



Electrochemical Nitrogen Reduction Under (Near) Ambient Conditions

Suzanne Zamany Andersen

Supervisor: Prof. Peter C. K. Vesborg

Co-supervisor: Prof. Ib Chorkendorff

Assoc. Prof. Jakob Kibsgaard

Department of Physics

Section of Surface Physics and Catalysis

Technical University of Denmark

Ph.D. Thesis

April 2020

Cover images

Top: Quotes regarding the Ph.D. work.

Bottom: Picture of ammonia molecule tattoo.

Abstract

The world population is expected to increase significantly over the next 80 years, reaching potentially 11 billion people before leveling off at the end of this century. All these people will need food, which can be grown more effectively by the application of synthetic fertilizer to the soil compared to traditional manure. Synthetic fertilizer, in the form of ammonia, is currently commercially produced via the large-scale catalytic Haber-Bosch process. This utilizes methane and nitrogen as reagents to produce ammonia over an iron-based catalyst, with carbon dioxide as a side product. Unfortunately, this process releases ~1 % of all the CO₂ emissions in the world, negatively impacting climate change. Furthermore, due to the large energy barriers required to split the inert dinitrogen molecule, high pressures and temperatures are needed, leading to huge centralized facilities for the production of ammonia.

In this thesis, the process of electrochemical nitrogen reduction is considered, where ammonia can potentially be made directly from nitrogen and hydrogen, using electricity as the energy source. This would theoretically lead to a carbon neutral process, wherein the electricity could be supplied via renewable sources, such as wind or solar power. Furthermore, the process should be able to run continuously at (near) ambient conditions, thereby enabling production at the point of use, cutting out the need for transportation and storage.

Unfortunately, this process is far from optimal, and while the field is relatively new, the activity and selectivity of the electrocatalytic process is horrifically dismal. Ammonia is sadly also ubiquitous in the environment in small, but similar (and often greater), amounts to those made from electrocatalysis, which leads to regrettably many false positives in the literature. Scientists are, for the most part, not nearly careful and stringent enough with background testing, therefore inadvertently misleading the field with wrong results. Therefore a central part of this work was in developing a thorough and rigorous testing protocol, which, if followed properly, can ascertain if the source of the measured ammonia is pervasive contamination or successful synthesis. The crucial and indispensable step of this protocol is the use of gas cleaning combined with quantifiable isotope labeled experiments, which is the definitive proof of a successful electrocatalytic process. Two different proposed processes for gas cleaning

were tested successfully (a home-made and a commercial system), along with nuclear magnetic resonance measurements for isotope sensitive quantification of ammonia.

Using this protocol, many different catalysts were tested, both in aqueous and non-aqueous conditions, based on published research. None of the tested pure metal candidates in aqueous conditions produced any measurable ammonia above the detection limit of the colorimetric indophenol method. Ruthenium, one of the most promising pure metal catalysts according to theoretical calculations, was tested in alkaline, neutral, and acidic conditions, as well as under different temperatures in both alkaline and acidic media, but to no avail. One of the more promising systems in non-aqueous electrolyte was also tested: the lithium-mediated system first proposed by Tsuneto et al. in 1993. This system finally gave a positive result. Rigorous testing validated the reported result by Tsuneto et al., bringing it up to be included as one of the few trustworthy reports from the electrochemical nitrogen reduction field. Different cathode materials were also tested in the system, along with different salts and proton sources, leading to the conclusion that the initial system with a molybdenum working electrode in lithium perchlorate in tetrahydrofuran with ethanol as the proton source was the best in terms of Faradaic efficiency.

However, there is a caveat to this ammonia synthesizing process. The lithium-mediated system is not stable over longer measurements, as initially observed by Tsuneto et al., and seen from our data as well. A cyclic stabilization method of the working electrode potential was therefore created. This method utilizes a short lithium deposition pulse, followed by a longer resting pulse below lithium deposition potentials, with the cycle repeated indefinitely. This allows the lithium species to chemically dissolve from the surface during the longer resting pulse, preventing a build-up of passivating species on the surface of the electrode. The electrodes were investigated with various *ex-situ* characterization techniques to determine the surface composition post-measurement. The continuous lithium deposition process originally proposed by Tsuneto et al. was compared to the newly developed cycling method. The new cyclic method was seen to keep the electrode surface clear of accumulated species, which could therefore keep the working electrode potential in a stable regime for days, improving both the Faradaic efficiency and the energy efficiency significantly. This suggested method is an incremental step towards commercialization of the lithium-mediated system, as continuous operation at increased energy efficiency is absolutely necessary for future industrial use.

Resume

Verdensbefolkningen forventes at stige drastisk de næste 80 år, før det stabiliseres på omkring 11 milliarder mennesker i slutningen af dette århundrede. Alle disse mennesker får brug for mad, som kan dyrkes mere effektivt ved anvendelse af syntetisk kunstgødning i forhold til traditionel gødning. Syntetisk gødning, i form af ammoniak, produceres på nuværende tidspunkt kommercielt via den katalytiske Haber-Bosch proces, som foregår på stor skala. Denne proces anvender metan og kvælstof som reagenser til at producere ammoniak over en jernbaseret katalysator med carbondioxid som et biprodukt. Desværre frigiver denne proces en betydelig mængde af den totale CO₂ udledning i verden, hvilket har negativ indflydelse på klimaændringerne. På grund af de store energibarrierer, der er forbundet med at splitte det inerte dinitrogenmolekyle, er der behov for høje tryk og temperaturer, hvilket fører til at faciliteter til produktion af ammoniak er enormt store og centralt placeret.

I denne afhandling arbejder jeg med elektrokemisk nitrogenreduktion; en proces, hvor ammoniak potentielt set kan fremstilles direkte fra kvælstof og brint ved at bruge elektricitet som energikilde. Dette vil teoretisk set føre til en kulstofneutral proces, hvor elektriciteten kan leveres af vedvarende energikilder, såsom vind- eller solenergi. Desuden kan processen køres decentralt, kontinuerligt og under (tilnærmelsesvis) standard tryk og temperatur, og derved muliggøre produktion dér hvor det skal bruges, hvilket fjerner behovet for transport og opbevaring.

Desværre er denne proces langt fra optimal, og selvom feltet er relativt nyt og nyligt blomstrende, er aktiviteten og selektiviteten af den elektrokatalytiske proces bedrøveligt lav. Ammoniak er desværre også tilstede i miljøet i små men lignende (og ofte større) mængder, end dem der er fremstillet ved elektrokatalyse. Dette fører beklageligt til mange falske positiver i litteraturen. Forskere er for det meste ikke omhyggelige og stringente nok med baggrundsprøver, og ofte får de derfor utilsigtet vildlede feltet med forkerte resultater. En central del af denne afhandling omhandler derfor en grunding og streng testprotokol, som, hvis den følges korrekt, kan konstatere, om kilden til det målte ammoniak er gennemgribende kontaminering eller vellykket syntese. Det afgørende og uundværlige trin i denne protokol er brugen af gasrensning

kombineret med kvantificerbare isotopmærkede eksperimenter, som er det endelige bevis på en vellykket elektrokatalytisk proces. To forskellige foreslåede opsætninger til gasrensning er testet med succes (et hjemmelavet og et kommercielt system) sammen med nuklear magnetisk resonansmåling til isotopfølsom kvantificering af ammoniak.

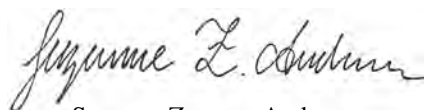
Ved hjælp af denne protokol testede jeg mange forskellige katalysatorer under både vandige og ikke-vandige forhold, baseret på offentliggjort forskning som udgangspunkt for valg af system. Alle de testede rene metalkandidater i vandig opløsning frembragte ingen målbar ammoniak over målegrænsen for den kolorimetrisk indofenol-metode. Ruthenium blev anvendt, da det er en af de mest lovende rene metalkatalysatorer ifølge teoretiske beregninger, og blev testet med basiske, neutrale og sure opløsninger såvel som ved forskellige temperaturer i både base- og syreopløsninger. Men alt dette til ingen nytte. Et af de mere lovende systemer i ikke-vandig elektrolyt blev også testet: det litiummedierede system, der først blev foreslået af Tsuneto et al. i 1993. Dette system gav endelig et positivt resultat. Rigorøse test validerede det rapporterede resultat fra Tsuneto et al., hvilket inddrager denne som en af de få pålidelige rapporter fra det elektrokemiske nitrogenreduktionsfelt. Forskellige katodematerialer blev også testet i systemet sammen med forskellige salte og protonkilder. Dette førte til konklusionen, at det oprindelige system med en Molybdæn-arbejdselektrode i litiumperchlorat med ætanol som protonkilde, var det bedste med hensyn til Faradisk effektivitet.

Det litiummedierede system er desværre ikke stabilt over længere målinger, hvilket både var observeret af Tsuneto et al., og data præsenteret i denne afhandling. Der blev derfor opfundet en cyklisk stabiliseringsmetode for arbejdslektrodepotentialet. Denne metode anvender en kort litiumdeponeringspuls, efterfulgt af en længere hvilepuls ved et potentiale lavere end litiumdeponeringspotentialet. Herefter gentages cyklussen kontinuerligt. Dette gør det muligt for diverse litium-arter at opløses kemisk fra overfladen under den længere hvilepuls, og hermed forhindre en opbygning af passiverende arter på overfladen af elektroden. Elektroderne blev undersøgt med forskellige *ex-situ* karakteriseringsteknikker for at bestemme overfladesammensætningen. Forsøg med den kontinuerlige litiumdeponeringsmetode, som oprindeligt var foreslået af Tsuneto et al., kunne hermed sammenlignes med den nyudviklede cykliske metode. Den nye metode kunne holde elektroden fri for akkumulerede arter og holdt derved arbejdslektrodepotentialet i et stabilt regime i flere dage. Dette forbedrede den Faradiske effektivitet samt energieffektiviteten markant. Denne foreslåede metode er et opadgående trin mod kommercialisering af det litiummedierede system, da kontinuerlig drift med øget energieffektivitet er absolut nødvendigt for fremtidig industriel anvendelse.

Preface

The work for this thesis was carried out at the Technical University of Denmark, Department of Physics, Section of Surface Physics and Catalysis (SurfCat) in the period between April 2017 and April 2020, including an external research stay at Stanford University, Department of Chemical Engineering, from October 2018 to December 2018.

My experimental work was carried out in close collaboration with other students, both from SurfCat and Stanford university, and with input from my supervisors and professors involved in this project. I will throughout this thesis use the pronoun "I" to denote work carried out exclusively by myself, while I reserve the pronoun "we" whenever there is overlap between my work and the work and ideas of my colleagues. The contributions from my colleagues will clearly be stated in the respective chapters.



Suzanne Zamany Andersen

April 2020

Acknowledgements

The work for this thesis was funded by the Villum Foundation V-SUSTAIN grant 9455 to the Villum Center for the Science of Sustainable Fuels and Chemicals. The 800 MHz NMR spectra were recorded on the spectrometers of the NMR Center at the Technical University of Denmark supported by the Villum Foundation. All the results reported in this thesis were possible due to extended collaboration with many people, both at DTU and Stanford University.

I am first and foremost grateful to my supervisors Prof. Peter C.K. Vesborg, Prof. Ib Chorkendorff and Assoc. Prof. Jakob Kibsgaard for giving me the opportunity to work on this exciting project. Weekly discussions regarding this project and my results, as well as their open door policy for questions, is what has led to a fun and interesting Ph.D. project. They had me hooked from the first moment describing the project as one of the hardest challenges in electrochemistry with the reward being "finding a golden needle in an immensely huge haystack". I would also like to especially thank Senior Lecturer Ifan E.L. Stephens for first teaching me about catalysis, and slipping in my application for the Ph.D. position past the application deadline. He was my main supervisor for the first 2 months of my Ph.D., and despite leaving for a prestigious position at Imperial College London in July 2017, he has continuously provided advice and support in my Ph.D., for which I am very grateful. Additionally I would like to thank Prof. Jens K. Nørskov, whose input in the regular ammonia meetings has greatly elucidated the mechanism behind the lithium mediated process, and Dr. Debasish Chakraborty for helping me with the patent application.

I would like to thank the entire DTU ammonia team for providing both help in times of need and for their support in experimentation. This started with the incredibly talented Dr. Viktor Čolić and Dr. Sungeun Yang, who were each half-time Post Docs on this project. They taught a very lost physicist much about chemistry, including everything from how to properly use a pipette, down to the basics of electrochemistry. I would also like to thank the meticulous and thorough Jakob B. Pedersen, both for helping me with carrying out experiments, and for letting me rope him into joining the International Physicists' Tournament. I greatly appreciate our talks about physics for the competition, and our trip to California for beamline experiments. I

am very happy that the incredibly skilful Dr. Mattia Saccoccio also joined the ammonia team, as he has an uncanny knack for understanding machinery/instrumentation, and always has a intelligent solution for any problem that might crop up in the lab. I am also very grateful for having met Kevin Krempel during my external stay at Stanford University, and then subsequently convincing him to join the ammonia team at DTU. Despite being one of his supervisors for his Master's Thesis, I am convinced he taught me more in those months than I him, and I consider our team very lucky to have him also join as a Ph.D. student. And last but not least the newest additions to the ammonia team: Katja Li and Dr. Rokas Sažinas, who I am very much looking forward to working more with in the future. The entire ammonia team has provided me with many fruitful discussions regarding various possible (and sometimes downright silly) ways to carry out ammonia synthesis, and I am very grateful that we are a tight-knit and overall supportive group.

Beyond the ammonia team, I want to thank all the amazing people at SurfCat, both for proving help professionally and for being a fun, social, and inviting group to work in. I appreciate all the exciting social events we do as a group, and all the fun weekly Friday bars, which creates a welcoming atmosphere for everyone. I want to particularly thank Anna Winiwarter, who has greatly helped me navigate the maze that is DTU administration. I want to thank my office mates, Jakob B. Pedersen, Jens-Peter Haralsted, Thomas Smitshuysen and Celia Cailloux for making the office a colorful and fun environment with enjoyable banter and delicious food. I further want to thank the very accomplished and capable floor managers Brian Knudsen, Patrick Strøm-Hansen and Jakob Ejler Sørensen for their technical support in making all the equipment at SurfCat function, and the diligent and caring Jacqueline McNulty for assistance in the chemistry lab, as well as Birgit Bohn for excellent organization and coordination of our entire section. I furthermore want to thank my collaborator Kasper Enemark-Rasmussen for measuring NMR samples, and gladly answering any question regarding NMR and the software used for data treatment. I also want to thank the exceptionally brilliant Michael Statt (Stanford University) and Dr. Vanessa J. Bukas for always being ready with an answer to theoretical questions, and explaining complicated processes in an easily digestible way.

In October-December 2018, I was on a external stay at Stanford Univeristy in Prof. Thomas Jaramillo's lab. I want to thank Prof. Jaramillo for this great opportunity that showed me the benefits of collaboration and knowledge-sharing, and Prof. Matteo Cargnello for letting me work in his lab while there. In particular I want to thank Dr. Jay Schwalbe whom I worked closely with during this stay, and who seems to be an infinite font of knowledge regarding electrochemistry. I want to thank Sarah J. Blair and Dr. Adam Nielander, from whom I have learned much about NMR and XRD. I also want to thank everyone in Prof. Jaramillo's group,

who made me feel very welcome during this stay, and included me in all the fun social activities. I acknowledge the Danish Ministry of Higher Education for financially supporting my stay.

I thank Jakob B. Pedersen, Doris Hoffmeyer, Mattia Saccoccio, Rasmus D. Engelsholm, Anna Winiwarter, Kevin Krempf, Søren B. Scott, Katja Li, Rokas Sažinas, Valeria Magri, and Daníel Björnsson for proof reading parts of my thesis, and giving me much needed and invaluable suggestions for improvements.

I want to especially thank Anna and Valeria for countless coffee breaks, talks about personal life, and fun yoga nights. I am very grateful for how close we have gotten, and despite neither of them being at DTU anymore, I have no doubt the friendship will continue to grow. I also want to thank Sarah G. Shapel, who I supervised for a small course in ammonia synthesis. Much of the experimentation on Otto was done together, and our friendship has grown through the many coffee breaks while monitoring the day long electrochemistry experiments. I also want to express my gratitude to Celia for the shared fun experiences and reminding me to enjoy life and take breaks sometimes (especially while extremely stressed with writing this dissertation), as well as Jens-Peter for all the great movie suggestions and fun hangouts. I also want to thank Chris for helping me rediscover myself during an especially hard time in my life.

Finally, I want to thank my family. My cousins, Atusa and Anahita, have always been a source of both constant encouragement and incredible inspiration, as they are both extremely talented and very creative. I want to thank my uncles Jamshid for challenging me intellectually, and Javad for supporting me in a caring family environment. My grandparents, from both sides, have always shown me love and compassion, and I dearly miss my paternal grandfather and maternal grandmother whom I lost in the last 3 years. I want to thank my ex-husband, Spencer. We were faced with much hardship to simply be together, but despite that we also had many happy times, and our marriage has made me a stronger person. I want to thank my parents, who have raised me in an environment filled with endless love and care. They have always instigated and encouraged scientific curiosity. My decision to become an engineer stemmed from my mother always capably fixing anything broken around the house, and my father inexhaustibly teaching me about the natural world around us. Last but not least, I thank my best friend and boyfriend Daníel for his encouragement, love, and understanding. These last few months of my Ph.D. have not been easy on either of us, and the only thing keeping me from a complete stress induced breakdown has been his continuous support, delicious and nutritious cooking, and constant reminders to eat, sleep, and take breaks.

List of publications

Paper I

A rigorous electrochemical ammonia synthesis protocol with quantitative isotope measurements

Suzanne Z. Andersen*, Viktor Čolić*, Sungeun Yang*, Jay A. Schwalbe, Adam C. Nielander, Joshua M. McEnaney, Kasper Enemark-Rasmussen, Jon G. Baker, Aayush R. Singh, Brian A. Rohr, Michael J. Statt, Sarah J. Blair, Stefano Mezzavilla, Jakob Kibsgaard, Peter C. K. Vesborg, Matteo Cargnello, Stacey F. Bent, Thomas F. Jaramillo, Ifan E. L. Stephens, Jens K. Nørskov and Ib Chorkendorff

Nature, **570**, 504-508, (2019)

* these authors contributed equally

Paper II

A Versatile Method for Ammonia Detection in a Range of Relevant Electrolytes via Direct Nuclear Magnetic Resonance Techniques

Adam C. Nielander, Joshua M. McEnaney, Jay A. Schwalbe, Jon G. Baker, Sarah J. Blair, Lei Wang, Jeffrey G. Pelton, Suzanne Z. Andersen, Kasper Enemark-Rasmussen, Viktor Čolić, Sungeun Yang, Stacey F. Bent, Matteo Cargnello, Jakob Kibsgaard, Peter C. K. Vesborg, Ib Chorkendorff, and Thomas F. Jaramillo

ACS Catal., 2019, **9**, 7, 5797-5802

Paper III

A Combined Theory-Experiment Analysis of the Surface Species in Lithium-Mediated NH_3 Electrosynthesis

Jay A. Schwalbe, Michael J. Statt, Cullen Chosy, Aayush R. Singh, Brian A. Rohr, Adam C. Nielander, Suzanne Z. Andersen, Joshua M. McEnaney, Jon G. Baker, Thomas F. Jaramillo, Jens K. Nørskov, and Matteo Cargnello

ChemElectroChem, 2020, 7, 7, 1542-1549

Paper IV

Cyclic Stabilization Method on Lithium-Mediated Electrochemical Nitrogen Reduction

Suzanne Z. Andersen*, Michael J. Statt*, Vanessa J. Bukas*, Sarah G. Shapel, Jakob B. Pedersen, Kevin Krempel, Mattia Saccoccio, Debasish Chakraborty, Jakob Kibsgaard, Peter C. K. Vesborg, Jens Nørskov, and Ib Chorkendorff

In preparation

* these authors contributed equally

Table of contents

Nomenclature	xix
1 Introduction	1
1.1 Once upon a time, more than 100 years ago	1
1.2 7.8 billion people, and counting...	3
1.3 11 billion people while the temperatures keep rising?	4
1.4 Outline of this thesis	8
2 (Electro)catalysis and Nitrogen Reduction	11
2.1 Electrocatalysis	11
2.1.1 What is catalysis?	11
2.1.2 Electrocatalysis and applied potential	14
2.1.3 Defining the potential scale	16
2.2 Reduction of nitrogen	16
2.2.1 The Haber-Bosch process	16
2.2.2 Electrochemical nitrogen reduction and the competing reaction	17
2.3 Aims of this dissertation	20
3 Experimental Methods	23
3.1 Electrochemical experimentation	23
3.1.1 Electrochemical set-up	23
3.1.2 Electrochemical autoclave: "Otto Clive"	25
3.1.3 Electrochemical methods	28
3.2 Ammonia quantification	32
3.2.1 The indophenol method	32
3.2.2 Nuclear magnetic resonance (NMR)	36

3.3	Electrode characterization	38
3.3.1	X-ray Diffraction (XRD)	38
3.3.2	X-ray Photoelectron Spectroscopy (XPS)	39
3.3.3	Scanning Electron Microscopy (SEM) and Energy-Dispersive X-ray spectroscopy (EDX)	40
4	The Rigorous Protocol	43
4.1	The simple background measurements	44
4.2	Possible sources of ammonia contamination	45
4.2.1	Membranes for two-compartment cells	45
4.2.2	The catalyst and other common contamination sources	47
4.2.3	Accounting for known impurities and determining performance assessment	49
4.3	Quantitative isotope measurements	50
4.4	Summary	53
5	Electrochemical Nitrogen Reduction in Aqueous Solution	55
5.1	Trapping efficiency in system	56
5.1.1	Ammonia solubility in electrolyte	56
5.1.2	Purging efficiency to acid trap	57
5.1.3	Closed system with gas circulation	58
5.1.4	Ammonia oxidation	58
5.2	Ammonia contamination	59
5.3	Systematic study in electrochemical nitrogen reduction	64
5.3.1	Pure metal foils	64
5.3.2	Temperature dependence	67
5.3.3	Electrolyte pH	68
5.4	Summary	70
6	Electrochemical Nitrogen Reduction in Non-Aqueous Solution	71
6.1	Lithium-mediated electrochemical nitrogen reduction	72
6.1.1	Referencing the potential	73
6.1.2	Electrolyte evaporation and NH ₃ oxidation	74
6.2	Systematic study	75
6.2.1	Rigorous quantified isotope labeled testing	75
6.2.2	The role of the WE metal	77

6.2.3	Testing other salts	78
6.2.4	The importance of the proton source	79
6.3	State-of-the-art	81
6.4	Summary	83
7	Cyclic Stabilization of the Lithium-Mediated Process	85
7.1	Constant current deposition	86
7.2	The cycling method	87
7.2.1	Quantitative isotope labeled study and background measurements	89
7.2.2	Long-term stability	92
7.2.3	Advantages of the cycling method	93
7.3	<i>Ex-situ</i> characterization of electrodes	95
7.3.1	SEM and EDX	95
7.3.2	XRD	99
7.3.3	XPS	101
7.4	Theoretical considerations	103
7.5	Summary	105
8	Conclusion and Outlook	107
8.1	Conclusion	107
8.2	Outlook	110
	References	113
	Appendix A Supporting Information	123
A.1	Appendant to Chapter 5: Electrochemical Measurements	123
A.1.1	Example of determining potential range for Figure 5.6	123
A.1.2	Example SGEIS spectra from Table 5.6	125
A.2	Appendant to Chapter 7: SEM images	126
	Appendix B Appended Publications	131

Nomenclature

Roman Symbols

A	Absorbance	[AU]
C	Concentration	[M]
c	Speed of light	299,792,458 [m/s]
C_{NH_3}	Concentration of ammonia	[$\mu\text{g/mL}$]
d	Distance between lattice planes	[m]
E	Energy	[J]
E_A	Activation energy	[J]
E_b	Binding energy	[eV]
E_k	Kinetic energy	[eV]
E_{photon}	Energy of photon	[eV]
F	Faraday's constant	96,485 [C/mol]
FE	Faradaic efficiency	[%]
FE_{cycling}	Faradaic efficiency for the cyclic method	[%]
FE_{dep}	Faradaic efficiency during lithium deposition	[%]
ΔG	Change in Gibbs free energy	[J]
ΔG_R	Free energy of the ammonia oxidation reaction	[J]

δg_R	Specific free energy of reaction gained from ammonia oxidation	[J/kg]
h	Planck's constant	$6.62607015 \times 10^{-34}$ [J s]
I	Current	[mA]
i	Current density	[mA/cm ²]
I_0	Incidence light intensity at a given wavelength	[W/m ²]
I_1	Transmitted light intensity at a given wavelength	[W/m ²]
L	Path length through sample	[m]
m	Mass	[kg]
m/z	Mass to charge ratio	[kg/C]
n	Moles of product	[mol]
Q	Total transferred charge	[C]
R	Resistance	[Ω]
r_H	Rate of proton diffusion through the SEI layer	[s ⁻¹]
r_{H_2}	Rate of outgoing hydrogen	[s ⁻¹]
r_{Li}	Rate of Li ⁺ diffusion through the SEI layer	[s ⁻¹]
r_{N_2}	Rate of N ₂ diffusion through the SEI layer	[s ⁻¹]
r_{NH_3}	Rate of outgoing ammonia	[s ⁻¹]
\vec{S}	Magnetic spin quantum number	[N m s]
$s_{Li \rightarrow NH_3}$	Fraction of electrons used for Li plating recovered to selectively produce ammonia during resting	[%]
TE	Trapping efficiency	[%]
U	Potential	[V]
U_{cell}	Cell potential	[V]
V	Volume	[mL]

z Moles of electrons transferred per mole product

Greek Symbols

ε	Extinction coefficient	$[(\text{M m})^{-1}]$
η	Energy efficiency	$[\%]$
λ	Wavelength	$[\text{m}]$
μ	Magnetic dipole moment	$[\text{N m T}^{-1}]$
ν	Wavenumber	$[\text{m}^{-1}]$
ϕ	Workfunction of spectrometer	$[\text{eV}]$
θ	X-ray incident angle in XRD	$[^\circ]$

Acronyms / Abbreviations

AC	Alternating current
CA	Chronoamperometry
CE	Counter electrode
CP	Chronopotentiometry
DC	Direct current
EDX	Energy-dispersive X-ray spectroscopy
EIS	Electrochemical impedance spectroscopy
HER	Hydrogen evolution reaction
LSV	Linear sweep voltametry
NMR	Nuclear magnetic resonance spectroscopy
NRR	Nitrogen reduction reaction
OCP	Open circuit potential
OER	Oxygen evolution reaction
QMS	Quadrupole mass spectrometer

Redox	Coupled reduction-oxidation reaction
RE	Reference electrode
RF	Radio frequency
RHE	Reversible hydrogen electrode
SEI	Solid electrolyte interface
SEM	Scanning electron microscopy
SHE	Standard hydrogen electrode
UHV	Ultra high vacuum
UV/Vis	Ultraviolet-visible spectroscopy
WE	Working electrode
XPS	X-ray photoelectron spectroscopy
XRD	X-ray diffraction

Chapter 1

Introduction

"All you really need to know for the moment is that the universe is a lot more complicated than you might think, even if you start from a position of thinking it's pretty damn complicated in the first place."

— Douglas Adams, *The Hitchhiker's Guide to the Galaxy*

The aim of this chapter is to provide the reader with a motivation for the work carried out for this project in a broad context, explained entirely in layman's terms. That is, a sort of "ammonia for dummies". I will start with a small history lesson of ammonia, go over why ammonia is important today, and touch upon everyone's favorite political issue; our future impending doom (*i.e.* the global climate crisis). This will be tied into over-population and groundwater pollution, as well as the need for fertilizer in developing countries, access to food, and clean water. Basically a wide range of the UN sustainable development goals, which I urge you to go take a look at [1]. So let's get started.

1.1 Once upon a time, more than 100 years ago

Our story starts with the rather tragic and intriguingly controversial figure of Fritz Haber: a Jewish turned Christian German patriot, born from incest in Prussia. I could spend much of this chapter talking about the duality of certain aspects of his life, such as how he is both the father of chemical warfare during World War I, killing millions of people through his invention of various poison gases, mirrored by the fact that half of us wouldn't be alive today if not for him. Or some of the increasingly tragic events of his life, such as the suicide of his wife, Dr.

Clara Immerwahr, presumably from guilt over his horrible war contributions, or how some of the chemicals he developed were later used to kill his extended Jewish family members in concentration camps, by the very country he so patriotically served. Instead, I'm going to refer you to his biography [2], which I highly recommend, as it's a very interesting read.

The key sentence in the previous paragraph important for my work, is how he managed to feed half the population of the world [3]. It has been known by farmers for thousands of years that spreading manure on the fields makes the plants produce more crops per acre [4]. Through much experimentation with different kinds of both natural and synthetic manure, it was discovered in the 19th century that particularly nitrogen containing manure worked well for increased crop yield [5]. Unfortunately, usable nitrogen is difficult to come by. Yes, yes, I know that the very air we breathe contains 80ish% nitrogen, but for chemical reasons, that form of nitrogen (N_2 to be specific), is not usable [6]. It is what is known as "inert", meaning the two nitrogen atoms like each other so much, that they don't want to play with any other atoms around them, unless they are *really* forced to. But I'll get back to that.

So, where could one find usable nitrogen (also called fixed nitrogen)? All the way in South America as it turned out. There was natural rock sediment in Chile, called caliche, which contained usable forms of nitrogen that could be mined. Additionally, certain islands around the world, and particularly around Peru, contains something called guano, which is, well, bird and bat poop. This also contains a lot of fixed nitrogen, and many previously undisturbed islands were cleaned out, much to the annoyance of the birds and bats [7]. The caliche and guano were collected, and shipped halfway across the world to be used as fertilizer by the Europeans and Americans. But, as anyone with a little common sense can see, this is neither particularly sustainable nor up-scalable. The caliche deposits would eventually dry out, and the bird and bats, who probably liked to poop in privacy, were increasingly driven away from their roosts. Sir William Crookes, the incoming president of the British Academy of Sciences, prophesied this as the biggest challenge of the 20th century in his 1898 inaugural speech; "It is through the laboratory, that starvation may ultimately be turned into plenty... It is the chemist, who must come to the rescue" [8]. He was more accurate than Nostradamus at predicting the future.

The solution to impending starvation came in 1909, where our very own chemist, Fritz Haber, succeeded in making ammonia (NH_3) in his laboratory. He managed to force the very inert N_2 molecule to play with hydrogen, by using something called catalysis [kuh-ta-luh-suhs] [9]. This turned out to be a great discovery for the guano pooping birds and bats. Less so for the Chilean economy unfortunately [10].

1.2 7.8 billion people, and counting...

The discovery of how to make ammonia from air was immediately bought by the German company BASF. They needed to up-scale the process, and put Carl Bosch in charge of figuring out how to do it. Germans are nothing if not efficient, and only one year later he had succeeded in up-scaling it from Haber's table-top model, to a full production facility. Already in 1913 Germany was capable of producing 20 tonnes of ammonia per day [7]. This was absolutely crucial for Germany, as the allied powers had blocked trade to Chile, and they would not have access to fertilizer otherwise. Ammonia can (unfortunately) also be converted into explosives, which greatly helped the German war effort, and prolonged World War II[9].

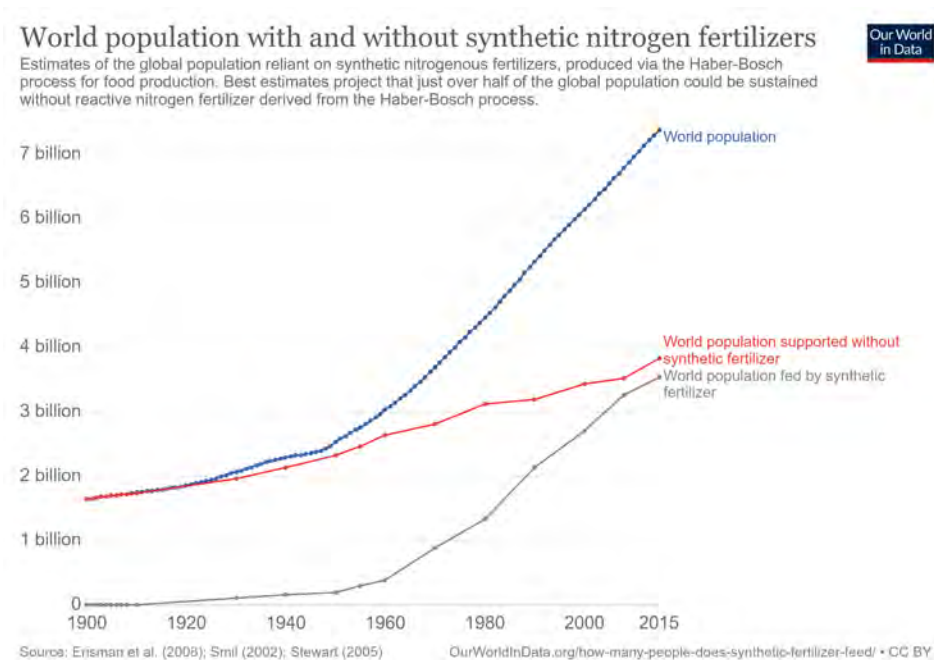


Figure 1.1 Global population from 1900 to 2015, with estimates of population without synthetic fertilizer. Erisman et al. (2008); Smil (2002); Stewart (2005) - "World population with and without synthetic nitrogen fertilizers". Published online at OurWorldInData.org. Retrieved from: <https://ourworldindata.org/grapher/world-population-with-and-without-fertilizer?time=1900..2015> [3, 11, 12].

After the war eventually ended, the newly invented Haber-Bosch process was commercialized, and spread across the world. Huge facilities were built, and ammonia was suddenly abundantly available to fertilize crops for the ever-growing population [13]. As more crops could

be grown, more people could eat, and this single discovery by Fritz Haber led to the explosive population boom of the past century [14], seen clearly in Figure 1.1. Today, half the nitrogen in our bodies have originated from the Haber-Bosch process [15]. Unfortunately, because the N_2 molecule is so inert, it requires high temperatures and high pressures to change it into ammonia. And pressure is a rather expensive commodity, requiring huge facilities, with reinforced valves and connections, and many safety measures. This means that the immense ammonia production facilities can only be built by countries that can afford it. The ammonia is then sold, at a mark up, and shipped to places that cannot afford to build the facilities. Furthermore, hydrogen also needs to come from somewhere, and while it is the most abundant element in the universe, it's not really accessible in a pure form. There's a lot of it in methane (CH_4) though, which, through the magic of catalysis, can be mixed with water (H_2O) to make pure hydrogen usable for making ammonia. Unfortunately, the carbon from the methane doesn't just disappear, and instead joins up with the oxygen from water to make CO_2 [16]. Unless you've been living under a rock the past few years, you'll know that most people (though sadly not all) are slowly starting to realize that CO_2 is something called a greenhouse gas [17]. And greenhouse gasses are bad for the environment. They essentially float around our atmosphere, acting like a giant blanket for the earth, slowly heating it up by trapping energy that would otherwise be sent out into space. As we are currently producing incredible amounts of ammonia, a total of around 1 % of our global CO_2 emissions is just from running the Haber-Bosch process [18].

1.3 11 billion people while the temperatures keep rising?

There's a sort of unspoken catch-22 in this particular field. I just claimed that ammonia is important, as half of us wouldn't be alive without it. But the more people we can feed, the more our population increases, which in turn is putting a huge strain on the resources of our planet, worsening the climate impact [19]. Over-population is another "hot topic" in debates, and ammonia production isn't exactly doing anything to help that. While the strain our consumption has on the planet is a problem, looking at Figure 1.2, it is clear that the growth rate of the population is actually decreasing since the 60s. This is due to things like overall decreased world poverty [20] and child mortality rates, and increases in education [21] and healthcare [22]. These all lead to women having fewer children, and to start conceiving later in life as well, both because women are more educated, and because more of the children will survive into adulthood. The more developed a country, the smaller the birth rate, which will eventually steady the population growth [23]. Globally, the growth rate is still positive, so barring any major world war or global viral pandemic (which isn't entirely unlikely in my unprofessional and

currently quarantined opinion), experts agree that we will probably hit an astounding 11 billion people before the population stabilizes [24].

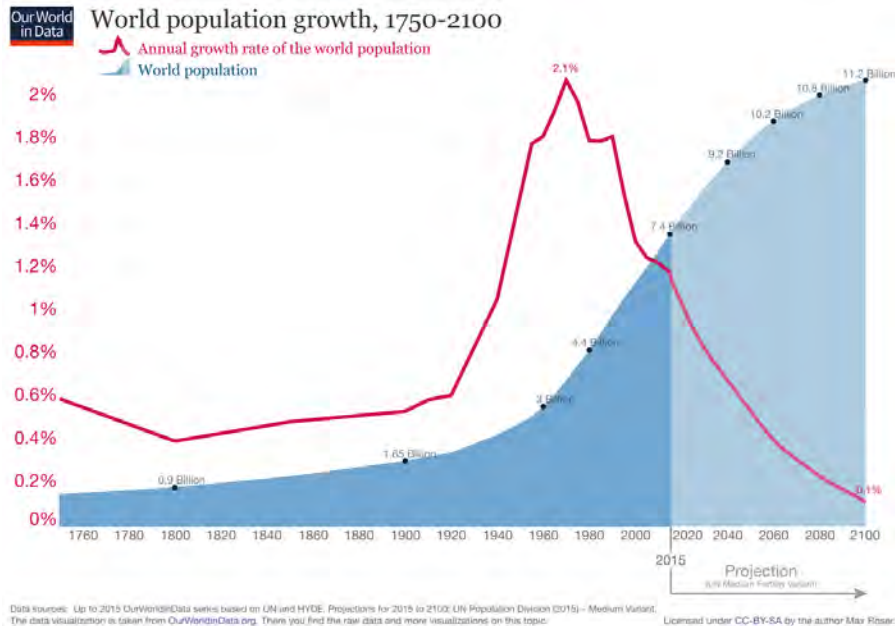


Figure 1.2 Global population and growth rate until 2015, with predictions of the future until 2100. Max Roser (2015) – "World population growth, 1750-2100". Published online at OurWorldInData.org. Retrieved from: '<https://ourworldindata.org/world-population-growth>'.

So, getting fertilizer to developing countries is important, because decreased hunger helps increase the standard of living, and thereby eventually zeroes the population growth rate, which is good for the planet. However, besides the downside of increased CO₂ due to the Haber-Bosch process, there's another issue. The way we fertilize our fields today is very inefficient [3]. The farmer buys fertilizer in bulk, then spreads it out over the field to increase crop growth. Now, in the farmer's mind, synthetic fertilizer = more crops. So, the more fertilizer used, the more crops can be grown. However, this is true only up to a certain biological limit, as the plant can only uptake so much fertilizer in one go [25]. And of course the farmer wants to make sure that limit is reached, to maximize profit. So if the farmer has access to cheap fertilizer, the farmer will use as much as possible. While that logic in theory works for maximizing crop yield, once the plant cannot uptake any more fertilizer, the excess is simply washed away. You might have heard about groundwater pollution and nitrate run-offs as another issue popping up [26]. It's partially from farmers over-fertilizing. And it's very hard to tell a farmer to use less fertilizer, as

they want to make sure they are getting the maximum yield per square meter of crops, meaning they would rather err on the side of using too much fertilizer rather than too little, inadvertently causing damage to the environment [27].

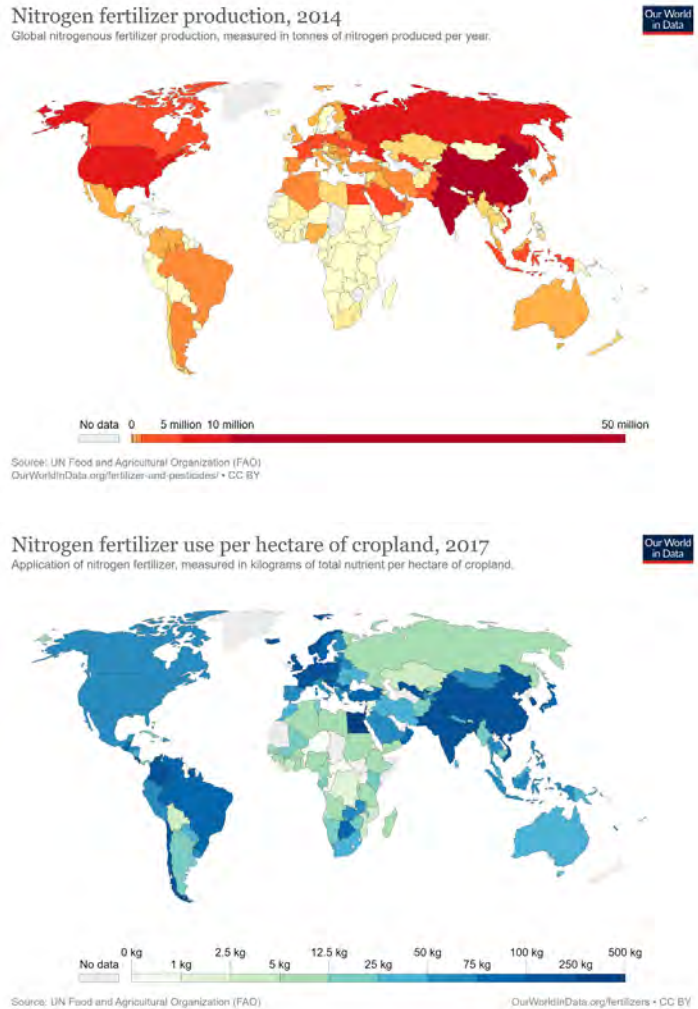


Figure 1.3 Top) Global ammonia production in 2014. Bottom) Global ammonia application in 2017. Food and Agriculture Organization of the United Nations (FAO) (2020). Published online at OurWorldInData.org/fertilizers.

These two quite large problems of CO₂ release and groundwater pollution will only become significantly worse for the planet when the regions that currently don't have the infrastructure or

initial capital to build Haber-Bosch plants gain access to fertilizer as they develop. Just consider sub-Saharan Africa, wherein currently 1.1 billion people live. It is estimated that the population will go up to anywhere from 2.6 [28] to a whopping 4.2 billion [29] by the end of this century. They produce and use very little synthetic fertilizer, seen in Figure 1.3, but with the expected advances in development, will require fertilizer to produce crops more efficiently. And that can currently only come through the Haber-Bosch process [30].

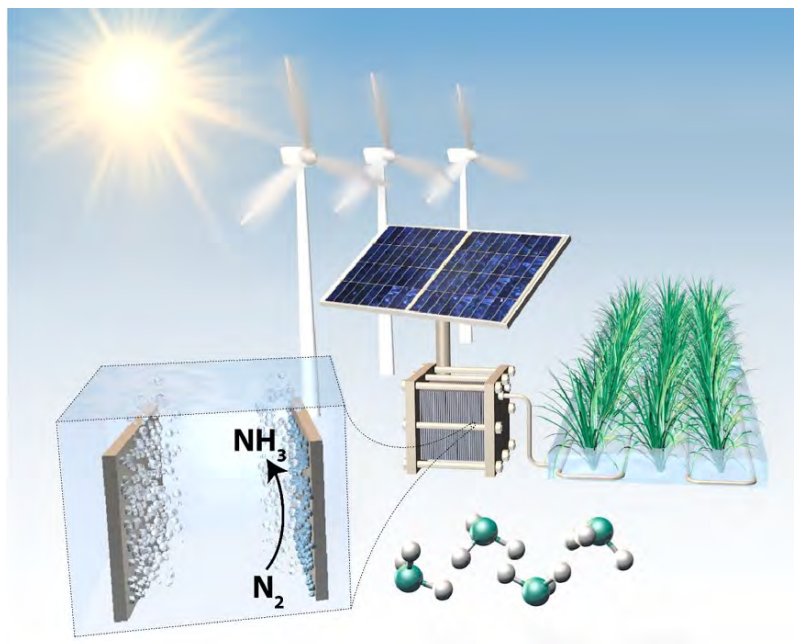


Figure 1.4 The dream when starting this project. A magic box, that the farmer can keep on the farm, requiring only electricity (of course from a renewable source), water and air. This would produce small amounts of ammonia, which can be distributed directly into the irrigation system in the proper amounts. Picture courtesy of Assoc. Prof. Jakob Kibsgaard.

It seems like a dire situation. We need ammonia, and we need to make a lot more of it in the future, but it worsens climate change, and causes groundwater pollution. Not to mention it requires a large capital investment to make the huge Haber-Bosch facility necessary to produce it [31]. So, what can be done to solve these issues? Cue angelic choir and trumpet music, because this is where my project comes in. Using the magic of catalysis, it should in principle be possible to convince the inert N_2 molecule to split using electricity instead of the high pressure and high temperature needed by the Haber-Bosch process [32–35]. If we don't need high pressure, we don't need huge facilities, because, as you might remember, high pressure means expensive

components, which, in turn, favor large plants to reach economy of scale. And the electricity supplied can even come from a renewable source, such as solar or wind energy. Furthermore, the hydrogen can in this case be supplied by water, rather than methane, making the whole process completely CO₂ neutral. This can all happen in a small device, similar to what is shown in Figure 1.4, placed locally at the farm, directly where the ammonia is needed, requiring only air, water, and electricity. The fertilizer can be fed directly and continuously into the irrigation system in small calibrated doses, enough that the plants can exactly uptake all of it, without any excess being washed away into our groundwater. This could in practice also be done today with Haber-Bosch produced fertilizer to reduce run-offs, but it would require additional storage of the fertilizer at the farm, throughout the growing season. Ammonia, if not handled correctly, can be a dangerous chemical in concentrated doses [36]. This risk of improper handling is increased if the farmer has to dilute it himself, rather than simply producing it diluted on-site *via* electrochemistry.

While this magic box sounds amazing, it is still quite far away from being realized [37, 38]. I will, rather optimistically, say that my work of the previous three years has brought us just a little closer to this goal, as you will see if you keep on reading. I expect to lose many of the readers when stuff becomes technical, or you might just skip to the conclusion to get the short version. But if nothing else, I hope by reading this introduction, that you, friend, family, colleague, opponent, or stranger that you might be, have learned something about the challenges we as humans face for the present and future. Climate change, access to clean water, and decreasing world hunger are all linked, and we can only hope to solve these issues by considering the broader picture. This starts by accepting evidence and data from experts, particularly in a political climate ripe with "fake news", where opinions can weigh more than facts. If we talk about the issues, and back our claims with facts, we can finally start tackling the upcoming challenges together.

1.4 Outline of this thesis

Chapter 2 includes a general overview of catalysis, the Haber-Bosch process, and electrochemical ammonia synthesis a bit more specifically. The end of this chapter will have specific aims of my Ph.D. project covered in this work.

Chapter 3 covers all the different experimental methods used throughout my project.

Chapter 4 will cover, in depth, the rigorous protocol for nitrogen reduction we developed that is necessary for carrying out proper experiments in ammonia synthesis, which includes quantifiable isotope measurements as a necessary keystone. This chapter will go through the

many pitfalls that unfortunately many people do not successfully navigate when it comes to measuring ammonia.

The three next chapters will deal with various experiments wherein I attempt, and sometimes succeed, at synthesizing ammonia. Chapter 5 and 6 will deal with electrochemical nitrogen reduction in respectively aqueous and non-aqueous conditions. Spoiler alert: one of them works, one of them does not. The end of Chapter 6 will have a state-of-the-art plot from 2018, along with some speculations regarding the work of others. Chapter 7 will then deal with a cyclic stabilization method, which vastly improves the efficiency towards synthesizing ammonia. This is compared to the state-of-the-art in the literature.

Lastly, in Chapter 8, I will draw the main conclusions from the previous four chapters. Finally, I will discuss the future of this project, as well as the future, as I see it, of electrochemical nitrogen reduction.

Chapter 2

(Electro)catalysis and Nitrogen Reduction

"The trouble with having an open mind, of course, is that people will insist on coming along and trying to put things in it."

— Terry Pratchett, *Diggers*

This chapter will be split into two parts: The first part covers a brief introduction into electrocatalysis, describing the general concepts and terms used. The second part describes the Haber-Bosch process and electrochemical nitrogen reduction. I will define some aims of this dissertation at the end, which I will attempt to answer throughout the following chapters. The experienced reader can simply skip ahead to the aims in Section 2.3.

2.1 Electrocatalysis

2.1.1 What is catalysis?

Catalysis is a process that increases the rate of a chemical reaction. It involves the use of a catalyst, a material that lowers the energy barrier for the chemical reaction, while the catalyst itself remains unchanged at the end of the reaction. The difference in energy between the starting reactants and the desired product is defined by the difference in Gibbs free energy, ΔG . Typically there will be some intermediate steps before forming a product, which deal with the breaking and forming of chemical bonds. These are energetically less favorable than the starting

point, and therefore require some activation energy, E_a , which is the difference between the initial state and the transition state. A catalyst provides another reaction pathway by interacting with the reactants, forming adsorbed intermediate steps, which lowers the activation energy required to form said intermediates, and thereby increases the reaction rate. One can imagine this energy landscape as a mountain. The reactants are on one side, while the desired product is on the other side. You have to pay a lot of energy to walk up the mountain to get to the product on the other side. Meanwhile, catalysis essentially is a tunnel through the mountain, and you have to pay less energy to get to the product by just walking through the tunnel. These are sketched in Figure 2.1 for the simple reaction $A + B \rightarrow AB$. If a catalyst is included (green pathway), a simplified intermediate step wherein the reactants are adsorbed onto the catalyst is shown, which "tunnels through the mountain" and lowers the required E_a for the reaction. The energy needed to drive the reaction can stem from applied pressure or temperature to the system, which overcomes this energy barrier.

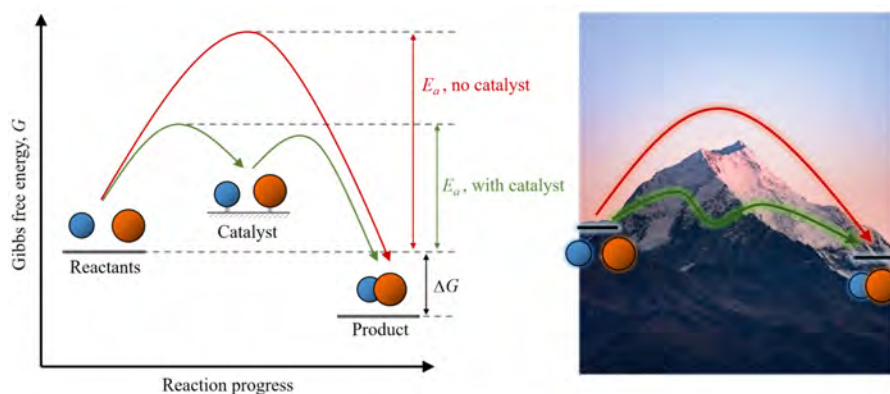


Figure 2.1 Left: schematic of chemical reaction between two molecules. Pathway without catalysts (red) requires a higher activation energy, while pathway with catalyst (green) has a lower activation energy, due to the interaction with the catalyst. Right: Catalysis explained through mountain energy landscape analogy. Photo by Mads Schmidt Rasmussen on Unsplash.

The activity and selectivity is the holy grail of a useful catalyst. Activity is a measure of how much product is formed as a function of time, while selectivity is a measure of how much desired product, as opposed to any side products, is formed. The former leads to high reaction rates, while the latter ensures that undesired side reactions are minimized. Furthermore, stability is another crucial parameter, as even the best catalyst is worthless if it rapidly degrades. One of these without the others is essentially useless for practical application of a catalyst, so one should always keep in mind to optimize all three parameters [16, 39].

Basic mechanisms of surface reactions

Heterogeneous catalysis is a type of catalysis wherein the phase of the catalyst and the reactants and products are different. The usual route for heterogeneous catalysis is through a surface reaction, wherein the catalyst itself remains unchanged at the end of the reaction. At least one reactant species is adsorbed onto the catalyst surface, which will lower the reaction energy barrier. There are different mechanisms for the reaction, depending on how the reaction occurs. One route is when only one reactant adsorbs, directly reacts with the other reactant(s), and desorbs (the Eley-Rideal mechanism). Another way is when the other reactant(s) are also adsorbed onto the surface, diffuse together and react, then desorb (Langmuir-Hinshelwood mechanism). There is also a variation of this wherein one reactant comes from the lattice of the catalyst, leaving a vacancy that can be filled with a new reactant (Mars-Van Krevelen mechanism). It is important to know the reaction pathway for a given reaction, as one needs to optimize the catalyst accordingly. One can determine the pathway of the reaction by determining the kinetic laws governing the reaction. [16]

Sabatier's principle and scaling relations

The schematic of an intermediate shown in Figure 2.1 is very simplified. There are many different intermediate steps involved, which can be split into reactant(s) adsorbing onto the surface, reactions between reactants on the catalyst, and desorption of the product(s) from the surface. Ideally one needs a catalyst which is reactive enough to adsorb the reactant onto the surface, thereby affecting the intra-molecular binding strength of the molecule, but not so reactive that it binds too strongly and cannot desorb again from the catalyst surface after reaction. This ideal binding is called Sabatier's principle, and can be visualized as a volcano plot, wherein the best metal catalyst that binds neither too strongly nor too weakly is at the top [40]. An example is shown in Figure 2.2, where the (111) surface of Rhenium (Re) and Ru appear to be the ideal binding catalysts for the black curve, while Platinum (Pt) is best for the blue curve for both (111) and (211) surfaces. This figure is quite important, and I will return to it throughout this chapter as we slowly build an understanding of catalysis, to fully explain what is shown.

Rather than just trying every catalyst for a given reaction (such as the work by Alwin Mittasch, who tested well over 20,000 catalysts for the Haber-Bosch process [7, 42]), one can use computational chemistry to determine which catalyst is best for a given reaction [38]. All the different intermediate steps must be determined, along with the adsorption energies these all have for a given catalyst surface. It can therefore be computationally heavy to calculate which catalyst is the best. For a given reaction, the number of intermediate steps can be quite large,

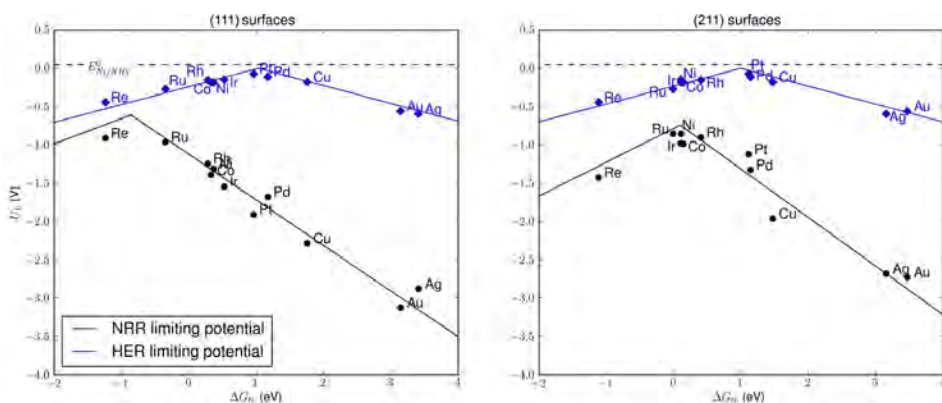


Figure 2.2 Volcano plot over the nitrogen reduction (black) and hydrogen evolution (blue) as a function of the *N binding-energy descriptor on a (111) and (211) surface. Figure reprinted with permission from Reference [41]. Copyright 2015 John Wiley & Sons, Inc.

each constructing different volcano plots, which additionally vary depending on the facet or site of the exposed metal surface. To lighten the computational load, scaling relations, which simply state that different intermediates bound to a surface through the same type of bond will have similar binding energies, can be used. These correlations of the adsorbates vastly simplify the calculations down to just a few parameters [43], and can be used to predict the binding energies of new materials. Micro-kinetic modeling can further be used to also consider the kinetics of the adsorption of molecules, reaction, and desorption from the surface as a function of pressure and temperature [44].

2.1.2 Electrocatalysis and applied potential

The observant or knowledgeable reader might have noticed that the y-axis on Figure 2.2 is potential. The work carried out in this thesis is through electrochemical reactions, wherein electricity is used as the driving force to overcome the activation energy needed to enable the desired reaction. This involves the transfer of charges and electrons between two electrically connected but spatially separated electrodes. The flow of electrons in an external circuit connecting the electrodes is generated via two coupled half-cell reactions, taking place at the electrode/electrolyte interface. On one electrode, an oxidation reaction will generate electrons and oxidized species due to a reactant being oxidized ($R \rightarrow O + ne^-$). Oppositely, on the other electrode, a reduction reaction occurs, where the electrons can reduce an oxidized species ($O + ne^- \rightarrow R$). The combination of both is called a redox reaction (reduction-oxidation), and the electrode where reduction happens is labeled the cathode, while at the anode oxidation occurs

[45]. There must be an equal number of electrons stemming from oxidation and leading to reduction in the system to maintain charge balance. If one reaction is less active, then that will be the limit of charge flow in the system. Furthermore, there must be a corresponding flow of ions through the electrolyte, meaning the electrolyte must be ionically conductive.

Since we just went over why energy is needed to overcome the barrier for reaction, and we are now talking about electrons and current flow, this naturally leads to the main parameter for electrochemical reactions, namely potential. Instead of pressure and temperature mentioned earlier, electric potential is what drives an electrochemical reaction. Temperature and pressure can of course still be used (and will throughout this thesis), but the additional parameter of applied potential at our electrode surface to drive the reaction is what defines electrocatalysis.

The link between the difference in Gibbs free energy and a reversible electrochemical process at constant temperature and pressure is defined as follows:

$$\Delta G = -z F U_{cell} \quad (2.1)$$

where z is the number of electrons transferred in the reaction, F is Faraday's constant, and U_{cell} is the cell potential. The reversible cell potential defines the point where reactions run forwards and backwards at the exact same rate, also defined as the open circuit potential (OCP) [46]. When applying a potential to an electrode, the electron energy level is correspondingly changed. If the energy level of the electron at the electrode is higher than an unoccupied molecular orbital in the reacting molecule, a reduction reaction occurs. Oppositely, electrons can be transferred to the electrode from the molecule, if the electron energy level at the electrode is lower than an occupied molecular orbital, resulting in oxidation of the molecule [45]. The applied potential at an electrode surface can therefore determine which reactions are possible. To tilt the balance towards either reduction or oxidation, one has to correspondingly increase or decrease the cell potential to make one of the reactions favorable. Though it is important to keep in mind that despite one reaction being thermodynamically favorable, it does not affect the rate. The reaction could still be favorable, but run on a time-scale of the lifetime of the universe. One therefore typically needs extra potential to overcome these kinetic limitations, referred to as overpotential. A good catalyst will lower this overpotential, thereby increasing the reaction rate. Consider Figure 2.2 again, which shows the nitrogen reduction reaction (NRR) and the competing hydrogen evolution reaction (HER) [41]. Both are reduction reactions wherein protons and electrons form a product (either NH_3 or H_2). But it can be seen that for a Pt (111) surface, very little overpotential needs to be applied to enable HER. However, on the same Pt electrode, one would need to apply at least -2.0 V for NRR to occur. This is why the top of

the volcano plot is the ideal catalyst for a given reaction, as it leads to the lowest overpotential required to run the desired reaction.

2.1.3 Defining the potential scale

To do electrochemistry, one needs to simultaneously run the reduction and oxidation reactions on two separate electrodes. This means a total cell voltage can be measured between the two electrodes submerged in electrolyte, but typically one would like to know the potential at the surface of one (or both) of the electrodes, as the applied potential is what drives the reaction. It is defined that the $2\text{H}^+ + 2\text{e}^- \rightleftharpoons \text{H}_2$ reaction using a Pt electrode in 1 atm H_2 and with a a_{H^+} hydrogen activity of 1 is the zero point, and all other reactions can be referenced in comparison to this standard hydrogen electrode (SHE) [45]. But this is for a pH of 0, which is not very useful for most experimental systems. Instead one can use the reversible hydrogen potential (RHE), which is the potential of the Pt electrode independent of pH, meaning a_{H^+} varies depending on the pH, but the measured potential does not vary, connecting the two scales:

$$E_{\text{RHE}} = E_{\text{SHE}} - 0.059 \cdot \text{pH} \quad (2.2)$$

For aqueous experiments, I will use RHE as the potential scale. The potential scale for non-aqueous electrolytes are slightly trickier to define, as the proton concentration is limited. Instead, as all work is done with Li deposition, the scale used is *vs* the reaction $\text{Li}^+ + \text{e}^- \rightleftharpoons \text{Li}_{(\text{s})}$, which has the reversible potential -3.04 V *vs* SHE at 1 atm and 25 °C with a_{Li^+} of 1.

2.2 Reduction of nitrogen

2.2.1 The Haber-Bosch process

Ammonia production by the Haber-Bosch process currently exceeds 172 Mt per year [47]. N_2 is held together by a triple bond, one of the strongest bonds in nature. It is therefore very unreactive, as the triple bond dissociation energy is 946 kJ/mol [48]. Catalysis is therefore required to lower the needed energy for bond dissociation in the Haber-Bosch process. The most common catalyst used in the Haber-Bosch process is a triple promoted iron-based catalyst (promoted with potassium oxide, alumina, and calcium oxide) [49], but more expensive catalysts, such as ruthenium on magnesia [50] also work well.

The reaction for ammonia synthesis runs according to:



This is an exothermic reaction, so heat is produced when the reaction runs towards ammonia. At room temperature and atmospheric pressure, ammonia is actually favored, but the reaction rate is immeasurably low. The equilibrium constant for the reaction at 1 atm is 1 around 150-200 °C, and quickly decreases above that temperature according to the van't Hoff equation. Unfortunately the iron-based catalyst needs ~400 °C to work well, which would decrease the equilibrium constant down to $\sim 10^{-4}$ [51]. What Fritz Haber realized was that increasing the pressure would affect the reaction rate, as it would shift the equilibrium relationship more favorably towards ammonia. This is due to Le Châtelier's principle, which states that increasing the pressure will shift the equilibrium of the reaction towards the side with fewer molecules in the gaseous state to counteract the applied change. Haber-Bosch plants are today operated at 150-250 bar and 400-450 °C [16]. As pressure is a precious commodity, requiring strengthened valves, pipes, etc. and an increased safety system, the Haber-Bosch process runs in immense centralized plants, from which the ammonia (and thereby fertilizer) can be distributed across countries and even continents.

2.2.2 Electrochemical nitrogen reduction and the competing reaction

Electrochemical nitrogen reduction on the other hand occur through a redox reaction:



where equation 2.4 is the NRR, and equation 2.5 is called hydrogen oxidation reaction (HOR), and occurs on the anode. This is the reaction that supplies the protons and electrons needed in NRR to form ammonia. These protons and electrons can also undergo HER on the cathode:



Unfortunately, as the overpotential for HER is significantly less than NRR, this reaction is much more likely to occur. Looking back to Figure 2.2, it is seen that for all catalysts plotted, HER will preferentially take place over NRR, since HER has less overpotential compared to NRR.

Aqueous electrochemical nitrogen reduction

In an aqueous electrolyte, the protons and electrons are supplied by the oxygen evolution reaction (OER) through water splitting rather than HOR:



which can, in combination with NRR, produce ammonia from N_2 and H_2O , as seen in Figure 2.3. This would be preferred, as supplying H_2 is more difficult compared to H_2O .

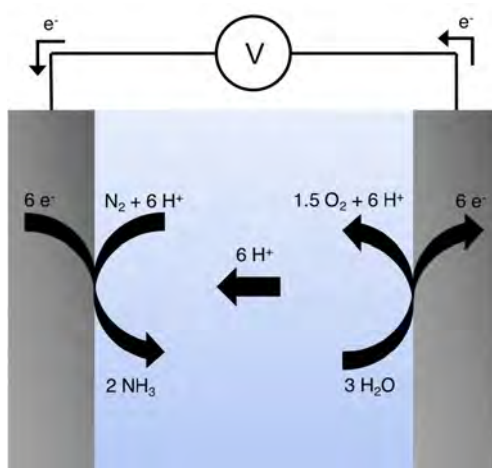


Figure 2.3 Schematic over aqueous electrochemical cell synthesizing ammonia from H_2O and N_2 . Courtesy of Kevin Krempf, and reprinted from Reference [52].

We would expect the aqueous system to run through a reaction pathway where the nitrogen is adsorbed onto the catalyst surface, protonated by the proton source in the electrolyte, thereby forming ammonia, and then desorbing from the catalyst. This can occur through either an alternating or distal route. In the alternating route, each of the N in the adsorbed N_2 molecule will alternately be protonated, while in the distal pathway, one N is fully protonated and dissociates, whereafter the other N is protonated and desorbs from the surface [32].

The lithium-mediated electrochemical process

For the non-aqueous system, the process is a little unusual. The hypothesized pathway for ammonia synthesis is *via* Li reduction of Li ions in the electrolyte, plating onto the surface of the cathode. Li metal is extremely reactive due to the single electron in the 2s orbital, which will easily be donated to create bonds and form Li compounds. This high reactivity is enough

to split the strong triple bond and dissociate the nitrogen molecule, forming a lithium nitride, Li_3N [53]. This reaction is a downhill chemical reaction at room temperature, and will therefore spontaneously occur when a nitrogen molecule impinges upon the freshly plated metallic Li surface. A proton source which impinges upon the Li_3N will protonate it, which is also a downhill reaction that spontaneously occurs, and after three protonations, NH_3 is formed and desorbs. This is the most accepted route of ammonia synthesis in the lithium-mediated literature [54, 55], and the steps are schematically shown in Figure 2.4.

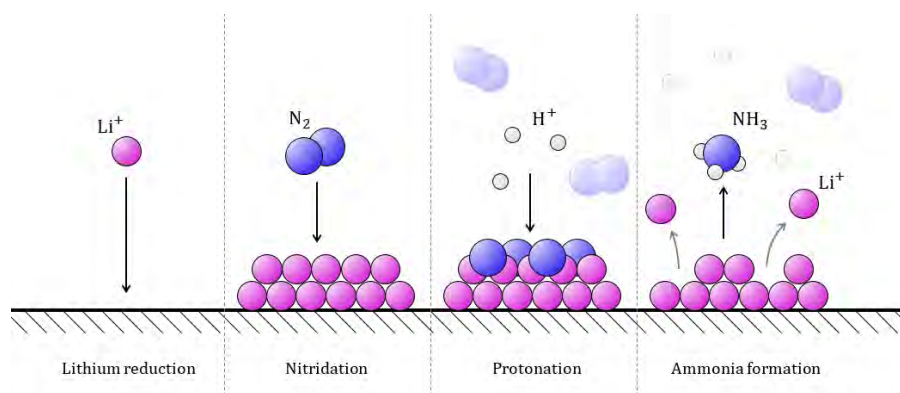


Figure 2.4 Schematic drawing of the lithium-mediated process. Courtesy of Jakob B. Pedersen.

Formation of the nitride is not the only reaction possible at the surface. If a proton source impinges upon the reduced Li, a LiH is expected to form, which leads to hydrogen evolution: the main competing reaction. Furthermore, micro-kinetic modelling of the surface (carried out by the talented Michael Statt and Dr. Vanessa Bukas) suggests that the most stable Li species on our surface is a lithium amide, LiNH_2 , under our reaction conditions. This species forms when sufficient amounts of ammonia have formed *via* the Li_3N route, and thereafter impinges upon the reduced Li surface, forming a stable amide. This amide can form ammonia again, if a proton impinges upon it. The various pathways are shown in Figure 2.5. I will get back to this in more detail in Section 7.4, which covers Paper IV.

Another controversial, well studied, but not very well understood phenomenon that affects the lithium-mediated system, is the solid electrolyte interface (SEI) layer. It is a passivation layer that forms on the electrode in the first sweep towards reducing potentials, consisting of decomposition products of the electrolyte [56]. It is claimed that the SEI layer consists of a multi-layered structure with an inorganic inner layer made of compounds like Li_2CO_3 and Li_2O [57, 58] and an outer layer of an organic compound ROLi , where R depends on the solvent [59]. The outer SEI layer is heterogeneous, porous, and permeable. It allows for the passage of Li

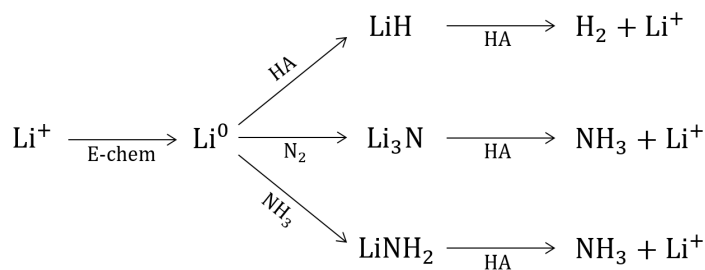


Figure 2.5 Expected reactions for the lithium-mediated process. HA is the proton source, while N_2 leads to nitridation of the Li. Reactions are not balanced.

ions while blocking the passage of electrons to prevent further electrolyte breakdown [60]. N_2 and the proton source must diffuse through this layer in order to react with the reduced Li on the surface of the WE. However, most of the battery literature wherein SEI layer formation is discussed is highly controversial and varies greatly between electrolytes and different additives. Much of the literature uses organic carbonates as solvents, whereas we use an ethereal solvent, which will affect the SEI layer differently [61]. Furthermore we also have protons present, whereas battery literature typically uses aprotic solutions. It is therefore not possible to directly compare our results to the battery literature, making any conclusions we can draw regarding the SEI layer speculative at best.

2.3 Aims of this dissertation

When starting this project, my group had already spent over a decade trying to synthesize ammonia. Despite much of the literature claiming successful ammonia synthesis, my earlier colleagues had neither managed to make any ammonia, nor reproduce any published results from the field, despite numerous claims of successful nitrogen reduction. My only goal was therefore to unquestionably reduce nitrogen electrochemically in any way possible. I have stumbled a lot along the way, and learned by many of my wrong turns. I have also realized that many other people in this field are quite lost, either without knowing it, or potentially purposefully (I'd like to believe it is the former, but I'm also an optimist at heart). In this work, I therefore aim at actually succeeding in nitrogen reduction, and at both improving my own understanding of electrochemistry, and helping others realize the pitfalls of this field.

Specifically, I list the aims in the following:

1. What are the pitfalls in electrochemical nitrogen reduction? How should I (and others) do proper nitrogen reduction experiments, and why can so many things lead to false positives? This is covered in Chapter 4.
2. Can I successfully reproduce any result from the literature? This is split into aqueous and non-aqueous literature, respectively covered in Chapter 5 and 6.
3. If I manage to make ammonia, can I improve the efficiency? Do I understand which reaction mechanism is used, and what is even happening? This will be addressed in Chapter 7.
4. And what can any of this be used for? Did I waste 3 years of my life? The thrilling conclusion will be revealed in Chapter 8.

Chapter 3

Experimental Methods

"We demand rigidly defined areas of doubt and uncertainty!"

— Douglas Adams, *The Hitchhiker's Guide to the Galaxy*

Throughout this work, I have utilized various different methods depending on the condition of the experiment. Different techniques have been used for both *in-situ* and *ex-situ* electrode characterization, and I have tweaked two well-known methods for ammonia detection. This chapter covers the theoretical background of the techniques utilized, as well as a methods description. It is split into three parts; electrochemical experimentation, ammonia quantification, and electrode characterization.

3.1 Electrochemical experimentation

The primary goal of this thesis is electrochemical nitrogen reduction. Because of the rather broad scope of that challenge, many different methods from the literature were attempted. If successful, low initial concentrations of ammonia would be expected based on published work in the field. This unfortunately makes the process of determining success very difficult, as ammonia is ubiquitous to the environment in small concentrations. Great care was therefore taken to keep the electrochemical set-up clean, as will be described below.

3.1.1 Electrochemical set-up

To carry out electrochemical experiments, either a 2- or 3-electrode setup was used. In the first configuration, a working electrode (WE) and counter electrode (CE) are immersed in

the electrolyte and are electrically connected. The WE is the electrode whereon the reaction of interest takes place, in this case the cathode where nitrogen reduction occurs. The CE, also called the anode in this case, runs the counter reaction generating the electrons needed, stemming from the oxidation reaction.

One can either set a desired current or a total cell potential to run a reaction. With only a 2-electrode set-up, the potential measured is the total cell potential between the electrodes, so *e.g.* the WE potential relative to the CE potential. This does not give any information about the absolute potential of the WE relative to a conventional scale. If a reference electrode (RE) with a known stable potential is included, the electrochemical cell becomes a 3-electrode system, wherein no current runs between the RE and the other electrodes. Since the potential of the RE is known and stable, one can determine the potential of the WE (and CE) relative to the known RE potential, and the potential at these electrodes can be correlated to a known potential scale, such as V vs SHE or RHE, introduced in Section 2.1.3.

Aqueous experiments

Throughout this work, borosilicate glass cells were used, where single compartment experiments were carried out with 6.0 mL electrolyte, while the H-cell experiments had 7.5 mL in each compartment. In experiments with gas purging, a P3 glass frit was used for increased gas solubility. All glassware were boiled once or twice as needed in ultrapure water (18.2 M Ω resistivity, Millipore, Synergy UV system), then dried overnight at 100 °C in air.

For aqueous experiments, the electrolyte was made in batches every month. A background sample would always be taken, testing ammonia contamination of the prepared electrolyte, and a new batch would be made if above 10 p.p.b. (see section 3.2 for details). A microporous polypropylene 25 μ m thick Celgard 3401 membrane was used in H-cell measurements, requiring no cleaning, and stored in 0.1 M KOH (99.995 %, Merck Suprapur). Proton-conducting Nafion (Nafion 117, Chemours) was also tested, both as received, and cleaned by boiling for 1 hour in 3 % H₂O₂ (30 %, Merck), then 1 hour in 0.1 M H₂SO₄ (Suprapur, Merck), followed by thorough rinsing in Millipore water to remove excess acid.

A Hg–Hg₂SO₄ reference electrode (SI Analytics) was used, separated in a chamber with a glass frit connected to the chamber containing the WE. The CE was Ir foil (+99.9 %, Goodfellow), and various different WE candidates were tested: Ru (+99.9 %, Goodfellow), Rh (+99.99 %, Goodfellow), Re (+99.99 %, MaTeCK), Au (+99.99 %, Goodfellow), Ni (+99.99 %, Goodfellow), and Fe (+99.9 %, Goodfellow). All foils were polished with polycrystalline diamond paste (Buehler), in order of grain sizes 3 μ m, 1 μ m, and 0.25 μ m, until mirror finish

was achieved, with an ultra-sonication in Millipore water and isopropanol ($\geq 99.8\%$, Merck) between each polishing step.

Non-aqueous experiments

For non-aqueous experiments, a fresh batch of electrolyte was prepared in a glovebox for every experiment. The solvent, tetrahydrofuran (THF, anhydrous, $\geq 99.9\%$, inhibitor-free, Sigma Aldrich), was mixed with a proton-source, typically 1 % ethanol (EtOH, 99.5 %, Extra Dry, AcroSeal or anhydrous, Honeywell) with 0.2 M LiClO₄ (battery grade, dry, 99.99 %, Sigma-Aldrich) unless denoted otherwise. Other salts were also tested: Ba(ClO₄)₂ (Anhydrous, Alfa Aesar), Mg(ClO₄)₂ (Anhydrous, Alfa Aesar), NaClO₄ ($\geq 98\%$, Anhydrous, Alfa Aesar), LiBF₄ ($\geq 98\%$, acid <200 p.p.m., anhydrous, Sigma Aldrich), and LiCF₃SO₃ (99.995 %, Sigma Aldrich).

Various WE candidates were tested: Mo (+99.9 %, Goodfellow), Ag (+99.9 %, Goodfellow), Ti (+99.7 %, Sigma Aldrich), Mg (+99.9 %, Goodfellow), Au (+99.9 %, Goodfellow), Carbon paper (Sigracet 29 BC, Fuel Cell Store), and Graphite rod (High Pure Graphite, Redoxme). All foils were polished with Si-C paper (Buehler, CarbiMet P1200) prior to experiments, and rinsed thoroughly in EtOH. If the foil was re-used, it was first dipped in 2 % HCl (VWR Chemicals) to dissolve any surface species of Li, then rinsed in ultrapure water and EtOH prior to polishing. A Pt mesh (+99.9 %, Goodfellow) was used as the CE. A Pt wire (+99.99 %, Goodfellow) was used as a pseudo-reference electrode. Both of these were flame annealed prior to measurements. The pseudo-reference was experimentally observed to have an error margin of 400 mV, as determined from the Li reduction potential onset (discussed further in Section 6.1.1).

3.1.2 Electrochemical autoclave: "Otto Clive"

Tsuneto et al. [62] reported that increasing pressure in the lithium-mediated system to 10 bar N₂ increases the FE to $\sim 29\%$, while 50 bar leads to an increase up to $\sim 50\%$. Increasing the N₂ pressure of the system will increase the N₂ solubility in the electrolyte according to Henry's law. If that leads to an increase in ammonia, it means that N₂ availability is a limiting factor for the system, which was also shown by Lazouski et al. [55]. To test the validity of this, an electrochemical autoclave was built based on the design by Gustav Wiberg [63]. The design was modified slightly by adding a 100 bar pressure gauge on the lid, as well as a safety relief valve, and included the option to replace the thermocouple with a quadrupole mass spectrometer (QMS) (Pfeiffer, OmniStar GSD 320) connection as needed. The electrochemical glass cell used in this design is 30 mL in electrolyte volume to accommodate the expected increase in

ammonia concentration, and the WE and CE are positioned horizontally, with ~ 0.5 cm distance between them, to allow for magnetic stirring below the WE. The RE is positioned between the anode and cathode. The autoclave (aptly named Otto Clive, and hereafter lovingly referred to as Otto) can be pressurized to 100 bar and heated to 250 °C, however throughout this work, I use only 10 bar.

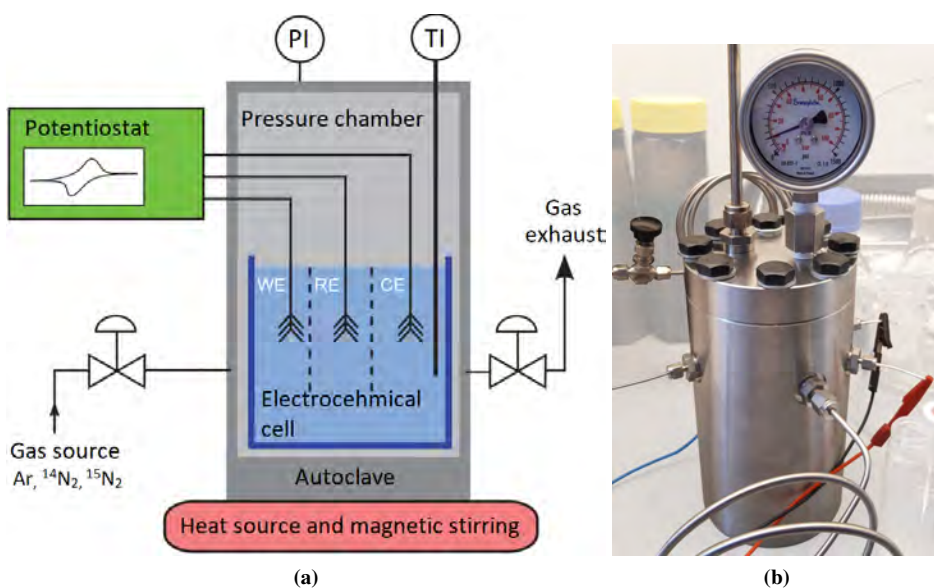


Figure 3.1 a) Schematic of autoclave. Modified and reprinted with permission from reference [63]. Copyright 2014, AIP Publishing. b.) Picture of Otto Clive.

A magnetic stirring bar (VWR, glass covered) cleaned in the same way as the glass cell, is added to the single compartment cell in all Otto experiments. The WE is a 1.8 cm^2 Mo foil and the CE is a Pt mesh placed 0.5 cm apart, with a Pt wire RE. Prior to an electrochemical experiment, Ar (N5.0, Air Liquide) gas is introduced into the empty assembled cell placed in the autoclave for 1 hour. The denser Ar gas can substantially displace the atmospheric N_2 and O_2 in the system, which is measured *via* mass spectrometry (MS). The electrolyte is made in the glovebox, and injected into the Ar atmosphere cell from a septum capped vial to reduce O_2 exposure, and the autoclave is closed. The pressure is increased to 10 bar with either N_2 (N6.0, Air Liquide) or Ar, depending on the intended experiment, and de-pressurized to 3 bar a total of 10 times. This pumping/evacuation procedure is done to flush out any remaining atmospheric contaminants. Even assuming a 20 % O_2 atmosphere at 1 bar when starting (which is not the

case as the Ar will displace most of the air), the O_2 concentration would only be ~ 0.4 p.p.m. after this procedure ¹.

Quadrupole Mass Spectrometer (QMS)

As the name implies, a QMS consists of four metal rods in a perfectly parallel configuration. Each opposite rod is electrically connected, and each set is applied with a radio frequency (RF) voltage, superposed on a direct current (DC) offset voltage, seen in Figure 3.2. The sample gas can be ionized by *e.g.* electron bombardment from a filament. When these ions enter the center of the QMS, they are subjected to a total electric field that consists of a quadrupolar alternating field, since the sets of rods will have opposite charge. When a positive ion enters this field, it will be drawn towards the negative rod. If the rod changes charge before the ion collides and discharges, it will propel the ion in a new direction [64]. The velocity will depend on the mass to charge ratio, m/z , of the ion, which can lead to a path down the center of the rods.

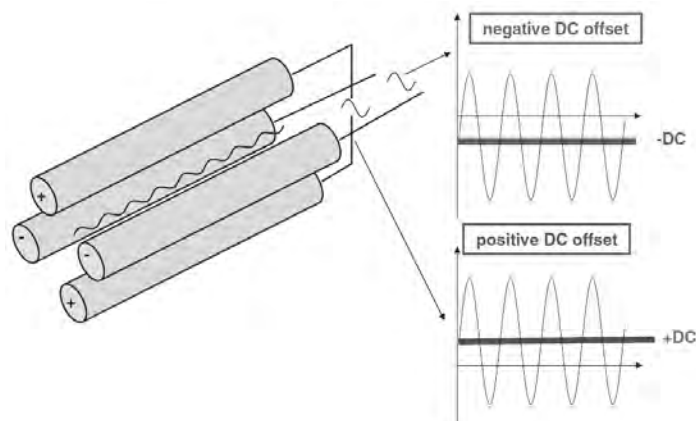


Figure 3.2 Schematic of QMS quadrupole, with voltage profile on the rods. Printed with permission from Reference [65]. Copyright 2008 Elsevier B.V.

By applying specified alternating current (AC) and DC voltages to the rods, one can create a band filter that only allows for the passage of a certain m/z through the rods. The detector at the end of the rods then detect only ions with the specified m/z . By varying the absolute values of the voltages, a mass spectrum across all the m/z values can be acquired, allowing for the detection of a variety of compounds, as each has a unique mass spectrum. The advantage of QMS over other mass spectrometers, is the low vacuum required ($\sim 10^{-7}$ mbar), and fast and

¹Start with $\sim 20\%$ O_2 , and add gas up to 10 bar: $20\%/10 = 0.02$. Then evacuate down to 3 bar, and add gas up to 10 bar, repeated 9 times: $0.02 \cdot \left(\frac{3}{10}\right)^9 = 0.4$ p.p.m.

simple operation. However, they have a low resolution and transmittance (compared to *e.g.* a sector MS) [65].

3.1.3 Electrochemical methods

Herein is a description of the various electrochemical techniques used. Full understanding of the inner workings of the potentiostat (Bio-Logic VMP2 and SP-300) is beyond the scope of this thesis, and the techniques will therefore only be explained in general terms.

Electrochemical impedance spectroscopy (EIS)

When it is needed to determine how resistant an electrochemical system is to the flow of electrical current, the electrical resistance for the direct current (DC) case does not suffice. Instead, one can use its generalized version for alternating current (AC) called impedance, wherein the response of the system is variable with frequency [66]. By applying a small perturbation to the system, *e.g.* a small AC potential (or current) and measuring the phase dilated current (or potential) response, one obtains much information about the types of processes happening in the system [67]. Conduction through different processes, such as Ohmic resistance across the system versus charge transfer resistance of reactions, respond differently at different applied frequencies in potential, as the time-scale for the electrical conduction in each process adapts differently. In the first case, one needs the high frequency response, while the latter case is prominent at lower frequencies.

One can, by the use of equivalent circuit diagrams with resistors, capacitors, inductors, etc., model the impedance of an electrochemical cell to elucidate which processes are happening in the system. However, this requires a much deeper understanding of the system than what is needed for this thesis. I have only used the high frequency response to determine the Ohmic resistance in my electrochemical systems, as shown in an example spectra in Figure 3.3.

Ohmic IR-drop compensation

As the electrolyte has Ohmic resistance, the potential measured for the WE by the potentiostat in the 3-electrode system needs to be corrected [69]. Using potentiostatic (P)EIS, the Ohmic resistance, R , can be determined, and the measured WE potential can be corrected to the actual potential at the surface of the electrode using the current, I , according to [45]:

$$U_{measured} = U_{actual} - IR \quad (3.1)$$

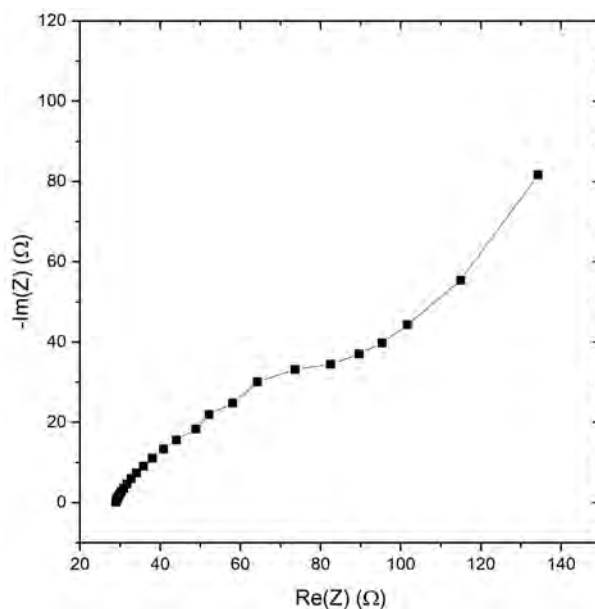


Figure 3.3 Example data of a Nyquist plot [68], showing the real and imaginary part of the impedance along respectively the x- and y-axis. The Ohmic resistance can be determined from the high frequency part (left of graph), where it crosses the x-axis, in this case at 29 Ω .

where the current is negative, due to the reaction at the surface. So an increase in R , *e.g.* by moving the CE and WE further apart, leads to an increase in $U_{measured}$.

There is a "manual IR compensation" technique in the EC-Lab software (Bio-Logic, V11.27), which can compensate for 85 % of the Ohmic drop. The remaining 15 % must be manually compensated, as a full (or over-) compensation would lead to positive feedback loops in the instrumentation, causing oscillations and instability in the measurements. For energy calculations (see Equation 3.3), the uncorrected potential was used, to determine the total energy input into the system by the potentiostat.

Linear sweep voltametry (LSV)

For some measurements, an initial linear sweep was used to ramp up to the desired WE potential. This was partially to determine the Li reduction onset in the non-aqueous system, as the RE had a bit of drift in the non-aqueous system (more on that in Section 6.1.1), and to prevent the potentiostat from overloading if switching suddenly to high currents or potentials in the aqueous system.

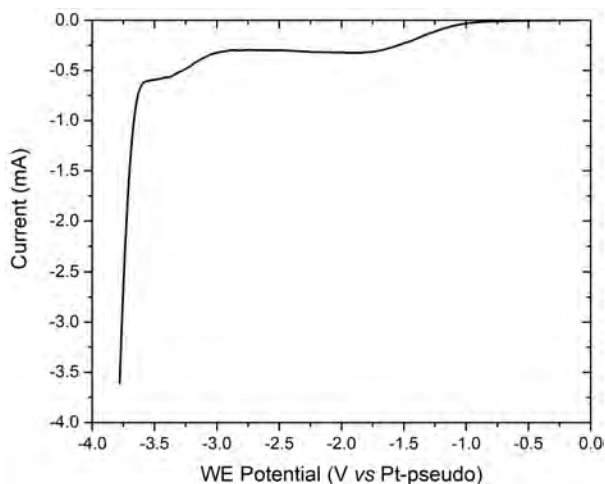


Figure 3.4 Example data of a LSV plot. The WE potential is plotted vs the Pt-pseudo RE. The Li reduction potential can be determined from this graph as occurring around -3.6 V based on the exponential onset of Li reduction, and the potential scale can be changed accordingly to the Li/Li⁺ scale.

Furthermore, LSV can show if there are unexpected amounts of H₂O or O₂ contamination, as the current would show a peak at a less negative potential. It is seen in Figure 3.4 that something is reduced at around -1.5 V and again at -3.1 V vs Pt-pseudo RE (corresponding to around +2.1 and +0.5 vs Li/Li⁺ respectively). These peaks might be ascribed to O₂ and H₂O, respectively [70], and a cleaning of the THF and EtOH with *e.g.* molecular sieves could improve this.

Chronoamperometry (CA) and chronopotentiometry (CP)

Chronoamperometry, as the name implies, measures the current over time. For this technique, a constant potential, either as total cell potential in the 2-electrode system, or a potential of the WE in the 3-electrode system, is applied, and the current adjusts accordingly, and is measured as a function of time. Oppositely, in chronopotentiometry, the current is set between the WE and CE, and the potential response of the system as a function of time is measured [45].

I used both techniques, depending on whether I needed control over the current passed in the system, or needed a set WE or cell potential. Another important measure, the total charge passed, Q , can be inferred by integrating the current over time throughout the entire experiment. For ease of data visibility, I will plot this value as a second y-axis, seen in the example Figure 3.5. The WE potential will always be blue, the CE potential green, the current density will be

red, and the total charge passed will be black (and stylistically chosen to be plotted as negative because the current is negative).

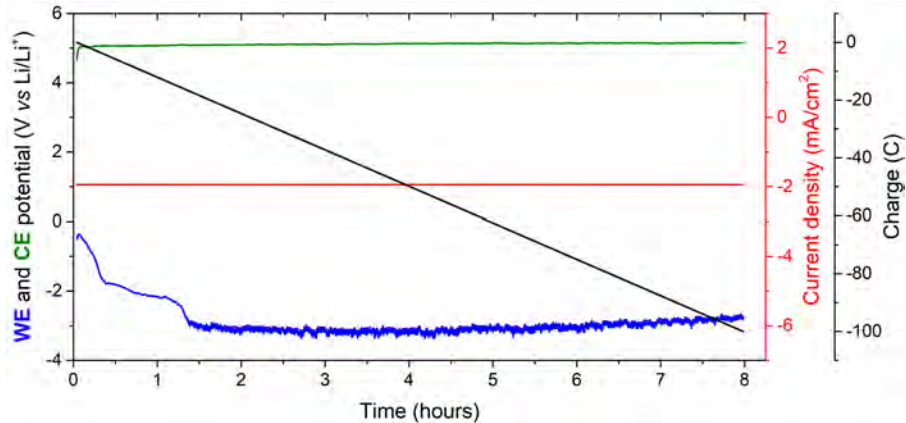


Figure 3.5 Example data of a CP plot. WE (blue) and CE (green) potential are plotted on the left y-axis, while current density (red) and charge (black) are plotted on separate y-axes on the right.

I use these techniques for testing nitrogen reduction. From the data, I can calculate two important parameters: the Faradaic efficiency (FE) and the energy efficiency, η . The FE is a measure of how much of the total passed charge directly makes a certain desired product. This is calculated via Faraday's law of electrolysis and given by:

$$FE = \frac{z \cdot F \cdot n}{Q} \cdot 100\% \quad (3.2)$$

where z is the moles of electrons transferred per mole of product, F is Faraday's constant, and n is moles of product. In my case, z is 3 for the transferred electrons, n is measured from the concentration of ammonia after the experiment, and Q is controlled by the CA or CP experiment parameters. Ideally, we want 100 % FE towards ammonia synthesis, but realistically HER is a competing side reaction, which will throughout this thesis, and in all the literature, dominate.

The energy efficiency is calculated by:

$$\eta = \frac{E_{out}}{E_{in}} \quad (3.3)$$

where the total energy put into the system by the potentiostat, E_{in} , is given by

$$E_{in} = \int \{U_{CE}(t) - U_{WE}(t)\} \cdot I(t) dt \quad (3.4)$$

as determined from the CA or CP measurement. It is important not to use the manual Ohmic drop correction for the energy efficiency calculation, otherwise the calculated energy efficiency will be over-estimated. The total energy which can be gained from the ammonia produced, E_{out} , is defined via the free energy of the reaction, ΔG_R . This can be calculated from the specific free energy of the reaction from ammonia oxidation to N_2 and H_2O , δg_R , multiplied with the amount of ammonia produced, m_{NH_3} :

$$E_{out} = \Delta G_R = \delta g_R \cdot m_{NH_3} \quad (3.5)$$

The energy efficiency was only calculated for experiments in the autoclave, as the FE was high enough to warrant the need for energy efficiency calculations.

3.2 Ammonia quantification

There are many different methods of determining ammonia concentration. For the purposes of this thesis, a modified version of the Berthelot method was used for everyday experiments [71]. This method can accurately determine the amount of ammonia in a given sample, but the measured result can be misleading, due to various possible sources of ammonia contamination. Since the method is so sensitive, measuring down to sub-p.p.m. levels with high accuracy, uncertainty from ubiquitous ammonia in the environment is significantly higher. As the colorimetric method cannot distinguish the origin of the ammonia measured, proper verification experiments with a quantitative isotope sensitive method must therefore also be used.

3.2.1 The indophenol method

The indophenol method, also known as the Berthelot method from its inventor, utilizes a chemical reaction between ammonia and a phenol. Under a suitably oxidizing environment, the reaction yields a blue indophenol dye that absorbs light very strongly around 630 nm, which can be used to quantify the initial ammonia concentration in the solution, even down to sub-p.p.m. levels [72].

Throughout this work, several calibration curves have been made for different measurement conditions. In aqueous electrolytes, a pre-determined concentration of NH_4Cl (99.8 %, Merck) was added to the 0.1 M KOH electrolyte, and neutralized with 0.5 M H_2SO_4 (Suprapur, Merck) to ~ 7 pH. A 2 mL aliquot of the sample was transferred to a cuvette, and 0.5 mL alkaline hypochlorite solution (A1727, Sigma-Aldrich) was added, which will form a monochloramine when reacting with ammonia. Another 0.5 mL phenol nitroprusside solution (P6994, Sigma-

Aldrich) is added, which will form a benzoquinonechlorimine. This reaction is accelerated by the addition of the coupling agent sodium nitroprusside, which affects the accuracy and reproducibility of the reaction. The benzoquinonechlorimine will subsequently react with another phenol to form the final indophenol dye, with a beautiful (and measurable) blue color [73]. Once the two reagents are added, the cuvette is vigorously shaken and left in the dark at room temperature for 30 minutes to develop.

The blue color comes from the intrinsic ability of energy absorption and emission in a molecule in the form of photons. This happens *via* a change of quantum state in the molecule, such as the excitation of an electron from a lower energy state into a higher energy state, which leads to absorption of the incoming photon if the energy of the photon corresponds to the energy needed to kick the electron to the higher state. The indophenol dye absorbs light particularly well in the range of 630 nm to 720 nm [72], which gives it the blue color, as the photon energy, E_{photon} is related to wavelength, λ , via the following equation:

$$E_{\text{photon}} = \frac{h \cdot c}{\lambda} \quad (3.6)$$

where h is Planck's constant, and c is the speed of light. One can measure the amount of indophenol, and thereby the amount of ammonia, by quantifying how much light is absorbed through the medium. This relation is derived from the Beer-Lambert law [74]:

$$A_{\lambda} = \log_{10} \frac{I_0}{I_1} = \epsilon \cdot C \cdot L \quad (3.7)$$

where A_{λ} is the measured absorbance, I_0 is the incident light intensity at a specific wavelength, and I_1 is the transmitted intensity at that wavelength. The absorbance is also equal to the product of the concentration of the absorbing species, C , the path length of the photon through the medium, L , and the extinction coefficient of the medium, ϵ , which is constant for each absorbing species at a set temperature and pressure. One should be aware that the linearity of the Beer-Lambert law only holds for low concentrations [75].

An ultraviolet-visible (UV/Vis) spectrometer (UV-2600, Shimadzu) can generate light with a known intensity and specified wavelength using a monochromator. As the light is passed through the sample, the transmitted light is measured with a photodiode, and the absorbance as a function of wavelength is determined. Since the concentration linearly depends on the absorption, one can determine the amount of ammonia in the sample by the use of a calibration curve with a known concentration of ammonia. Nitrite and hydrazine detection kits were also used, which utilizes a similar reaction and method. The step by step procedure for these is covered in the Methods section of Paper I, in Appendix B.

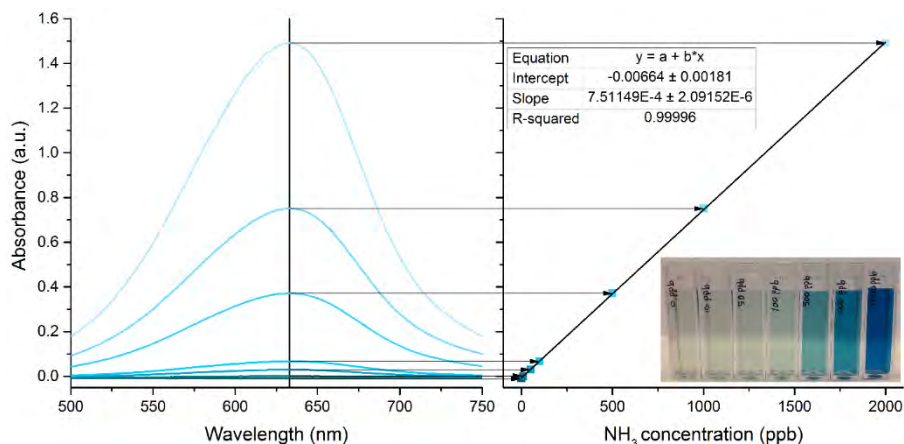


Figure 3.6 Calibration curve for the Berthelot reaction used for colorimetric quantification of NH₃ in aqueous solution. Inset with visible increasing blue colors for increasing concentrations of ammonia.

For indophenol in aqueous solutions, we investigated the range 400-800 nm. By varying the initial concentration of NH₄Cl, a calibration was created, as shown in Figure 3.6, based on the absorbance peak at 630 nm. To ensure a proper calibration curve, this was repeated occasionally by others on the project, and the curves were compared, to ensure that someone's mistake in *e.g.* weighing out the initial NH₄Cl did not lead us to falsely measure higher ammonia concentrations in our samples. It happened once, and no one is infallible (especially not a physicist trying to do chemistry), so it is good practice to make at least two calibration curves independently, and re-do the calibration curves every few months to account for changes in the UV/vis instrument. It is also imperative to make a blank measurement of the electrolyte for every experiment, as this ensures no major contamination of the chemicals.

For the non-aqueous electrolyte, the indophenol method had to be slightly modified, as we empirically saw that THF would interfere with the reagents, decreasing the absorption peak. The NH₄Cl was dissolved in anhydrous EtOH, as it was not soluble in THF at the needed concentrations, which was diluted with the proper ratio into our electrolyte (typically 0.2 M LiClO₄ in 1 % EtOH/99 % THF), and a 0.5 mL aliquot was taken. 10 μ L of 4 M HCl (37 %, VWR Chemicals) was added to this, similar to the experiment samples, and the solution was dried in a water bath at 61 °C for 40 minutes. This will evaporate the THF and EtOH, while leaving the ammonia as ammonium chloride salt. The salt can then be dissolved in 2 mL of Milli-Q water, and the indophenol reagents can be added, as described above.

Typically most work in the literature uses the peak-based absorbance spectrum to determine ammonia concentration, shown in Figure 3.7a as Method-I. It does not appear to be an issue

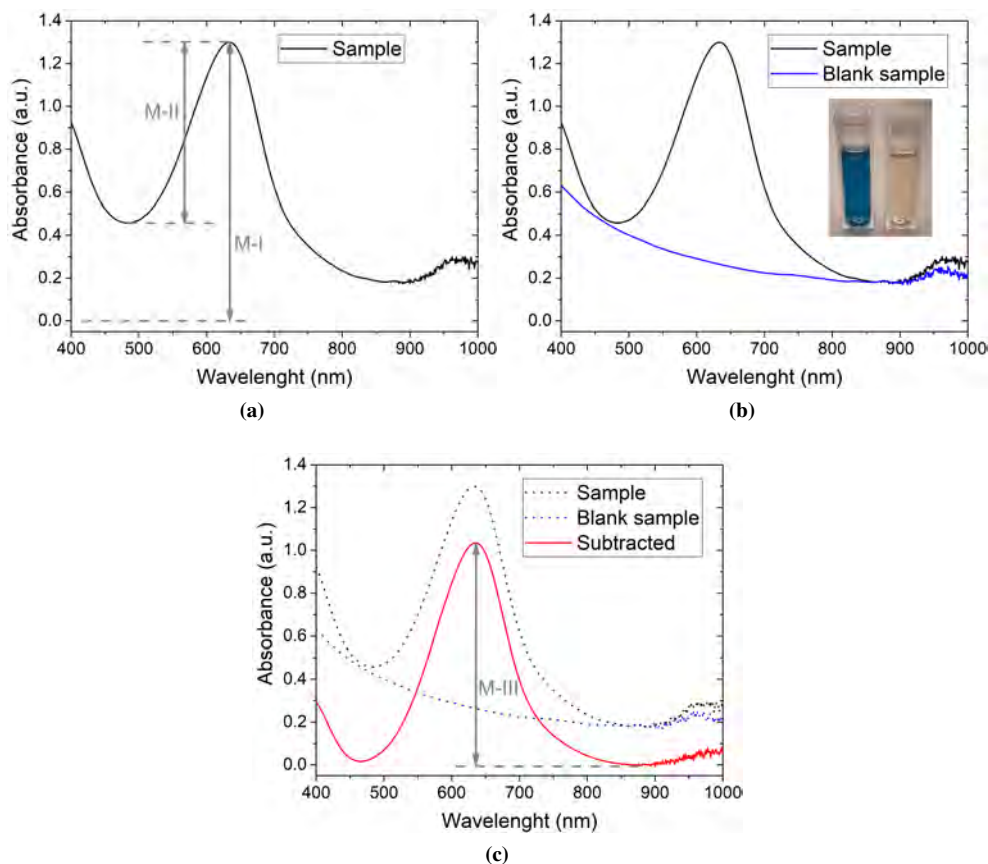


Figure 3.7 a) UV/Vis spectrum of a non-aqueous sample, with noticeable asymmetry of peak. Most papers use method-I to determine ammonia concentration, with a single paper suggesting method-II. b) UV/Vis spectrum of background electrolyte without added indophenol reagents. The background electrolyte is tinged yellow due to solvent decomposition, which raises the low wavelength absorbance peaks. c) Spectrum with subtracted background. Method-III is used in this work to calculate ammonia concentration.

in aqueous electrolyte, but many non-aqueous electrolytes, particularly THF, seem to slowly become tinged yellow over time, probably due to solvent breakdown. This leads to an increased absorbance in the lower wavelength region, which falsely increases the absorbance spectra of the indophenol sample. Most reports in the literature simply use the peak value of the indophenol spectra to determine ammonia concentration, which gives a falsely high value due to this up-shift. In the case shown in Figure 3.7a, the measured concentration based on this method, would lead to a FE of 4.9%. Method-II was proposed by [55], wherein a peak to trough value is

used instead. While this is much more accurate, it actually underestimates the concentration in our case, giving a FE of 3.5 %. This is due to the yellow color of the post-measurement electrolyte, which gives an up-shift of the lower wavelengths, thereby increasing the trough absorbance for our samples, seen in Figure 3.7b. Instead, if the background of the electrolyte without any added indophenol reagents is subtracted, we get a much more symmetric peak. Now the peak to trough can more accurately be used, defined as Method-III, giving an accurate ammonia concentration of our sample, and leading to the FE of 4.0 % in the example spectra shown in Figure 3.7c.

3.2.2 Nuclear magnetic resonance (NMR)

NMR is a technique that relies on the magnetic properties of nuclei. All nuclei that have a non-zero spin, $|\vec{S}| > 0$, will also have a non-zero magnetic dipole moment, $\vec{\mu} \propto -\vec{S}$. When such a nucleus is exposed to a strong magnetic field, \vec{B}_0 , the nuclear magnetic moment will align either parallel or antiparallel to the field, acquiring polarization. A weak oscillating perpendicular electromagnetic pulse is then applied, referred to as a RF pulse. Because of the Heisenberg uncertainty principle, each nucleus will exhibit Larmor precession about an external magnetic field. This occurs at a set resonance frequency, which, if matched with the RF pulse, will force the magnetic moments into a perpendicular plane to \vec{B}_0 . Each nucleus will be shielded slightly differently due to the surrounding nuclei and electrons from the chemical environment of the molecular structure. The RF pulse required to change the alignment of each nucleus will therefore vary depending on the strength of B_0 , the chemical bonds, and other atoms around the nucleus of interest. The frequency difference is typically on the order of p.p.m. of the basic resonance frequency, and leads to a characteristic shift in the spectra as well.

Once the magnetic moment is in the perpendicular plane, it precesses in this plane with a frequency dependent on B_0 , the type of nuclei, and the nuclei's chemical bonds in the molecule. This can all be used to determine the composition of the molecule by using a NMR spectrometer, which is essentially a coil with the sample inside, wherein the precession induces an AC current. Over time, the precession will gradually start aligning with B_0 again, which causes the amplitude of the AC signal to decrease. The time scale of this shift also contains information about the nuclei. Additionally, the spin alignment of the surrounding atoms influences the excitation pulse, resulting in splitting of the signal depending on the number of neighboring spins. Fourier-transform of the signal from all these excited nuclei creates the NMR spectrum we are familiar with, wherein the composition of the sample can be determined based on the characteristic frequencies for each molecule. Furthermore, one can use NMR to determine the

concentration, as the area of the signal is directly proportional with the total amount of nuclei affected by the RF pulse [76].

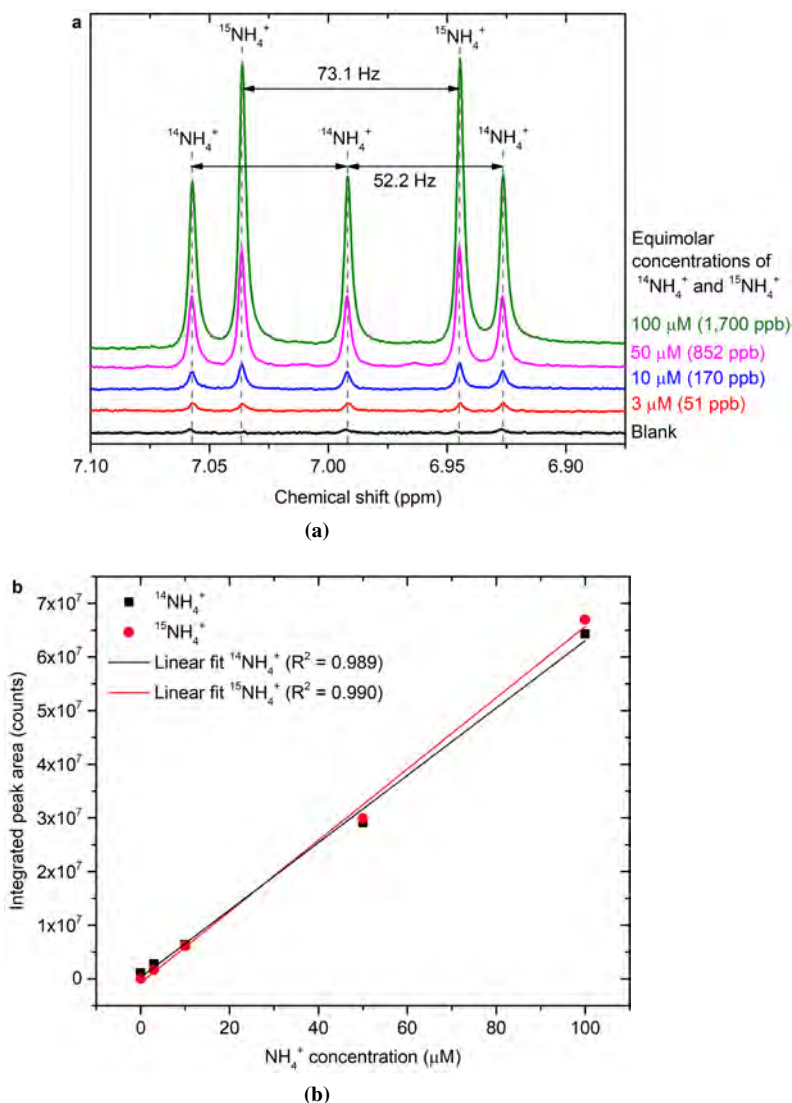


Figure 3.8 a) NMR spectra of 0.1 M KOH solutions containing equal concentrations of $^{14}\text{NH}_4^+$ and $^{15}\text{NH}_4^+$ from NH_4Cl . The solution is acidified with 0.5 M H_2SO_4 to a pH of 1, and CH_3OH was used as an internal reference. b) Integrated signal peak areas for both $^{14}\text{NH}_4^+$ and $^{15}\text{NH}_4^+$ as a function of the added ammonia concentration.

For isotopically sensitive ammonia detection, ^1H NMR can be used to differentiate isotopes of ammonia. Because ^{14}N has spin 1, while ^{15}N has spin 1/2, the scalar interaction of ^1H with the former causes a triplet splitting with 52 Hz as a characteristic spacing, while the latter causes a doublet splitting of 73 Hz. These peaks are distinguishable and easily identifiable, as seen in the calibration for NMR data shown in Figure 3.8. Spectra were acquired using a Bruker AVANCE III HD 800 MHz spectrometer equipped with a 5 mm TCI CryoProbe. The high $B_0 = 18.8$ T magnetic field in combination with a cryo-cooled NMR probe makes the signal accurately quantifiable down to 50 p.p.b., and even distinguishable for concentrations as low as 10 p.p.b. One does not necessarily need an 800 MHz NMR system, as we could also get a 50 p.p.b. resolution with a 400 MHz NMR, however all spectra for this thesis were recorded with the better 800 MHz system. Because the concentration of the solvent, whether it was aqueous or THF, is many orders of magnitude higher than the ammonia, the signal from the solvent would dominate. To account for this, an RF-pulse with the resonance frequency of the solvent can be applied first, before the multi-frequency pulse used for probing basically everything else. This technique was used for signal suppression of water, while a slightly more complicated version of this was used for THF suppression [77, 78].

3.3 Electrode characterization

The electrodes were characterized *ex-situ* with several different techniques, some surface sensitive, others useful for bulk crystalline thin films. The electrodes were measured both before (plain polished metal foil) and after electrochemistry. In the case of the lithium-mediated process, *ex-situ* characterization has limited overlap with *in-situ* processes, as the surface composition will vastly change upon air exposure.

3.3.1 X-ray Diffraction (XRD)

X-Ray Diffraction (XRD) is used to determine the composition of a bulk crystalline material *via* the crystal structure of said solid. One can probe the lattice structure of a material with X-rays, as the wavelength is comparable to the lattice distances in the crystalline structure. Each arrayed crystalline atoms will elastically scatter the incoming X-rays in a spherical wave, which interferes with the scattered waves from the surrounding arrayed atoms. In most directions, these waves will cancel each other out, but they can constructively interfere in specific directions called diffraction, determined by Bragg's law:

$$n\lambda = 2d \sin(\theta), \quad n = 1, 2, 3, \dots \quad (3.8)$$

where n is an integer, λ is the wavelength of the X-ray, d is the distance between lattice planes, and θ is the incident angle.

Conventionally, the sample is exposed to monochromatic X-rays, the incidence angle is varied, and the diffracted angle is measured as a function of 2θ , making a characteristic composition spectrum. In order for XRD to be useful, the crystal structure must be greater than ~ 100 nm, otherwise destructive interference leads to peak broadening [16]. For powder diffraction, the intensity of each peak is related to the intensity of the other diffraction peaks of the sample. For thin films however, contribution from the substrate must be limited. This can be achieved by fixing the incidence angle to a very low value, called grazing incidence (GI)-XRD, and measuring the diffracted beam over a wide angle range. Because the thin films typically grow preferentially in certain directions, the peak intensities will therefore not be related, as they are in powder diffraction [79].

XRD was recorded with a Malvern PANanalytical Empyrean X-ray diffractometer, equipped with parallel beam optics and a parallel plate collimator of 0.18° . The source is an Empyrean Cu LFF HR gun operated at 45 kV and 40 mA, with $K_\alpha = 1.540598 \text{ \AA}$. Grazing incidence geometry was used to minimize the contribution of the substrate, *i.e.* the Mo foil, with an incident radiation beam fixed at a grazing angle of 0.4° .

3.3.2 X-ray Photoelectron Spectroscopy (XPS)

X-ray Photoelectron Spectroscopy (XPS) is an extremely useful surface sensitive technique for determining catalyst composition and oxidation states. The basis of XPS is the photoelectric effect, wherein a photon of energy $h\nu$ is absorbed by an atom, leading to a core or valance electron with a certain binding energy, E_b , being ejected from the atom. This happens with a certain kinetic energy, E_k , which can be measured, and E_b can inversely be determined by:

$$E_k = h\nu - E_b - \phi \quad (3.9)$$

where ϕ is the work function of the spectrometer. Since E_b is a characteristic fingerprint for each element, the composition of the atom that ejected the photoelectron can be determined. Auger is a process wherein the hole left by the ejected photoelectron is filled with a higher energy electron, emitting a photon with a characteristic energy, which in turn excites and ejects an Auger photoelectron. An important distinction between the two processes is that Auger electrons have a fixed kinetic energy, completely independent from the energy of the initial X-ray source used [16]. Both processes are schematically shown in Figure 3.9.

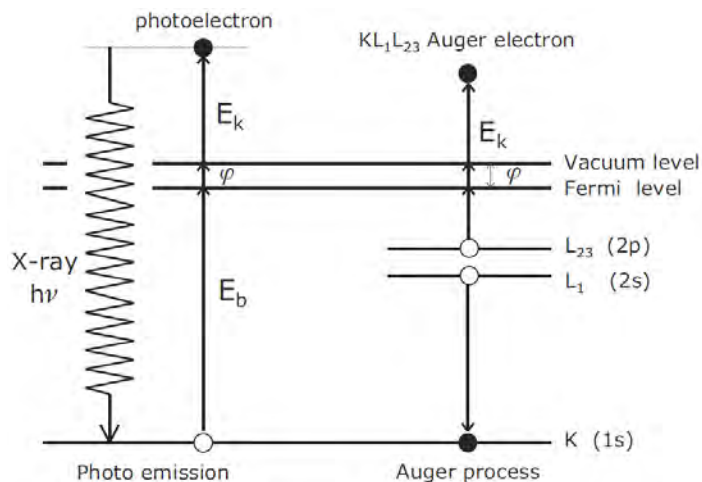


Figure 3.9 XPS and Auger photoelectron generation. Reprinted with permission from Reference [16]. Copyright 2005, John Wiley and Sons.

XPS is extremely surface sensitive because the mean free path of the ejected photoelectron is very short, on the order <2 nm dependent on the material and electron kinetic energy. The initial X-rays are generated through either Mg K_{α} ($h\nu = 1253.6$ eV) or Al K_{α} ($h\nu = 1486.3$ eV) radiation, and to ensure a high signal, XPS analysis must be done in ultra high vacuum (UHV). Usually a hemispherical electron analyser is used, wherein a variable applied voltage difference between two concentric hemispheres filters electrons as a function of kinetic energy.

XPS was done using a ThermoScientific Thetaprobe instrument equipped with an Al K_{α} X-ray source. Survey spectra were recorded with 20 scans at 50 ms dwell time per 1 eV step. Elemental detail spectra were recorded with 5-50 scans in 0.1 eV steps with 50 ms dwell time. The chamber pressure was $2 \cdot 10^{-7}$ mbar, and the lateral resolution was 400 μm . A Flood Gun in Charge Neutralization mode was used during the measurement. The data was acquired and analyzed using Thermo Advantage v5.979 by Thermo Fischer Scientific.

3.3.3 Scanning Electron Microscopy (SEM) and Energy-Dispersive X-ray spectroscopy (EDX)

Scanning Electron Microscopy (SEM) is a technique used to generate images of a conductive sample surface beyond what visible light optics can accomplish. The images are made by scanning an incident electron beam across a sample, and detecting the intensity of the response at each point from either elastically BackScattered Electrons (BSE), inelastically scattered

Secondary Electrons (SE), or Energy Dispersive X-rays (EDX) [80]. BSE typically have energies of 1 keV or more, and can therefore be generated from deeper in the sample, typically 50-300 nm, giving more depth information. SE on the other hand are low energy electrons on the order of ~50 eV generated from the outer shells of atoms, and therefore have a limited information depth of around 5-50 nm of the sample. EDX depth of analysis highly depends on the material and the acceleration voltage used, ranging from 100 nm - 1 μm [81]. The SEM used was a Quanta FEG 250 SEM from FEI, equipped with an Oxford Instruments 80 mm² X-Max silicon drift EDX detector for elemental mapping. EDX quantification was done with AZtec software from Oxford Instruments.

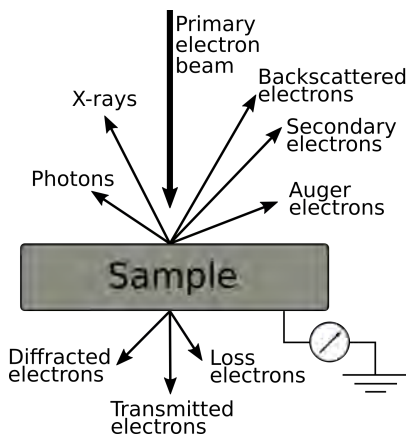


Figure 3.10 Possible interactions with a primary electron beam in SEM. Reprinted and modified with permission from Reference [16]. Copyright 2005, John Wiley and Sons.

Figure 3.10 shows the many different responses in a sample to an electron beam. For this work, SE electrons are used for imaging of the sample surface, and EDX is used for elemental composition. The former is measured via an Everhart-Thornley detector, wherein the electrons are accelerated with a ~250 V bias thereby enhancing the collection efficiency in the detector. Because SE escape more easily from sharp corners, edges, and tips, this is a useful technique for determining morphology of 3D structures.

Emitted X-ray photons have characteristic energies useful for determining and mapping out the chemical composition of the sample as the primary electron beam is scanned across the sample, generating elemental maps. The X-rays are commonly detected with silicon drift detectors, wherein the incoming photon energy is determined by the ionization of the detector material (high purity silicon).

The sample material must be conductive to avoid charging effects from the electron beam. Due to the dependence on pressure for the mean free path of electrons, sufficiently high vacuum ($\sim 10^{-6}$ mbar) is necessary for acceptable signals in SEM [82].

Chapter 4

The Rigorous Protocol

"If they don't keep exercising their lips, he thought, their brains start working."

— Douglas Adams, *The Hitchhiker's Guide to the Galaxy*

The focus of this chapter is to provide the foundation for proper measurements of electrochemically synthesized ammonia. It is an unfortunate truth that the rates of electrochemical ammonia synthesis in *all* published literature is dismal, *i.e.* very little (if any) is produced. Typical experiments are in the sub-p.p.m. range of ammonia concentration. Now this in itself is not a problem, though it is a bit disheartening. The issue is that ammonia is ubiquitous in the environment in small concentrations, which are annoyingly similar to the amounts reported for ammonia synthesis (I have a personal and unprofessional theory that the ammonia molecules particularly likes to gather on the set-ups of electrochemical nitrogen reduction scientists much more than any other places, because the ammonia can feel the desire we have for measuring it).

The chapter is split into three main sections: the initial nitrogen reduction measurements, considerations for cleanliness, and the vital quantitative isotope measurements. The entire chapter can be summarized into the flowchart presented in Figure 4.1, which will be explained step-by-step. The work in this chapter was carried out by myself and the very talented and knowledgeable Dr. Viktor Čolić and Dr. Sungeun Yang.

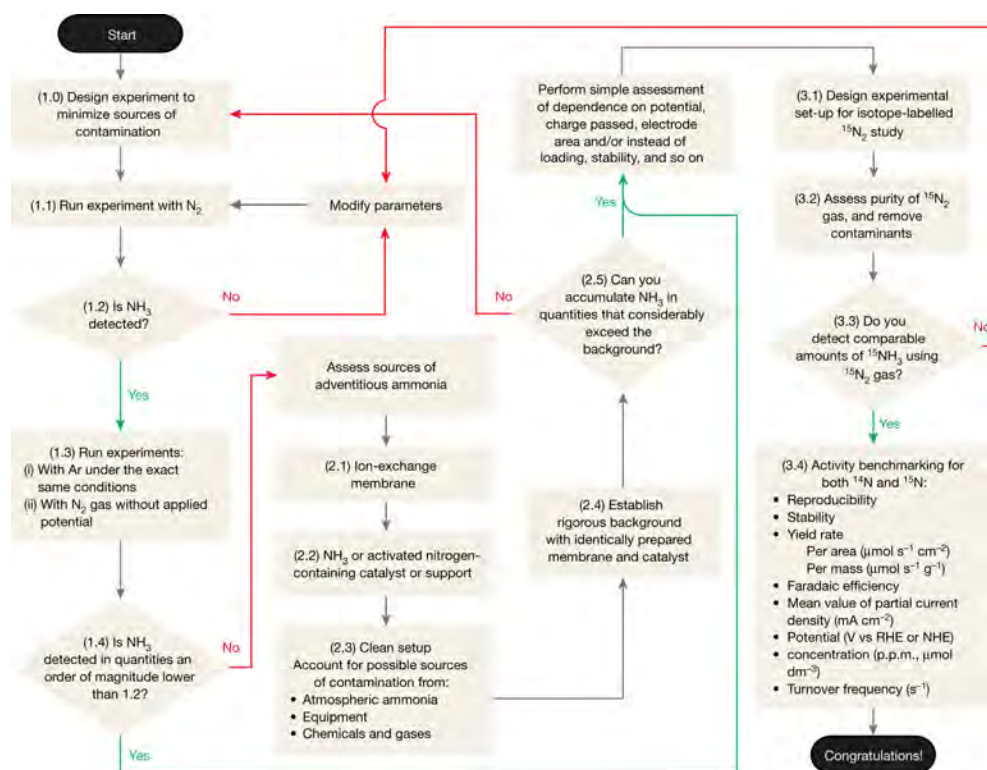


Figure 4.1 Flowchart covering the route for successful electrochemical nitrogen reduction experiments. Printed with permission from Reference [77].

4.1 The simple background measurements

Here I will go through the boxes 1.0-1.4 of the protocol. These are the absolute minimum amount of experiments needed to determine if you *might* be synthesizing ammonia, but is unquestionably not enough as a singular proof.

1.0-1.1 There are some important experiment design considerations one should contemplate before setting up the experiment. This can range from whether or not there is fixed nitrogen in the electrodes/electrolyte, to the cell design used, as single and double-compartment cells each have their advantages and drawbacks. The single-compartment cell has the advantage of a low cell potential, but the drawback of possible ammonia oxidation at the CE. This is directly opposite to the two-compartment cell, wherein the membrane hinders ammonia oxidation [83]. Unfortunately, the choice of membrane adds ohmic resistance to the system, and might be a source of contamination (more on that in Section 4.2.1).

1.2 The Berthelot reaction, also called indophenol and described in section 3.2.1, is one of the most common methods for ammonia detection. Other simple colorimetric methods, such as Nessler's reagents or ammonia assay kits, can also be used. We can distinguish the ammonia signal down to 10 p.p.b. and up to 15 p.p.m. using indophenol. The advisable upper bound for indophenol is around 5 p.p.m. [84], as concentrations greater than this appear to give falsely high absorbance values, leading to overestimation of the ammonia concentration. One can stay within the advisable measurement range by diluting the aliquot with H₂O if the expected ammonia concentration is above the upper bound.

1.3 If ammonia is detected, some very simple control experiments are necessary. These must be run under the exact same conditions as previously to be representative. The first is an Ar blank experiment, where the N₂ gas is replaced with Ar. This will elucidate whether the measured ammonia stems from external sources, such as contamination of the electrolyte, electrodes, chemicals, gloves used, etc. The Ar blank experiment must show either no or significantly less ammonia compared to the N₂ experiment. If that is indeed the case, the second experiment to run is with N₂, but without any potential applied. This will show if there is any ammonia contamination of the N₂ gas itself. The work by Dabundo et al. [85] clearly demonstrated that some gas bottles can have significant amounts of contamination, even above the claims from the manufacturer. Unfortunately, the N₂ bottles can also contain contamination of other fixed sources of nitrogen, such as NO_x and N₂O, which will be much easier reduce to ammonia compared to N₂ [86]. One must therefore clean the N₂ gas accordingly to remove all potential labile nitrogen contaminants, as described further in Section 5.2.

1.4 If the two control experiments in **1.3** show less than one order of magnitude ammonia than the measurement in **1.2**, then the next step is considering isotope labeled experiments. If, however, the ammonia concentration is within one order of magnitude, but it is still suspected that the system might be making ammonia regardless, one can take steps to reduce the contamination levels, as described in the next section.

4.2 Possible sources of ammonia contamination

4.2.1 Membranes for two-compartment cells

2.1 Many studies [87–90] on 2-compartment cells will utilize Nafion, a co-polymer of tetrafluoroethylene and a perfluoro-sulfonic acid, as the membrane. It is ionically conductive due to the incorporation of perfluorovinyl ether groups terminated with sulfonate groups on a tetrafluoroethylene (PTFE) structure. Each study cleans the Nafion differently prior to use, or even use it as received. Unfortunately, the ammonium ion can also be ionically exchanged with protons on

Amount of NH ₃ added to cell	Gas	Condition of Nafion	WE potential [vs RHE]	Measured NH ₃ in WE compartment	Measured NH ₃ in CE compartment
0	None	Untreated	0 V	-9.7 nmol (-22 p.p.b.)	
0	N ₂	Cleaned	0 V	37 nmol (85 p.p.b.)	
0	N ₂	Cleaned	0 V	16 nmol (37 p.p.b.)	
44 nmol (1000 p.p.b.)	None	Untreated	0 V	410 nmol (910 p.p.b.)	-48 nmol (-110 p.p.b.)
440 nmol (1000 p.p.b.)	N ₂	Cleaned	0 V	417 nmol (945 p.p.b.)	78 nmol (178 p.p.b.)
440 nmol (1000 p.p.b.)	Ar	Cleaned	-0.5 V	407 nmol (925 p.p.b.)	-8.8 nmol (-20 p.p.b.)

Table 4.1 Ammonia contamination in Nafion 117 membrane for various conditions, with and without added ammonia. Each measurement is conducted after the membrane has been in contact with 0.1 M KOH for 1 hour in a two-compartment cell. The membrane is cleaned with hydrogen peroxide, sulfuric acid, and ultra-pure water, as described in reference [77].

the sulfonic acid groups [91]. This means Nafion can also act as a source or sink for ammonia, as it can uptake ammonia from the environment or the cleaning reagents used, and then release it continuously throughout the electrochemical measurement. Furthermore, Nafion actually degrades if exposed to even 0.1 p.p.m. of ammonia [92], and the conductivity will drastically decrease due to this poisoning [93].

We tested Nafion 117, both as received, and after a cleaning in a 2-compartment cell, to both determine how permeable the membrane was to ammonia, and how much contamination the use of Nafion can lead to. The negative value of ammonia seen in Table 4.1 is due to it being a comparison with a blank from the electrolyte, and if the Nafion soaks up the inherent ammonia contamination from our electrolyte, the measured amount will be "negative" in comparison. The as-received, untreated Nafion was seen to soak up ammonia, while the cleaned membrane would contaminate the set-up. We expect that cleaning the membrane in highly acidic solutions might introduce ammonia during the cleaning, as acidic solutions can much more easily uptake environmental ammonia. This contaminant in the acidic solution is soaked up by the membrane, and then subsequently released into the electrolyte. It was also seen that with added ammonia and no applied potential, the membrane actually allows for considerable crossover to the CE

compartment. With an applied potential, the measured ammonia in the CE compartment is negative, probably due to ammonia oxidation at the CE. Because Nafion degrades in the presence of ammonia, and can act as a source or sink, we (and others [91]) would highly discourage the use of Nafion membranes for electrochemical nitrogen reduction.

Amount of NH ₃ added before test	Gas	WE potential [vs RHE]	Measured NH ₃ in WE compartment	Measured NH ₃ in CE compartment
0	None	0 V	<4.4 nmol (<10 p.p.b.)	
440 nmol (1000 p.p.b.)	None	0 V	438 nmol (995 p.p.b.)	8.8 nmol (20 p.p.b.)
440 nmol (1000 p.p.b.)	Ar	-2.0 V	348 nmol (791 p.p.b.)	39 nmol (89 p.p.b.)

Table 4.2 Ammonia contamination in Celgard 3401 for various conditions. Each measurement is after the membrane has been in contact with 0.1 M KOH for 1 hour in a two-compartment cell. The membrane is not cleaned, and is stored in 0.1 M KOH.

We also tested Celgard 3401, a 25 μm thick microporous polypropylene membrane. We ran three repeated measurements leaving equally sized Nafion and Celgard membranes in 0.1 M KOH for 1 hour each, and measured the ammonia contamination compared to the blank electrolyte. The cleaned Nafion was seen to overall increase the measured ammonia, while the as-received Nafion soaked up ammonia contamination from our stock solution. The Celgard appeared to give a slight positive measure, below the 10 p.p.b. detection range. This is shown in Figure 4.2. Even when adding 1 p.p.m. of ammonia to the WE compartment, we could recover all of the ammonia within detection limits, as seen in Table 4.2. However, when we apply a potential, a significant amount of the ammonia is seen to cross over the membrane, and we overall lose some ammonia in the system, probably due to oxidation at the counter electrode. In this case we lost around 12 % of the added ammonia. However, we have the firm stance that underestimating synthesized ammonia is far better than a false positive, and have therefore chosen to continue using Celgard for all aqueous experiments.

4.2.2 The catalyst and other common contamination sources

2.2 If the catalyst or the support for the catalyst contains any amount of fixed nitrogen, one must be very careful to properly measure the levels of ammonia from these sources, and determine any nitrogen depletion in the substance before and after electrochemical measurements [94].

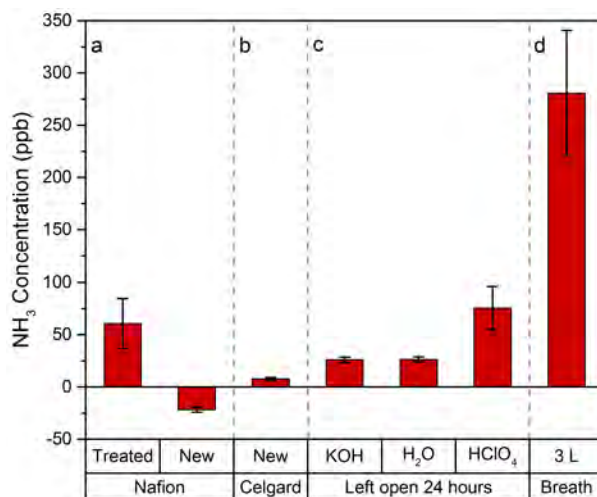


Figure 4.2 Ammonia contamination from various different sources used in experiments, or sources which the sample might be exposed to in lab. Printed with permission from reference [77].

Fixed nitrogen means anything that is not N_2 , such as imides, amides, nitriles, nitrates, nitrites, etc. One should be mindful if the expected reaction mechanism is the Mars-van-Krevelen mechanism, as the nitride might initially form ammonia even in Ar gas, due to the depletion of nitrogen from the lattice [95]. I would recommend reading the work by Du et al. [96] for a critical take.

2.3 Ammonia is ubiquitous in the environment in variable amounts of 0.05-250 p.p.m. [97], depending on whether you are in a clean room or literally standing in a pig sty. If chemicals are left standing open, they can accumulate ammonia over time, even in the cleaner laboratory air. This is seen for various chemicals in Figure 4.2. Ensuring a closed system, also for the cell itself, is therefore imperative for proper measurements. An anecdotal story about air contamination actually occurred in our lab. We went from measuring <10 p.p.b. of ammonia on Ru for everything we did, to suddenly measuring 44 p.p.b. when cleaning the Ru differently. We thought that somehow we had hit the holy grail of aqueous electrochemical nitrogen reduction. It later turned out that the extra ammonia contamination was due to the building site next door. They had just started digging up the earth to put in support pillars, increasing the environmental ammonia in our lab, and therefore on our glassware and chemicals too. It takes that little to get a false positive.

Environmental ammonia also means that most surfaces, to some extent, might have ammonia on them, including the surface of the electrochemical cell itself. A thorough cleaning is therefore required between each experiment, particularly if the prior experiment included a lot

of ammonia. Additionally the human breath also contains ammonia, as it is a by-product of protein metabolism. It is produced from the degradation of protein that is converted into urea by the liver, and is expelled from the body. Due to the slight alkalinity of blood, some ammonia diffuses into the bloodstream and is expelled through the exhaled breath. The concentration of ammonia which human breath contains varies from 0.1 to 3.0 p.p.m. depending on age, gender, health, diet, etc. [98]. We carried out some simple measurements where we each exhaled one full breath of 3 L [99], and measured the amount of ammonia. Interestingly mine was the highest, which is in accordance with women, on average, exhaling more ammonia [98]. Professor Ib Chorkendorff saw this as an opportunity to be directly involved in lab experiments. He ate a big steak dinner (sacrifices must be made for science), and showed up early the next day ready to measure ammonia. Well, the result is interesting (and funny), as seen in Figure 4.3.

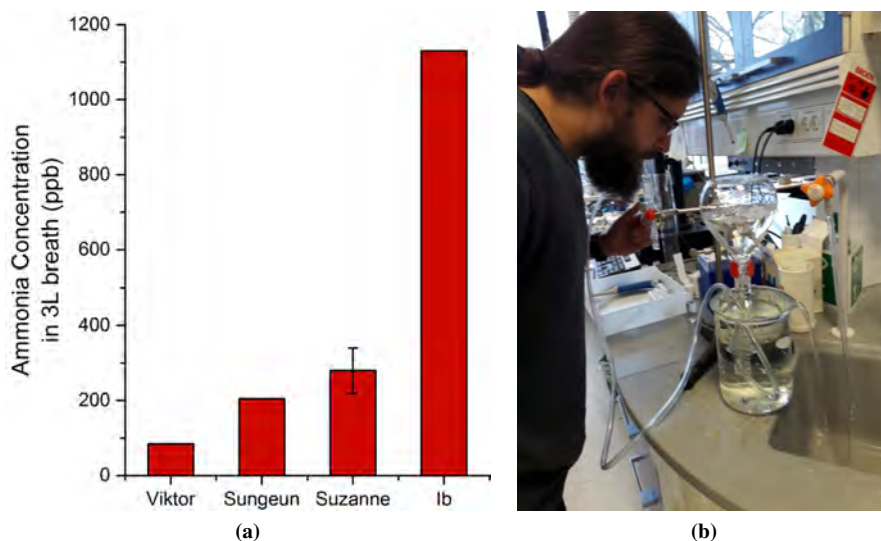


Figure 4.3 a) Ammonia measured in breath. Repeated 3 times for me, to show mean and standard deviation as error bars. b) Viktor breathing into our home-made test set-up consisting of an upside down flask to accurately measure a single full exhaled breath.

4.2.3 Accounting for known impurities and determining performance assessment

2.4 Once all these factors are been taken into account, it is important to establish rigorous background measurements, to account for possible sources of ammonia, particularly if a mem-

brane or nitrogen containing catalyst is used. This could *e.g.* be several repeated measurements with Ar gas to establish a baseline for the contamination, thereby determining the variance of adventitious ammonia within each measurement, and to measure possible changes as a function of time.

2.5 Once ammonia is measured in concentrations that significantly exceed those of the background contamination experiments with Ar over the same time period, one can move onto the next phase of the flow chart.

Before starting isotope measurements, a simple assessment of the performance of the catalyst is needed. This can be done by determining the stability and reproducibility of experiments, the activity in *e.g.* $\mu\text{mol s}^{-1} \text{cm}^{-2}$, dependence on the applied WE potential, etc. It is also important to report the ammonia concentration and volume of electrolyte, as well as the background contamination levels. Ensuring that ammonia is continuously produced over time, increases with higher catalyst area or loading, etc. is a good indication (but not proof in itself) of successful ammonia synthesis.

4.3 Quantitative isotope measurements

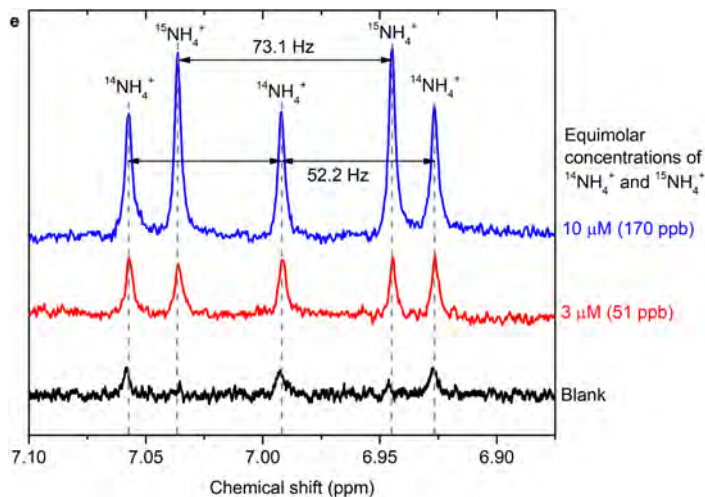


Figure 4.4 Zoom in of NMR calibration curve from Figure 3.8, with equimolar concentrations of $^{14}\text{NH}_3$ and $^{15}\text{NH}_3$ added. The blank sample is measured to contain 10 p.p.b. of ammonia via indophenol. Printed with permission from Reference [77].

3.1 Finally, in order to provide definite proof that the nitrogen in the detected ammonia originates from the reduction of N_2 gas supplied to the system, it is imperative to conduct

isotope labeled measurements with $^{15}\text{N}_2$ gas. The isotope labeled ammonia can then be detected by NMR, Fourier transform infra-red (FTIR) spectroscopy [53], or MS. Because we at DTU have access to NMR, thanks to spectrometers of the NMR Center at the Technical University of Denmark supported by the Villum Foundation, we chose to use NMR. We were able to clearly distinguish concentrations down to 50 p.p.b., and even concentrations as low as 10 p.p.b. were visible, seen as the small peaks in the blank in Figure 4.4, where the 10 p.p.b. was detected with indophenol as our inherent ammonia background contamination. Once the ammonia peaks are identified, the integrated area under each peak can be used to determine the amount of ammonia synthesized when compared to a calibration curve.

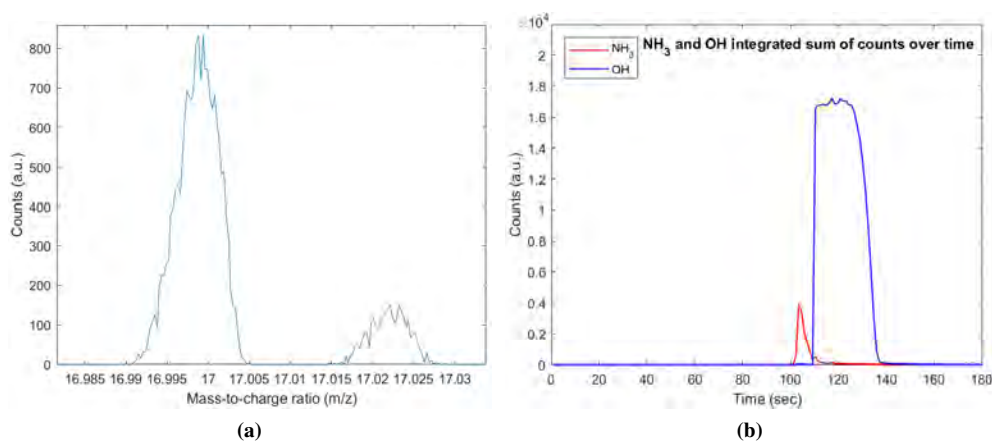


Figure 4.5 a) MS spectrum clearly showing that the OH peak (m/z of 17.008) is clearly distinguishable from the $^{14}\text{NH}_3$ peak (m/z of 17.026). The spectrum is not calibrated, so the m/z is slightly off, and the amounts shown are not quantified. b) GC-MS spectrum of 20 p.p.m. $^{14}\text{NH}_3$ in aqueous electrolyte. Clear timely separation of the NH_3 is seen from the interfering peak of OH from water. Deconvolution is possible due to timely resolution by the GC.

Isotope labeled ammonia can also be detected via MS. Due to the atomic weight difference between $^{14}\text{NH}_3$ and $^{15}\text{NH}_3$, the product originating from the isotope labeled $^{15}\text{N}_2$ gas is mass distinguishable. Unfortunately, H_2O has a mass very similar to that of isotope labeled $^{15}\text{NH}_3$, so a very high resolution and suppression of the water signal is needed to directly quantify the $^{15}\text{NH}_3$ signal, *e.g.* by lowering the ionization potential. With a good enough gas chromatography (GC)-MS, equipped with an optimal column for NH_3 separation from water, and a MS with high enough resolution, one can separate the NH_3 peak from H_2O , even though they otherwise would overlap. We are fortunate enough to have such an instrument at SurfCat, and the result can be seen in Figure 4.5. As sector MSs of that quality are rather expensive, there are other methods

to get around the interfering water signal by *e.g.* measuring on a compound that selectively reacts with the ammonia in the solution, which has been done successfully in some literature [100, 101].

3.2 In isotope labeled $^{15}\text{N}_2$ nitrogen gas, ammonia and reducible nitrogen are a common and experimentally significant impurity [85]. This is an additional concern which is generally not addressed in the literature. It necessitates the use of an ammonia trap before the gas enters the electrochemical cell, which can remove $^{15}\text{NH}_3$ impurities from the $^{15}\text{N}_2$ gas. Control measurements with $^{15}\text{N}_2$ gas flowing through the cell under OCP must be conducted to establish the level of ammonia contamination from the gas feed, in the same manner as in measurements with $^{14}\text{N}_2$ gas. Furthermore, the gas supply might contain NO_x and other sources of reduced nitrogen, which must be accounted for and cleaned from the gas stream. This can be done with *e.g.* a Cu catalyst or a gas purifying system, which will be described in Section 5.2.

3.3 The amount of ammonia detected when the potential is applied with isotope labeled gas must be significantly higher than the detected amounts in the control measurements. The results must also be reproducible, and quantitatively show the same level of activity as with $^{14}\text{N}_2$ gas. Furthermore, a single point for isotope sensitive studies is not enough to prove successful synthesis, even if that point correlates well with the non-isotope studies. One must repeat both isotope and non-isotope measurements at least 3 times, estimating a mean and standard deviation for the proposed electrochemical process with both gasses.

3.4 In order to ensure meaningful evaluation of data collected under different conditions in different experimental set-ups, in addition to the usually reported yield rate and faradaic efficiency, it is necessary to report the actual concentration of the detected ammonia. This should be reported in combination with the concentration in control measurements with Ar, and with N_2 at OCP, along with the volume of the electrolyte in the cell, as we typically see that concentrations of ~ 100 p.p.b. can easily originate from contamination. The turnover frequency (TOF) (per site per second) and the yield rate particularly per surface area or gram of catalyst, as measures of activity need to be reported, in order to ensure a robust assessment of the possible catalytic activity of different materials. It should also be assessed whether these values are stable with time, or if the activity degrades quickly. All these values need to be compared for $^{14}\text{N}_2$ and $^{15}\text{N}_2$ measurements, and similar values should be obtained.

Once all of these steps are carried out successfully, ammonia synthesis is proven. The sources of contamination and suggested control experiments, while intended for electrochemical ammonia synthesis, can also be applied to photoelectrochemical experiments and for nitrogen oxidation to NO_x ; the main points regarding the importance of carrying out blank tests and utilizing isotope labeled $^{15}\text{N}_2$ are still valid and should be utilized across these fields as

well. Quantitative isotope labeled experiments is the keystone of this protocol, and without it, ammonia synthesis is simply not proven.

4.4 Summary

In this chapter, I presented a protocol for rigorously benchmarking electrochemical nitrogen reduction. This covered all the common pitfalls and possible false positives the inattentive scientist might encounter. The first validation step when any ammonia is measured from an electrochemical experiment, is to perform Ar blank and N₂ at OCV tests, to determine if the measured ammonia is an external contamination. Sources of possible contamination must be accounted for, particularly if the set-up contains any fixed nitrogen. However, simply performing Ar and N₂ blank experiments are not enough to definitively prove ammonia synthesis, and quantitative isotope labeled experiments with proper gas cleaning is absolutely paramount for proper scientific studies. Without proper isotope labeled experiments, none of the reported data can be trusted. The only exception to this rule is if the amounts of ammonia produced are beyond question, *i.e.* if the synthesized ammonia can literally be smelled or seen.

Chapter 5

Electrochemical Nitrogen Reduction in Aqueous Solution

"For a moment, nothing happened. Then, after a second or so, nothing continued to happen."
— Douglas Adams, *The Hitchhiker's Guide to the Galaxy*

The primary goal of this chapter is to synthesize any amount of ammonia in aqueous solutions, following the protocol from Chapter 4. The chapter will first cover topics that are all essential before starting ammonia synthesis experiments:

- How well does ammonia stay in the system? If we add a certain amount of ammonia, can we recover all of it? Does electrochemistry affect the ammonia in the system?
- What contamination sources do we have in our system, and where could any adventitious ammonia stem from?

After ensuring we have dealt with these questions, we can start measurements. Many published reports claim successful nitrogen reduction on various pure metal electrodes in aqueous solution, and we attempt to reproduce some of those results. We also try changing the temperature of the system, and test out various different aqueous electrolytes. I want to emphasize here that while I report values in p.p.b., I personally consider anything less than 100 p.p.b. in the experiments in the beginning of the chapter (as we were just learning about ammonia contamination) to simply be measurement uncertainties from pipetting/contamination of stock chemicals. It was not until the end of the chapter (~6 months into my Ph.D.) where we consistently measured <10 p.p.b. in

our blank solutions. So please be aware of a high uncertainty on the order of ~ 100 p.p.b. in Section 5.1.

All experiments reported are carried out in collaboration with the shared first authors of Paper I: Dr. Viktor Čolić and Dr. Sungeun Yang. The work presented is therefore entirely shared work, with guidance from my 3 supervisors, and Prof. Ifan Stephens. I will therefore use "we" throughout this chapter.

5.1 Trapping efficiency in system

Before starting any form of experiments, we need to ensure that our system is capable of trapping the produced ammonia, and to determine how much of our ammonia we might lose, if any. This section presents experiments carried out purely in 0.1 M KOH electrolyte, with a 0.5 M H₂SO₄ acid trap when stated.

5.1.1 Ammonia solubility in electrolyte

The very first step is to determine the trapping efficiency (TE) of ammonia. This is defined in this context as:

$$\text{TE (\%)} = \frac{\text{Amount of NH}_3 \text{ measured in system}}{\text{Amount of NH}_3 \text{ added to system}} \quad (5.1)$$

As we will later on experiment with temperature variations, the first thing we tested was how well ammonia stays in stagnant solution as a function of temperature and time. We made an ammonia concentration of 2 p.p.m. in a closed 10 mL glass vial placed in a water bath, and measured the ammonia concentration as seen in Figure 5.1. Experiments at room temperature and up to 40 °C have reasonable TE. But if higher temperature experiments are carried out, one needs to be aware that ammonia will significantly escape into the headspace of the cell.

We also tried two different cell materials, as seen in Table 5.1, with and without the addition of gas purging at ~ 10 mL/min N₂. Interestingly more ammonia was measured the next day in the glass cell than was added. I suspect there might have been a leak, and adventitious ammonia from the atmosphere could have dissolved into the solution. Both systems appear to lose quite a significant amount of the added ammonia if purging with gas. As gas bubbling during electrochemical nitrogen reduction experiments is necessary, a downstream acid trap can be used to trap the gaseous ammonia.

Because glass cells are easier to clean and can be custom ordered cheaply, we chose to continue use with glass cells. We were aware that KOH might dissolve the glass, and tested our solutions with inductively coupled plasma mass spectrometry after leaving 0.1 M KOH

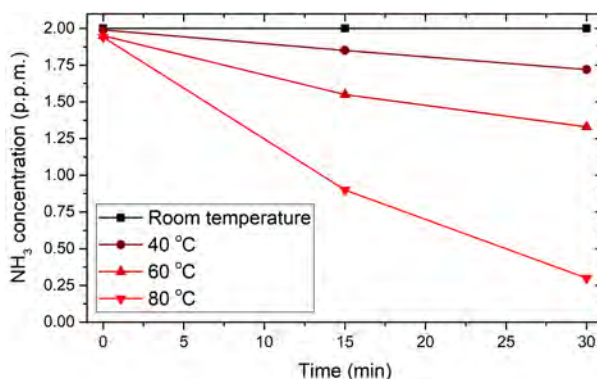


Figure 5.1 Initially 2 p.p.m. of NH_3 was added to 10 mL 0.1 M KOH at different temperatures. Ammonia concentration is then measured as a function of time for the different temperatures.

Time (hour)	NH_3 concentration (p.p.m.)				
	Glass cell	Glass cell + glass frit	Glass cell + bubbling	PP tube	PP tube + bubbling
2	10.1	10.0	4.9	9.8	4.7
20	10.3			9.9	

Table 5.1 A 10 p.p.m. concentration of NH_3 in 5 mL 0.1 M KOH in either glass or polypropylene (PP) tube. Ammonia concentration is measured via indophenol as a function of time. The PP tube was used as a cell with PP tubing as the bubbler. Glass frit was tested to see if ammonia would diffuse through it.

overnight in the glass cell. No significant impurities were measured from this, and glass cells are therefore used in the rest of the work.

5.1.2 Purging efficiency to acid trap

Adding an acid trap is a common way to capture any gaseous ammonia that escapes due to gas bubbling during the experiment. As gaseous ammonia is passed through an acidic solution, it will neutralize some of the acid, making ammonium ions, which stays in solution. However, due to its high polarity, ammonia is also very easily dissolved in water, leading it to remain in even high pH solutions [102]. To increase the TE, an acidic solution is added in a downstream trap.

Table 5.2 shows the results of adding a downstream acid trap, and adding ammonia to either the cell or the acid trap, and measuring the TE of the system after purging N_2 for 1.5 hours. Since ammonia is detected in the electrolyte upstream from the acid trap wherein the ammonia was added, our 5.0 purity N_2 gas or our chemicals must have some ammonia contamination,

Electrolyte/ acid trap	Added NH ₃ (p.p.b.)	Measured NH ₃ (p.p.b.)	Trapping efficiency (%)
Electrolyte	400	318	80
Acid trap	0	31	87 (total)
Electrolyte	0	10	
Acid trap	400	392	98

Table 5.2 0.1 M KOH electrolyte with a downstream glass 0.5 M H₂SO₄ acid trap connected via stainless steel swagelok tube connectors. TE of each component measured after 1.5 hours bubbling with ~10 mL/min N₂.

however, it is seen that the acid trap does indeed trap some of the ammonia which escapes the electrolyte. Some ammonia is still lost in the transfer from the cell to the downstream trap, which is expected as ammonia is a sticky molecule [103, 104], and will sit on the walls of the glass cell and stainless steel connector when transferred downstream.

5.1.3 Closed system with gas circulation

To reduce the inflow of N₂, and therefore potential contaminants, a gas circulation set-up with a glass pump was built. The first iteration of the system was very simple, with only the glass pump and an electrochemical cell. Because the glass pump has an internal volume of roughly 200 mL, some of the ammonia in gas phase will stay inside the glass pump during the re-circulation. An experiment was therefore tested where 10 p.p.m. of ammonia is added to 0.1 M KOH, and gas was re-circulated for 2 hours. Some H₂SO₄ is then added to the electrolyte to bring the pH down to 2, and the gas was recirculated for another hour, in an attempt to re-trap the gaseous ammonia in the now acidic electrolyte. This was tried twice, and the amount of ammonia measured after each attempt was 7.4 and 7.9 p.p.m. While the TE of the gas-circulation set-up is not ideal, it is still better than the values obtained in Table 5.1. In a second iteration of this system, the gas is circulated for 2 hours in the cell, then the outlet is switched, and the whole system (glass pump and cell) is purged for 1 hour through a downstream acid trap with Ar after measurements. The total TE was 86 % in this system (5.0 p.p.m. recovered in cell and 3.6 p.p.m. in acid trap). While still not close to 100%, this was the system used for remaining experiments in aqueous solution, as it was the highest TE we could obtain.

5.1.4 Ammonia oxidation

Once we determined how much is lost due to purging, we also wanted to determine if any ammonia is lost during electrolysis. Experiments shown in Table 5.3 were carried out with a flow

of 10 mL/min Ar, except for the first experiment which did not have any flow (denoted stagnant). Clearly electrolysis alone can significantly oxidize ammonia, as 3.8 p.p.m. disappeared from the first experiment alone. When Ar purging was added, even more ammonia was lost. When reducing the added amount to only 1 p.p.m., almost all the ammonia was oxidized. Adding a downstream acid trap did not help, as it appears that very little was transferred to the trap.

Electrolyte/ acid trap	Added NH ₃ (p.p.m.)	Time (hours)	Potential (V vs RHE)	Measured NH ₃ (p.p.m.)
Electrolyte (stagnant)	10	2	-[2.7, 3.0]	6.2
Electrolyte	10	2	-[2.7, 3.1]	4.2
Electrolyte	1	1.5	-[2.4, 3.2]	0.05
Electrolyte	1	1.5	-[2.9, 3.8]	0.05
Acid trap	0	1.5		0.02

Table 5.3 0.1 M KOH electrolyte with a downstream glass 0.5 M H₂SO₄ acid trap connected via stainless steel swagelok tube connectors. The electrochemical set-up was a Ru WE, with 100 mA applied current, where the potential range shown denotes the change in WE potential during the measurement.

Considering the literature on aqueous nitrogen reduction (see Extended Data Table 1 of Paper I, Appendix B), the amounts of ammonia measured are very small (except for the reported literature where either fixed nitrogen or even ammonia is used in the preparation of the experiment, which makes one wonder whether a connection exists). This means that if ammonia is produced, and there is no separation of the anolyte and catholyte, any synthesized ammonia will most likely be oxidized again. One therefore needs to carefully consider the use of a single-compartment cell vs a two-compartment cell with a membrane. As was discussed in Chapter 4, a Celgard membrane leads to less contamination of the system, so all electrochemical experiments in aqueous solution will hereafter use a two-compartment set-up with a Celgard membrane.

5.2 Ammonia contamination

Another issue that needs to be addressed before electrochemical experiments can be started, is possible contamination sources, as discussed in Section 4.2.

One source of contamination we encountered in the lab was the chemicals used, particularly the strong acids. We used, amongst other chemicals, HClO₄ as an electrolyte. When using 0.1 M HClO₄, we suddenly started measuring ammonia concentrations around 300-400 p.p.b.

even in the blanks. After ordering a new batch of HClO_4 , the ammonia contamination was back around the expected 10 p.p.b. for our background levels. Another (rather surprising) source of contamination, was the pipettes used. Each person has a personal set of pipettes, so the history of the pipette is known to the user. Even though disposable fresh pipette tips are used each time, for some inexplicable reason, the 100-1000 μL pipette Dr. Sungeun Yang used for adding indophenol reagents was narrowed down to give falsely high results. We suspect a student might have grabbed it, and wrongly used it to pipette a strong acid or even ammonia, getting a bit of solution into the main pipette body. Although we have no way of knowing if this happened, I only mention this, to highlight the ease of random ammonia contamination which might occur in a lab. It took us 2 full weeks to realize the contamination (variable but on the order 10-300 p.p.b. ammonia in *every* sample) was coming from the pipette used, and not from successful ammonia synthesis.

Electrolyte/ acid trap	Gas	Voltage (V vs RHE)	NH_3 conc. (p.p.b.)
Electrolyte	N_2		<10
Acid trap	N_2		18
Electrolyte	Ar	[-1.7, 3.4]	<10
Acid trap	Ar		<10

Table 5.4 Ammonia measured in system when purging with ~ 10 mL/min N_2 or Ar gas with electrolysis (-90 mA), both for 1.5 hours.

Time (hours)	NH_3 conc. (p.p.b.)	
	Without cold trap	With cold trap
0	0	0
1	17	<10
2	21	12

Table 5.5 Ammonia measured in 0.1 M HClO_4 when bubbling with ~ 10 mL/min N_2 with and without a cold trap.

Another serious source of contamination that everyone absolutely *needs* to consider, is the N_2 gas used (N5.0, AGA in this chapter). Dabundo et al. [85] reported significant contamination of stock $^{15}\text{N}_2$ gas, which has to be cleaned before isotope measurements can be done (box 3.1-3.3 of the flowchart in Figure 4.1). And $^{14}\text{N}_2$ gas can unfortunately equally also be contaminated.

Table 5.4 shows measurements of ammonia from simply purging with N_2 gas. Up to ~ 10 p.p.b. is simply measurement uncertainty from the indophenol method, but the 18 p.p.b. is contamination. If we used a cold trap instead, as shown in Table 5.5, reduced levels of contamination was measured. A cold trap can freeze any ammonia in the gas stream, as the melting point of ammonia is -78 $^\circ\text{C}$. By submerging part of the inlet tube into an EtOH slurry (EtOH cooled by liquid N_2 , around -115 $^\circ\text{C}$), the ammonia in the gas stream will freeze onto the internal tube walls submerged in the slurry. This is seen to reduce the ammonia contamination.

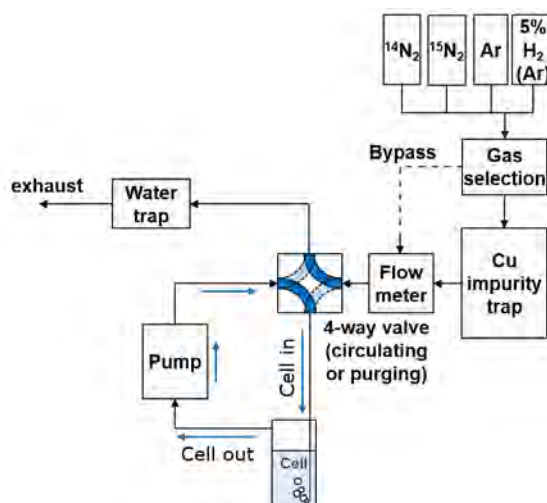
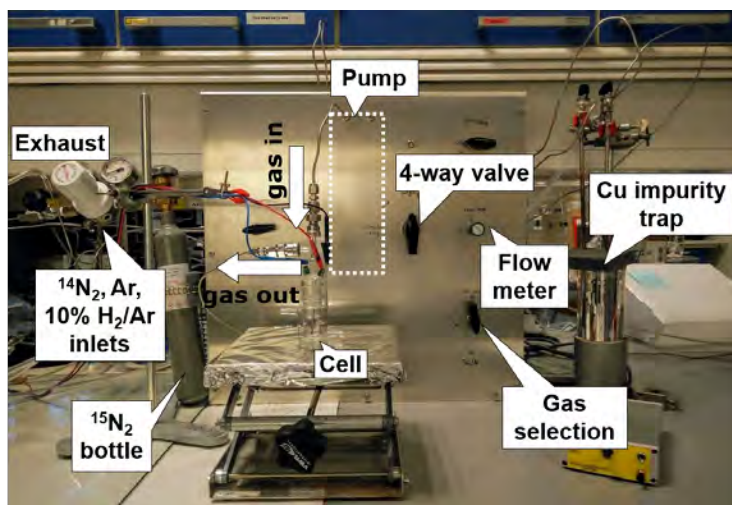


Figure 5.2 Full gas circulation set-up photo and schematic. The glass circulation pump is placed behind the metal valve panel, outlined with the white rectangle. Modified and reprinted from Reference [77].

Unfortunately, the report by Dabundo et al. pointed out that nitrate, nitrite, and nitrous oxide contamination is also quite common in $^{15}\text{N}_2$, and logically therefore also in $^{14}\text{N}_2$. Fixed nitrogen, *e.g.* in the form of nitrite and nitrate, is more easily reducible than N_2 , so a method to clean the gas stream of all contaminants is necessary. Reduced Cu can remove these contaminants [105, 106] in combination with the cold trap for ammonia. A Cu impurity trap was therefore made with 2 g of a Cu-Zn-Al oxide catalyst in a U-shaped swagelok stainless steel tubing that

could be submerged in EtOH slurry. This was added to the inlet of our circulation set-up with the option to bypass the Cu impurity trap, as shown in Figure 5.2. The set-up allows for the selection of 4 different gasses: $^{14}\text{N}_2$, $^{15}\text{N}_2$, Ar, and 5% H_2 in Ar. The Cu must be reduced before use, which can be done in 5% H_2/Ar at $\sim 300^\circ\text{C}$ for 2 hours. The gas flow is then switched to Ar while the tube is kept at 300°C for 0.5 hours to remove any residual H_2 , and the electrolyte can be injected into the cell at this point to purge out any dissolved air from the solution. The tube is subsequently lowered into the prepared EtOH slurry, so the Cu impurity trap also freezes out ammonia from the gas stream.

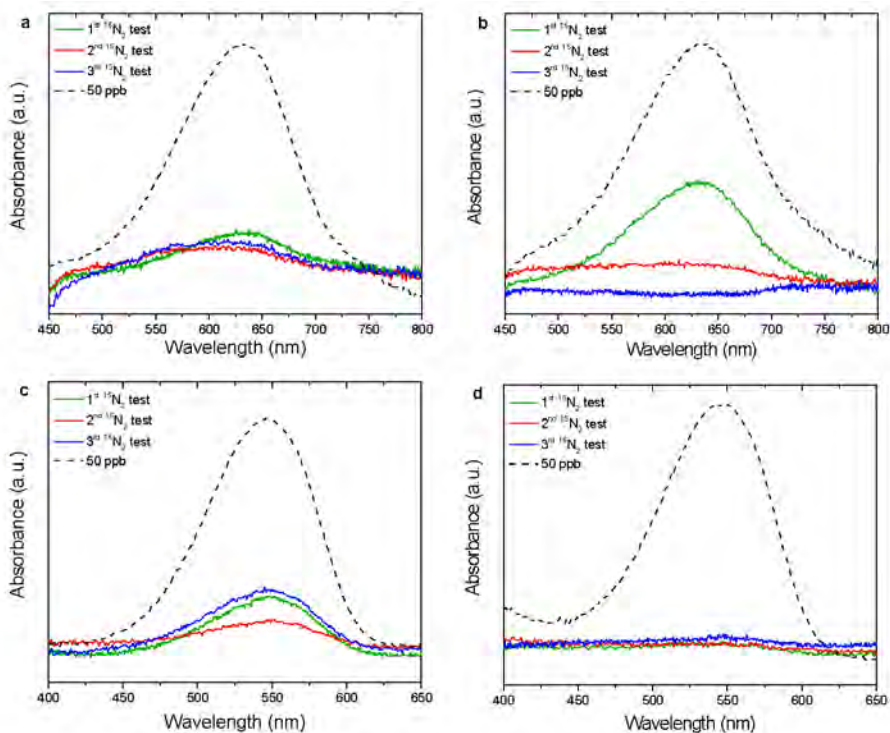


Figure 5.3 Concentration of ammonia and nitrite in the $^{15}\text{N}_2$ gas stream, measured as 3 subsequent measurements of the concentrations of: a) ammonia without cleaning the gas stream, b) ammonia with the impurity trap, c) nitrite without cleaning the gas stream, and d) nitrite with the impurity trap. Reprinted from Reference [77]

A systematic study of the purity of our $^{15}\text{N}_2$ was needed. Ar is purged through the system for 30 mins in the bypass mode, avoiding the Cu impurity trap. Electrolyte is injected under Ar flow and purged with Ar to remove any dissolved $^{14}\text{N}_2$ before the gas is switched to $^{15}\text{N}_2$. Roughly 200 mL is passed, then switched to the gas circulating mode. The system is then left

to circulate the gas for 1 hour to duplicate experimental conditions. Aliquots of the solution is used to measure ammonia, nitrite, and hydrazine concentrations. This was repeated 3 times for reproducibility. The results are shown in Figure 5.3a and c for ammonia and nitrite respectively. No hydrazine was detected. Unfortunately the gas stream appears to have around 10 p.p.b. of ammonia and 10-20 p.p.b. of nitrite, which can more easily reduce to ammonia than our isotopically labelled $^{15}\text{N}_2$, giving a false positive.

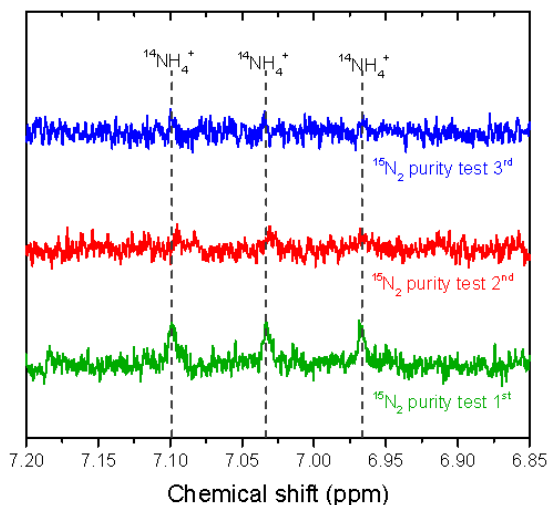


Figure 5.4 NMR of ammonia concentration of samples shown in Figure 5.3b after gas cleaning, to determine source of ammonia contamination from the 1st purity test. Reprinted from Reference [77]

When repeating these three subsequent measurements with the newly incorporated and freshly reduced Cu impurity trap, all nitrite was seen to disappear from the gas stream (Figure 5.3d). The first ammonia measurement interestingly had a higher ammonia content (Figure 5.3b). We suspect that this spike is due to contamination of the Cu catalyst used, as this was the first reduction of said catalyst. Luckily each subsequent measurement (also some not shown), had no additional ammonia contamination after that first purity test. The reason we think this was ammonia from an unaccounted source rather than the gas stream, is because NMR shows it to be $^{14}\text{NH}_3$ rather than the expected $^{15}\text{NH}_3$ from the $^{15}\text{N}_2$ gas, seen in Figure 5.4.

The gas cleaning procedure with the reduced Cu catalyst mentioned here is used for the remainder of this chapter, as well as for some measurements in Chapter 6, unless otherwise stated. When we acquired a glovebox for non-aqueous experiments (Chapter 6), we switched to using a commercial gas purifier instead (MicroTorr MC1-902F, SAES Pure Gas), certified for <5 p.p.t.V of NH_3 and <1 p.p.t.V of NO_x impurities.

5.3 Systematic study in electrochemical nitrogen reduction

Once all sources of contamination are accounted for, and the gas stream is clean, we can finally start investigating the possibility of electrochemical nitrogen reduction. All metals were cleaned and prepared according to the procedure outlined in Section 3.1.1.

5.3.1 Pure metal foils

Looking back to Figure 2.2 [41], theoretical calculations suggest that Re, Ru, Rh, Ni, Ir, and Pt, might be the best pure metal candidates for the NRR, as they comparatively have the smallest overpotential. Additionally, Fe [107] and Au [108] might also work, as there are previously reported data of successful nitrogen reduction on these metals (without rigorous testing).

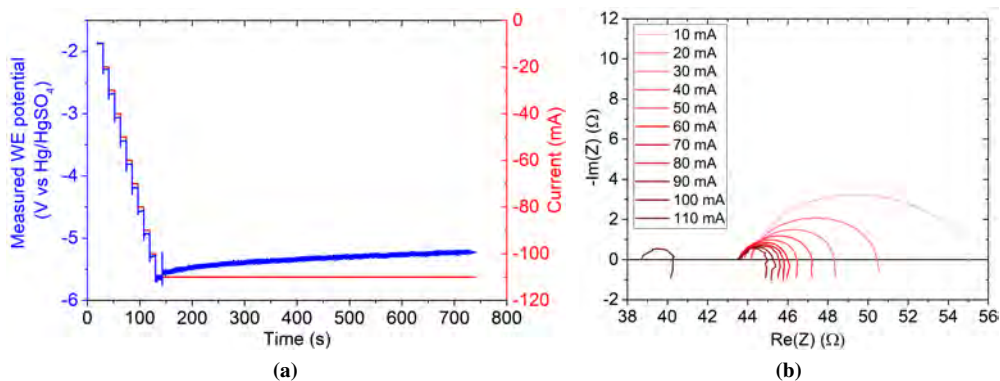


Figure 5.5 a) Staircase CP measurements with increasing current (red), showing change in measured potential (blue) in V vs Hg/HgSO₄. b) EIS measurements after each CP section shown as a Nyquist plot.

For a pure metal catalyst in this system, during a CP measurement, the potential and the Ohmic resistance changes over time. As we can only use at most 85% IR correction, the changing resistance during the measurement will affect the manual IR correction, thereby changing the actual WE potential during a CP. The measured potential of the WE also varied throughout the measurement. The drift in both is probably due to bubble formation on the WE, a change in temperature during the measurement, and/or a change in electrolyte volume during the measurement. We used a special technique called staircase galvanostatic (SG)EIS, which is essentially EIS then CP looped with incrementally increasing applied currents. With this, we could track the change in impedance and measured potential during a measurement. An example is shown in Figure 5.5. For the short increases in current, the overall Ohmic resistance does not change much, although the change in the shape of the semi-circle indicates changes in

the electrolyte resistance [109]. After just 10 minutes of CP at -110 mA, the Ohmic resistance is seen to drop from around 44 Ω to 39 Ω , and the potential is seen to change on the order of 300 mV. This means that the manual 85 % IR-drop correction is not quite correct, as the resistance changes during the measurement. The measured potential is uncompensated by $15\% \cdot 0.11 \text{ A} \cdot 44 \Omega = 726 \text{ mV}$, and the wrongly over-compensated $0.11 \text{ A} \cdot (44-39) \Omega = 550 \text{ mV}$, additional to the 300 mV shift during the measurement. Because of the change in these values, we have chosen to show the applied WE potential as a range rather than a discrete point, based on post-measurement correction. We therefore carried out SGEIS measurements for each metal, incrementally increasing the applied current in discrete and equivalent steps, with EIS between each measurement to determine the change in resistance.

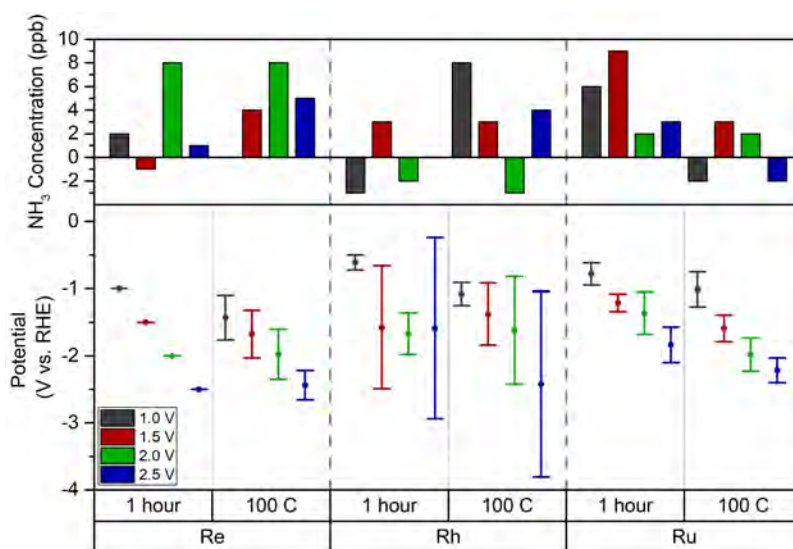


Figure 5.6 Potential vs RHE for CA measurements of Ru, Rh, and Re catalysts, with the measured concentration of ammonia for each experiment. As each measured concentration is below the 10 p.p.b. detection limit, the reported values are meaningless (hence some being negative). Each metal was tested either for 1 hour, or until 100 C of charge was passed for the potentials -1.0 , -1.5 , -2.0 and -2.5 V vs RHE . The bars span the change in potential throughout the measurement due to a changing Ohmic resistance. Reprinted from Reference [77]

We wanted to test the most promising pure metal catalysts (Ru, Re, and Rh) at set potentials. We therefore did measurements of EIS before, then ran a CA wherein we estimated based on the Ohmic resistance measured by EIS what the expected actual potential of the WE would be, and ended with another EIS. The Ohmic resistance after the measurement was used to estimate the range of potential which the WE actually experienced throughout the experiment. Appendix A.1.1 goes through the calculations of the WE potential. Some metals (particularly Rh) showed

very vigorous bubble formation, leading to huge changes in current, and therefore changes in the actual potential during the measurement. We aimed at carrying out measurements at four potentials, namely -1.0 V to -2.5 V in 0.5 V increments. Each experiment was carried out with CA either for 1 hour, or by passing a total of 100 C. The actual applied potential range is shown in Figure 5.6, additionally plotted with the measured ammonia concentration for each experiment. The measurement uncertainty of the indophenol method is ~10 p.p.b., meaning for all these pure metal catalysts in these potential intervals, no ammonia was synthesized.

WE / CE	Surface area (cm²)	Current (mA)	Potential range (V vs RHE)	Time (mins)	Comment
Ru / Ir	0.5	70-90	-[1.3, 3.3]	91.5	
		90-100	-[2.4, 4.2]	91.5	
		50-70	-[1.1, 1.6]	10	
		70-90	-[1.6, 2.1]	10	
		90-110	-[1.9, 2.5]	10	
		90-110	-[1.8, 2.3]	20	
		110-130	-[2.3, 2.9]	20	
		130-150	-[2.7, 3.0]	20	
		180-200	-[3.3, 3.9]	20	
Ir / Pt	1.5	50-70	-[1.0, 1.1]	10	
		90-100	-[1.3, 1.7]	17.5	
Fe / Ir	0.4	80-100	-[2.0, 2.6]	27	
		80-100	-[1.9, 2.4]	27	
		80-100	-[1.9, 2.4]	27	
		80-100	-[1.8, 2.4]	27	
		80-100	-[2.0, 2.6]	27	
		80-90	-[2.0, 2.4]	48	
		90-100	-[1.9, 2.4]	48	
Au / Ir	1.0	30-50	-[0.4, 0.7]	17.5	
		50-70	-[0.5, 0.8]	17.5	
		70-90	-[0.6, 0.9]	17.5	
		90-110	-[0.9, 1.1]	17.5	
		110-130	-[1.1, 1.5]	17.5	

WE / CE	Surface area (cm ²)	Current (mA)	Potential range (V vs RHE)	Time (mins)	Comment
Re / Ir	1.4	30-50	-[1.9, 2.5]	21.5	
		50-70	-[2.1, 2.7]	21.5	
		70-90	-[2.8, 3.4]	21.5	
		90-110	-[2.1, 2.6]	17.5	
		90-110	-[2.5, 3.1]	17.5	
Ni / Ir	1.2	6-8	-[0.9, 1.1]	140	100 C passed
		10-33	-[0.8, 2.0]	114	100 C passed
		13-45	-[1.4, 1.7]	77	100 C passed
		10-50	-[1.3, 2.3]	50	100 C passed

Table 5.6 All experiments with pure metal foils in two-compartment cell with Celgard membrane, 0.1 M KOH, and purified N₂. Applied current and estimated potential range shown. All metals (except Ni) done with SGEIS with equivalent steps. Ni experiments done with EIS, CA, then EIS. Not a single experiment synthesized ammonia. Example SGEIS spectra shown in Appendix A.1.2.

We also tested many other pure metal catalysts under various applied potentials by SGEIS. Some of the work is summarized in Table 5.6, wherein not a single experiment yielded any ammonia. The testing time might seem short, but an experiment with *e.g.* 100 mA for just 10 minutes gives 60 C of total charge passed. If we assume a FE of just 0.1% in our standard 7.5 mL volume of electrolyte, we can reorganize Equation 3.2 to yield:

$$C_{NH_3} = \frac{Q \cdot FE}{z \cdot F \cdot V} = \frac{60C \cdot 0.0001 \cdot 17.031 \text{ g/mol}}{3 \cdot 96485 \text{ C/mol} \cdot 7.5 \text{ mL}} = 0.047 \mu\text{g/mL} = 47 \text{ p.p.b.} \quad (5.2)$$

which should be detectable, as our background is <10 p.p.b. with gas cleaning.

5.3.2 Temperature dependence

A change in temperature was also investigated on a Ru catalyst, as this can change the equilibrium of the reaction. We used a heating/cooling jacket that allows for temperature control of the cell. For the experiments shown in Table 5.7, for the cooling experiments we used CP with PEIS before and after to measure the change in potential, and for the heating experiments we used SGEIS. It was seen that the potential and resistance change during these experiments was minimal, probably due to the temperature control of the cooling/heating jacket. Unfortunately,

this was only discovered after most of the foils had already been studied, so temperature control is not applied to Table 5.6.

Temperature (°C)	Current (mA)	Potential range (V vs RHE)	Time (mins)	Comment
2	50	-[2.3, 2.3]	10	
2	75	-[2.7, 2.8]	10	
2	100	-[3.0, 3.1]	10	CP with EIS
4	100	-[4.6, 4.7]	10	
6	130	-[5.6, 5.7]	10	
27	100-110	-[2.0, 2.3]	10	
40	100-110	-[1.8, 2.0]	10	SGEIS
60	130-110	-[1.4, 1.6]	10	

Table 5.7 Ru WE and Ir CE in 0.1 M KOH. The cell has a heating/cooling jacket to control the temperature. Applied current and estimated potential range shown. No synthesized ammonia measured.

5.3.3 Electrolyte pH

The choice of 0.1 M KOH as electrolyte was partially due to the reported literature, but also due to the competing HER. The overpotential for HER in alkaline media tends to be higher compared to acidic media [110]. This is due to the proton availability, as acidic media will have plenty of protons for HER to occur, while under alkaline conditions water splitting must supply the protons, which slows down the reaction rate. As HER is the dominating reaction for NRR in aqueous media, and limiting proton availability is a possible strategy for increased NRR [37], it was obvious to choose an alkaline electrolyte for the bulk experimentation. But we did also investigate both acidic electrolyte (0.1 M HClO₄) and neutral electrolyte (0.1 M NaClO₄).

Temperature (°C)	Current (mA)	Potential range (V vs RHE)	Time (mins)	Special comment
Room temp	80	-[4.5, 7.0]	10	CP + EIS
24	40-60	-[3.9, 4.2]	22	

Table 5.8 Two-compartment experiments with Ru WE, Ir CE in 0.1 NaClO₄. Applied current and estimated potential range shown. Neither experiment synthesized ammonia.

Table 5.8 shows the extent of experiments with 0.1 M NaClO₄, chosen as a neutral electrolyte. The measured WE potential for the neutral electrolyte was much higher than the alkaline electrolyte, and the resistance also changed significantly more throughout even a short 10 minute measurement. We suspect this was due to electrolyte heating near the electrode surface, as the cell noticeable heated throughout the measurement. The application of a 24 °C temperature controlled water bath helped decrease the change in resistance, but the measurement nonetheless yielded no ammonia.

Temperature (°C)	Current (mA)	Potential range (V vs RHE)	Time (mins)	Comment
Room temp	60-70	[-2.5, 3.1]	10	No temp control
	70-80	[-2.7, 3.5]	10	
	80-90	[-2.7, 3.6]	10	
	90-100	[-2.8, 3.9]	10	
	100-110	[-2.3, 3.7]	10	
	100-110	[-1.5, 2.6]	10	
	100-110	[-1.8, 2.7]	10	
	90-110	[-1.7, 2.2]	53	
	100-110	[-1.8, 2.7]	17	
	27	100-110	[-2.5, 2.7]	
100-110		[-3.1, 3.3]	10	
70-80		[-1.4, 1.9]	10	
80-90		[-1.7, 2.3]	10	
90-100		[-2.0, 2.5]	10	
100-110		[-2.3, 2.7]	10	
60	100-110	[-2.1, 2.3]	10	Heating jacket

Table 5.9 Two-compartment experiments with Ru WE, Ir CE in 0.1 HClO₄. Applied current and estimated potential range shown. No significant ammonia concentration was measured.

Table 5.9 shows some of the experiments with 0.1 M HClO₄, using a Ru WE, as that should be on top of the volcano plot for NRR [41]. The WE potential behaved similar to the alkaline electrolyte under acidic conditions. We also experimented with increased temperature, utilizing the heating jacket on the cell. None of these experiments yielded any quantifiable amounts of ammonia.

5.4 Summary

In this chapter, we attempted to do electrochemical nitrogen reduction in various different pH ranges for aqueous media. Before any electrochemical experiments could be started, the level of ammonia contamination and TE of the system needed to be addressed. In our experiments we found that:

- We could trap ammonia in the gas recirculation system with a TE up to 86 %, where the rest of the ammonia is expected to stick to the walls and pipes of the system.
- Ammonia oxidation on the CE is a serious issue in this system, and a two-compartment cell with a Celgard membrane (see Section 4.2.1) was used.
- The ammonia contamination in our lab was mainly from old chemicals, one of our pipettes, and the N₂ gas.

Once these sources of contamination were addressed, and the expected TE of the system was determined, electrochemical measurements were carried out. We tested some of the most promising pure metal candidates over a wide range of potentials in 0.1 M KOH. We also tested Ru as the WE at different temperatures, and in both neutral and acidic media. Ru was chosen for this, as the overpotential for this catalyst for NRR was comparatively low. Unfortunately none of these experiments yielded any significant amounts of ammonia compared to the background.

The conclusion to the aim mentioned in Chapter 2 regarding reproduction of any results from the literature is therefore an unfortunate "No" for aqueous media.

Chapter 6

Electrochemical Nitrogen Reduction in Non-Aqueous Solution

"Ford!" he said, "there's an infinite number of monkeys outside who want to talk to us about this script for Hamlet they've worked out."

— Douglas Adams, *The Hitchhiker's Guide to the Galaxy*

No matter what was attempted in Chapter 5, we had no success with electrochemical nitrogen reduction in aqueous solutions. This was roughly 1 year into my Ph.D., and the frustration we felt was almost palpable. When starting on non-aqueous systems, the very capable Dr. Jay Schwalbe, a friend and collaborator from Stanford, mentioned the work by Tsuneto et al. [54, 62] as a promising result. However, the reports had only verified their findings with simple blank tests. We (Dr. Viktor Čolić, Dr. Sungeun Yang, and I) therefore decided to attempt to replicate that experiment.

In this chapter, the following questions are addressed:

- Can we replicate the work by Tsuneto et al. with similar rates and efficiencies?
- What things do we need to be aware of in this system? What are the major sources of contamination? What might prohibit ammonia synthesis?

- Can we prove, with quantitative isotope labeled experiments, that we synthesize ammonia electrochemically in non-aqueous solution?

Since I already mentioned in Section 1.4 that managed to synthesize ammonia, it will not be a surprise to the reader that this system does indeed work. As we have quite thoroughly scoured the literature for any believable reports, a state-of-the-art is included at the end of this chapter, along with a discussion of the validity of most reported data in the literature.

The work in this chapter was carried out with the help of many different people, and I will therefore use "we". The work reported in Paper I, and partially discussed here, was carried out with Dr. Viktor Čolić and Dr. Sungeun Yang. The testing of various metals and salts was done in collaboration with the skilled Jakob B. Pedersen and Kevin Kreml, and the determination of the accuracy of our RE was done with Jakob B. Pedersen.

6.1 Lithium-mediated electrochemical nitrogen reduction

Working in non-aqueous electrolyte introduces a host of challenges that aqueous electrolyte does not have. To start with, we simply wanted to directly replicate the Tsuneto et al. experiment, and determine if any significant amount of ammonia was measured (box 1.1 and 1.2 in the flowchart of Figure 4.1).

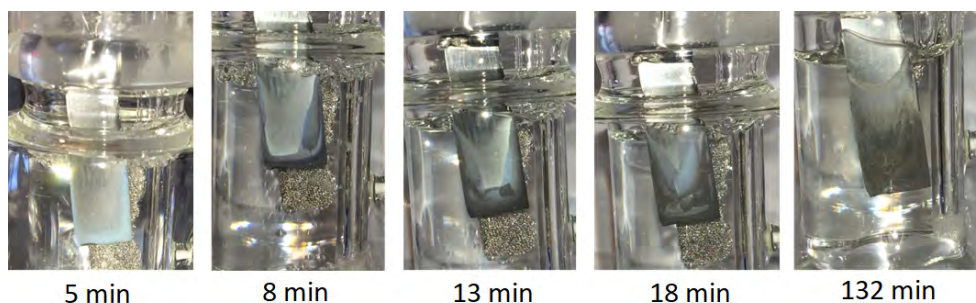


Figure 6.1 Backside of Mo foil electrode in 0.1 M LiClO₄ in THF with 1 % EtOH during electrolysis. Pt mesh CE visible in back.

Throughout the measurement, shown in Figure 6.1, the backside of the submerged foil was seen to gradually be covered by a white-ish film from the sides. This would creep towards the center of the backside, and started to slowly turn black. Presumably, this is reduced Li, that upon reacting (more on this in Section 7.4), turns black. The measurement was a 2-electrode measurement, with -9 V applied on the WE vs the CE, passing 20 C of charge just over 2 hours. The frontside of the foil was entirely black by the end of the measurement, while the back was

slowly covered. Within seconds of the electrode being exposed to air, the deposit turns white. Incredibly, when indophenol was done, the solution turned a bright blue (Eureka!).

As we had already developed a thorough procedure for ammonia contamination, the ammonia background was negligible for our measurements with simple Ar and N₂ blank experiments. However, we did have to develop a modified indophenol procedure, as the intensity of the ammonia peak was very dependent on the water content of the sample (the new procedure is described in Section 3.2.1). Once a calibration curve was made, we could start determining some of the important parameters of the system.

6.1.1 Referencing the potential

Unlike aqueous solutions, the use of a RE in non-aqueous solutions can be quite tricky, and is easily done wrong [111]. This is due to the lack of an established method to measure the electrode potential, as there is neither a primary RE, such as the SHE for aqueous systems, nor a redox reaction as stable as the Ag/AgCl available for the non-aqueous case [112].

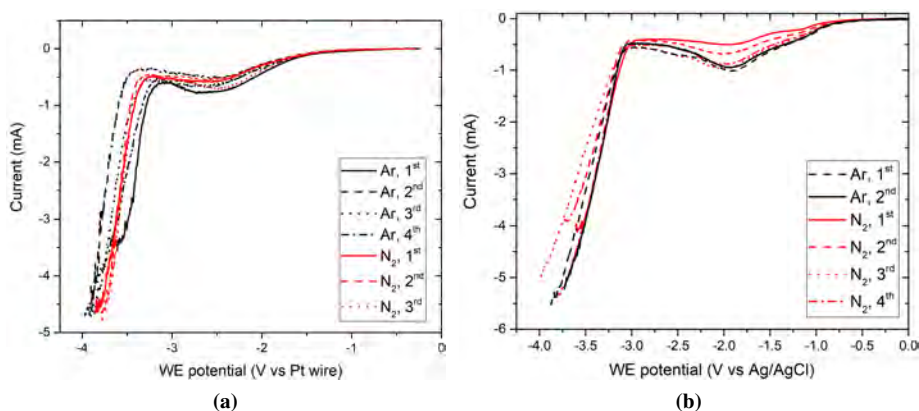


Figure 6.2 LSV graphs of a Mo WE and Pt mesh CE in 0.2 M LiClO₄ THF with 1 % EtOH. Repeated tests in N₂ or Ar gas, with a) a Pt wire as pseudo-RE, and b) a leakless Ag/AgCl RE.

A Pt wire can act as a pseudo-RE in a non-aqueous system [113]. This RE will lack a thermodynamic equilibrium and can exhibit drift in the potential during measurements. However, the use of a simple Pt wire minimizes possible contamination sources as it can easily be cleaned. It is seen in Figure 6.2a that the potential drift is around 400 mV for this pseudo-RE, as determined by the onset of Li reduction. We also tested a leakless Ag/AgCl reference electrode (eDAQ, ET-072) in PEEK. This RE was seen to initially be more reproducible for Li reduction (Figure 6.2b), however, over time, the Ag/AgCl RE degraded from use, and was therefore not

reliable. For all work in the lithium-mediated system, the Pt pseudo-RE is therefore used. The Li reduction potential is determined from the initial LSV, and the potential scale is referenced according to the Li/Li^+ scale. For the few measurements without Li reduction, the scale is roughly referenced *vs* RHE.

6.1.2 Electrolyte evaporation and NH_3 oxidation

THF has a very high vapor pressure of around 150 Torr at room temperature [114], and significant amounts of the electrolyte would therefore evaporate throughout a measurement. If the electrolyte is evaporating, a concern is that the ammonia might also evaporate. A test was therefore carried out with electrolyte with added ammonia from NH_4Cl salt. This electrolyte was injected into a cell under Ar atmosphere (not in the gas-circulation set-up), and 2 samples were taken to determine the concentration. The electrolyte was Ar purged for 2 hours, then another 2 samples were taken to estimate the concentration after $\sim 20\%$ electrolyte evaporation. Electrolysis in Ar with a current density of $2\text{ mA}/\text{cm}^2$ passing 20 C was done, and lastly another 2 samples were taken. This was repeated twice, and the result is shown in Figure 6.3.

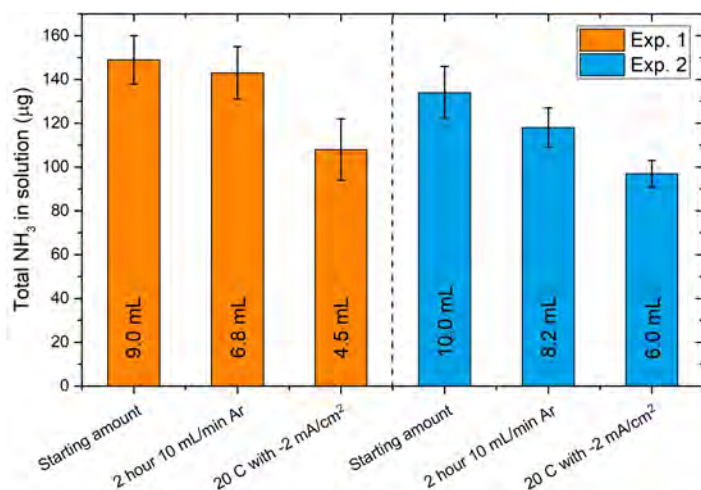


Figure 6.3 2 separate but similar experiments of electrolyte evaporation and oxidation. A Mo WE, Ir CE, and Pt RE was used in Ar atmosphere, with 0.2 M LiClO_4 in THF with 1% EtOH, with added ammonia from NH_4Cl salt. The NH_3 concentration is measured before each experiment, after 2 hours of purging with Ar, where some electrolyte has evaporated, and again after passing 20 C of charge with $-2\text{ mA}/\text{cm}^2$. Mean and standard deviation from 2 indophenol measurements of the same sample.

It is seen that some of the ammonia appears to leave the system with electrolyte evaporation, and that electrolysis additionally decreases the total amount of ammonia in solution. In a

closed system with recirculation of the gas and subsequent acid trapping/Ar purging after each experiment, one can re-trap some of the ammonia lost from electrolyte evaporation. A pre-bubbler with THF can also saturate the dry gas with THF prior to entering the cell, thereby significantly decreasing electrolyte evaporation in the first place. This was seen to completely eliminate the loss of ammonia due to gas purging over a 2 hour experiment. The amount lost to oxidation is, however, unrecoverable in this system. If a two-compartment system with a proper membrane is used, ammonia oxidation on the CE could be completely avoided. We unfortunately did not find a durable membrane for the use in non-aqueous electrolytes, and therefore had to accept the losses due to ammonia oxidation. This does however mean that our reported amounts of ammonia synthesized in this system are most likely underestimated, and our Faradaic and energy efficiencies are actually higher, if we could simply recover all the ammonia directly after synthesis. We currently have very little control (or knowledge) of the oxidation reaction on the CE. Ideally it should be HOR, if we could supply hydrogen straight to the anode, but that is not the case so far, and we therefore suspect the anode reaction is unfortunately solvent oxidation [115]. While this (if indeed that is the anode reaction) is a problem over long time, for now, it is not addressed in this thesis.

6.2 Systematic study

In this section, the lithium-mediated system proposed by Tsuneto et al. is rigorously proven to synthesize ammonia by isotope sensitive quantification. Different variations of the system are then explored, wherein the NH_3 concentration is determined by the indophenol method of a single sample from the electrolyte only (hence the lack of mean and standard deviations).

6.2.1 Rigorous quantified isotope labeled testing

Following the rigorous protocol suggested in Chapter 4, the reported system by Tsuneto et al. [62] that lacked the imperative isotope sensitive experiments was proven to synthesize ammonia. We used a two-electrode set-up with Mo WE and Pt CE in a single-compartment cell. Measurements were done in the gas recirculation system, passing the gas through the Cu impurity trap for cleaning. First, two simple background experiments were done, one with Ar gas wherein 20 C of charge was passed with an applied cell potential of -9 V, and two with respectively $^{14}\text{N}_2$ and $^{15}\text{N}_2$ gas at OCV for 1.5 hours. Neither experiment lead to any significant amounts of ammonia. Measurements with N_2 gas and a total applied cell potential of -9 V was then started, with 2 samples taken every 5 C, until a total of 20 C was passed in the system. This was repeated 3 times for both $^{14}\text{N}_2$ and $^{15}\text{N}_2$, and the resulting ammonia concentration was

determined both by the isotope sensitive NMR method and the colorimetric indophenol method (one sample for each method). The NH_3 measured in each experiment was quantified, and a comparison of the mean and standard deviation of the 3 identical experiments show overlap between the two methods, as expected for a proper NRR experiment.

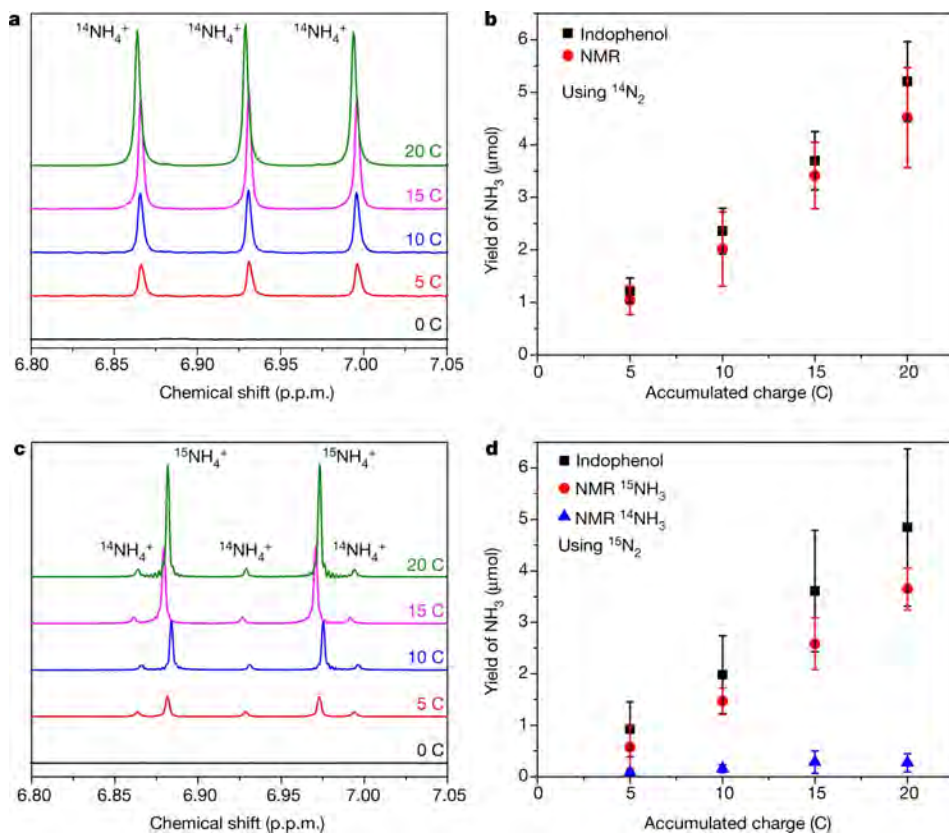


Figure 6.4 Mo WE with Pt CE in 0.2 M LiClO_4 in THF with 1% EtOH. Experiments with -9 V total cell potential with samples taken every 5 C from 0 C to 20 C charge passed. a), c) Representative NMR data from one experiment in respectively $^{14}\text{N}_2$ and 98% $^{15}\text{N}_2$ gas. b), d) Data of mean and standard deviation of 3 repeated experiments in respectively $^{14}\text{N}_2$ and 98% $^{15}\text{N}_2$, with ammonia measured either by indophenol or NMR. Reprinted from Paper I, Reference [77].

When using the 98% $^{15}\text{N}_2$ gas, NMR shows that some $^{14}\text{NH}_3$ is also formed due to $^{14}\text{N}_2$ impurities in the gas, which the colorimetric indophenol method cannot distinguish. As seen both from Figure 6.4 and the reported values in Table 6.1, there is similar amounts of NH_3 synthesized with the cleaned $^{14}\text{N}_2$ and $^{15}\text{N}_2$, proving the validity of the lithium-mediated system proposed by Tsuneto et al. conclusively.

Gas	Method	Mean yield rate ($\mu\text{mol h}^{-1} \text{cm}_{\text{geo}}^{-2}$)	Mean conc. for 20 C (p.p.m.)	FE (%)
$^{14}\text{N}_2$	NMR	0.7 ± 0.2	9.6 ± 1.6	6.5 ± 1.4
	Indophenol	0.8 ± 0.1	11.1 ± 1.3	7.5 ± 1.1
$^{15}\text{N}_2$	NMR	0.6 ± 0.1	8.3 ± 0.9	5.7 ± 0.7
	Indophenol	0.7 ± 0.2	10.3 ± 2.7	7.0 ± 2.2

Table 6.1 Reported values for the measurements shown in Figure 6.4

6.2.2 The role of the WE metal

As the process is now rigorously proven to synthesize ammonia, different variations of the system can be explored. One of the things tested by Tsuneto et al. was the WE metal. They concluded that the activity of the WE towards NH_3 is lowered if the WE metal alloys with Li. This is clearly seen for *e.g.* Au in Table 6.2 with a very low FE, which is due to the alloying of Au with Li in organic electrolytes [116]. Carbon paper and a graphite rod was interestingly also seen to work, albeit with a lower FE. One might expect something like Li_2C_2 to form, or - with enough O_2 - Li_2CO_3 . It is possible that the potential makes it unfavorable in this system, or that NH_3 synthesis might be possible regardless of the reaction with Li.

WE metal	WE potential (V vs Li/Li^+)	Current (mA)	Charge passed (C)	NH_3 conc. (p.p.m.)	FE (%)
Mo	-2.5	-[4.2, 4.5]	11.3	8.6	7.0
Ag	-3.0	-[3.3, 3.9]	16.0	7.5	6.6
Ti	-2.5	-[3.8, 5.1]	10.3	7.7	6.4
Ni	-2.4	-[2.2, 2.5]	5.5	6.5	4.1
Mg	-2.5	-[4.3, 5.8]	11.4	6.6	2.4
Au	-0.4	-[4.1, 8.9]	24.8	1.0	0.3
Carbon paper	-2.5	-[3.1, 4.2]	10.2	1.7	2.7
Graphite rod	-1.5	-[1.2, 3.0]	11.9	2.4	2.0

Table 6.2 CA measurements of different WE metal in 0.2 M LiClO_4 in THF with 1 % EtOH for 1 hour.

As we had plenty of high purity Mo available in the lab, we continued to use Mo for lithium-mediated nitrogen reduction experiments. Cu (tested by my colleagues, but not included here)

also gives similar results to Mo, however these were not used, as the performance deteriorates with re-use of the foils [55].

6.2.3 Testing other salts

Elements in the same group can exhibit similar chemical behavior due to the number of valence electrons available for bonding [51]. We therefore tested metal salts with the same or similar number of valence electrons as Li, shown in Table 6.3, as these might be similarly reactive. Tsuneto et al. [62] had previously claimed a very small activity towards ammonia synthesis on NaClO_4 under 50 bar. Interestingly, Na_3N is an extremely unstable alkali metal nitride, contrary to Li_3N [117]. It is not expected to form under these conditions, and their reported data therefore runs counter to their proposed mechanism of nitride formation, suggesting mild ammonia contamination of their set-up. Interestingly, our NaClO_4 salt also contained ammonia (easily determined and quantified by Ar blank experiments).

Salt (M)	WE potential (V vs Li/Li ⁺)	Current (mA)	Charge passed (C)	Comment
0.1 M $\text{Ba}(\text{ClO}_4)_2$	-7	<-0.1	1.0	Huge ionic resistance, even when electrodes were <0.5 cm apart
0.2 M $\text{Ba}(\text{ClO}_4)_2$	-6	<-0.1	1.0	Huge ionic resistance still
0.5 M $\text{Ba}(\text{ClO}_4)_2$	-4	-0.1	6.7	Small visible deposition
0.5 M $\text{Mg}(\text{ClO}_4)_2$	-9	-20 nA	-	Small resistance (40 Ω) but negligible currents
0.5 M NaClO_4	-4	-[2.2, 3.0]	10.1	Contamination of salt. Ar blank showed same amount of NH_3
0.2 M LiCF_3SO_3	-3.0	-[1.2, 2.0]	12.5	3.5 p.p.m. with 2.7 % FE
0.2 M LiBF_4	-0.5	-[1.0, 2.1]	4.0	1.1 p.p.m. with 2.0 % FE

Table 6.3 Testing of different salts with a Mo WE in THF with 1 vol.% EtOH with 10 mL/min N_2 flow. No ammonia was produced greater than the background contamination. The measured potential in the systems without Li is estimated from the Pt RE, since Li reduction cannot be used to scale after.

We had issues dissolving $\text{Ba}(\text{ClO}_4)_2$ salt in the electrolyte, leading to a huge ionic resistance in the system. With a molar concentration 0.5 M added to the electrolyte (although nominally the actual concentration is lower due to the dissolution issues), we could see a small visible deposition on the surface of the Mo electrode. Unfortunately, no ammonia greater than the

background was measured in any salt that did not include Li. For our system, LiClO₄ gives the highest yields, and is therefore used for the rest of the lithium-mediated nitrogen reduction measurements.

6.2.4 The importance of the proton source

In the current system, EtOH is a sacrificial proton source. Dr. Viktor Čolić carried out experiments with CH₃-CH₂-OD (deuterated EtOH on the OH group), which, via ¹H and ²H (or D) NMR, proved that the proton source in the system was the -OH group (measurements not included here, as I had no part in them).

Proton source (vol.%)	WE potential (V vs Li/Li ⁺)	Current (mA)	Charge passed (C)	Special comment or	
				NH ₃ conc. (p.p.m.)	FE (%)
0.1 % H ₂ O	-0.5	-[2, 8]	21.1	Unstable. Black dendrite growth	
1 % H ₂ O	-0.5	-1	3.8	Very stable. No visible deposit	
1 % 3-OH-THF	-0.4	[2, -10]	9.5	Highly unstable. Fluffy grey 0.5 mm deposit	
1 % 3-OH-THF 0.1 % EtOH	-0.3	-[2, 8]	13.3	Unstable. Fluffy black 0.5 mm deposit	
4 % H ₂	-0.1	-[5, 8]	6.4	Long, needle-like deposits. Electrolyte turned brown.	
4 % H ₂ 1 % EtOH	-0.5	-[1.5, 2]	6.2	2.4	3.6
1 % 2-butanol	-0.5	-[1.5, 2.0]	10	6.7	5.2
1 % 2-propanol	-0.5	-[1.0, 1.5]	10.5	7.9	7.9
1 % glycerol	-0.5	-[2.0, 2.5]	10	0	0

Table 6.4 Testing of different proton sources with a Mo WE in 0.2 M LiClO₄ in THF with 10 mL/min N₂ flow for 1 hour each. If no ammonia was produced, a comment on the stability of the CA measurement, along with any interesting observations, is noted instead. H₂ vol.% is in regards to N₂ supplied.

Experiments without EtOH (or a similar alcohol) as the proton source simply did not synthesize any ammonia, summarized in Table 6.4. Interestingly, glycerol also did not synthesize ammonia. We speculate this could be due to the structure of the molecule, as both

2-propanol and 2-butanol are secondary alcohols, and therefore more similar to EtOH compared to glycerol, which is a triole. A combination of H₂ and EtOH was also tried, in the hope that HOR occurs on the anode, and $\text{LiEtO} + \text{H}^+ \rightarrow \text{EtOH} + \text{Li}^+$ in solution, so the EtOH is not a sacrificial proton source and the Li ions can be reduced again. An interesting test (which will be done soon), is the use of D₂ gas and D NMR to prove the validity of this claim. Regardless, it seems that while adding some H₂ to the N₂ does synthesize ammonia, it also reduces the FE of the reaction. This could be because the excess H₂ in the system will form LiH on the cathode instead (as metallic Li also can reduce H₂), competing with nitride formation and thereby lowering the selectivity towards ammonia synthesis. In the ideal system, the anode and cathode are separated by a membrane, *e.g.* as the optimized system suggested by Lazouski et al. [55], which would enable the use of H₂ only on the anode.

Many of the experiments without EtOH lead to some interesting deposits forming on the WE. The experiment with 0.1 vol.% H₂O did not produce ammonia, but instead formed some long ~0.5 mm dendrites, seen in Figure 6.5. No ammonia was detected in any of the solutions which created these dendrites. Before taking out the electrode, 1 vol.% EtOH was added, causing the black deposits to dissolve rapidly. Unfortunately this did not lead to any detectable ammonia in the solution either, implying that the dendrite deposits are not Li₃N.

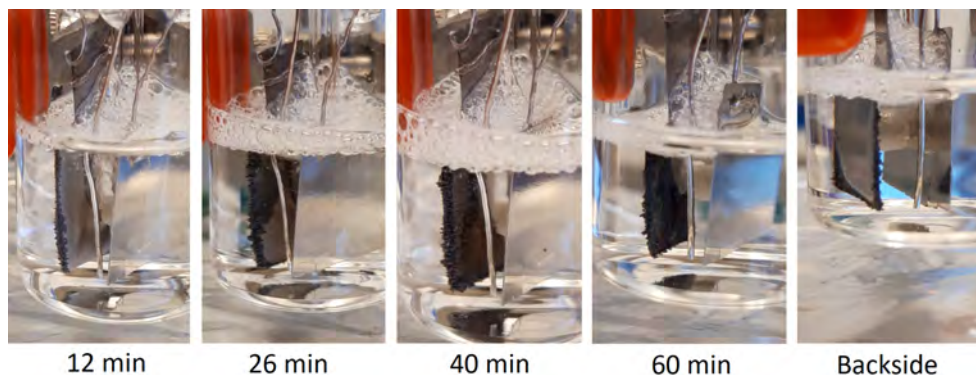


Figure 6.5 Mo foil electrode in 0.2 M LiClO₄ in THF with 0.1 % H₂O during 1 hour electrolysis at -0.5 V vs Li/Li⁺. Thick and "fluffy" looking 0.5 mm deposit on electrode clearly visible. Ir foil CE and Pt wire pseudo-RE also seen.

It was observed that for all samples without EtOH (or similar alcohols), thick, porous, or long dendritic deposits were observed on the surface (except for 1 % H₂O where nothing was visually observed). This could be because EtOH is somehow important for the formation of an SEI layer that allows the lithium-mediated process to occur [118], however this is highly speculative and difficult to prove.

6.3 State-of-the-art

We carried out an extensive literature study for both Chapter 5 and 6. The full list is included in Paper I, Extended Data Tables 1-4, Appendix B. Some of the more promising reports under near ambient conditions for electrochemical nitrogen reduction from 2018 and earlier is shown in Figure 6.6. We considered the extent of cleaning done prior to experimentation, and plotted the important values for these reports. It was clearly seen that very few reports actually carried out the necessary isotope labeled studies (red), and only a single study had quantitative isotope experiments with gas cleaning [119], which is the point labeled Fe/SS on Figure 6.6.

One of the more promising works with simple background tests was the reported data by Tsuneto et al. [62], now proven to synthesize ammonia earlier in this Chapter. Additionally, we have included a point for the data in Chapter 5 over aqueous NRR even though no appreciable amounts of ammonia exceeding the impurity level of our system was measured.

From Figure 6.6 and Extended Data Table 1 [77], it is easy to see that some of the "best" reported data in the literature do not bother with rigorous testing. Most do not even carry out simple blank tests to confirm if ammonia is a contaminant of the N_2 gas used [107, 120, 121], while some reports even include ammonia in the preparation steps [88, 122–124] without Ar blank testing. Other reports include fixed nitrogen compounds, like nitrate [125], amine [126, 127], nitrite, nitrous oxide, etc., which reduce much easier to NH_3 than N_2 . Simple Ar blank tests are *absolutely necessary* as a *first* approach to exclude these sources of contamination. Unfortunately, many reports do not even do this, and yet still claim high rates towards nitrogen reduction. We chose to exclude most of these works in the state-of-the-art overview figure, yet even when excluding many of these works, most of the remaining reports fall below a partial current density towards ammonia of $10 \mu A/cm^2$, leading to low concentration of detected ammonia. The contamination problem combined with the low catalytic performances results in high uncertainties in activity and selectivity benchmarking, bringing much of the published data on nitrogen reduction into question.

Furthermore, very few report the concentrations of ammonia measured in their experiment (starred data is our estimates based on information given in the reported work), which we believe to be quite important. If one has 100 mL electrolyte, and measures 0.1 p.p.m. of ammonia, one might conclude 10 μg of ammonia was synthesized. Similarly if one only has 1 mL electrolyte, but measures 10 p.p.m., the amount reported as synthesized is the same. However, we easily saw contamination of stock chemicals on the order of 0.1-0.3 p.p.m. if great care was not taken, which would render the first report completely invalid, while not altering the second report much. This alone is a reason to carry out simple blank measurements, and to report the concentrations measured, as this (along with all the other steps of the protocol) strengthens the

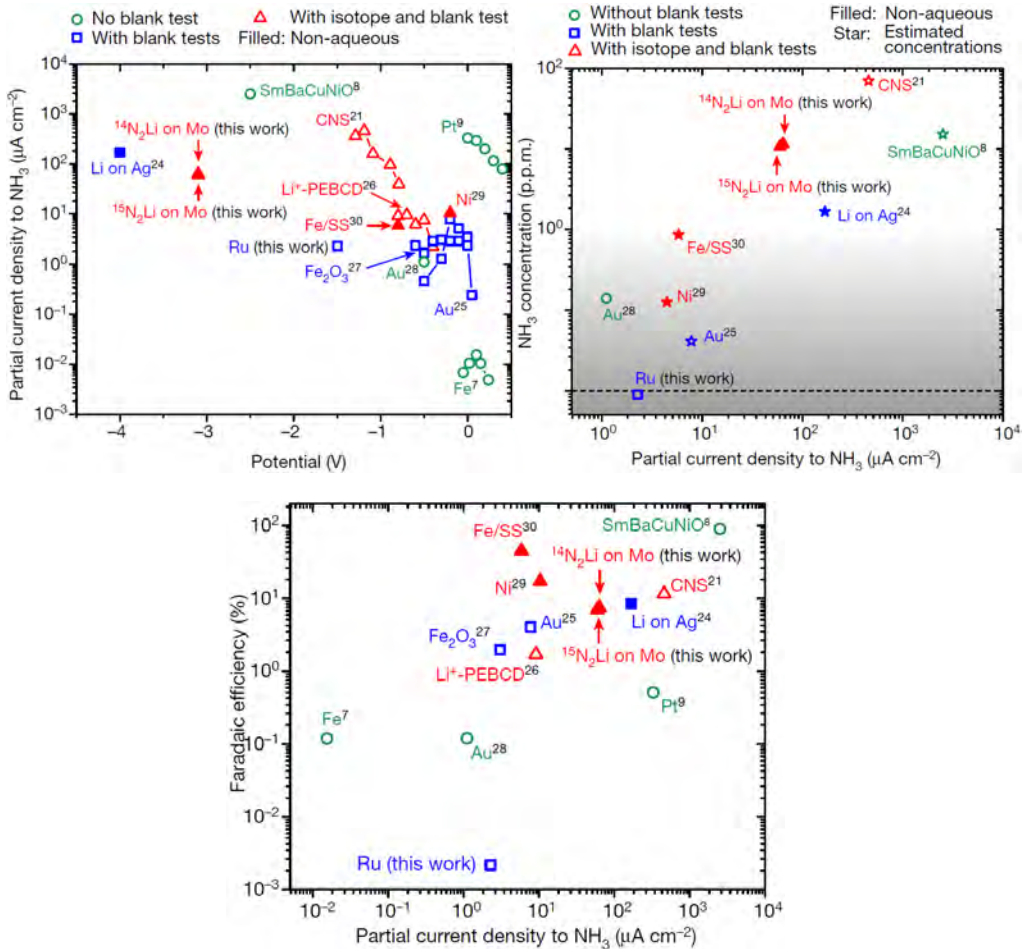


Figure 6.6 State-of-the-art up to 2018. Green colors are without any background measurements, blue colors include argon blanks and N_2 purging at OCV, while red denotes isotope labeled experiments. Filled symbols denote non-aqueous, and starred symbols are calculated estimations based on written information in the report. Citations do not correspond with references in this thesis. Reprinted from Reference [77] and included in Appendix B, wherein the accurate citation key is located.

claim of validity. Luckily, some scientists are starting to look through old data with greater rigour [128–130], leading to the discovery of published false positives. I can therefore only urge scientists to go through their procedure again, following the protocol, and thereafter correcting or retracting any work with false positives, as these works hinder or slow down the development of the field towards more efficient processes with higher yields.

6.4 Summary

This chapter validated the lithium-mediated system first proposed by Tsuneto et al. [54] as a way to synthesize ammonia. This was done by following the strict protocol suggested in Chapter 4. Some of the things we needed to consider when changing to non-aqueous solutions were:

- How to reference the potential.
- Electrolyte evaporation due to the higher vapor pressure of THF, and therefore the trapping efficiency in the system.

Once these new challenges were addressed, we could move on to rigorous and systematic testing of the lithium-mediated electrochemical nitrogen reduction process. This included:

- Quantitative isotope labeled experiments (!!!).
- Testing various different parameters, such as the WE metal, other Li and non-Li based salts, and various proton sources.

The results concluded that the original report was indeed a true positive in the literature. This leads to a resounding "YES!" to the aim mentioned in Chapter 2 regarding reproducing any result from the literature. Most of the literature considered was plotted in a state-of-the-art overview at the end of this chapter, along with some mild considerations towards the validity of much of the published data.

Chapter 7

Cyclic Stabilization of the Lithium-Mediated Process

"I may not have gone where I intended to go, but I think I have ended up where I needed to be."
— Douglas Adam, *The Long Dark Tea-Time of the Soul*

In Chapter 6, I reported data on the non-aqueous lithium-mediated process, first proposed by Tsuneto et al. in 1993 [54]. All data in that chapter utilized either continuous CP or CA techniques, running for a few hours at most. During that time, the total cell potential would be slowly increasing, and in some cases, the system would overload since our potentiostat is limited to the range [-10 V, 10 V].

I have developed a method which is proven to be stable over days, far beyond anything every reported in literature, while continuously synthesizing ammonia. This method increases the FE by almost a factor 2, and the energy efficiency by a factor 3. A patent is filed for this method, and all the data presented will be covered in Paper IV, which is currently in preparation. I have personally carried out all the experimental work, with help from Sarah G. Shapel as a M.Sc. student who took a special course in electrochemical nitrogen reduction with me. All work in this chapter is done in a home-built electrochemical autoclave (Otto) at 10 bar, covered in Section 3.1.2. The chapter will cover the usual method to do lithium-mediated experiments, then my cycling method for comparison. *Ex-situ* measurements of electrode composition before and after both methods for comparison will also be shown, as well as a discussion of the advantages and disadvantages of the method. Lastly, I will briefly cover some theoretical work for this method, which is entirely made by the talented Michael Statt and Dr. Vanessa Bukas.

7.1 Constant current deposition

When attempting to carry out long time CP measurements, the WE potential was always seen to initially drop in the first 20 minutes, then semi-stabilize for some time, only to then suddenly start dropping rapidly. This is seen very clearly in Figure 7.1, for 3 repeated experiments in Otto with 2 mA/cm^2 applied current density, that all overload the potentiostat. The mean and standard deviation for all three experiments was $21.2 \pm 1.6 \%$ in FE and $2.3 \pm 0.3 \%$ in energy efficiency.

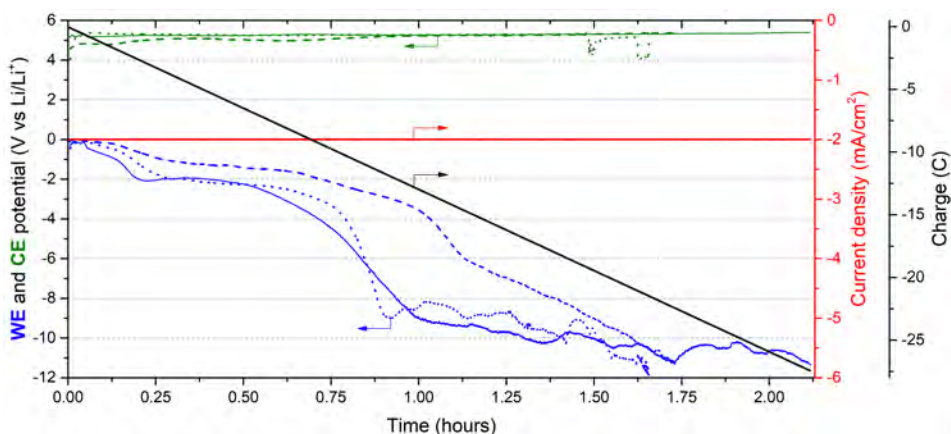


Figure 7.1 CP of three repeated experiments in Otto at 10 bar N_2 . Constant current applied at 2 mA/cm^2 in system with Mo WE, Pt CE and RE, in 0.3 M LiClO_4 in THF with 1 % EtOH.

For the lithium-mediated process, it is hard to achieve stability during a constant deposition experiment. Even Tsuneto et al. experienced "*in most cases, the uncorrected electrode potential was initially about -4 V and shifted gradually in the negative direction during the electrolysis, whereas it was difficult to measure the electrode potential precisely because of IR drop*" [54]. We have seen this for most experiments as well, and published literature on this system does not acknowledge this. In Figure 7.2, a representative figure of CP in literature is shown, and a total cell potential of -9 V estimated. I have plotted the first 40 minutes of one of the curves from Figure 7.1 for comparison. The report [55], which is in many other ways one of the best papers in the field due to its use of thorough experimentation and quantifiable isotope labeled experiments, does not at any point mention anything about the stability of their system, which is a huge issue for the lithium-mediated process. It is of course possible that their system does not behave similar to mine after 40 minutes, but for the data shown, there is a clear drift in the total cell potential over time, and the system is not stable in this operational window. The main

difference between the report and my data is the use of a membrane. This will prevent ammonia oxidation at the CE, which the report showed was quite significant in their system. It allows control of the CE reaction, so HOR can become the source of protons, rather than EtOH or solvent break-down, which is the case for my system. The membrane does however add to the Ohmic resistance, increasing the total cell voltage of the system.

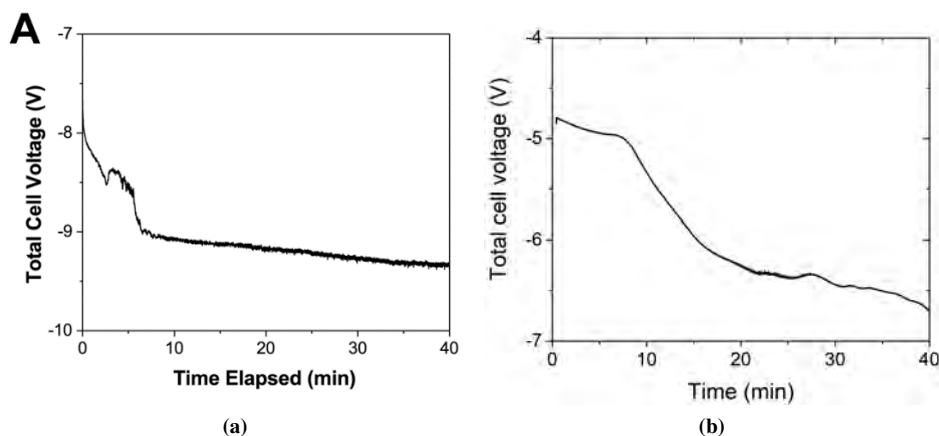


Figure 7.2 a) Typical CP, which only shows a 40 minutes experiment at 3 mA/cm² with a membrane. Figure reprinted with permission from Reference [55]. Copyright 2019 Elsevier Inc. b) Total cell potential for one of the experiments shown in Figure 7.1 shortened to only show a similar time range with 2 mA/cm² in a single compartment cell.

I suspect that the instability of the lithium-mediated process is due to a build-up of passivating Li species on the electrode surface. It was previously speculated that if the Li reduction happens at a very high rate, metallic Li will deposit onto Li species that has yet to react [55]. This is both inefficient, as current is basically wasted forming species that do not undergo a favorable reaction, and leads to increased resistance in the cell, as the Li ions in solution are slowly depleted. The electrode surface can also slowly passivate due to this gradual build-up, which increases the WE potential.

7.2 The cycling method

To circumvent the issue of build-up of Li species on the electrode surface, I developed a cycling method. This method involves switching between different current densities during a CP measurement. The first is a short Li reduction step, where I apply -2 mA/cm² for 1 minute, hereafter called the "deposition" step. The second step is a longer "resting" step, wherein the

current density needs to either be so low that Li reduction does not occur, 0 mA, or slightly positive. The resting time is variable, typically starting with 3 minutes, then increasing up to 4-8 minutes, depending on how stable the experiment is. The measurement shown in Figure 7.3a is representative data of 2 repeated stable 100 C experiments, which had a mean and standard deviation of $36.8 \pm 1.3\%$ in FE, and $7.1 \pm 0.2\%$ in energy efficiency.

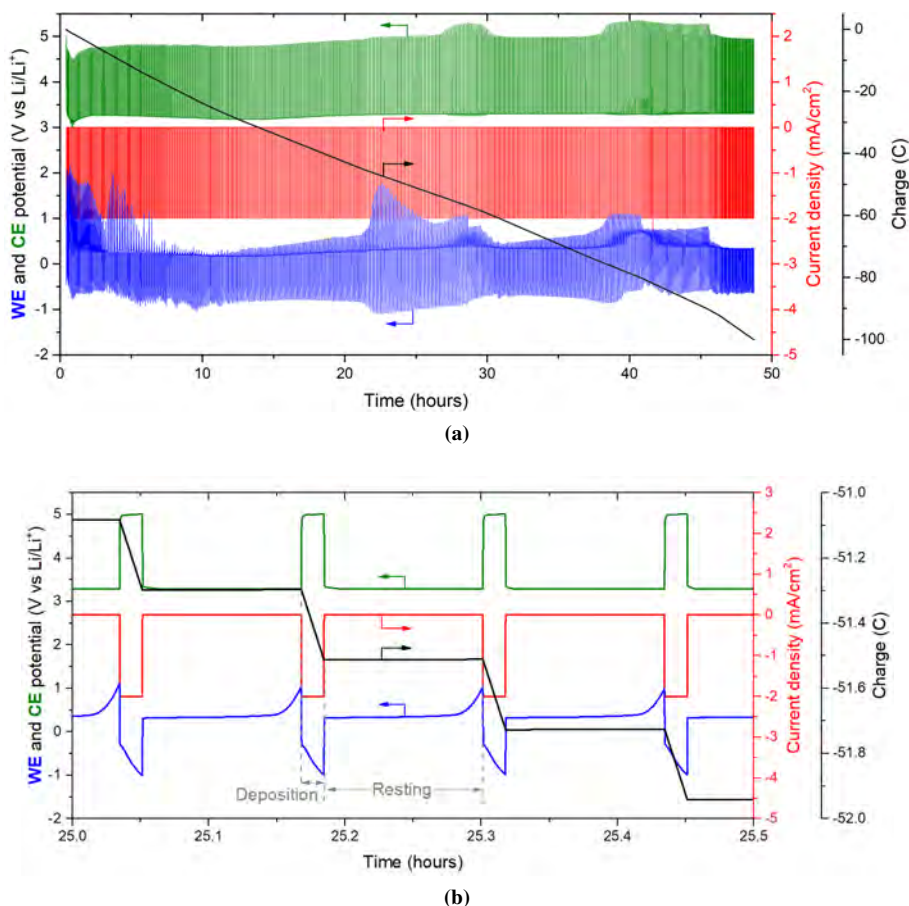


Figure 7.3 a) Cycling between -2.0 and 0.0 mA/cm² (red), passing 100 C of charge (black), with the WE potential (blue) and CE potential (green) as stable across the experiment. The potential is controlled by varying the resting time, which can be seen as the slope of the charge passed. b) A close-up of the cycling. When applying a deposition current, the WE potential increases cathodically across the entire 1 minute deposition. When switching back to resting, the WE potential is initially stable just positive of 0 V vs Li/Li⁺, until it eventually starts increasing anodically due to Li species fully dissolving from the surface. At this point, another Li depositing pulse is applied. System with Mo WE, Pt CE and RE, in 0.3 M LiClO₄ in THF with 1 % EtOH at 10 bar N₂.

By applying these short deposition pulses, a small amount of Li ions are reduced onto the electrode surface. The subsequent resting pulse then gives enough time for the deposited Li to chemically react and dissolve off the surface. This prevents a build-up of Li species, and significantly prevents the WE potential from drifting cathodic over time. Essentially, during the resting step, the surface is more or less "reset" in each cycle, which additionally can replenish the Li in solution. During the resting step, the WE potential appears stable for some time, before increasing anodically, as seen in Figure 7.3b. I interpret this anodic shift as the point at which all the Li species is dissolved, and the deposition pulse can therefore be applied again, restarting the whole cycle. By varying the resting time, the WE potential during deposition is kept below -1 V vs Li/Li^+ , which increases the energy efficiency of the system, as the gradual drift to highly cathodic potentials is prevented. Over these day-long experiments, I would check the measurement every 1.5 hours (even waking up repeatedly during the night), and adjust the resting time as needed. When the WE potential during the resting reaches the point of changing anodically, a new deposition pulse should be applied. The change in resting time is reflected in the change of the slope of the charge passed, which looks continuous when looking at the whole spectrum in Figure 7.3a, but is in fact in discrete intervals as seen in Figure 7.3b. The variations in the potential is due to this 1.5 hour checking, as sometimes the resting time was not changed fast enough (*e.g.* near the 21-22 hour mark).

Interestingly, in both the constant current case and the cycling, and really any measurement I have done on the lithium-mediated process, there is an initial increase in total cell voltage in the very beginning of the measurement. This is seen most clearly on Figure 7.1 occurring from 1-15 minutes, but it also appears on the cycling experiments. I hypothesize that this initial increase in WE potential stems from increasing thickness of the initial SEI layer formation, which remains throughout the experiment. During the deposition and resting steps of the cycling process, the SEI layer will probably increase/decrease in thickness, causing changes in the WE potential. It could however also be due to an initial build-up of passivating Li species from inherent oxygen and water contamination in the set-up. These might not chemically dissolve off the surface, as lithium hydroxide and lithium oxide are stable species.

7.2.1 Quantitative isotope labeled study and background measurements

In Chapter 6, the lithium-mediated system was proven to synthesize ammonia by following the rigorous quantitative protocol presented in Chapter 4. However, since Otto is a slightly different system, background testing it still necessary.

An Ar blank measurement with Ar purged electrolyte and 10 bar of Ar gas was carried out with the cycling method, passing 100.7 C (the extra 0.7 C is due to me being *slightly*

sleep-deprived throughout these day-long experiments). A total of $15 \pm 2 \mu\text{g}$ of ammonia was measured, corresponding to around 0.5 p.p.m. of ammonia. Another experiment with N_2 purged electrolyte at 10 bar N_2 was also set up, and left to measure OCP for 24 hours. This yielded $11 \pm 1 \mu\text{g}$ ammonia, for a total of 0.4 p.p.m in the electrolyte. There is an inherent amount of contamination in Otto, simply because each long cycling experiment makes comparatively large amounts of ammonia, even above 100 p.p.m. for some measurements. Ammonia is a rather sticky molecule [103, 104], so it will stay on Otto's walls and pipes, and is therefore hard to clean completely. However, as we are making 1-2 orders of magnitude more ammonia in *each* electrochemical measurement, this contamination is insignificant in comparison, as long as it is accounted for and regularly checked.

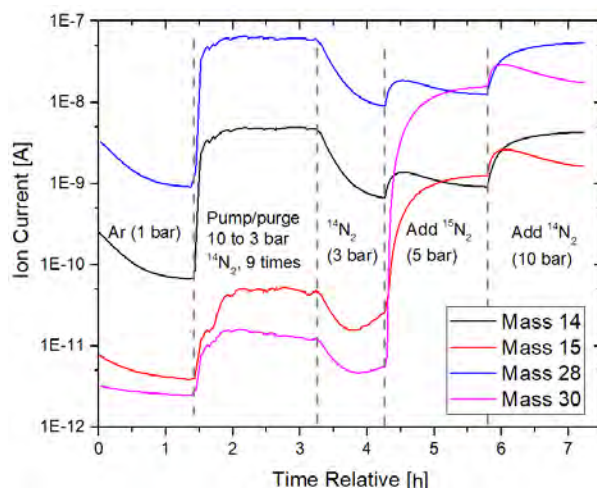


Figure 7.4 MS spectrum of masses 14, 15, 28, and 30 during the set-up procedure for the isotope labeled experiment in Otto. Absolute pressure denoted in parentheses for different steps.

I spent all of Chapter 4 and Paper IV preaching that quantitative isotope measurements are necessary to prove ammonia synthesis, so of course that needed to be done. Because the lithium-mediated system has already been proven to synthesize ammonia, I did a single isotope measurement for the cycling method in Otto (counter to what I state in the flowchart). I only need to show that quantitative isotope NMR corresponds to the colorimetric indophenol, not prove that the system synthesizes ammonia, as that has already been done. Because Otto's internal volume is $\sim 380 \text{ cm}^3$, and all autoclave experiments use 10 bar, Otto could not be entirely filled with only $^{15}\text{N}_2$ (that would also be prohibitively expensive). The purchased $^{15}\text{N}_2$ gas bottles are 416 mL in volume, with roughly 5 L compressed gas. A pump/purge procedure was done 9 times (as described in Section 3.1.2), ending with an absolute pressure of 3 bar with

$^{14}\text{N}_2$ in Otto. $^{15}\text{N}_2$ was then added until the absolute pressure was 5 bar, followed by filling the remaining 5 bar with $^{14}\text{N}_2$, ending at a total of 10 bar with a $^{14}\text{N}_2$ and $^{15}\text{N}_2$ gas mixture. The pressure gauge on Otto goes up to 100 bar, so it is not very exact for measuring small differences in pressure. Since the exact composition of the gas prior to starting measurements was needed, a QMS was connected to Otto.

The connection is a 1 μm gasket placed with $\sim 5\text{ cm}^3$ of dead volume, so the MS data stabilizes with roughly 1 hour delay from the moment the pressure is changed in Otto. This is clearly seen in Figure 7.4, wherein the dashed lines denote changes in pressure. To estimate the gas ratio, the main MS peaks (masses 28 and 30) and the double ionization peaks (masses 14 and 15) can be used for $^{14}\text{N}_2$ and $^{15}\text{N}_2$ respectively. Due to electrolyte evaporation, mass 15 is convoluted with contributions from both EtOH and THF. These contributions are significant in the regime before $^{15}\text{N}_2$ is added, but does not contribute significantly when fully pressurized. To determine the final ratio of $^{14}\text{N}_2$ to $^{15}\text{N}_2$, the ratio between respectively mass 28 vs 30 and mass 14 vs 15 is used. The final amount is $78 \pm 2\text{ rel.}\%$ $^{14}\text{N}_2$ and $22 \pm 2\text{ rel.}\%$ $^{15}\text{N}_2$, where the amount is the mean and the uncertainty is the standard deviation of the 2 ratios.

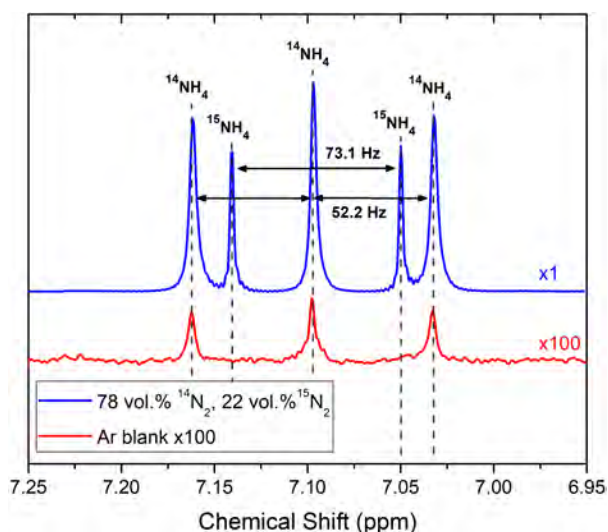


Figure 7.5 NMR spectra of the ammonia composition in the isotope labeled cycling experiment with a mixture of $^{14}\text{N}_2$ and $^{15}\text{N}_2$ (blue), and the ammonia concentration in the cycling 100.7 C Ar blank experiment (red) multiplied by 100 for ease of viewing.

Once electrolysis is started, similar ratios of $^{14}\text{NH}_3$ and $^{15}\text{NH}_3$ should be measured using isotope sensitive NMR as those of the supplied $^{14}\text{N}_2$ and $^{15}\text{N}_2$. The total amount of ammonia measured in NMR should additionally be similar to the amount measured by indophenol. A CP

measurement identical to the 2 repeated measurements for the cycling method in the previous section, passing a total of 100 C cycling between -2 mA/cm^2 for deposition and 0 mA/cm^2 for resting, yielded a $^{15}\text{NH}_3$ concentration of 15.6 p.p.m. and a $^{14}\text{NH}_3$ concentration of 67.1 p.p.m, adding up to 82.6 p.p.m. in total. This makes the ratio 82 rel.% $^{14}\text{NH}_3$ to 18 rel.% $^{15}\text{NH}_3$, not far from the ratio of gasses added. Indophenol on the sample gave $81.3 \pm 4.2 \text{ p.p.m.}$, in perfect accordance with the NMR. The mean and standard deviation determined by indophenol was $37.6 \pm 1.9 \%$ for FE, and $6.2 \pm 0.3 \%$ in energy efficiency. These values also match with the identical experiments using $^{14}\text{N}_2$ gas in the previous section, proving the system makes equal amounts of ammonia, regardless of the isotope of N_2 gas used (as is to be expected).

7.2.2 Long-term stability

To prove that the cycling method works for even longer than just 100 C, I set out to do a week long experiment. The CP shown in Figure 7.6 spans 5 days; an unprecedented long measurement time in electrochemical nitrogen reduction (not quite a week, but I was exhausted from sleep deprivation). This measurement passed over 180 C, and by varying the resting time, I could control the WE potential. There is a drift of the CE potential throughout the measurements, and interestingly the Pt RE had turned black at the end of the measurement. I suspect this could be due to Li intercalation into the Pt, as flame-annealing it afterwards turned the flame a bright white in the first few seconds. Unfortunately, this means the potentials are not very exact, but assuming they are, the experiment yielded a mean and standard deviation of $33.1 \pm 0.1 \%$ in FE and $5.2 \pm 0.2 \%$ in energy efficiency. The measured ammonia concentration was $111 \pm 4 \text{ p.p.m.}$ in 29.5 mL electrolyte, the highest recorded in my Ph.D. (hurrah!).

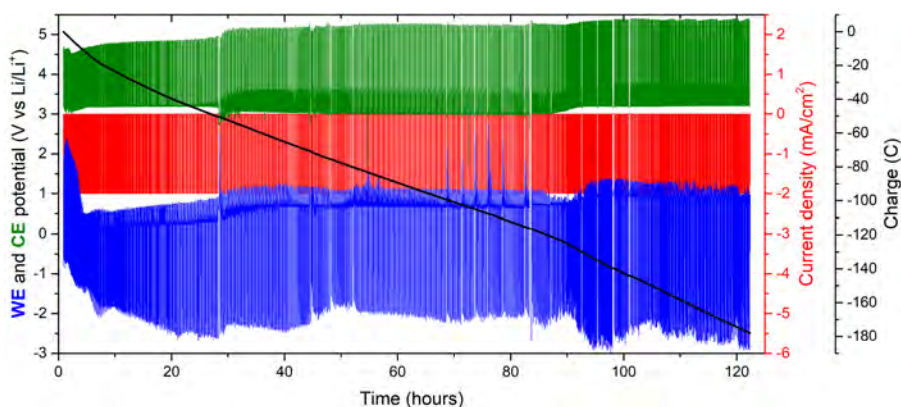


Figure 7.6 CP of longer measurement. System with Mo WE, Pt CE and RE, in 0.3 M LiClO_4 in THF with 2% EtOH at 10 bar N_2 .

I believe the FE was slightly lower due to the increase in EtOH concentration. As I expected to pass a significant amount of charge, I used 2 % EtOH instead of the standard 1 %. Under the assumption that every single proton comes from EtOH and makes either H₂ or NH₃, 180 C leads to 1.9 mmol of EtOH consumed. 1 % EtOH in 30 mL electrolyte corresponds to 5.2 mmol EtOH, and 1.9 mmol of this would therefore decrease the EtOH concentration by 37 %. To avoid a possibly detrimentally low EtOH regime observed previously in a similar system by Lazouski et al. [55], I therefore used 2 % EtOH for this experiment. An increased EtOH concentration was also shown to negatively impact FE [55, 62] due to increased availability of protons towards H₂ formation. But an increase from 1 to 2 % should not decrease the FE prohibitively much, which was also observed, as the FE went down to 33.1 ± 0.1 %, instead of the 37.6 ± 1.9 % reported for 1 % EtOH.

7.2.3 Advantages of the cycling method

Hypothetically, it should be possible to do a continuous deposition experiment with Li, wherein there is a perfect balance between the amount deposited, and the amount of Li dissolving when synthesizing ammonia. In actuality, all the deposited Li cannot completely form a nitride, especially not at a high deposition rate. Some will be covered with more reduced Li before it has time to react, while some will react with *e.g.* EtOH to form a hydride, or even with contamination in the set-up forming some unreactive or passive Li species, which will cover the electrode slowly. When applying a resting time, these species are given time to chemically dissolve off the surface, clearing away the build-up of Li species on the electrode. Additionally, as seen from the data in Table 7.1, the cycling method also leads to increased FE and energy efficiency compared to the constant deposition experiments. The main disadvantage of this method is the increase in time, and therefore the rate of ammonia formation. For the constant deposition, the rate is on the order ~ 150 $\mu\text{g}/\text{hour}$, with the caveat that it is not sustainable for much more than 2 hours in this system. The cycling sample (assuming a continuous production) has an average ammonia formation rate around ~ 45 $\mu\text{g}/\text{hour}$ for the same electrode, but can operate for days. All measured experimental values for each experiment in this chapter is summarized in Table 7.1.

Visual inspection of the electrodes show quite a significant difference between constant deposition and the cycling method, as seen in Figure 7.7. The constant deposition electrode, despite passing much less charge and running for much shorter time, had significant build-up of Li species on the surface. These deposits were as thick as 1 mm, completely changing the morphology of the surface. The cycling method on the other hand has no visual build-up. There is a bit of dried electrolyte on this sample, as I did not rinse the electrodes, due to the

Sample name	FE (%)	Charge passed (C)	NH ₃ (μg)	Conc. (p.p.m.)	Vol. (mL)	Energy efficiency (%)
Constant 1 (IP)	20.2 ± 1.0	27.4	325 ± 16	10.0 ± 0.5	32.5	1.8 ± 0.1
Constant 2 (IP)	21.3 ± 1.2	21.4	267 ± 15	9.4 ± 0.5	28.5	2.2 ± 0.2
Constant 3 (IP)	22.2 ± 0.5	22.3	293 ± 6	11.0 ± 0.2	26.7	2.8 ± 0.1
Cycling 1 (IP)	36.4 ± 0.4	100.0	2143 ± 22	72.6 ± 0.7	29.5	7.4 ± 0.1
Cycling 2 (IP)	37.2 ± 1.2	100.0	2188 ± 70	53.7 ± 1.9	37.8	6.8 ± 0.2
Cycling 3 (Isotope, IP)	37.6 ± 1.9	100.0	2212 ± 114	81.3 ± 4.2	27.2	6.5 ± 0.4
Cycling 3 (NMR: ¹⁵ NH ₃ / ¹⁴ NH ₃)	38.2	100.0	423 / 1823	15.6 / 67.1	27.2	6.6
Cycling long (IP)	33.1 ± 1.0	178.3	3470 ± 104	111.0 ± 3.5	29.5	5.3 ± 0.2
Ar blank (IP)		100.7	15 ± 2	0.5 ± 0.1	28.0	
Ar blank (NMR)		100.7	12	0.4	28.0	
N ₂ OCV (IP)			11 ± 1	0.4 ± 0.1	30.4	

Table 7.1 The mean and standard deviation for each experiment stems from 3 indophenol (IP) samples of the electrolyte, which has minor spread due to human inaccuracy when pipetting. Each repeated sample name denotes identical experiments. Cycling 3 used isotope labeled gas, and was therefore measured with both indophenol and NMR. NMR was done on 2 samples; 1 diluted to be in the correct calibration range, and 1 not diluted to check that the dilution ratio was accurate. The data for the diluted sample multiplied by the dilution ratio is included here, while the NMR spectrum for the undiluted sample is shown in Figure 7.5. The amount of ammonia in μg is the total ammonia measured in both electrolyte and water trap, whereas the concentration only denotes ammonia in the electrolyte.

lack of mechanical stability of the deposited Li flakes on the constant deposition sample. The cleanliness of the cycling method sample correlates with the theory that the experiment is stable due to the cyclic reduction of Li and subsequent chemical dissolution of Li species from the

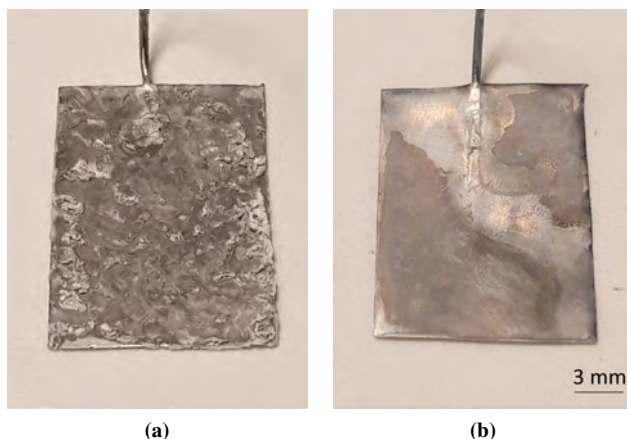


Figure 7.7 a) Picture of Mo electrode after constant deposition CP, passing around 20 C. b) Picture of Mo electrode with cycling method, passing a total of 180 C.

surface during resting. This method will not clog up the surface with passive species, leaving the electrode much cleaner and smoother after measurements, leading to stable and reproducible experiments.

7.3 *Ex-situ* characterization of electrodes

Although air exposure will significantly change the electrode composition, *ex-situ* characterization of the electrodes can still give some information about the difference in composition between the constant deposition sample and the cycling method sample.

7.3.1 SEM and EDX

SEM was used to look at the surface morphology of the different samples. This worked well for the plain Mo foil and the constant deposition sample, but the cycling sample was inexplicably difficult to look at. A low energy (5 kV) electron beam had to be used at all time, and magnifying the sample more than x1000 was impossible, as the surface of the sample would simply evaporate due to beam damage (seen in Appendix A.2). This beam damage effect occurred on the entire cycling sample surface, but not on the Mo foil or constant deposition sample, wherein a higher (15 kV) beam energy could even be used for better imaging, even up to x5000 magnification.

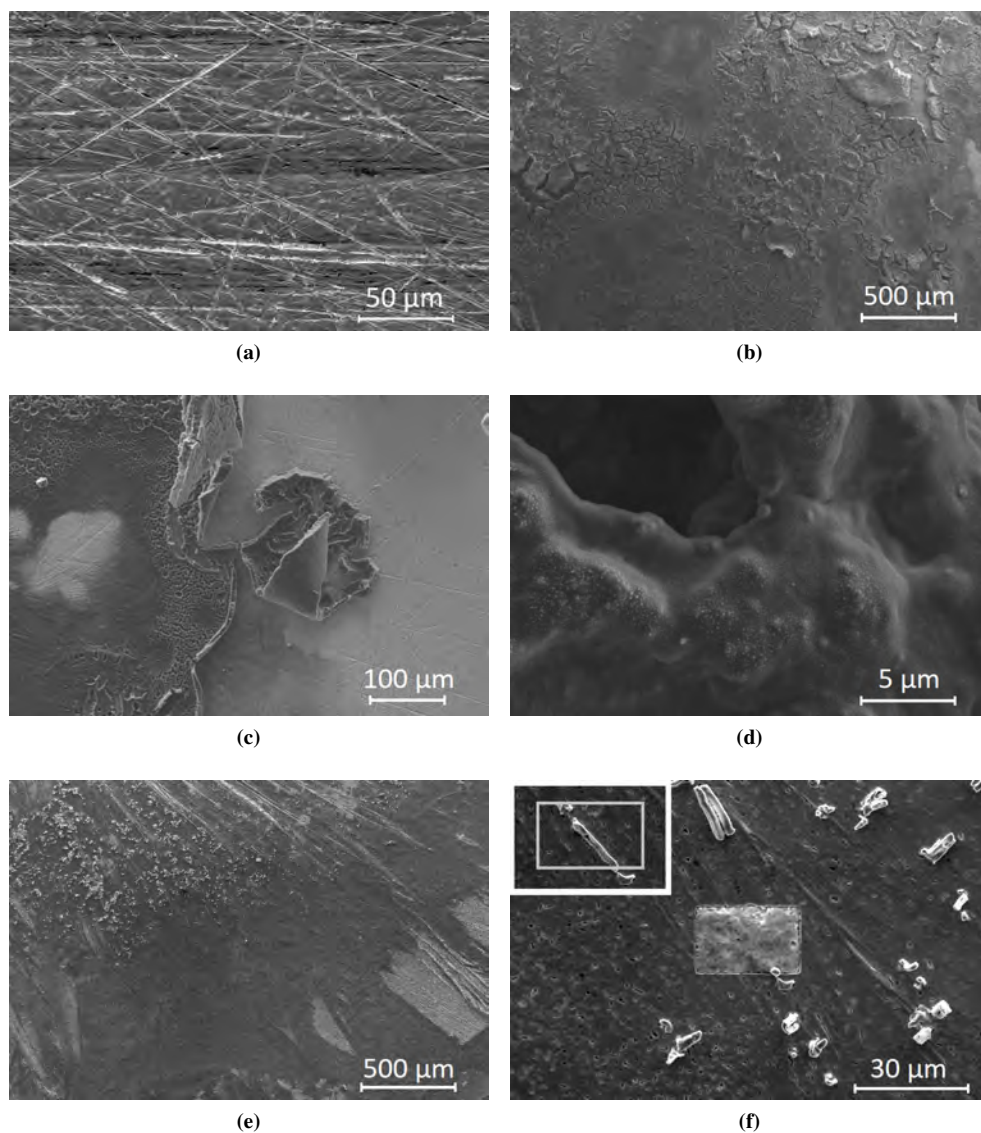


Figure 7.8 SEM image of a) polished Mo electrode b) constant deposition sample c) constant deposition Li species flake clearly almost de-attached from Mo foil surface d) zoom of constant deposition surface e) cycling sample overview with area of whiskers f) whisker before (inset) and after attempting to zoom.

The polished Mo foil seen in Figure 7.8a has a quite rough surface structure. Various different grains of polish had been tested, but appeared to make no difference on the amount

of ammonia produced, so a simple Si-C paper was used. Figure 7.8b-d shows the constant deposition sample. This had a very rough sample surface, with big flakes that look as if they have peeled off the Mo foil. After experiments, there is a lot of flakes suspended in the electrolyte, which gradually dissolve. These are expected to form on the WE surface, then disconnect due to stirring, and eventually dissolve in the electrolyte. One such flake is clearly seen on top of the Mo foil surface in Figure 7.8c, which appears to be around $\sim 10 \mu\text{m}$ thick. A close up of the deposited Li species reveals an uneven and rough surface. The cycling sample (Figure 7.8e-f) looked quite different. On most of the sample, the Mo foil was visible underneath a thin layer of Li species. There was interestingly also a spot roughly 1.5 mm^2 wherein whiskers had formed, seen in the upper left corner of Figure 7.8e. Any attempt at getting a closer look at these whiskers (or on any part of the sample really), resulted in the surface literally disappearing under the applied electron beam, as seen in Figure 7.8f, wherein the inset shows the whisker before attempting magnification. The whiskers can stochastically grow through the inhomogeneous SEI layer [131], which certainly changes during the cycling, due to the various chemical reactions and dissolutions taking place. More SEM images is included in Appendix A.2.

To get an idea of the surface composition of the samples, EDX was also carried out. The Mo foil (not shown) mainly contained Mo, C, and O, but also showed a small Ca peak (0.08 at.%) as a contaminant. The place for EDX on the constant deposition sample clearly showed both the Mo foil substrate, and the deposited Li species on top, seen in Figure 7.9. Li can unfortunately not be seen via EDX [132], but the Mo substrate is easily distinguishable, and the oxygenated Li species is also quite clearly seen as appearing on top of the Mo foil. C and Cl is seen everywhere, originating from dried electrolyte, although the Cl atomic percentage is quite low for the constant deposition sample. Oppositely, the cycling method sample shows relatively much less C, but much more O and Cl, seen in Figure 7.10. Each element is more spread out over the entire surface, as the Li species layer on top of the Mo foil is quite thin. The Si and Al seen in both samples stem from respectively the sample stub and detector, and are therefore contaminants from the EDX measurement, and not present in the actual samples.

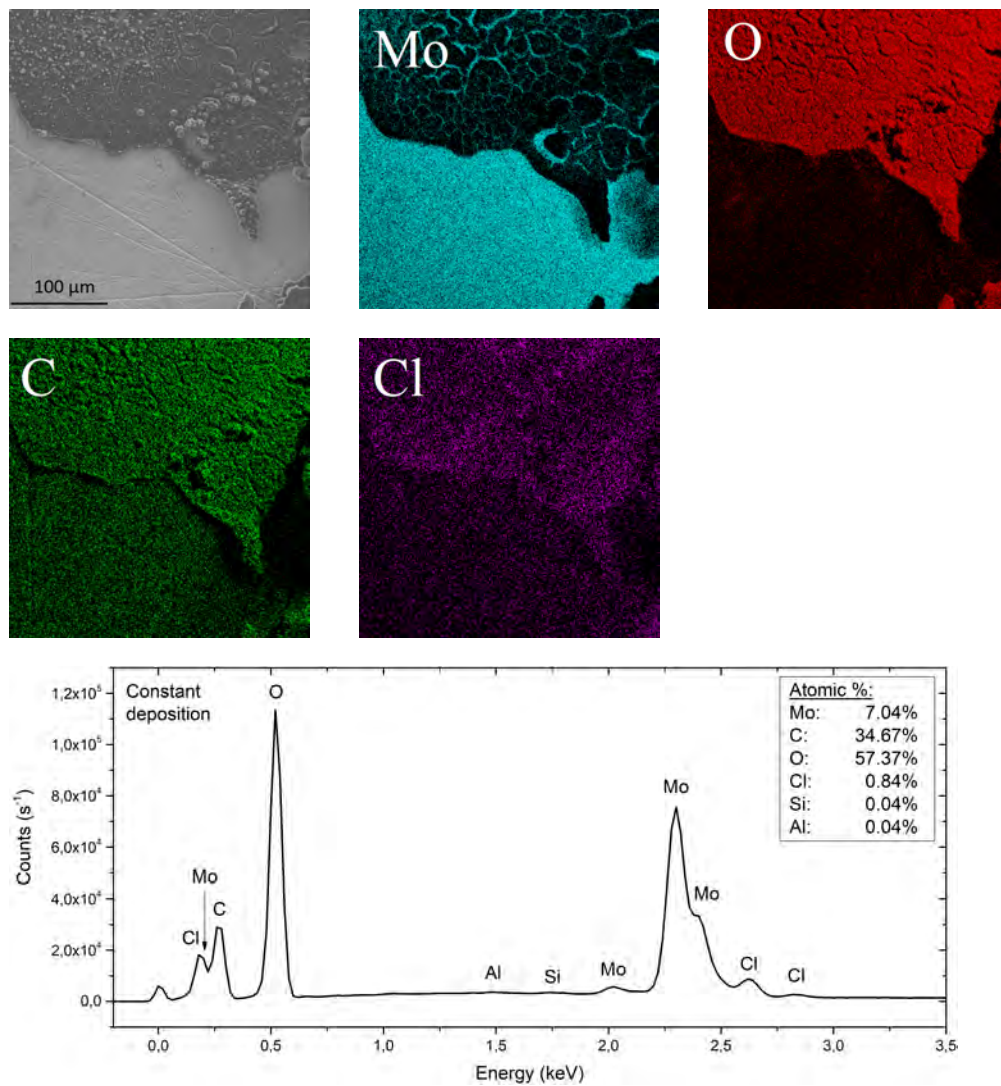


Figure 7.9 EDX images and spectrum of the constant deposition sample. The colors are auto-corrected for lightning and visibility. There are faint Al and Si peaks visible, which stem from the detector and sample stub. There are no peaks above 3.5 keV.

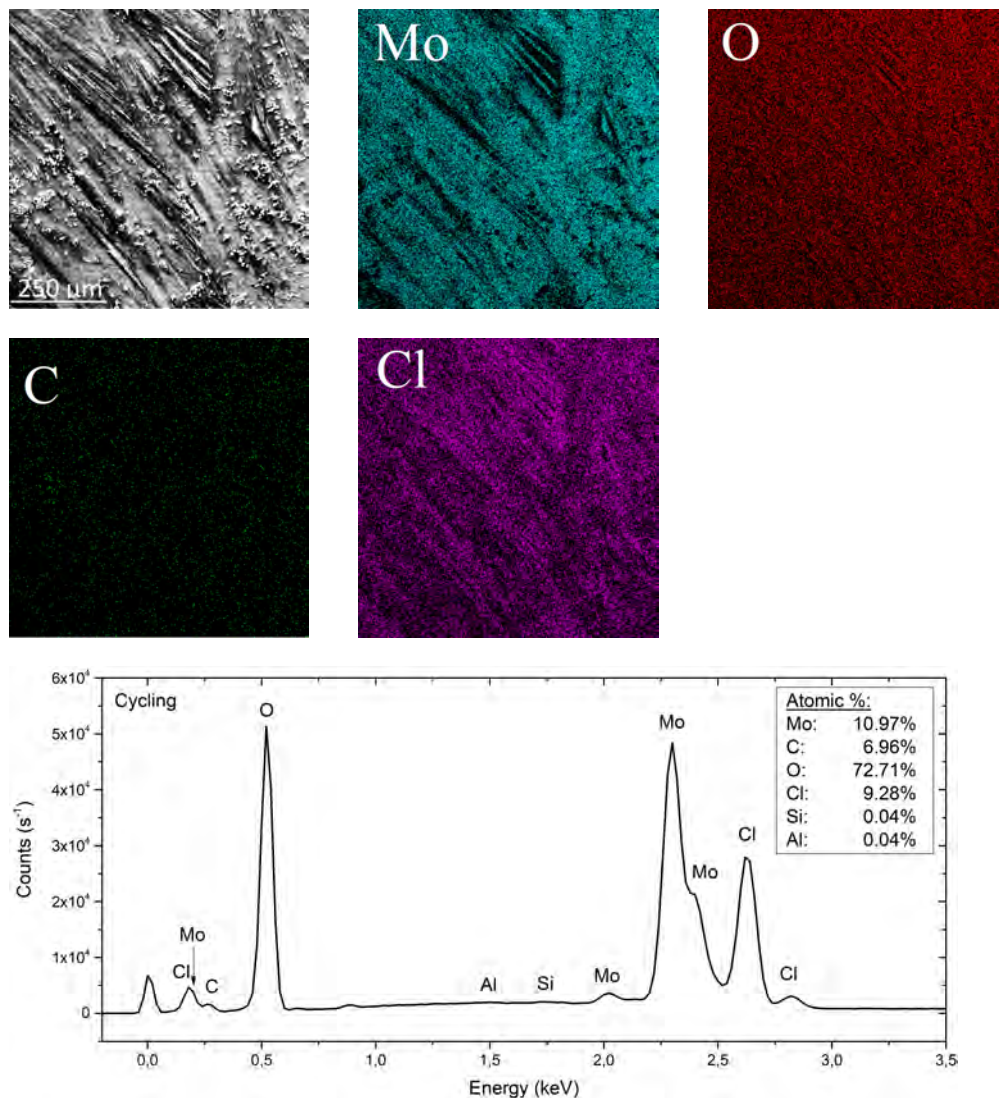


Figure 7.10 EDX images and spectrum of the cycling method sample. The colors are auto-corrected for lightning and visibility. There are faint Al and Si peaks visible, which stem from the detector and sample stub. There are no peaks above 3.5 keV.

7.3.2 XRD

Grazing incidence XRD was used to limit the Mo foil substrate contribution. With XRD it is expected that crystalline compounds on the sample generate peaks, and we can therefore expect

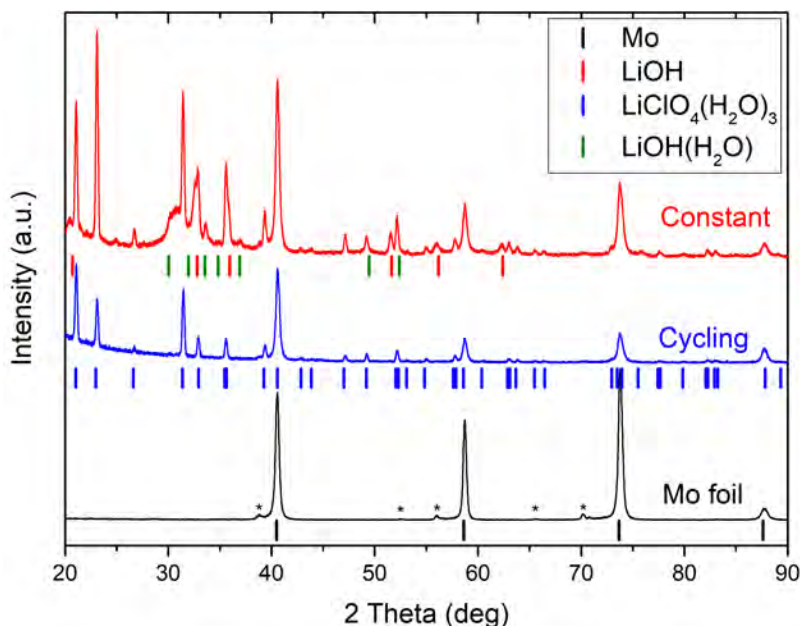


Figure 7.11 GI-XRD spectrum of three samples. The peaks with * on the Mo foil are simply beta lines from the main Mo (ICSD:52267) peaks. The beta peaks are not visible in the other samples, due to limited substrate contribution from GI geometry. Hydrated lithium perchlorate (ICSD:26737) is clearly visible on both E-chem samples, which is simply dried electrolyte from lack of rinsing and air exposure. Additionally, lithium hydroxide (ICSD:26892) and hydrated lithium hydroxide (ICSD:98-003-5155) is seen on the constant current sample, along with an amorphous phase.

to "see" the whole thickness of the deposited thin film. Figure 7.11 clearly shows the Mo foil sample, where the additional peaks are simply beta line from the main Mo peaks. A Ni filter could be used to remove these artefact peaks, but the Ni filter would also overall reduce the peak intensity of all peaks, enough that some of the smaller peaks on the electrochemical samples were no longer visible. The cycling sample only shows hydrated LiClO₄ on the surface, which is simply dried electrolyte that has been exposed to air and subsequently hydrated, present due to the lack of rinsing of the samples. The constant deposition sample showed some extra peaks additional to the hydrated LiClO₄, which most likely corresponds to LiOH and hydrated LiOH, as well as an amorphous phase (the big blob around 30-35°). As this is an *ex-situ* measurement, it is difficult to conclude whether these compounds are formed *in-situ* or after air exposure. The hydrated LiOH could be a surface species which becomes hydrated when exposed to air, while the non-hydrated LiOH lies underneath, and is protected from air exposure. There could also be a combination of both on the surface, which is formed throughout measurements. They could

also both form from something else as soon as the sample is exposed to air. LiOH is expected to be one of the most stable oxidized Li species [133], but the time of formation depends on the oxygen exposure, which could happen *in-situ* as well, as oxygen is an expected contaminant of the set-up.

7.3.3 XPS

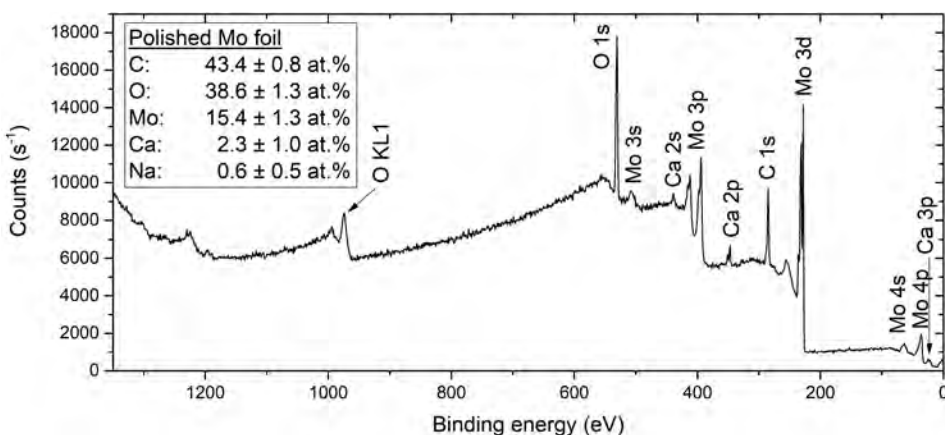


Figure 7.12 Representative XPS spectrum of polished Mo foil, with mean and standard deviation of at.% calculated based on fitting of individual peak scans on 3 different spots.

XPS survey spectra and individual peak scans were carried out on three separate points for each sample. Representative survey spectra are shown in Figures 7.12 and 7.13. A small Ca contamination is seen in our plain Mo foil, which was also seen in the EDX spectrum. Additionally, a bit of Na was also present on 2 out of the 3 investigated spots, which is presumably also a small contamination from the manufacturer. The sputtering gun was unfortunately off-line during these measurements, so depth profiling of the samples was not possible. The constant deposition and cycling sample did not show any of the Mo substrate, as XPS is a very surface sensitive method. Interestingly, the constant deposition sample had significantly more C in it, and much less Cl compared to the cycling sample, similar to what was seen with EDX (although relative composition is different, as EDX is not a surface sensitive method).

Since an amorphous phase was seen with XRD, and the XPS and EDX data both show significantly more C for the constant deposition sample, it is suspected that there is a build-up of a passivating SEI layer on the constant deposition sample formed from decomposition products of the electrolyte, which is consistent with an amorphous carbon species on the surface of this sample. The SEI layer will in this type of electrolyte consist of, among other things, lithium

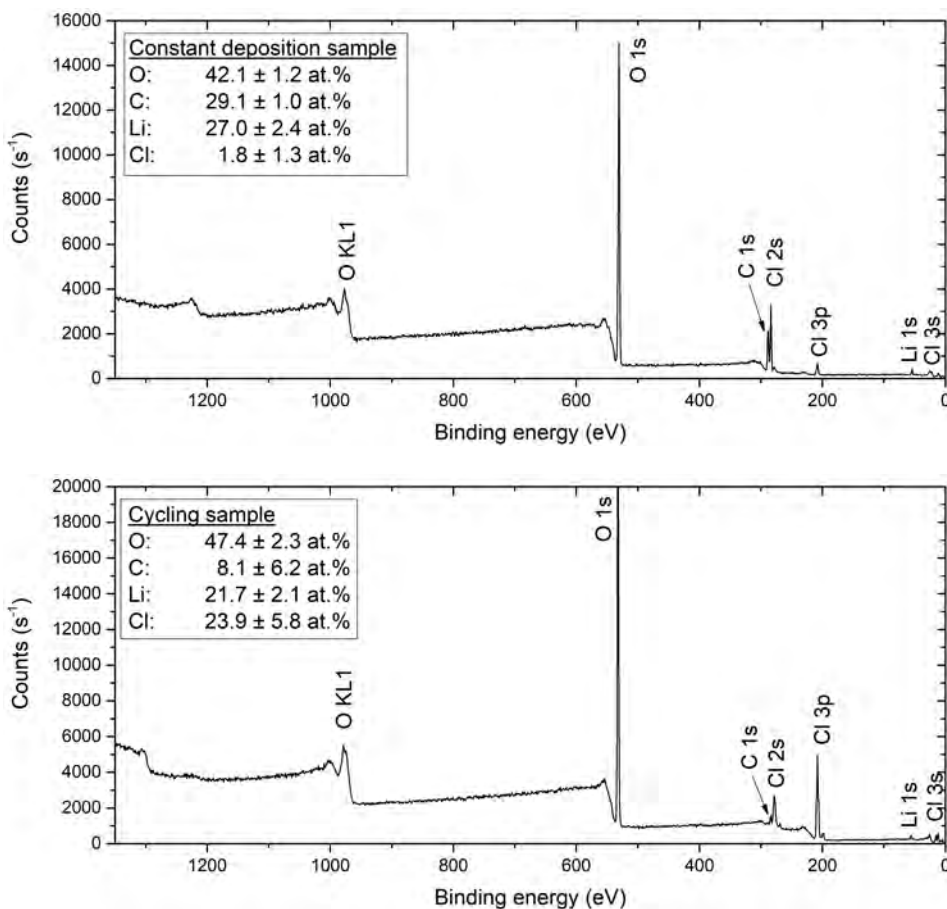


Figure 7.13 Representative XPS spectrum of different samples, with mean and standard deviation at.% calculated based on fitting of individual peak scans on 3 different spots for each sample.

carbonate and/or alkyl carbonate species, that allows Li ion transport through the layer [60, 134]. In the cycling sample, the SEI layer thickness is most likely increasing/decreasing with the cycling [135], which overall keeps it quite thin. The constant deposition sample might have a much thicker SEI layer, which might be what is measured through these *ex-situ* techniques, as significantly more C is observed on this sample.

7.4 Theoretical considerations

To explain the increase in FE during the cycling method, the exceptionally accomplished Michael Statt and Dr. Vanessa J. Bukas have developed a model for what happens in the resting period, which I will summarize here.

By considering all the elementary steps that can occur during Li deposition, the rate limiting steps are assumed to be the diffusion of reactants through the SEI layer [136]. The subsequent electrochemical steps are assumed to have negligible activation energy, and are driven irreversibly forward, thus occurring extremely fast in comparison to the diffusion [137]. This is due to the applied potential at the WE, which is high for the needed Li reduction. The same assumption is used for the non-electrochemical step of nitrogen dissociation, which occurs with a negligible kinetic barrier [53].

According to this model, ammonia formation is always limited by the arrival of reactant species, and is therefore either proton or nitrogen mass transfer limited. In the regime of proton mass transport limitations, the excess nitrogen likely reacts to form Li_3N , and increasing the N_2 (e.g. by an increase in pressure) will have little to no effect on the FE. In the case of nitrogen mass transport limitations, all the incoming N_2 is balanced with outgoing ammonia. These two regimes are reflected in the following expression for FE for constant deposition under steady-state conditions:

$$FE_{dep} = \begin{cases} \frac{\frac{3}{2} r_{N_2}}{2r_{H_2} + 3r_{NH_3} + r_{Li}}, & r_H \gg \frac{3}{2} r_{N_2} \\ \frac{\frac{1}{3} r_H}{2r_{H_2} + 3r_{NH_3} + r_{Li}}, & r_H \ll \frac{3}{2} r_{N_2} \end{cases} \quad (7.1)$$

$$(7.2)$$

where r_x denotes rates of reagents impinging upon the surface (r_{N_2}, r_H, r_{Li}) and products leaving (r_{NH_3}, r_{H_2}). The denominator is simply the total current passed in the system, assuming H_2 and NH_3 are the only formed products. Assuming a constant Li deposition rate, the FE during deposition can be graphically represented in a heat map as a function of N_2 and proton availability, seen in Figure 7.14. A horizontal movement denotes a change in N_2 availability, e.g. by increasing the pressure by 10 bar as shown with the stars. This can push the system from a nitrogen mass transport limited region (above the red line), to the proton limited region (below the red line). Increasing the pressure further will not affect the FE, but increasing the proton concentration at this point will move the star upwards. If the increase in concentration is just right, one might hit the red dashed line, and thereby the optimum for that given pressure of N_2 .

This optimum in proton concentration has previously been experimentally proven [55, 62, 138]. However, this peak was explained with other kinetic models assuming a constant,

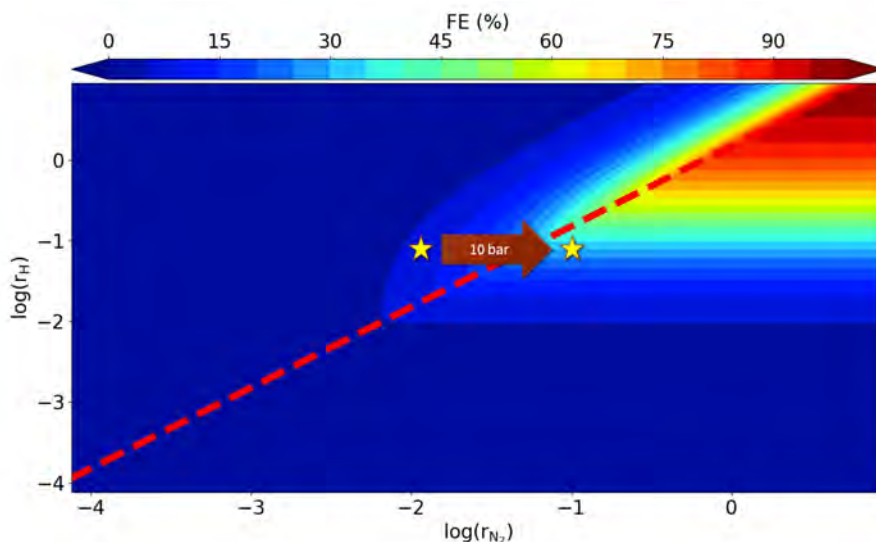


Figure 7.14 Heatmap showing FE as a function of the rate of proton and nitrogen diffusion in the lithium-mediated system. The dashed red line represents the edge of the N_2 (upper left) and H^+ (lower right) transport limitations. The arrow illustrates a 10 bar increase in N_2 pressure. Courtesy of Michael Statt, and included in Paper IV.

sub-monolayer Li deposition on the surface, rather than our assumptions of transitions between proton and nitrogen limited regimes. Since we clearly see a build-up of Li species on the surface of the electrode during constant deposition (Figure 7.7), the assumption of a constant Li layer does not seem feasible in our system.

The model can be modified to explain how ammonia synthesis is possible even during resting. During this step, there is no current flow in the external circuit, which would in principle restrict NRR and HER. However, in the lithium-mediated process, there are high-energy electrons available from the excess build-up of reduced Li on the surface of the electrode. This means the reduced Li can donate an electron, acting like a pseudo-battery for electron storage. This replaces the step $H^+ + e^-$ with $H^+ + Li\cdot$, where $Li\cdot$ denotes an active surface site of reduced Li, and adds Li^+ as a product. As the stored electrons will effectively have the potential of Li, *i.e.* 0 V vs Li/Li^+ , the previous assumption of fast reaction for the electrochemical steps still hold. Some fraction of electrons used for Li plating can therefore be recovered to selectively produce ammonia during the resting step, denoted as $s_{Li \rightarrow NH_3}$. The FE_{dep} of the deposition case for both regimes (Equations 7.1 and 7.2) can therefore be changed to a $FE_{cycling}$ of the cycling method for both regimes by adding $r_{Li} s_{Li \rightarrow NH_3}$ to both numerators. The $s_{Li \rightarrow NH_3}$ will be affected by the available Li on the surface. If all the reduced Li has already reacted (*e.g.* to form LiH), then

there are no available high-energy electrons for ammonia formation, and no additional ammonia is formed during the resting step. This motivates the need for the reaction to occur in a slightly proton limited regime, as the FE towards ammonia (compared to H_2) will overall be higher, both during deposition and resting. The increase of FE when applying the cycling method is therefore due to the possible recovery of electrons stored in metallic Li, enabling NRR even without an external current flow.

7.5 Summary

Long-term continuous measurements using CA or CP techniques appear to be impossible, as the total cell potential prohibitively increases to the point of no operation. To keep a stable cell voltage, a cycling method is developed, wherein a Li deposition pulse at -2 mA/cm^2 for 1 minute is applied, followed by a resting pulse at 0 mA/cm^2 , which varies from 3-8 minutes depending on the intended result, and this cycle is repeated. It is seen that the system remains stable, and can operate for days, passing unprecedented charge towards ammonia for an electrochemical nitrogen reduction system. Both the FE and energy efficiency is significantly improved by the cycling method, and while the average ammonia formation rate is lower, continuous operation for more than 120 hours was achieved. This is a significant improvement over anything reported in the literature, and is therefore an overwhelming "Yes" to the aim mentioned in chapter 2 of improving efficiency.

The proposed reaction mechanism developed by Michael Statt and Dr. Vanessa Bukas explain what might be happening on the surface of the electrode during the cycling method. The model provides a possible answer for the improved efficiency seen in the experimental data when using the cycling method. This successfully answers the aim in Chapter 2 regarding understanding (and improving) the mechanism of the lithium-mediated system.

Chapter 8

Conclusion and Outlook

"I read the whole Hitchhiker's Guide to the Galaxy thinking that due to the hype, there would be something interesting towards the end of it. It was crap all the way through."

— Ib Chorkendorff, February 2020

In Chapter 4, I presented a protocol enabling rigorous testing to prove successful ammonia synthesis. The following three chapters investigated electrochemical nitrogen reduction in both aqueous and non-aqueous media. This final chapter is split into two parts: first a general conclusion and overview of my findings throughout this work, followed by an outlook over the future, and the work that is needed to push electrochemical nitrogen reduction towards commercial application.

8.1 Conclusion

The very first step in electrochemical nitrogen reduction was developing a systematic way to carry out experiments. This was seen as absolutely necessary, as small amounts of ammonia is a persistent contamination source, even in the "clean" laboratory environment. We would see ammonia contamination in the glassware, the chemicals, the pipettes, the gas, etc. if we were not careful. Unfortunately, many papers in electrochemical nitrogen reduction are published without carrying out simple background tests. These tests, which are very simple and easy to do, cover an experiment with Ar instead of N₂, which can rule out external environmental contamination, as well as possible contamination of the electrodes, chemicals, membranes, and the cell itself, coupled with N₂ tests without applied potential, to rule out ammonia contamination of the gas

itself. However, the only definitive way to track the origin of the ammonia, is by the use of isotope labeled $^{15}\text{N}_2$, and subsequently measuring $^{15}\text{NH}_3$ after electrochemistry. Even this proved to not be enough, as commercial $^{15}\text{N}_2$ gas bottles can also contain both ammonia and other fixed nitrogen species as a contaminant [85]. The amount of ammonia can easily be determined by purging the system with the isotope labeled $^{15}\text{N}_2$ gas without applied potential for the same duration of time as a regular experiment, and then measuring the ammonia afterwards. This method will unfortunately not account for other fixed nitrogen compounds, such as NO_x , N_2O , nitrites, nitrates, etc., which are much more easily reduced than N_2 . We therefore added a Cu impurity trap with a reduced Cu catalyst to catch any fixed nitrogen species, and simultaneously used an ethanol slurry to freeze any ammonia contamination in the gas stream. Furthermore, to save on cost for the expensive $^{15}\text{N}_2$ gas, we used a glass pump to circulate the gas in the set-up, which has the additional benefit of increasing the trapping efficiency of the system, as ammonia does not as readily escape.

As we were developing all these systems and processes, we created a flow chart based protocol that was easy to follow, published in Paper I, Reference [77]. This tool would enable us (and others in the field) to accurately determine if an electrochemical experiment achieves successful ammonia synthesis. The crucial step in this protocol is the use of repeated quantitative isotope labeled experiments, with an acceptable overlap between an isotope sensitive method and a colorimetric method. The amount of ammonia produced should furthermore also correlate with the amount produced with non-isotope labeled N_2 . Without these tests, successful electrochemical nitrogen reduction is simply not proven.

We used this rigorous protocol to test some of the most promising pure metal catalysts from the literature in aqueous conditions [41]. A wide variety of pure metal electrodes were tested in alkaline conditions, with no significant amount of ammonia produced. Ru was tested in acidic and neutral condition as well, and at different temperatures for acidic and alkaline media, without any positive result. When moving on to non-aqueous media, the report by Tsuneto et al. [54, 62] seemed promising, as they claimed a high Faradaic efficiency with much current passed and high concentrations of ammonia measured. Their system used a lithium-mediated process, wherein they plate Li on the cathode. They claim the mechanism for the process involved the reaction of the reduced Li with N_2 , which forms a lithium nitride, Li_3N . This nitride can subsequently be protonated three times from ethanol in solution, producing ammonia and lithium ethoxide, LiEtO .

Following the protocol we developed, we validated their results with quantified isotope labeled studies. This was the first major breakthrough, as over a decade of attempted electrochemical nitrogen reduction in our group had lead to nothing. Once the system was proven to

work, we wanted to elucidate the mechanism of ammonia synthesis, and improve the system in terms of activity, selectivity, and stability. The biggest issue in the system, as presented, was the slow increase of the total cell potential, eventually leading to an overload of the potentiostat. When continuously applying a current or potential, a thick deposition layer of Li species were visible on the cathode surface, which we believe is due to the deposited Li not having enough time to react with our N_2 (or ethanol). This leads to fresh deposition of Li on top of unreacted and/or passivated Li species. We suspect that this gradual build-up leads to the increase in total cell voltage, and eventual overloading of the system.

I therefore developed a cycling strategy, wherein a short 1 minute pulse with Li deposition is applied, followed by a longer 3-8 minute resting pulse below Li deposition, which allows for the deposited Li species to chemically react and dissolve off the surface of the electrode. This was tested in a home built electrochemical autoclave (based on the design by Reference [63]) at 10 bar. The increase in N_2 pressure is expected to increase the ammonia yield, because one of the limiting factors in the ambient system is N_2 availability, and increase in pressure will increase N_2 solubility in the electrolyte due to Henry's law. This overall increase in yield due to increase in pressure will make small differences in yield due to changes in procedure more clear. Using the cycling method significantly increased the Faradaic efficiency and energy efficiency of the system, the calculations of both covered in Section 3.1.3. The continuous lithium deposition method previously reported [54, 55, 62, 77, 138] was used in the electrochemical autoclave at 10 bar N_2 , and gave a Faradaic efficiency of $21.2 \pm 1.6 \%$ and an energy efficiency of $2.3 \pm 0.3 \%$ in my system. Using my newly developed cycling method increased the Faradaic efficiency to $36.8 \pm 1.3 \%$, and the energy efficiency to $7.1 \pm 0.2 \%$ in comparison. It also enabled long experiments with a stable cell potential, even over several days, completely unheard of within the field. The vast improvement of the system in terms of both stability and efficiency was theorized by Michael Statt and Dr. Vanessa Bukas to be due to ammonia formation during resting. This is presumed to be possible because newly reduced Li has high-energy electrons available. If any proton source from the electrolyte impinges upon Li_3N , the high-energy electrons from reduced Li can be used to form ammonia without any external current flow. This significantly reduces inefficiencies in the system, and prevents the gradual build-up of species on the electrode, leading to excellent stability of the overall cell potential, even over days.

8.2 Outlook

Although the work presented in this thesis overall made a rather satisfying Ph.D. project, there are still many unanswered questions. My group and I will focus on understanding more about the lithium-mediated process. We believe that major improvements are possible, and that if we can reach a target of 100 mA/cm^2 at 50 % Faradaic efficiency, that the system is close to commercial application.

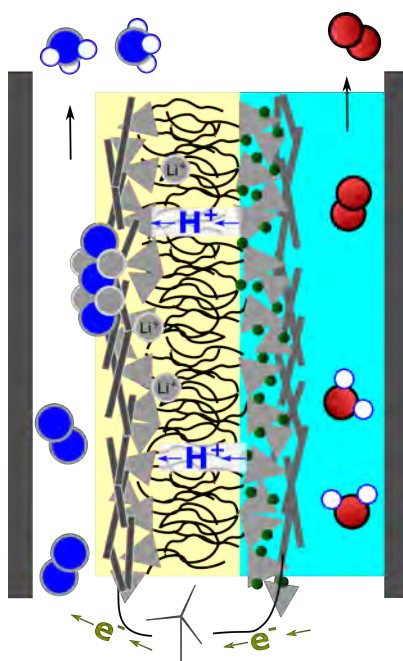


Figure 8.1 Idealized version of a flow cell, producing ammonia and oxygen from water and nitrogen *via* a lithium-mediated process. Courtesy of Søren B. Scott.

The ideal end prototype would be something along the lines of the flow cell shown in Figure 8.1. Some of the major questions and experiments left to answer in the near future are the following:

- Measure H₂ produced, to determine whether any charge is "lost" in the system, *i.e.* if there is an unexpected reaction taking place.
- Use D₂ gas recycling in combination with EtOH to determine if ammonia can be produced from purely N₂ and H₂. If deuterated ammonia is measured and increases over time,

this means the EtOH can be replenished during measurements, which is a crucial step in pushing the system towards commercialization.

- Understand the anode reaction, and prevent solvent breakdown (if that is what currently occurs on the anode).
- Set up a continuous flow cell type system, with a membrane separating the anolyte and catholyte. This will enable the use of H₂ at the anode as the proton source (if that does indeed replenish the EtOH), and is another crucial step in commercialization of the system.
- Find proper gas diffusion layers for the fuel cell type system, as N₂ availability at the cathode surface due to low solubility in the electrolyte is a limiting factor for ammonia synthesis.
- Determine if there are any other alkali or alkaline earth metals that work in a similar way, as this could replace Li and potentially lower the required energy for metal ion reduction.

There are many different directions to investigate, and much work to be done. Luckily there is also a great interest in commercializing electrochemical nitrogen reduction, fueling the funding for more research on this topic. Ammonia is not only used as a fertilizer, but it can also be used as an energy carrier [139]. This ties into the hydrogen economy, as ammonia is easier to transport and store compared to liquid hydrogen, and has a high energy density almost comparable to coal and oil [140]. Much work has gone into making ammonia fuel cells [141, 142], because ammonia can be a carbon free energy carrier at the end user, which is highly desirable considering the recent push for renewable and green energy. If ammonia can also be produced in a CO₂ neutral process (*e.g.* through electrochemistry), then a future with an "ammonia economy" [143] suddenly seems very attractive as an alternative to our current environmentally harmful fossil fuel based economy.

I'd like to think the work of my Ph.D. is a small step towards making this desirable future just a little more feasible, but I'll let you, dear reader, be the judge of that.

References

- [1] United Nations Department of Public Information. *Sustainable Development Goals*. 2015.
- [2] D. Charles. *Mastermind: The Rise and Fall of Fritz Haber, the Nobel Laureate Who Launched the Age of Chemical Warfare*. 1e. Ecco, 2005, p. 336.
- [3] V. Smil. “Nitrogen and Food Production: Proteins for Human Diets”. In: *AMBIO: A Journal of the Human Environment* 31.2 (2002), pp. 126–131.
- [4] R. Fraser, A. Bogaard, R. Fraser, T. H. E. Heaton, M. Wallace, P. Vaiglova, M. Charles, and G. Jones. “Crop manuring and intensive land management by Europe’s first farmers”. In: *Proceedings of the National Academy of Sciences of the United States of America* 110.31 (2013), pp. 12589–12594.
- [5] J. Silvertown, P. Poulton, E. Johnston, G. Edwards, P. M. Biss, J. Silvertown, P. Poulton, E. Johnston, G. Edwardst, M. Heardi, and P. M. Biss. “The Park Grass Experiment 1856-2006: Its Contribution to Ecology”. In: *Journal of Ecology* 94.4 (2006), pp. 801–814.
- [6] H.-P. Jia and E. A. Quadrelli. “Mechanistic aspects of dinitrogen cleavage and hydrogenation to produce ammonia in catalysis and organometallic chemistry: relevance of metal hydride bonds and dihydrogen”. In: *Chem. Soc. Rev.* 43.2 (2014), pp. 547–564.
- [7] T. Hager. *The Alchemy of Air: A Jewish Genius, a Doomed Tycoon, and the Discovery that Changed the Course of History*. Broadway Books, 2008, p. 336.
- [8] “Science and Food Supplies”. In: *Nature* 126.3171 (1930), pp. 193–194.
- [9] V. Smil. *Enriching the Earth: Fritz Haber, Carl Bosch, and the Transformation of World Food Production*. Cambridge, Massachusetts: The MIT Press, 2001, p. 338.
- [10] S. R. Bown. *A most damnable invention: dynamite, nitrates, and the making of the modern world*. New York, NY: Thomas Dunne Books, 2005, p. 272.
- [11] J. W. Erisman, M. a. Sutton, J. Galloway, Z. Klimont, and W. Winiwarter. “How a century of ammonia synthesis changed the world”. In: *Nature Geoscience* 1.10 (2008), pp. 636–639.
- [12] W. M. Stewart, D. W. Dibb, A. E. Johnston, and T. J. Smyth. “The Contribution of Commercial Fertilizer Nutrients to Food Production”. In: *Agronomy Journal* 97.1 (2005), pp. 1–6.
- [13] V. Smil. “Detonator of the population explosion”. In: *Nature* 400.6743 (1999), pp. 415–415.

- [14] G. Ertl. "Reactions at surfaces: From atoms to complexity (nobel lecture)". In: *Angewandte Chemie - International Edition* 47.19 (2008), pp. 3524–3535.
- [15] D. R. Montgomery and A. Biklé. *The Hidden Half of Nature: The Microbial Roots of Life and Health*. W. W. Norton & Company, 2016, p. 320.
- [16] I. Chorkendorff and J. W. Niemantsverdriet. *Concepts of Modern Catalysis and Kinetics*. Weinheim: Wiley-VCH Verlag GmbH & Co. KGaA, 2003.
- [17] T. R. Karl and K. E. Trenberth. "Modern Global Climate Change". In: *Science* 302.5651 (2003), pp. 1719–1723.
- [18] International Fertilizer Association. "Fertilizers , Climate Change and Enhancing Agricultural Productivity Sustainably". In: *Ifa* (2009), p. 30.
- [19] P. A. Murtaugh and M. G. Schlax. "Reproduction and the carbon legacies of individuals". In: 19 (2009), pp. 14–20.
- [20] S. Peltzman. "Mortality inequality". In: *Journal of Economic Perspectives* 23.4 (2009), pp. 175–190.
- [21] E. Gakidou, K. Cowling, R. Lozano, and C. J. Murray. "Increased educational attainment and its effect on child mortality in 175 countries between 1970 and 2009: A systematic analysis". In: *The Lancet* 376.9745 (2010), pp. 959–974.
- [22] O. Galor. "The demographic transition: Causes and consequences". In: *Demetrica* 6.1 (2012), pp. 1–28.
- [23] W. Lutz, W. Sanderson, S. Scherbov, and S. Asia. "The coming acceleration of global population ageing". In: *Nature* 451. February (2008), pp. 12–15.
- [24] Department of Economic and Social Affairs. "Population Division". In: *United Nations ST/ESA/SER* (2015), pp. 1–148.
- [25] N. D. Mueller, J. S. Gerber, M. Johnston, D. K. Ray, N. Ramankutty, and J. A. Foley. "Closing yield gaps through nutrient and water management". In: *Nature* 490 (2012), pp. 254–257.
- [26] J. W. Erisman, A. Bleeker, J. Galloway, and M. S. Sutton. "Reduced nitrogen in ecology and the environment". In: *Environmental Pollution* 150 (2007), pp. 140–149.
- [27] A. G. Good and P. H. Beatty. "Fertilizing nature: A tragedy of excess in the commons". In: *PLoS Biology* 9.8 (2011), pp. 1–9.
- [28] S. J. Karam. *How many people will live in Africa in 2050 and 2100?* 2015.
- [29] United Nations Department of Economic and Social Affairs Population Division. *World Population Prospects 2019*. 2019.
- [30] L. K. Boerner. "Taking the CO₂ out of NH₃". In: *Chemical and Engineering News* 97.24 (2019), pp. 18–21.
- [31] Yara. *Yara and BASF open world-scale ammonia plant in Freeport, Texas*. 2018.
- [32] M. A. Shipman and M. D. Symes. "Recent progress towards the electrosynthesis of ammonia from sustainable resources". In: *Catalysis Today* 286 (2016), pp. 57–68.
- [33] M. Jewess and R. H. Crabtree. "Electrocatalytic Nitrogen Fixation for Distributed Fertilizer Production?" In: *ACS Sustainable Chemistry & Engineering* 4.11 (2016), pp. 5855–5858.

- [34] J. Nørskov, J. Chen, R. Miranda, T. Fitzsimmons, and R. Stack. *Sustainable Ammonia Synthesis – Exploring the scientific challenges associated with discovering alternative, sustainable processes for ammonia production*. Tech. rep. USDOE Office of Science (SC) (United States), 2016, p. 33.
- [35] L. Ye, R. Nayak-Luke, R. Bañares-Alcántara, and E. Tsang. “Reaction: “Green” Ammonia Production”. In: *Chem* 3.5 (2017), pp. 712–714.
- [36] New York State Department of Health. “The fact about ammonia”. In: *Technical Information* July (2004).
- [37] A. R. Singh, B. A. Rohr, J. A. Schwalbe, M. Cargnello, K. Chan, T. F. Jaramillo, I. Chorkendorff, and J. K. Nørskov. “Electrochemical Ammonia Synthesis—The Selectivity Challenge”. In: *ACS Catalysis* 7.1 (2017), pp. 706–709.
- [38] E. Skúlason, T. Bligaard, S. Gudmundsdóttir, F. Studt, J. Rossmeisl, F. Abild-Pedersen, T. Vegge, H. Jónsson, and J. K. Nørskov. “A theoretical evaluation of possible transition metal electro-catalysts for N₂ reduction”. In: *Physical Chemistry Chemical Physics* 14.3 (2012), pp. 1235–1245.
- [39] J. K. Nørskov, F. Studt, F. Abild-Pedersen, and T. Bligaard. *Fundamental Concepts in Heterogeneous Catalysis*. Hoboken, NJ, USA: John Wiley & Sons, Inc, 2014.
- [40] A. B. Laursen, I. C. Man, O. L. Trinhammer, J. Rossmeisl, and S. Dahl. “The Sabatier Principle Illustrated by Catalytic H₂O₂ Decomposition on Metal Surfaces”. In: *Journal of Chemical Education* 88.12 (2011), pp. 1711–1715.
- [41] J. H. Montoya, C. Tsai, A. Vojvodic, and J. K. Nørskov. “The Challenge of Electrochemical Ammonia Synthesis: A New Perspective on the Role of Nitrogen Scaling Relations”. In: *ChemSusChem* 8.13 (2015), pp. 2180–2186.
- [42] R. E. Oesper. “Alwin mittasch”. In: *Journal of Chemical Education* (1948), pp. 531–532.
- [43] A. Vojvodic and J. K. Nørskov. “New design paradigm for heterogeneous catalysts”. In: *National Science Review* 2.2 (2015), pp. 140–143.
- [44] A. J. Medford, C. Shi, M. J. Hoffmann, A. C. Lausche, S. R. Fitzgibbon, T. Bligaard, and J. K. Nørskov. “CatMAP: A Software Package for Descriptor-Based Microkinetic Mapping of Catalytic Trends”. In: *Catalysis Letters* 145.3 (2015), pp. 794–807.
- [45] A. J. Bard and L. F. Faulkner. *Electrochemical Methods - Fundamentals and Applications*. 2nd. John Wiley & Sons, Inc., 2000, p. 833.
- [46] N. Elgrishi, K. J. Rountree, B. D. McCarthy, E. S. Rountree, T. T. Eisenhart, and J. L. Dempsey. “A Practical Beginner’s Guide to Cyclic Voltammetry”. In: *Journal of Chemical Education* 95.2 (2018), pp. 197–206.
- [47] L. E. Apodaca. *Nitrogen (fixed) — Ammonia*. 2019.
- [48] S. W. Benson. “Resource papers - III bond energies”. In: *Journal of Chemical Education* 42.9 (1965), pp. 502–515.
- [49] H. Chen and R. Andersen. “Studies of the triply promoted ammonia syntehsis catalyst with an electron-probe microanalyzer”. In: *Journal of Catalysis* 28.1 (1973), pp. 161–173.
- [50] F. Rosowski, A. Hornung, O. Hinrichsen, D. Herein, and M. Muhler. “Ruthenium catalysts for ammonia synthesis at high pressures: Preparation, characterization, and power-law kinetics”. In: *Applied Catalysis A: General* 151 (1997), pp. 443–460.

- [51] T. E. Brown, H. E. H. LeMay, B. E. Bursten, C. Murphy, and P. Woodward. *Chemistry: The Central Science*. 11e. Upper Saddle River, NJ: Prentice Hall, 2008, p. 1230.
- [52] K. Krempel. “Electrochemical ammonia synthesis in organic electrolytes”. PhD thesis. Technical University of Denmark, 2019.
- [53] J. M. McEnaney, A. R. Singh, J. A. Schwalbe, J. Kibsgaard, J. C. Lin, M. Cargnello, T. F. Jaramillo, and J. K. Nørskov. “Ammonia synthesis from N₂ and H₂O using a lithium cycling electrification strategy at atmospheric pressure”. In: *Energy & Environmental Science* 10.7 (2017), pp. 1621–1630.
- [54] A. Tsuneto, A. Kudo, and T. Sakata. “Efficient Electrochemical Reduction of N₂ to NH₃ Catalyzed by Lithium”. In: *Chemistry Letters* 22.5 (1993), pp. 851–854.
- [55] N. Lazouski, Z. J. Schiffer, K. Williams, and K. Manthiram. “Understanding Continuous Lithium-Mediated Electrochemical Nitrogen Reduction”. In: *Joule* 3.4 (2019), pp. 1127–1139.
- [56] P. G. Kitz, M. J. Lacey, P. Nova, and E. J. Berg. “Operando EQCM-D with Simultaneous in Situ EIS: New Insights into Interphase Formation in Li Ion Batteries”. In: *Analytical Chemistry* 91 (2019), pp. 2296–2303.
- [57] G. Nazri, R. H. Muller, and J. E. Soc. “Composition of Surface Layers on Li Electrodes in PC, LiClO₄ of Very Low Water Content”. In: *Journal of the Electrochemical Society* 132.9 (1985), pp. 2050–2054.
- [58] D. Aurbach, M. L. Daroux, P. W. Faguy, and E. Yeager. “Identification of Surface Films Formed on Lithium in Propylene Carbonate Solutions”. In: *Journal of the electrochemical society* 134.7 (1987), pp. 1611–1620.
- [59] P. Lu and S. J. Harris. “Lithium transport within the solid electrolyte interphase”. In: *Electrochemistry Communications* 13.10 (2011), pp. 1035–1037.
- [60] A. Wang, S. Kadam, H. Li, S. Shi, and Y. Qi. “Review on modeling of the anode solid electrolyte interphase (SEI) for lithium-ion batteries”. In: *npj Computational Materials* 4.1 (2018).
- [61] G. Zhuang and P. N. J. Ross. “Contrasting film formation reactions of etheral and carbonate solvents on metallic lithium”. In: *Journal of power sources* 89 (2000), pp. 143–148.
- [62] A. Tsuneto, A. Kudo, and T. Sakata. “Lithium-mediated electrochemical reduction of high pressure N₂ to NH₃”. In: *Journal of Electroanalytical Chemistry* 367.1-2 (1994), pp. 183–188.
- [63] G. K. Wiberg, M. J. Fleige, and M. Arenz. “Design and test of a flexible electrochemical setup for measurements in aqueous electrolyte solutions at elevated temperature and pressure”. In: *Review of Scientific Instruments* 85.8 (2014).
- [64] E. de Hoffmann and V. Stroobant. *Mass Spectrometry: Principles and Applications*. John Wiley & Sons Ltd, 2007, p. 502.
- [65] Á. Somogyi. “Chapter 6 - Mass spectrometry instrumentation and techniques”. In: *Medical Applications of Mass Spectrometry*. Elsevier B.V, 2008, pp. 93–140.
- [66] M. E. Orazem and B. Tribollet. *Electrochemical Impedance Spectroscopy*. Boston: John Wiley & Sons, Inc., 2008, pp. 287–357.
- [67] Gamry Instruments. *Basics of Electrochemical Impedance Spectroscopy*. 1990.

- [68] J. Li, C. Arbizzani, S. Kjelstrup, J. Xiao, Y. Yao Xia, Y. Yu, Y. Yang, I. Belharouak, T. Zawodzinski, S. T. Myung, R. Raccichini, and S. Passerini. "Good practice guide for papers on batteries for the Journal of Power Sources". In: *Journal of Power Sources* 452 (2020), p. 227824.
- [69] Gamry Instruments. "Understanding iR Compensation". In: *Gamry Application Notes* (2014), pp. 1–19.
- [70] D. Aurbach, M. Daroux, P. Faguy, and E. Yeager. "The electrochemistry of noble metal electrodes in aprotic organic solvents containing lithium salts". In: *Journal of Electroanalytical Chemistry* 297.1 (1991), pp. 225–244.
- [71] D. Cogan, J. Cleary, C. Fay, A. Rickard, K. Jankowski, T. Phelan, M. Bowkett, and D. Diamond. "The development of an autonomous sensing platform for the monitoring of ammonia in water using a simplified Berthelot method". In: *Anal. Methods* 6.19 (2014), pp. 7606–7614.
- [72] P. L. Searle. "The berthelot or indophenol reaction and its use in the analytical chemistry of nitrogen. A review". In: *The Analyst* 109.5 (1984), p. 549.
- [73] R. Harfmann and S. Crouch. "Kinetic study of Berthelot reaction steps in the absence and presence of coupling reagents". In: *Talanta* 36.1-2 (1989), pp. 261–269.
- [74] G. Wypych. "Photophysics". In: *Handbook of Material Weathering*. 6e. ChemTec Publishing, 2018. Chap. 1, pp. 1–26.
- [75] A. D. McNaught and A. Wilkinson. *Compendium of Chemical Terminology (the "Gold Book")*. 2nd. Oxford, UK: Blackwell Scientific Publications, 1997.
- [76] Bruker. *What Is NMR?* 2010.
- [77] S. Z. Andersen, V. Čolić, S. Yang, J. A. Schwalbe, A. C. Nielander, J. M. McEnaney, K. Enemark-Rasmussen, J. G. Baker, A. R. Singh, B. A. Rohr, M. J. Statt, S. J. Blair, S. Mezzavilla, J. Kibsgaard, P. C. Vesborg, M. Cargnello, S. F. Bent, T. F. Jaramillo, I. E. Stephens, J. K. Nørskov, and I. Chorkendorff. "A rigorous electrochemical ammonia synthesis protocol with quantitative isotope measurements". In: *Nature* 570.7762 (2019), pp. 504–508.
- [78] A. C. Nielander, J. M. McEnaney, J. A. Schwalbe, J. G. Baker, S. J. Blair, L. Wang, J. G. Pelton, S. Z. Andersen, K. Enemark-Rasmussen, V. Čolić, S. Yang, S. F. Bent, M. Cargnello, J. Kibsgaard, P. C. K. Vesborg, I. Chorkendorff, and T. F. Jaramillo. "A Versatile Method for Ammonia Detection in a Range of Relevant Electrolytes via Direct Nuclear Magnetic Resonance Techniques". In: *ACS Catalysis* 9.7 (2019), pp. 5797–5802.
- [79] G. L. Parrish, C. Ortiz, M. Hart, and M. Bellotto. "Grazing incidence synchrotron x-ray diffraction method for analyzing thin films". In: *Journal of Materials Research* 2.4 (1987), pp. 471–477.
- [80] W. C. Nixon. "Scanning electron microscopy". In: *Contemporary Physics* 10.1 (1969), pp. 71–96.
- [81] D. Brandon and W. D. Kaplan. *Microstructural Characterization of Materials: 2nd Edition*. 2008, p. 536.
- [82] J. I. Goldstein, D. E. Newbury, P. Echlin, D. C. Joy, C. Fiori, E. Lifshin, J. I. Goldstein, D. E. Newbury, P. Echlin, D. C. Joy, C. Fiori, and E. Lifshin. *Electron-Beam-Specimen Interactions*. 1981, pp. 53–122.

- [83] Y. Yao, J. Wang, U. B. Shahid, M. Gu, H. Wang, H. Li, and M. Shao. “Electrochemical Synthesis of Ammonia from Nitrogen Under Mild Conditions: Current Status and Challenges”. In: *Electrochemical Energy Reviews* (2020), pp. 1–32.
- [84] Y. Zhao, R. Shi, X. Bian, C. Zhou, Y. Zhao, S. Zhang, F. Wu, G. I. N. Waterhouse, L.-Z. Wu, C.-H. Tung, and T. Zhang. “Ammonia Detection Methods in Photocatalytic and Electrocatalytic Experiments: How to Improve the Reliability of NH₃ Production Rates?” In: *Advanced Science* 6.8 (2019), p. 1802109.
- [85] R. Dabundo, M. F. Lehmann, L. Treibergs, C. R. Tobias, M. A. Altabet, P. H. Moisaner, and J. Granger. “The Contamination of Commercial 15N₂ Gas Stocks with 15N–Labeled Nitrate and Ammonium and Consequences for Nitrogen Fixation Measurements”. In: *PLoS ONE* 9.10 (2014). Ed. by J. B. Love, e110335.
- [86] J. M. McEnaney, S. J. Blair, A. C. Nielander, J. A. Schwalbe, D. M. Koshy, M. Cargnello, and T. F. Jaramillo. “Electrolyte engineering for efficient electrochemical nitrate reduction to ammonia on a titanium electrode”. In: *ACS Sustainable Chemistry and Engineering* 8.7 (2020), pp. 2672–2681.
- [87] M.-M. Shi, D. Bao, B.-R. Wulan, Y.-H. Li, Y.-F. Zhang, J.-M. Yan, and Q. Jiang. “Au Sub-Nanoclusters on TiO₂ toward Highly Efficient and Selective Electrocatalyst for N₂ Conversion to NH₃ at Ambient Conditions”. In: *Advanced Materials* 29.17 (2017), p. 1606550.
- [88] R. Lan, J. T. S. Irvine, and S. Tao. “Synthesis of ammonia directly from air and water at ambient temperature and pressure”. In: *Scientific Reports* 3.1 (2013), p. 1145.
- [89] V. Kordali, G. Kyriacou, and C. Lambrou. “Electrochemical synthesis of ammonia at atmospheric pressure and low temperature in a solid polymer electrolyte cell”. In: *Chemical Communications* 17 (2000), pp. 1673–1674.
- [90] S. Chen, S. Perathoner, C. Ampelli, C. Mebrahtu, D. Su, and G. Centi. “Electrocatalytic Synthesis of Ammonia at Room Temperature and Atmospheric Pressure from Water and Nitrogen on a Carbon-Nanotube-Based Electrocatalyst”. In: *Angewandte Chemie International Edition* 56.10 (2017), pp. 2699–2703.
- [91] Y. Ren, C. Yu, X. Tan, X. Han, H. Huang, H. Huang, and J. Qiu. “Is It Appropriate to Use the Nafion Membrane in Electrocatalytic N₂ Reduction?” In: *Small Methods* 3.12 (2019), p. 1900474.
- [92] K. Hongsirikarn, J. G. Goodwin, S. Greenway, and S. Creager. “Influence of ammonia on the conductivity of Nafion membranes”. In: *Journal of Power Sources* 195.1 (2010), pp. 30–38.
- [93] R. Halseid, P. J. S. Vie, and R. Tunold. “Influence of Ammonium on Conductivity and Water Content of Nafion 117 Membranes”. In: *Journal of The Electrochemical Society* 151.3 (2004), A381.
- [94] B. Hu, M. Hu, L. Seefeldt, and T. L. Liu. “Electrochemical Dinitrogen Reduction to Ammonia by Mo₂N: Catalysis or Decomposition?” In: *ACS Energy Letters* 4.5 (2019), pp. 1053–1054.
- [95] X. Yang, S. Kattel, J. Nash, X. Chang, J. H. Lee, Y. Yan, J. G. Chen, and B. Xu. “Quantification of Active Sites and Elucidation of the Reaction Mechanism of the Electrochemical Nitrogen Reduction Reaction on Vanadium Nitride”. In: *Angewandte Chemie* 131.39 (2019), pp. 13906–13910.

- [96] H.-L. Du, T. R. Gengenbach, R. Hodgetts, D. R. MacFarlane, and A. N. Simonov. “Critical Assessment of the Electrocatalytic Activity of Vanadium and Niobium Nitrides toward Dinitrogen Reduction to Ammonia”. In: *ACS Sustainable Chemistry & Engineering* 7.7 (2019), pp. 6839–6850.
- [97] W. Schlesinger and A. Hartley. “A global budget for atmospheric NH₃”. In: *Biogeochemistry* 15.3 (1992), pp. 191–211.
- [98] C. Turner, P. Španěl, and D. Smith. “A longitudinal study of ammonia, acetone and propanol in the exhaled breath of 30 subjects using selected ion flow tube mass spectrometry, SIFT-MS”. In: *Physiological Measurement* 27.4 (2006), pp. 321–337.
- [99] J. E. Cotes, D. J. Chinn, and M. R. Miller. *Lung Function*. Oxford, UK: Blackwell Publishing Ltd., 2006, p. 636.
- [100] Y. Song, D. Johnson, R. Peng, D. K. Hensley, P. V. Bonnesen, L. Liang, J. Huang, F. Yang, F. Zhang, R. Qiao, A. P. Baddorf, T. J. Tschaplinski, N. L. Engle, M. C. Hatzell, Z. Wu, D. A. Cullen, H. M. Meyer, B. G. Sumpter, and A. J. Rondinone. “A physical catalyst for the electrolysis of nitrogen to ammonia”. In: *Science Advances* 4.4 (2018), e1700336.
- [101] J. B. Spinelli, L. P. Kelley, and M. C. Haigis. “An LC-MS Approach to Quantitative Measurement of Ammonia Isotopologues”. In: *Scientific Reports* 7.1 (2017), p. 10304.
- [102] M. Brass, T. Pritzel, E. Schulte, and J. U. Keller. “Measurements of Vapor-Liquid Equilibria in the Systems NH₃-H₂O-NaOH and NH₃-H₂O-KOH at Temperatures of 303 and 318 K and Pressures 0.1 MPa p 1.3 MPa”. In: *International Journal of Thermophysics* 21.4 (2000), pp. 883–898.
- [103] R. J. Yokelson. “Evaluation of adsorption effects on measurements of ammonia, acetic acid, and methanol”. In: *Journal of Geophysical Research* 108.D20 (2003), p. 4649.
- [104] F. Bianchi, J. Dommen, S. Mathot, and U. Baltensperger. “On-line determination of ammonia at low pptv mixing ratios in the CLOUD chamber”. In: *Atmospheric Measurement Techniques* 5.7 (2012), pp. 1719–1725.
- [105] L. Ma, Y. Cheng, G. Cavataio, R. W. McCabe, L. Fu, and J. Li. “Characterization of commercial Cu-SSZ-13 and Cu-SAPO-34 catalysts with hydrothermal treatment for NH₃-SCR of NO_x in diesel exhaust”. In: *Chemical Engineering Journal* 225 (2013), pp. 323–330.
- [106] L. Ma, Y. Cheng, G. Cavataio, R. W. McCabe, L. Fu, and J. Li. “In situ DRIFTS and temperature-programmed technology study on NH₃-SCR of NO over Cu-SSZ-13 and Cu-SAPO-34 catalysts”. In: *Applied Catalysis B: Environmental* 156-157 (2014), pp. 428–437.
- [107] N. Furuya and H. Yoshida. “Electroreduction of nitrogen to ammonia on gas-diffusion electrodes loaded with inorganic catalyst”. In: *Journal of Electroanalytical Chemistry and Interfacial Electrochemistry* 291.1-2 (1990), pp. 269–272.
- [108] Y. Yao, S. Zhu, H. Wang, H. Li, and M. Shao. “A Spectroscopic Study on the Nitrogen Electrochemical Reduction Reaction on Gold and Platinum Surfaces”. In: *Journal of the American Chemical Society* 140.4 (2018), pp. 1496–1501.
- [109] B.-A. Mei, O. Munteshari, J. Lau, B. Dunn, and L. Pilon. “Physical Interpretations of Nyquist Plots for EDLC Electrodes and Devices”. In: *The Journal of Physical Chemistry C* 122.1 (2018), pp. 194–206.

- [110] J. Kibsgaard and I. Chorkendorff. “Considerations for the scaling-up of water splitting catalysts”. In: *Nature Energy* (2019).
- [111] N. Mozzhukhina and E. J. Calvo. “Perspective—The Correct Assessment of Standard Potentials of Reference Electrodes in Non-Aqueous Solution”. In: *Journal of The Electrochemical Society* 164.12 (2017), A2295–A2297.
- [112] K. Izutsu. *Electrodeposition from Ionic Liquids Nanostructured Materials in Electrochemistry Electrochemistry*. WILEY-VCH Verlag GmbH & Co. KGaA, Weinheim, 2009, p. 408.
- [113] G. Inzelt, A. Lewenstam, and F. Scholz. “Handbook of reference electrodes”. In: *Handbook of Reference Electrodes* (2013), pp. 1–344.
- [114] D. Scott. “Tetrahydrofuran: vibrational assignment, chemical thermodynamic properties, and vapor pressure”. In: *The Journal of Chemical Thermodynamics* 2.6 (1970), pp. 833–837.
- [115] A. N. Dey and E. J. Rudd. “Electroinitiated Polymerization of Tetrahydrofuran”. In: *Journal of The Electrochemical Society* 121.10 (1974), p. 1294.
- [116] A. N. Dey. “Electrochemical Alloying of Lithium in Organic Electrolytes”. In: *Journal of The Electrochemical Society* 118.10 (1971), p. 1547.
- [117] D. Fischer and M. Jansen. “Synthesis and Structure of Na₃N”. In: *Angewandte Chemie International Edition* 41.10 (2002), pp. 1755–1756.
- [118] E. Peled and S. Menkin. “Review—SEI: Past, Present and Future”. In: *Journal of The Electrochemical Society* 164.7 (2017), A1703–A1719.
- [119] F. Zhou, L. M. Azofra, M. Ali, M. Kar, A. N. Simonov, C. McDonnell-Worth, C. Sun, X. Zhang, and D. R. MacFarlane. “Electro-synthesis of ammonia from nitrogen at ambient temperature and pressure in ionic liquids”. In: *Energy & Environmental Science* 10.12 (2017), pp. 2516–2520.
- [120] A. Sclafani, V. Augugliaro, and M. Schiavello. “Dinitrogen Electrochemical Reduction to Ammonia over Iron Cathode in Aqueous Medium”. In: *Journal of The Electrochemical Society* 130.3 (1983), p. 734.
- [121] N. Furuya and H. Yoshida. “Electroreduction of nitrogen to ammonia on gas-diffusion electrodes modified by Fe-phthalocyanine”. In: *Journal of Electroanalytical Chemistry and Interfacial Electrochemistry* 263.1 (1989), pp. 171–174.
- [122] G. Xu, R. Liu, and J. Wang. “Electrochemical synthesis of ammonia using a cell with a Nafion membrane and SmFe_{0.7}Cu_{0.3-x}Ni_xO₃ (x = 0–0.3) cathode at atmospheric pressure and lower temperature”. In: *Science in China Series B: Chemistry* 52.8 (2009), pp. 1171–1175.
- [123] Z. Zhang, Z. Zhong, and R. Liu. “Cathode catalysis performance of SmBaCuMO_{5+d} (M=Fe, Co, Ni) in ammonia synthesis”. In: *Journal of Rare Earths* 28.4 (2010), pp. 556–559.
- [124] K. Kugler, M. Luhn, J. A. Schramm, K. Rahimi, and M. Wessling. “Galvanic deposition of Rh and Ru on randomly structured Ti felts for the electrochemical NH₃ synthesis”. In: *Physical Chemistry Chemical Physics* 17.5 (2015), pp. 3768–3782.
- [125] D. Bao, Q. Zhang, F.-L. Meng, H.-X. Zhong, M.-M. Shi, Y. Zhang, J.-M. Yan, Q. Jiang, and X.-B. Zhang. “Electrochemical Reduction of N₂ under Ambient Conditions for Artificial N₂ Fixation and Renewable Energy Storage Using N₂/NH₃ Cycle”. In: *Advanced Materials* 29.3 (2017), p. 1604799.

- [126] G.-F. Chen, X. Cao, S. Wu, X. Zeng, L.-X. Ding, M. Zhu, and H. Wang. “Ammonia Electrosynthesis with High Selectivity under Ambient Conditions via a Li⁺ Incorporation Strategy”. In: *Journal of the American Chemical Society* 139.29 (2017), pp. 9771–9774.
- [127] K. Kim, C.-Y. Yoo, J.-N. Kim, H. C. Yoon, and J.-I. Han. “Electrochemical Synthesis of Ammonia from Water and Nitrogen in Ethylenediamine under Ambient Temperature and Pressure”. In: *Journal of The Electrochemical Society* 163.14 (2016), F1523–F1526.
- [128] D. L. Boucher, J. A. Davies, J. G. Edwards, and A. Mennad. “An investigation of the putative photosynthesis of ammonia on iron-doped titania and other metal oxides”. In: *Journal of Photochemistry and Photobiology A: Chemistry* 88.1 (1995), pp. 53–64.
- [129] M. A. Shipman and M. D. Symes. “A re-evaluation of Sn(II) phthalocyanine as a catalyst for the electrosynthesis of ammonia”. In: *Electrochimica Acta* 258 (2017), pp. 618–622.
- [130] J. Choi, H.-L. Du, M. Chatti, B. H. R. Suryanto, A. Simonov, and D. Macfarlane. “Promoting nitrogen electroreduction to ammonia with bismuth nanocrystals and potassium cations in water”. In: *ChemRxiv, preprint* (2020).
- [131] K. Nishikawa, T. Mori, T. Nishida, Y. Fukunaka, M. Rosso, and T. Homma. “In Situ Observation of Dendrite Growth of Electrodeposited Li Metal”. In: *Journal of The Electrochemical Society* 157.11 (2010), A1212.
- [132] Bruker. *Periodic Table of Elements and X-ray Energies*. 2015.
- [133] D. D. Wagman, W. H. Evans, V. B. Parker, R. H. Schumm, I. Halow, S. M. Bailey, K. L. Churney, and R. L. Nuttall. “The NBS tables of chemical thermodynamic properties. Selected values for inorganic and C1 and C2 organic substances in SI units [J. Phys. Chem. Ref. Data 11, Suppl. 2 (1982)]”. In: *Journal of Physical and Chemical Reference Data* 18.4 (1989), pp. 1807–1812.
- [134] K. Kanamura. “XPS Analysis of Lithium Surfaces Following Immersion in Various Solvents Containing LiBF₄”. In: *Journal of The Electrochemical Society* 142.2 (1995), p. 340.
- [135] F. Shi, A. Pei, D. Thomas, J. Xie, X. Yu, X. Zhang, and Y. Cui. “Lithium metal stripping beneath the solid electrolyte interphase”. In: *PNAS* 115.34 (2018), pp. 8529–8534.
- [136] K. Xu. “Electrolytes and interphases in Li-ion batteries and beyond”. In: *Chemical Reviews* 114.23 (2014), pp. 11503–11618.
- [137] A. R. Singh, B. A. Rohr, M. J. Statt, J. A. Schwalbe, M. Cargnello, and J. K. Nørskov. “Strategies toward Selective Electrochemical Ammonia Synthesis”. In: *ACS Catalysis* 9.9 (2019), pp. 8316–8324.
- [138] J. A. Schwalbe, M. J. Statt, C. Chosy, A. R. Singh, B. A. Rohr, A. C. Nielander, S. Z. Andersen, J. M. McEnaney, J. G. Baker, T. F. Jaramillo, J. K. Nørskov, and M. Cargnello. “A Combined Theory-Experiment Analysis of the Surface Species in Lithium-Mediated NH₃ Electrosynthesis”. In: *ChemElectroChem* 7 (2020), pp. 1542–1549.
- [139] A. Valera-Medina, H. Xiao, M. Owen-Jones, W. I. David, and P. J. Bowen. “Ammonia for power”. In: *Progress in Energy and Combustion Science* 69 (2018), pp. 63–102.
- [140] R. Lan, J. T. Irvine, and S. Tao. “Ammonia and related chemicals as potential indirect hydrogen storage materials”. In: *International Journal of Hydrogen Energy* 37.2 (2012), pp. 1482–1494.
- [141] N. V. Rees and R. G. Compton. “Carbon-free energy: A review of ammonia- and hydrazine-based electrochemical fuel cells”. In: *Energy and Environmental Science* 4.4 (2011), pp. 1255–1260.

- [142] S. Suzuki, H. Muroyama, T. Matsui, and K. Eguchi. “Fundamental studies on direct ammonia fuel cell employing anion exchange membrane”. In: *Journal of Power Sources* 208 (2012), pp. 257–262.
- [143] R. F. Service. “Liquid Sunshine”. In: *Science* 361.6398 (2018), pp. 120–123.

Appendix A

Supporting Information

A.1 Appendant to Chapter 5: Electrochemical Measurements

A.1.1 Example of determining potential range for Figure 5.6

Getting the desired WE potential was not entirely trivial for these measurements, as our current and our Ohmic resistance in the system would change throughout the measurement.

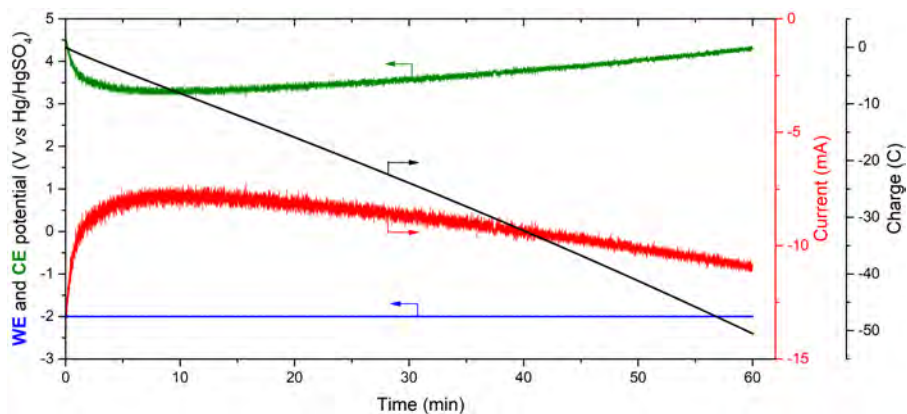


Figure A.1 CA spectrum from Figure 5.6 for Ru with 1 hour of electrochemistry at -1 V vs Hg/HgSO₄.

Figure A.1 shows an example of the acquired CA spectrum. We would first run PEIS, as seen in black on Figure A.2, to determine R in the system. First we need to convert from the saturated Hg/HgSO₄ RE used to SHE. The difference between the potential scales is 0.64 V at room temperature [45]. Then we can convert to RHE. As our electrolyte is 0.1 M KOH, the pH

is 13. The conversion is therefore:

$$U_{RHE} = U_{\text{Hg}/\text{HgSO}_4} + 0.64 + 0.0591 \cdot \text{pH} \quad (\text{A.1})$$

The potentiostat would only manually IR correct for 85 %, so we need to add the rest ourselves. From Figure A.2 it was seen that the initial R was around 70Ω , from which 85 % will be manually corrected. We applied $-2.0 \text{ V vs Hg}/\text{HgSO}_4$ as the WE potential (based on a "guesstimate" of how much the current and Ohmic resistance might vary). It was seen in Figure A.1 that the current varied from -14.0 to -7.5 mA . We chose to simplify the calculation, and use a weighted average current for these calculations. In this case, the weighted average current is -8.9 mA .

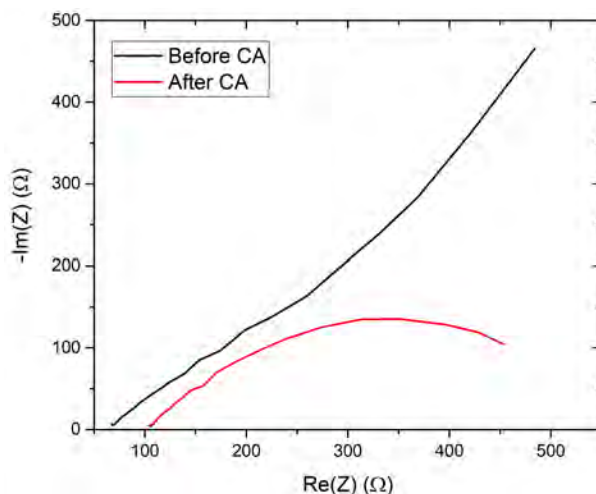


Figure A.2 PEIS spectra from Figure 5.6 for Ru with 1 hour of electrochemistry at -1 V vs RHE before and after CA

We can then calculate that the starting WE potential is:

$$U_{\text{before}} = -2.0 \text{ V} + 0.64 + 0.0591 \cdot 13 - (0.15 \cdot 70\Omega \cdot 8.9 \text{ mA}) = -0.6 \text{ V vs RHE} \quad (\text{A.2})$$

Unfortunately, R is seen to change after the measurement, most likely due to changes in temperature during the measurement. From Figure A.2, it is seen that R after running 1 hour of CA is around 105Ω . This is completely uncompensated for, and will change the actual potential by $(105 \Omega - 90 \Omega) \cdot (-8.9 \text{ mA}) = -0.3 \text{ V}$. So from these calculations, we estimate that the actual potential range during this measurement is $[-0.6, -0.9] \text{ V vs RHE}$.

A.1.2 Example SGEIS spectra from Table 5.6

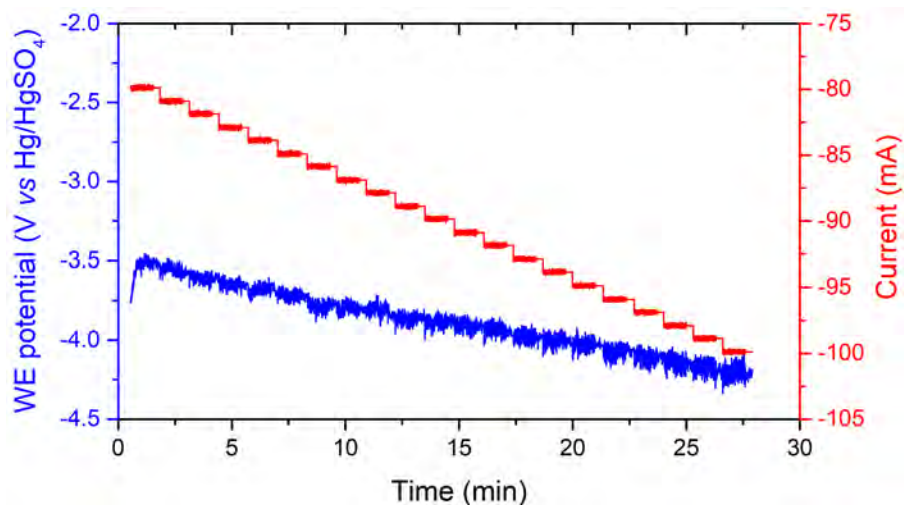


Figure A.3 SGEIS spectrum from Table 5.6 for Fe from 80-100 mA with 27 minutes of electrochemistry at $[-2.0, 2.6]$ V vs RHE.

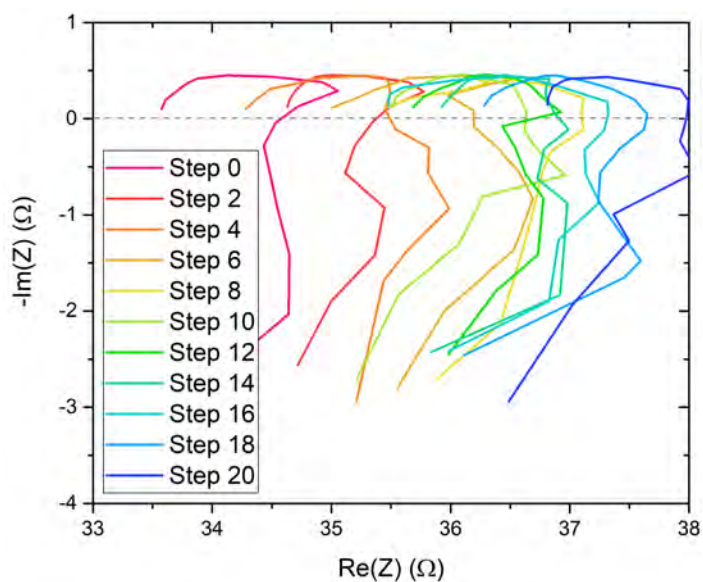


Figure A.4 Nyquist plots of impedance between the increases in current from the SGEIS spectrum for Fe from 80-100 mA with 27 minutes of electrochemistry at $[-2.0, 2.6]$ V vs RHE shown in Figure A.3.

A.2 Appendant to Chapter 7: SEM images

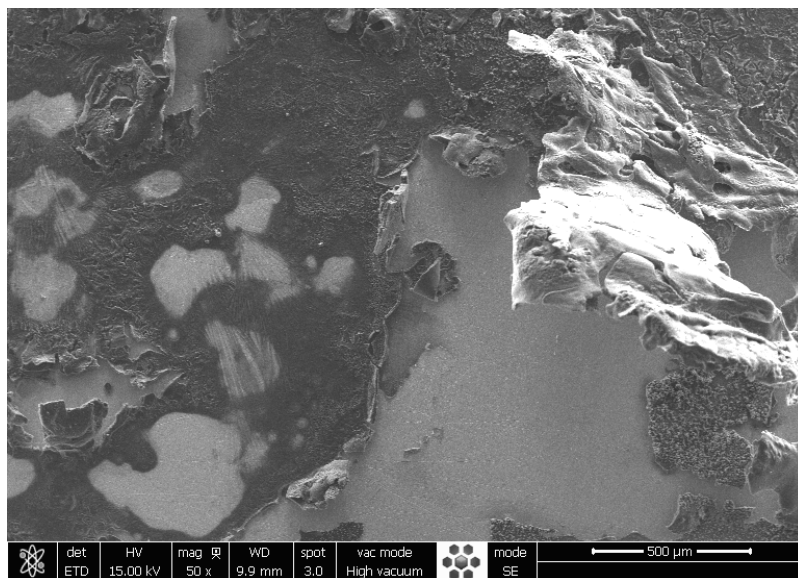


Figure A.5 SEM image of constant deposition sample. Same spot as Figure 7.8c, just zoomed out.

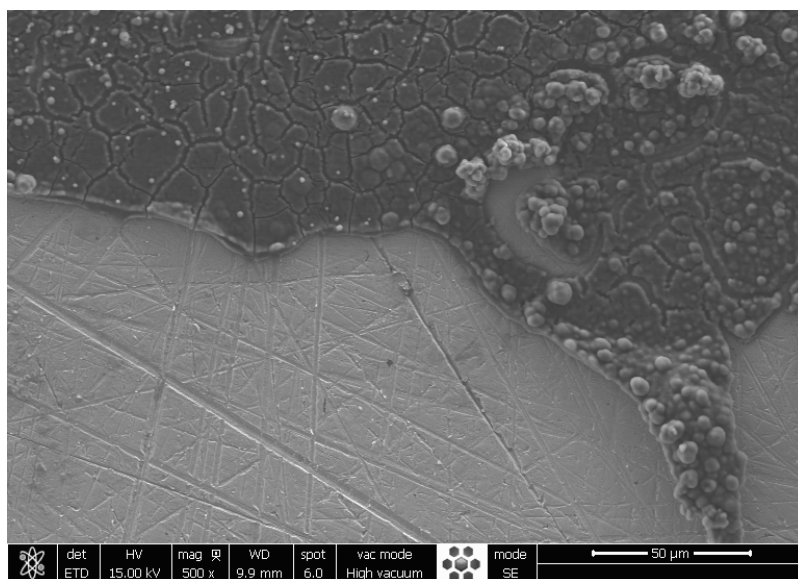


Figure A.6 SEM image of constant deposition sample. Same spot as Figure 7.9.

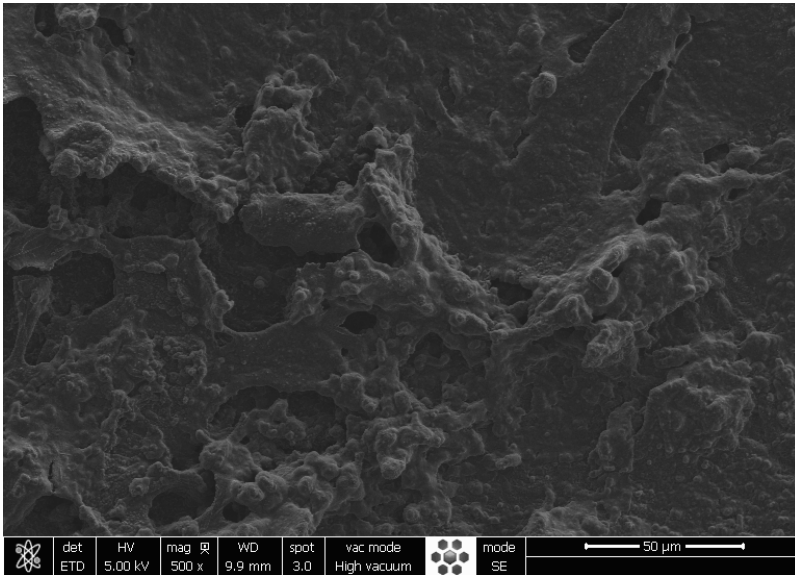


Figure A.7 SEM image of constant deposition sample. Same spot as Figure 7.8d, just zoomed out.

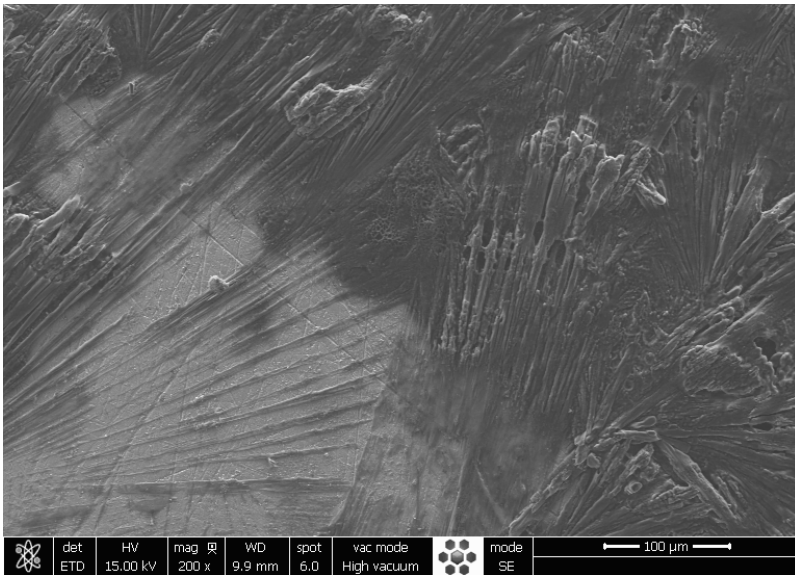


Figure A.8 SEM image of constant deposition sample. New area shown. The Mo foil underneath is clearly visible on parts of the surface.

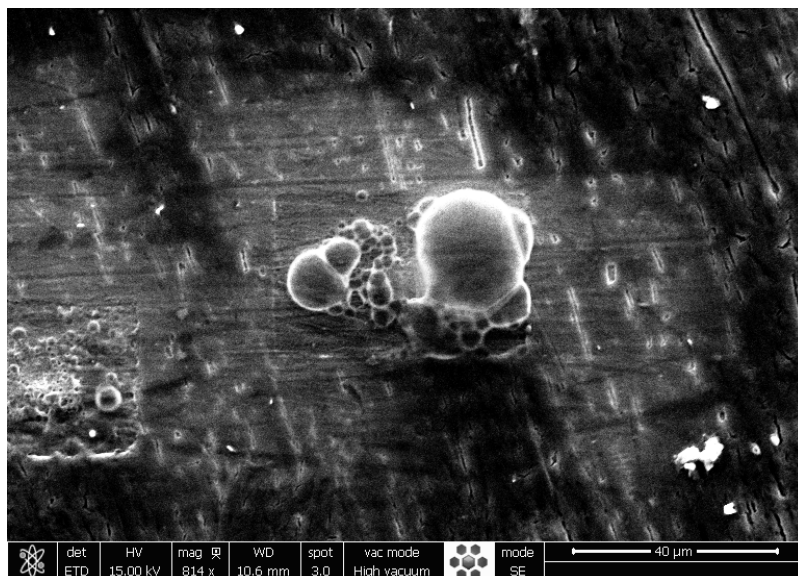


Figure A.9 SEM image of cycling method sample show in Figure 7.8. High-energy electron beam used (15 kV), which "boiled" away sample. Bubbles appeared, grew, and burst on the scale of seconds. Mo foil underneath became more visible.

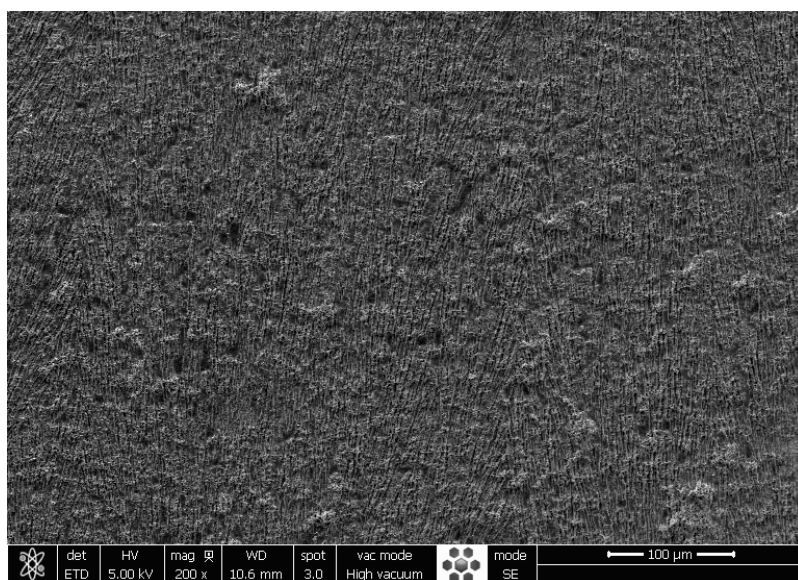


Figure A.10 SEM image of cycling sample on a new area of sample.

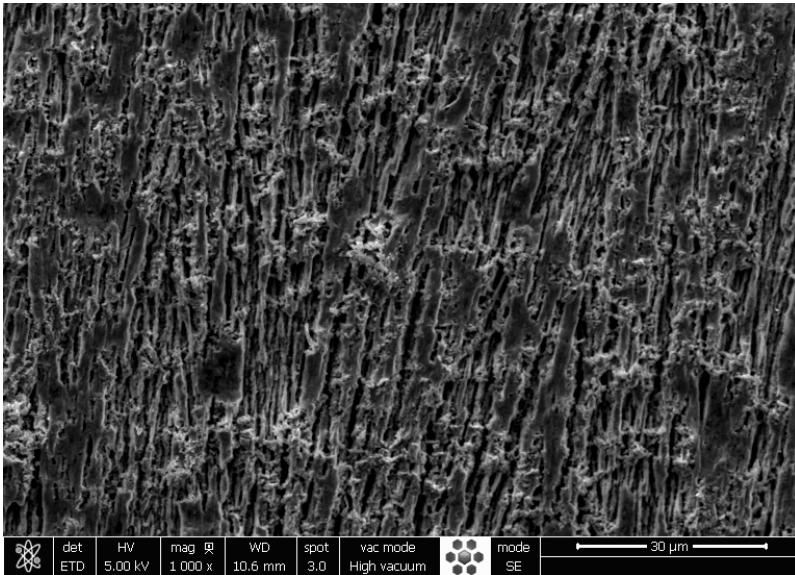


Figure A.11 SEM image of cycling sample shown in Figure A.10, just zoomed in.

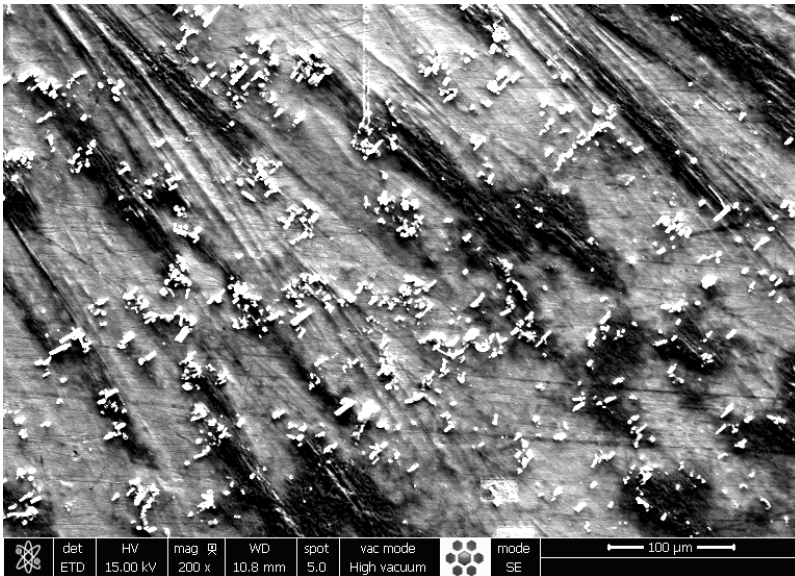


Figure A.12 SEM image of cycling sample. High contrast applied on section with whisker growth. Mo foil underneath becomes visible with increased contrast.

Appendix B

Appended Publications

Paper I

A rigorous electrochemical ammonia synthesis protocol with quantitative isotope measurements

Suzanne Z. Andersen*, Viktor Čolić*, Sungeun Yang*, Jay A. Schwalbe, Adam C. Nielander, Joshua M. McEnaney, Kasper Enemark-Rasmussen, Jon G. Baker, Aayush R. Singh, Brian A. Rohr, Michael J. Statt, Sarah J. Blair, Stefano Mezzavilla, Jakob Kibsgaard, Peter C. K. Vesborg, Matteo Cargnello, Stacey F. Bent, Thomas F. Jaramillo, Ifan E. L. Stephens, Jens K. Nørskov and Ib Chorkendorff

Nature, **570**, 504-508, (2019)

* these authors contributed equally

A rigorous electrochemical ammonia synthesis protocol with quantitative isotope measurements

Suzanne Z. Andersen^{1,6}, Viktor Čolić^{1,6}, Sungeun Yang^{1,5,6}, Jay A. Schwalbe², Adam C. Nielander², Joshua M. McEnaney², Kasper Enemark-Rasmussen³, Jon G. Baker², Aayush R. Singh², Brian A. Rohr², Michael J. Statt², Sarah J. Blair², Stefano Mezzavilla⁴, Jakob Kibsgaard¹, Peter C. K. Vesborg¹, Matteo Cargnello², Stacey F. Bent², Thomas F. Jaramillo², Ifan E. L. Stephens⁴, Jens K. Nørskov² & Ib Chorkendorff^{1*}

The electrochemical synthesis of ammonia from nitrogen under mild conditions using renewable electricity is an attractive alternative^{1–4} to the energy-intensive Haber–Bosch process, which dominates industrial ammonia production. However, there are considerable scientific and technical challenges^{5,6} facing the electrochemical alternative, and most experimental studies reported so far have achieved only low selectivities and conversions. The amount of ammonia produced is usually so small that it cannot be firmly attributed to electrochemical nitrogen fixation^{7–9} rather than contamination from ammonia that is either present in air, human breath or ion-conducting membranes⁹, or generated from labile nitrogen-containing compounds (for example, nitrates, amines, nitrites and nitrogen oxides) that are typically present in the nitrogen gas stream¹⁰, in the atmosphere or even in the catalyst itself. Although these sources of experimental artefacts are beginning to be recognized and managed^{11,12}, concerted efforts to develop effective electrochemical nitrogen reduction processes would benefit from benchmarking protocols for the reaction and from a standardized set of control experiments designed to identify and then eliminate or quantify the sources of contamination. Here we propose a rigorous procedure using ¹⁵N₂ that enables us to reliably detect and quantify the electrochemical reduction of nitrogen to ammonia. We demonstrate experimentally the importance of various sources of contamination, and show how to remove labile nitrogen-containing compounds from the nitrogen gas as well as how to perform quantitative isotope measurements with cycling of ¹⁵N₂ gas to reduce both contamination and the cost of isotope measurements. Following this protocol, we find that no ammonia is produced when using the most promising pure-metal catalysts for this reaction in aqueous media, and we successfully confirm and quantify ammonia synthesis using lithium electrodeposition in tetrahydrofuran¹³. The use of this rigorous protocol should help to prevent false positives from appearing in the literature, thus enabling the field to focus on viable pathways towards the practical electrochemical reduction of nitrogen to ammonia.

Ruthenium, rhenium and rhodium are the most promising pure metal catalysts¹⁴, for which our electrochemical benchmarking experiments in aqueous electrolyte yielded no more ammonia than the background level of around 10 parts per billion (p.p.b.) (Fig. 1). We conclude that under these conditions no ammonia is synthesized, and that the competing hydrogen evolution reaction dominates in an aqueous environment⁵. Figure 2a–c compares the amounts of ammonia produced in this negative-result experiment with those reported in the literature, and illustrates that the reported ammonia production rates and concentrations are often close to the common background levels that we also explicitly quantify (see Extended Data Fig. 1). Reporting only ammonia production rates, without careful control experiments, is thus clearly

not sufficient to reliably document the formation of ammonia. The problem of spurious nitrogen¹⁵ giving rise to experimental artefacts is well recognized in other fields, and probably explains the inability to reproduce¹⁶ the photochemical synthesis of ammonia over titanium dioxide under rigorous conditions. This problem is also increasingly recognized in the context of electrochemical ammonia synthesis, in which recent re-testing of a putative phthalocyanine-based ammonia electrosynthesis catalyst attributed the detected ammonia to contaminants or catalyst decomposition¹⁷. Measurement protocols are currently being developed to ensure that false positives can be distinguished from breakthrough results^{11,12}.

Previous studies have discussed the need to improve measurements and control studies in the synthesis of ammonia^{11,12}, and have identified a range of factors that must be considered to ensure that any ammonia detected is produced from dinitrogen rather than as a result of adventitious contamination. To this end, we implement a systematic benchmarking protocol that also quantifies the electroreduction of nitrogen. This protocol is presented in Fig. 3 in the form of a flow chart.

Previous studies^{11,12} have stated that, as a first control, it is essential to perform measurements with argon under exactly the same conditions as the nitrogen electroreduction experiments, in order to quantify ammonia that originates from contamination within the cell or from within the catalyst itself. A control with nitrogen at open circuit potential over the same duration as the electroreduction experiment is equally important, to investigate contamination in the feed-gas stream. However, we note that even high-purity nitrogen gas can contain, in addition to ammonia itself, other easily reduced nitrogen sources such as NO_x. As such, in order to reduce adventitious contamination, nitrogen gas should first be passed over an appropriate adsorbent—for example, copper (see Methods).

Other sources of contamination may also be present, which may lead to activity tests indicating that comparable amounts of ammonia are present in both samples and controls. These sources include Nafion, which is used in some N₂ electroreduction experiments as a separating membrane or electrolyte^{9,18} and which accumulates and releases ammonium ions (NH₄⁺) through ion exchange with acid groups (see Methods). Ambient air also contains a non-negligible amount of ammonia (ranging from 0.05–250 parts per million (p.p.m.)¹⁹) that can accumulate in chemicals and/or the experimental set-up, making the use of a closed system imperative. Similarly, human breath contains 0.3–3.0 p.p.m. ammonia²⁰ and therefore must be carefully excluded. The presence and the strength of these sources of contamination vary enormously, such that persuasive evidence for the successful electrochemical synthesis of ammonia requires the accumulation of ammonia in concentrations that substantially exceed those obtained in control measurements, including those with argon and those with nitrogen at open circuit potential over the duration of the experiment.

¹Department of Physics, Technical University of Denmark, Kongens Lyngby, Denmark. ²SUNCAT Center for Interface Science and Catalysis, Department of Chemical Engineering, Stanford University, Stanford, CA, USA. ³Department of Chemistry, Technical University of Denmark, Kongens Lyngby, Denmark. ⁴Department of Materials, Imperial College London, London, UK. ⁵Present address: Center for Energy Materials Research, Korea Institute of Science and Technology (KIST), Seoul, South Korea. ⁶These authors contributed equally: Suzanne Z. Andersen, Viktor Čolić, Sungeun Yang. *e-mail: ibchork@fysik.dtu.dk

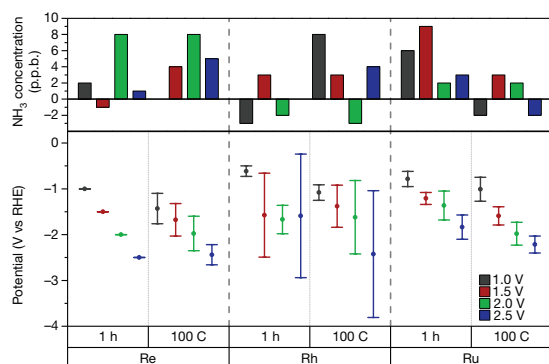


Fig. 1 | Potential range for chronoamperometric measurements of pure-metal catalysts and the detected amounts of ammonia in each measurement. Each catalyst was tested both for 1 h and by passing 100 C of charge at -1.0 , -1.5 , -2.0 and -2.5 V vs reversible hydrogen electrode (RHE), where the error bars represent a change in potential during the measurement due to a changing IR (Ohmic)-drop correction (see Methods).

More definite proof that any detected ammonia originates from the electroreduction of N_2 requires experiments using isotopically labelled $^{15}N_2$ gas; the $^{15}NH_3$ produced is then detected with an isotope-sensitive method. In this control experiment, the amount of $^{15}NH_3$ produced should be in quantitative agreement with the amount of $^{14}NH_3$ produced in the equivalent $^{14}N_2$ reduction tests. We note that, although recent studies included in Fig. 2 include isotope-labelling experiments, most of these lack quantitative data and would fail the requirements of our protocol.

Methods such as mass spectrometry²¹ and infrared spectroscopy²² can discriminate $^{15}NH_3$ from $^{14}NH_3$ (see Methods and Extended Data Fig. 3). We focus here on nuclear magnetic resonance (NMR) spectroscopy, which we found to be the most convenient. 1H NMR can differentiate between the isotopes, because the scalar interaction between 1H and ^{15}N in $^{15}NH_4^+$ results in a splitting of the 1H resonance into two

symmetric signals with a spacing of 73 Hz, whereas the 1H resonance coupled to ^{14}N in $^{14}NH_4^+$ is split into three symmetric signals with a spacing of 52 Hz. A solution with no added ammonia still shows weak peaks for $^{14}NH_4^+$, due to the aforementioned background contamination. Under the conditions described in Methods using an 800 MHz NMR instrument, the peaks for $^{15}NH_4^+$ are detectable at concentrations as low as 51 p.p.b., and the amounts of $^{14}NH_4^+$ and $^{15}NH_4^+$ can be quantified from the integrated peak areas. We have also demonstrated this strategy using a lower-field (and more common) 400 MHz NMR instrument (see Extended Data Fig. 2).

Isotope-labelled $^{15}N_2$ gas usually contains not only ammonia as an impurity, but also reducible, labile nitrogen-containing compounds such as NO_x ¹⁰. As an illustration of the potential effect of such impurities, we consider a recent study that reports microgram NH_3 yields obtained through the electroreduction of a very small fraction of the nitrogen reactant gas over the course of several days²³. The isotope-labelling control used $^{15}N_2$ gas with a purity of 99.13%, bubbled for 28 h at a rate of 10 ml min⁻¹. In such a case, the 0.87% of impurities could potentially lead to 3,600 μg of ammonia or other nitrogen-containing species per hour, which over the course of the experiment would equate to 100 mg and would vastly exceed the reported yield of ammonia. This illustrates the great care that must be taken when dealing with the almost inevitable contamination of the nitrogen gas, as even impurity levels that are restricted to a few p.p.m. can be highly problematic. Although control measurements with $^{15}N_2$ gas flowing through the cell under open circuit potential must be conducted to establish the level of ammonia contamination from the gas feed, in the same manner as for measurements with $^{14}N_2$ gas, additional purification is essential before the gas enters the electrochemical cell, to mitigate the contribution of contaminants such as NO_x and other labile nitrogen compounds. This can be effectively achieved through adsorption on a reduced copper catalyst (see Methods). We have implemented a gas recycling set-up (see Methods), which enables us to reduce impurity levels and reuse expensive $^{15}N_2$ when conducting isotope-labelling control experiments.

In cases in which the electroreduction of nitrogen to ammonia is successfully observed, experiments will need to be repeated in order to establish reproducible results with error bars and so that the mean and variance of the data can be determined. To enable the meaningful comparison of data collected under different conditions in different

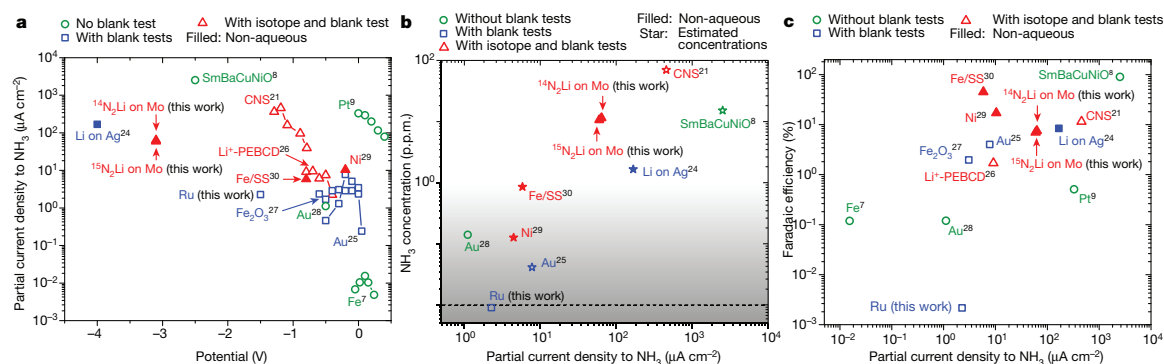


Fig. 2 | An overview of literature data on the electrochemical synthesis of ammonia. For further details, including the experimental conditions under which these data were obtained, see Extended Data Tables 1–4. Green dots represent data without a blank test, blue squares present data from experiments in which a blank test was performed, red triangles represent data with $^{15}N_2$ isotope tests with blank tests, filled symbols indicate non-aqueous systems, and stars are estimated values using data provided in the literature. **a**, Partial current densities for electrochemical ammonia production plotted against applied potential (vs RHE unless otherwise specified). **b**, Ammonia concentrations as a function of partial current density towards ammonia formation. The dashed line at 10 p.p.b. indicates the lower limit of detection of ammonia in our system, and the grey

gradient indicates concentrations wherein we have seen false positives, with a darker colour indicating a higher probability for false positives (see Extended Data Fig. 1). **c**, Faradaic efficiency of the detected ammonia as a function of partial current density towards ammonia. Data adapted from: ref. 7 for Fe; ref. 8 for SmBaCuNiO; ref. 9 for Pt; ref. 25 for Au; ref. 26 for Li⁺-PEBCD (Li⁺ incorporated into poly(*N*-ethyl-benzene-1,2,4,5-tetracarboxylic diimide)); ref. 27 for Fe₂O₃; ref. 28 for Au; ref. 29 for Ni with a potential of 1.8 V between two electrodes; ref. 30 for Fe/stainless steel (SS) with a potential vs normal hydrogen electrode (NHE); ref. 21 for nitrogen-doped carbon nanospikes (CNS); ref. 24 for Li on Ag with a potential vs Ag/AgCl/AgCl (sat), LiCl, LiClO₄/THF reference. The potential for Li on Mo in this work is -3.1 V vs standard hydrogen electrode (SHE).

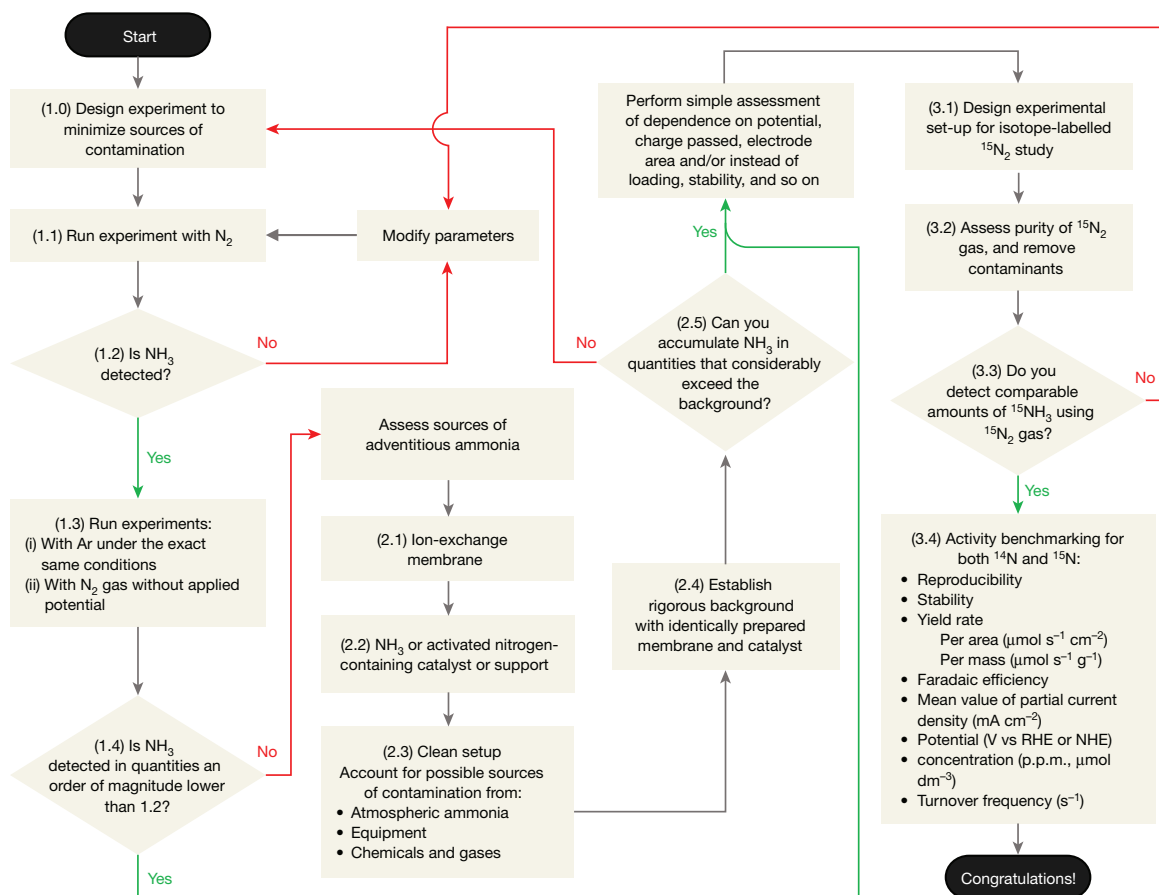


Fig. 3 | Suggested protocol for the benchmarking of electrochemical nitrogen reduction. Part 1 of the flow chart enables determination of adventitious background contamination of ammonia and other nitrogen containing compounds in the setup. Part 2 is only necessary

if the measured contamination levels are within an order of magnitude of the ammonia produced. Part 3 leads to isotope-sensitive quantitative measurements of synthesized ammonia, which should be comparable to the ammonia measured in part 1.

experimental set-ups, we suggest reporting the actual concentration of detected ammonia, the concentrations measured in control measurements and the electrolyte volume. Useful figures of merit that should be reported include the partial current density under which ammonia is synthesized, stated in mA cm^{-2} and normalized to geometric and electrochemically active surface area; the turnover frequency per site per second; the working electrode potential; the faradaic efficiency; the yield rate normalized to the electrode surface area; and the mass of the catalyst. The amount of ammonia produced can be quantified using isotope-specific NMR and colorimetric measurements (see Methods), which must give similar results. There must also be a 1:1 agreement between the amounts of ammonia produced in the $^{14}\text{N}_2$ and $^{15}\text{N}_2$ reduction tests performed under the same conditions.

We have used our proposed protocol to test several of the more promising processes and catalysts shown in Fig. 2. So far, we have been able to reproduce only the lithium-mediated nitrogen electroreduction experiment²⁴, which measured high current densities and determined ammonia concentrations using a colorimetric indophenol test and an ammonia gas-sensing electrode. However, the original study lacked crucial isotope-labelled measurements. In an experiment using a molybdenum foil and $^{14}\text{N}_2$ gas we were able to confirm the formation of ammonia by determining $^{14}\text{NH}_3$ using a colorimetric method and NMR (Fig. 4a, b). Two control experiments, one with argon accumulating 20 C of charge and another with cleaned $^{14}\text{N}_2$ gas at open

circuit potential for 1.5 h, gave no discernible quantity of ammonia. Finally, experiments using isotopically labelled $^{15}\text{N}_2$ (containing 2% $^{14}\text{N}_2$, with the gas cleaned using copper catalyst as an impurity trap; see Methods) confirmed the electrochemical production of $^{15}\text{NH}_3$ from $^{15}\text{N}_2$ (Fig. 4c), and the amount of accumulated ammonia correlated with the amount of charge passed through the system (Fig. 4d). When using $^{14}\text{N}_2$ gas, the quantification of ammonia by NMR and indophenol measurements resulted in a mean faradaic efficiency of $6.5 \pm 1.4\%$ and $7.5 \pm 1.1\%$, respectively; a mean yield rate of $0.7 \pm 0.2 \mu\text{mol h}^{-1} \text{cm}_{\text{geo}}^{-2}$ and $0.8 \pm 0.1 \mu\text{mol h}^{-1} \text{cm}_{\text{geo}}^{-2}$ (where 'geo' indicates that it is the geometric surface area that is stated); and a mean concentration after 20 C of charge had passed of $0.56 \pm 0.10 \text{ mM}$ ($9.6 \pm 1.6 \text{ p.p.m.}$) and $0.65 \pm 0.08 \text{ mM}$ ($11.1 \pm 1.3 \text{ p.p.m.}$). When using $^{15}\text{N}_2$ gas, ammonia determined by NMR and indophenol measurements gave a mean faradaic efficiency of $5.7 \pm 0.7\%$ and $7.0 \pm 2.2\%$, respectively; a mean yield rate of $0.6 \pm 0.1 \mu\text{mol h}^{-1} \text{cm}_{\text{geo}}^{-2}$ and $0.7 \pm 0.2 \mu\text{mol h}^{-1} \text{cm}_{\text{geo}}^{-2}$; and a mean concentration after 20 C charge had passed of $0.49 \pm 0.05 \text{ mM}$ ($8.3 \pm 0.9 \text{ p.p.m.}$) and $0.61 \pm 0.16 \text{ mM}$ ($10.3 \pm 2.7 \text{ p.p.m.}$). Although the exact nature of the lithium-mediated ammonia synthesis mechanism will be the subject of a future report, our observations validate the lithium-mediated strategy for the electrochemical production of ammonia, and illustrate that ammonia can be synthesized in similar quantities from $^{14}\text{N}_2$ and $^{15}\text{N}_2$ as well as demonstrating the use of our benchmarking protocol.

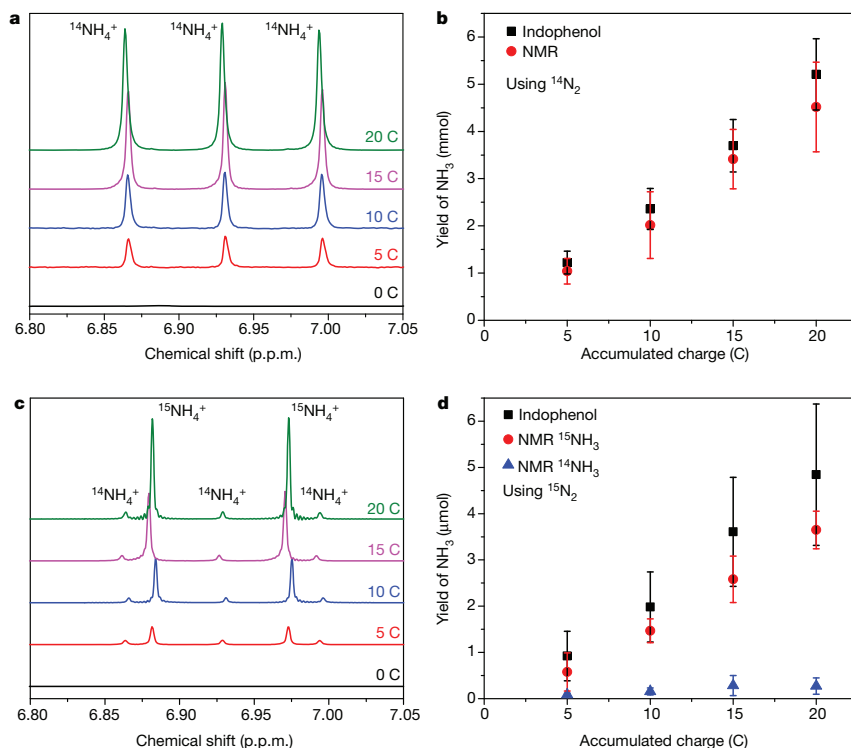


Fig. 4 | Ammonia synthesized at -3.1 V and more negative potentials vs SHE. Potentials were IR-drop corrected, and the experiments were conducted using a Mo cathode and Pt anode in an electrolyte of 0.2 M LiClO₄ in 1% ethanol and 99% THF, in the system reported in ref. ²⁴. Here, the formation of ammonia is successfully proven by repeated regular and isotope-labelled experiments. **a**, Representative NMR data from an experiment in which samples were taken at 5 C, 10 C, 15 C and 20 C using ¹⁴N₂ with THF suppression (see Methods for details). **b**, Data show mean \pm s.d. of three measurements of ¹⁴NH₃ yield, obtained from the

integrated peak area of the NMR data calibrated with the data from Extended Data Fig. 2b, c and the indophenol method. **c**, Representative NMR data from experiments with ¹⁵N₂ with samples taken at 5 C, 10 C, 15 C and 20 C. **d**, Data show mean \pm s.d. of three measurements of ¹⁵NH₃ yield, obtained from the integrated peak area from NMR data calibrated with data from Extended Data Fig. 2c, d and the indophenol method. The ¹H spectra were referenced by setting the chemical shift of the methyl resonance of ethanol to 1.15 p.p.m. (TMS = 0.0 p.p.m.). The slight shift in the NMR peaks is due to slight differences in the pH, volume, and/or temperature of samples.

We anticipate that our rigorous protocol will enable a more effective identification of electrochemical systems that are truly capable of reducing nitrogen to ammonia. In addition, by preventing false positives from appearing in the literature, it may ultimately aid the development of more efficient processes that yield substantially larger amounts of ammonia than are currently achieved. Once ammonia can be produced at concentrations beyond the parts-per-million range, rigorous protocols with quantitative isotope-sensitive experiments may no longer be necessary for every measurement. However, the varied sources of potential contamination will remain, and our suggested control experiments thus remain important and relevant when exploring nitrogen-conversion processes, including photoelectrochemical reduction and oxidation to NO_x species.

Online content

Any methods, additional references, Nature Research reporting summaries, source data, statements of data availability and associated accession codes are available at <https://doi.org/10.1038/s41586-019-1260-x>.

Received: 8 June 2018; Accepted: 9 May 2019;

Published online 22 May 2019.

- Shipman, M. A. & Symes, M. D. Recent progress towards the electrosynthesis of ammonia from sustainable resources. *Catal. Today* **286**, 57–68 (2017).
- Jewess, M. & Crabtree, R. H. Electrocatalytic nitrogen fixation for distributed fertilizer production? *ACS Sustainable Chem. Eng.* **4**, 5855–5858 (2016).

- Nørskov, J. et al. *Sustainable Ammonia Synthesis – Exploring the Scientific Challenges Associated with Discovering Alternative, Sustainable Processes for Ammonia Production*. <https://doi.org/10.2172/1283146> (United States Department of Energy, 2016).
- Ye, L., Nayak-Luke, R., Bañares-Alcántara, R. & Tsang, E. Reaction: “green” ammonia production. *Chem* **3**, 712–714 (2017).
- Singh, A. R. et al. Electrochemical ammonia synthesis—the selectivity challenge. *ACS Catal.* **7**, 706–709 (2017).
- Skúlason, E. et al. A theoretical evaluation of possible transition metal electro-catalysts for N₂ reduction. *Phys. Chem. Chem. Phys.* **14**, 1235–1245 (2012).
- Sclafani, A., Augugliaro, V. & Schiavello, M. Dinitrogen electrochemical reduction to ammonia over iron cathode in aqueous medium. *J. Electrochem. Soc.* **130**, 734–736 (1983).
- Zhang, Z., Zhong, Z. & Liu, R. Cathode catalysis performance of SmBaCuMO_{5+δ} (M = Fe, Co, Ni) in ammonia synthesis. *J. Rare Earths* **28**, 556–559 (2010).
- Lan, R., Irvine, J. T. S. & Tao, S. Synthesis of ammonia directly from air and water at ambient temperature and pressure. *Sci. Rep.* **3**, 1145 (2013).
- Dabundo, R. et al. The contamination of commercial ¹⁵N₂ gas stocks with ¹⁵N-labeled nitrate and ammonium and consequences for nitrogen fixation measurements. *PLoS One* **9**, e110335 (2014).
- Greenlee, L. F., Renner, J. N. & Foster, S. L. The use of controls for consistent and accurate measurements of electrocatalytic ammonia synthesis from dinitrogen. *ACS Catal.* **8**, 7820–7827 (2018).
- Chen, G.-F. et al. Advances in electrocatalytic N₂ reduction—strategies to tackle the selectivity challenge. *Small Methods* 1800337 (2018).
- Tsuneto, A., Kudo, A. & Sakata, T. Efficient electrochemical reduction of N₂ to NH₃ catalyzed by lithium. *Chem. Lett.* **22**, 851–854 (1993).
- Montoya, J. H., Tsai, C., Vojvodica, A. & Nørskov, J. K. The challenge of electrochemical ammonia synthesis: a new perspective on the role of nitrogen scaling relations. *ChemSusChem* **8**, 2180–2186 (2015).
- Hager, T. *The Alchemy of Air* (Harmony Books, 2008).

16. Boucher, D. L., Davies, J. A., Edwards, J. G. & Mennad, A. An investigation of the putative photosynthesis of ammonia on iron-doped titania and other metal oxides. *J. Photochem. Photobiol. Chem.* **88**, 53–64 (1995).
 17. Shipman, M. A. & Symes, M. D. A re-evaluation of Sn(II) phthalocyanine as a catalyst for the electrosynthesis of ammonia. *Electrochim. Acta* **258**, 618–622 (2017).
 18. Shi, M.-M. et al. Au sub-nanoclusters on TiO₂ toward highly efficient and selective electrocatalyst for N₂ conversion to NH₃ at ambient conditions. *Adv. Mater.* **29**, 1606550 (2017).
 19. Schlesinger, W. & Hartley, A. A global budget for atmospheric NH₃. *Biogeochemistry* **15**, 191–211 (1992).
 20. Turner, C., Španěl, P. & Smith, D. A longitudinal study of ammonia, acetone and propanol in the exhaled breath of 30 subjects using selected ion flow tube mass spectrometry, SIFT-MS. *Physiol. Meas.* **27**, 321–337 (2006).
 21. Song, Y. et al. A physical catalyst for the electrolysis of nitrogen to ammonia. *Sci. Adv.* **4**, e1700336 (2018).
 22. McEnaney, J. M. et al. Ammonia synthesis from N₂ and H₂O using a lithium cycling electrification strategy at atmospheric pressure. *Energy Environ. Sci.* **10**, 1621–1630 (2017).
 23. Wang, H. et al. Ambient electrosynthesis of ammonia: electrode porosity and composition engineering. *Angew. Chem. Int. Ed.* **57**, 12360–12364 (2018).
 24. Tsuneto, A., Kudo, A. & Sakata, T. Lithium-mediated electrochemical reduction of high pressure N₂ to NH₃. *J. Electroanal. Chem. (Lausanne)* **367**, 183–188 (1994).
 25. Bao, D. et al. Electrochemical reduction of N₂ under ambient conditions for artificial N₂ fixation and renewable energy storage using N₂/NH₃ cycle. *Adv. Mater.* **29**, 1604799 (2017).
 26. Chen, G.-F. et al. Ammonia electrosynthesis with high selectivity under ambient conditions via a Li⁺ incorporation strategy. *J. Am. Chem. Soc.* **139**, 9771–9774 (2017).
 27. Kong, J. et al. Electrochemical synthesis of NH₃ at low temperature and atmospheric pressure using a γ-Fe₂O₃ catalyst. *ACS Sustainable Chem. Eng.* **5**, 10986–10995 (2017).
 28. Yao, Y., Zhu, S., Wang, H., Li, H. & Shao, M. A spectroscopic study on the nitrogen electrochemical reduction reaction on gold and platinum surfaces. *J. Am. Chem. Soc.* **140**, 1496–1501 (2018).
 29. Kim, K., Yoo, C.-Y., Kim, J.-N., Yoon, H. C. & Han, J.-I. Electrochemical synthesis of ammonia from water and nitrogen in ethylenediamine under ambient temperature and pressure. *J. Electrochem. Soc.* **163**, F1523–F1526 (2016).
 30. Zhou, F. et al. Electro-synthesis of ammonia from nitrogen at ambient temperature and pressure in ionic liquids. *Energy Environ. Sci.* **10**, 2516–2520 (2017).
- Acknowledgements** This work was supported by the Villum Foundation V-SUSTAIN grant 9455 to the Villum Center for the Science of Sustainable Fuels and Chemicals. 400 MHz and 800 MHz NMR spectra were recorded on the spectrometers of the NMR Center at the Technical University of Denmark supported by the Villum Foundation. We acknowledge the contribution of Albert Kravos in setting up the analytical methods to detect ammonia.
- Reviewer information** *Nature* thanks Lauren Greenlee, Mark Symes and the other anonymous reviewer(s) for their contribution to the peer review of this work.
- Author contributions** S.Z.A., V.C., S.Y., J.K., S.M., P.C.K.V., I.E.L.S. and I.C. conceived the idea for the protocol and experimental design. S.Z.A., V.C., S.M. and S.Y. performed the experiments; V.C. performed potential scale determination and Ohmic-drop correction; S.Y. performed isotope measurements; K.E.-R. performed NMR measurements and wrote the NMR section; J.A.S., A.C.N. and J.M.M. performed Fourier transform infrared spectroscopy and wrote the corresponding section; J.K., P.C.K.V., I.E.L.S. and I.C. supervised the work; S.Z.A., V.C. and S.Y. drafted the manuscript; and all authors contributed to the editing of the manuscript.
- Competing interests** The authors declare no competing interests.
- Additional information**
Extended data is available for this paper at <https://doi.org/10.1038/s41586-019-1260-x>.
Reprints and permissions information is available at <http://www.nature.com/reprints>.
Correspondence and requests for materials should be addressed to I.C.
Publisher's note: Springer Nature remains neutral with regard to jurisdictional claims in published maps and institutional affiliations.
- © The Author(s), under exclusive licence to Springer Nature Limited 2019

METHODS

Electrochemical measurements in aqueous electrolyte. Bio-Logic VMP2 and SP-300 (Bio-Logic) potentiostats were used for all electrochemical experiments. A borosilicate glass H-cell was used, with working electrode and counter electrode chambers each 7.5 ml in volume, connected by a joint separated by a membrane. The Hg–Hg₂SO₄ reference electrode (SI Analytics) chamber was connected to the working electrode compartment by a glass frit. The electrolyte used was 0.1 M KOH (99.995%, Merck Suprapur) in ultrapure water (Millipore Synergy UV). The glassware was boiled and rinsed twice in Millipore water, then oven-dried overnight at 120 °C between each measurement. We used the microporous polypropylene Celgard 3401 membrane, with a thickness of 25 µm and a porosity of 41%, to separate working electrode and counter electrode chambers. Because it is a porous membrane—as opposed to a proton- or anion-exchange membrane—it does not act as a source or a sink for ammonia, requires no cleaning procedure, and can be kept in 0.1 M KOH. Ruthenium (6 × 6 × 1 mm², 99.9%), rhodium (10 × 10 × 2 mm³, 99.99%, Goodfellow), and rhodium (5 × 10 × 0.25 mm³, 99.9% purity, MaTeCK), were tested at four different potentials: –1.0 V, –1.5 V, –2.0 V and –2.5 V vs RHE, for 1 hour or until 100 C of charge was accumulated. The counter electrode was an iridium foil (25 × 25 × 0.125 mm³, 99.9%, Goodfellow). The electrodes were polished several times using polycrystalline diamond paste (Buehler) of sizes 3 µm, 1 µm, and 0.25 µm, respectively, until the surface had a mirror finish, followed by an ultra-sonication process in Millipore water and isopropanol (>99.8%, Merck) between each polishing step, to dislodge any remaining diamond particles. The working electrodes were annealed at 700–800 °C by induction heating with an Ar/5% H₂ (AGA Gas AB) atmosphere for 5 min. Given the generally low faradaic efficiencies observed for nitrogen reduction in the literature, we applied relatively high currents (10–50 mA) to maximise the ammonia in the system. The Ohmic resistance was measured at open circuit potential, by obtaining electrochemical impedance spectra from 30 kHz to 1 Hz before and after each measurement, fitted using EC-Laboratory V11.02. A shunt capacitance of 2 µF was connected between the reference electrode and the counter electrode to eliminate high-frequency artefacts. Bubble formation during the measurement would result in additional uncorrected IR drops. The electrochemical impedance spectra were fitted using the software to determine the uncompensated resistance. The IR-drop correction was carried out taking into account the current flowing at the given potential. Measurements were conducted with an 85% IR-drop automatic compensation, based on the pre-test resistance; the remaining 15% IR-drop was corrected a posteriori. The pre-test IR drop was higher than the post-test value, due to rising electrolyte levels in the working electrode compartment and temperature increases; we thus represent the potential as a range of values to account for this change in potentials. Additionally, when we attempted to measure the IR drop in operando, we measured an additional increase of at least 6% relative to the open circuit potential, due to bubble formation;³¹ typically such in operando measurements were impractical, owing to the potentiostat overloading. Thus, in order to account for uncertainty in the IR drop, we represent it as a range of values rather than a discrete data point. The higher hydrogen evolution activity of rhodium at very negative potentials resulted in particularly large differences between the pre-test and post-test IR drop value, manifested as a large uncertainty in potential.

Figure 1 displays the potential measured for each metal during chronoamperometry. All of the pure metal catalysts resulted in less than 10 p.p.b. NH₃, detected via the colorimetric indophenol method at the measured potentials, within the levels of background contamination of the set-up. These catalysts show much higher selectivity towards the competing hydrogen evolution reaction in aqueous solutions, consistent with DFT-based models¹⁴.

Electrochemical measurements in non-aqueous electrolyte. The experiments were performed in an OMNI-LABORATORY (Vacuum Atmospheres) glovebox and a home-made closed system with N₂ gas recirculation. The single compartment borosilicate glass cell had an electrolyte volume of 8 ml. It had a two-electrode configuration with a molybdenum foil (0.125 mm, 99.9%, Goodfellow) working electrode and a platinum-mesh (99.9%, Goodfellow) counter electrode. Experiments in non-aqueous electrolytes were conducted in 0.2 M LiClO₄ (battery grade, 99.99%, Sigma-Aldrich) in a mixture of 1 vol% ethanol (99.5%, AcroSeal, Sigma-Aldrich) and 99 vol% tetrahydrofuran (THF, anhydrous, 99.9%, inhibitor-free, Sigma-Aldrich). The exact potential vs SHE was difficult to determine owing to the large IR drop and fluctuating current. It was estimated in a three-electrode system using a Ag/Ag⁺ electrode prepared by immersing a silver wire (Dansk Hollandsk Edelmetal) in 0.1 M AgClO₄ (Sigma-Aldrich) in THF, separated from the main chamber with a P4 glass frit. The potential of this electrode was calculated to be 0.77 V vs SHE using data from ref.³² The IR drop was measured by electrochemical impedance spectroscopy. It was generally in the range of 900–1,600 Ω for the 0.2 M solution of LiClO₄. For the catalytic tests, a bias of –9 V was applied between the electrodes; the current was in the range of 2–3 mA. Using this system, we estimate the initial working electrode potential to be approximately –3.1 V under reaction conditions; it became more negative during the experiment.

Colorimetric tests to determine the concentrations of ammonia, nitrite and hydrazine. Ammonia in the electrolyte was quantified by the indophenol method, which works well for aqueous electrolytes and can be modified to work for non-aqueous electrolytes. For calibration in aqueous electrolytes, a known concentration of NH₄Cl (99.8%, Merck) was added to 0.1 M KOH, then neutralized by adding 0.5 M H₂SO₄ (Suprapur, Merck). 500 µl of phenol nitroprusside solution (P6994, Sigma-Aldrich) and 500 µl of alkaline hypochlorite solution (A1727, Sigma-Aldrich) was then added to 2 ml of the neutralized sample. The solution was incubated for 30 min at room temperature in the dark, and the sample absorbance was analysed by UV-vis spectroscopy (UV-2600, Shimadzu) from 400 nm to 800 nm. The calibration curve was constructed for ammonia with the following concentrations: blank, 10 p.p.b., 50 p.p.b., 100 p.p.b., 500 p.p.b., 1 p.p.m. and 2 p.p.m., and a fitted curve of the absorbance peak of each concentration showed a linear regression with an R² value of 0.99965. For the non-aqueous electrolyte (0.2 M LiClO₄ in 1% ethanol/99% THF), 20 µl of 4 M HCl (37%, VWR Chemicals) was added to 400 µl of the electrolyte, and the solution was dried at 60 °C for 30 min, evaporating the solvent while leaving ammonia in the form of the NH₄Cl salt. The remaining salts were dissolved in 2 ml of Milli-Q H₂O, and the indophenol method proceeded as described for the aqueous case. The calibration curve was constructed for ammonia with the same concentrations as for the aqueous case, and a fitted curve of the absorbance peak of each concentration showed a linear regression with an R² value of 0.99737. It is imperative to make a blank measurement for every sample using the same batch of chemicals; this ensures no major contamination of the chemicals.

NO_x contamination is often present in N₂ gas bottles. NO_x can be reduced to ammonia much more easily than can N₂; consequently, because its presence could lead to a false positive, it is important to account for it. Nitrite (NO₂[–]) can easily be detected down to 10 p.p.b. with colorimetric tests. For the aqueous electrolyte, a known concentration of KNO₂ (>96.0%, Sigma-Aldrich) was added to 0.1 M KOH, then neutralized by adding 0.5 M H₂SO₄. Subsequently 35 mg of powder was added from a nitrite test kit (photometric 0.002–1.00 mg l^{–1} NO₂-N, 0.007–3.28 mg l^{–1} NO₂[–], Spectroquant, Merck), containing sulfanilic acid and diazonium salt, to 3 ml of the neutralized solution. This was incubated for 10 min at room temperature before being analysed by UV-vis spectroscopy. A calibration curve was constructed with the same nitrite concentrations as the ammonia calibration; the fitted curve for the calibration showed a linear regression with an R² value of 0.99933.

Hydrazine can potentially be produced during the synthesis of ammonia. For the aqueous electrolyte, a known concentration of hydrazine monohydrate (~64%, Sigma-Aldrich) was added to 0.1 M KOH, then neutralized by adding 0.5 M H₂SO₄. This was followed by adding 1 ml of the reagent solution from the hydrazine test kit (photometric 0.005–2.00 mg l^{–1} N₂H₄, Spectroquant, Merck), containing 4-(dimethylamino)benzaldehyde, to 2.5 ml of the neutralized solution, and the new solution was incubated for 5 min at room temperature before analysis by UV-vis spectroscopy. A calibration curve was constructed with the same hydrazine concentrations as for the ammonia calibration; the fitted curve for the calibration showed a linear regression with an R² value of 0.99999.

Single-compartment cells. Single-compartment cells have the advantage of removing one source of possible ammonia contamination: the membrane. The single-compartment cell used in this work consisted of a clean glass cell containing 5 ml 0.1 M KOH electrolyte, with Ru as working electrode and Ir as counter electrode, using a glass bubbler to saturate the electrolyte with N₂ gas. However, when we added 1 p.p.m. of ammonia to such a set-up in order to evaluate the efficiency of ammonia retrieval, using Ar gas (5.0, AGA Gas AB, Sweden) instead of N₂ (to exclude contamination from the gas stream), and applied potentials around –2.5 V vs RHE for 1 hour, only 46 p.p.b. and 54 p.p.b. of the added ammonia could be recovered in two separate experiments. Ammonia was removed from the electrolyte, either by hydrogen bubble formation at the working electrode or by oxidation at the counter electrode.

Downstream trap. An acid or water trap downstream of the electrochemical cell is often used to capture gaseous ammonia. However, owing to the high solubility of ammonia in water, it tends to remain in aqueous electrolytes even at very high pH values³³. Therefore, one must evaluate the need for a downstream trap, as it is potentially redundant. Moreover, such a downstream trap could also be a serious source of contamination between experiments. We have not implemented a downstream trap in this work.

Nafion. Nafion is a frequently used membrane and binder. In order to assess the influence of a Nafion membrane, we conducted a series of measurements in the two-compartment cell with 7.5 ml 0.1 M KOH as electrolyte, Ru as working electrode and Ir as counter electrode, both with the ‘as-used’ working electrolyte and after the addition of a set amount of ammonia. The Nafion (Nafion 117, Chemours) was either used as received, or pre-cleaned by boiling for 1 h in 3% H₂O₂ (30%, Merck), boiling for 1 h in 0.1 M H₂SO₄ and then rinsing in Millipore water to remove excess acid. We observed a reduction in the concentration of ammonia in

0.1 M KOH solutions in contact with fresh Nafion. This is due to the membrane soaking up background contamination of ammonia from the electrolyte in which it is submerged, relative to a blank sample from the same batch of 0.1 M KOH that had not been in contact with Nafion. This leads to a 'negative' concentration relative to the blank, as shown in Extended Data Fig. 1a. Conversely, when the Nafion is pre-cleaned using the aforementioned method, the membrane becomes a source of ammonia contamination. The membrane probably absorbs ammonia from the acid during cleaning, and it is later released. Moreover, with no applied potential, the membrane enables considerable crossover of ammonia from the working electrode compartment to the counter electrode compartment (1 p.p.m. added to working electrode, 945 p.p.b. recovered in working electrode and 178 p.p.b. recovered in counter electrode after 1 h). With applied potential, the ammonia from the counter electrode compartment becomes negative (1 p.p.m. added to working electrode, 925 p.p.b. recovered in working electrode and -20 p.p.b. recovered in counter electrode after 1 h at -2.5 V vs RHE with Ar), most likely due to a combination of oxidation at the counter electrode and absorption into the membrane. Because Nafion can be both a sink and a source of ammonia, it should be used with great care in ammonia synthesis.

Celgard. The Celgard 3401 membrane is a 25- μm -thick microporous polypropylene membrane. No substantial increase or decrease in the detected levels of adventitious ammonia was measured with this membrane, as shown in Extended Data Fig. 1b. When 1 p.p.m. of ammonia was added to the working electrode compartment at open circuit potential, all of the ammonia was recovered. With an applied potential of -2.5 V vs RHE using Ar gas, crossover across the membrane increases, and 791 p.p.b. of the 1 p.p.m. of ammonia added was recovered from the working electrode compartment, while 89 p.p.b. was recovered at the counter electrode compartment. An H-cell with the Celgard membrane was therefore used for all aqueous experiments.

Additional sources of contamination. Three clean glass vials, containing separately 2 ml 0.1 M KOH, 2 ml Millipore H₂O and 2 ml 0.1 M HClO₄, were left open in the laboratory. After 24 hours, they contained considerable amounts of ammonia, as shown in Extended Data Fig. 1c; the experiment was repeated three times on different days. To show the possible contamination from human breath, an experiment in which one participant exhaled 3 l (close to the average capacity of a human full breath) through a glass tube inserted into 2 ml of 0.1 M KOH was conducted and repeated for a total of three measurements. Extended Data Fig. 1d shows that the amount of ammonia accumulated in this manner can be considerable. Additionally, nitrile rubber gloves are commonly used in laboratory work. Nitrile rubber is a copolymer of acrylonitrile and butadiene. Acrylonitrile is typically produced by the catalytic ammoxidation of propylene, in which ammonia is used as a reactant. We sonicated approximately 5 cm² of a nitrile glove (Pharma und Kosmetik) in 10 ml deionized water for 1 h, and 2.8 p.p.m. of ammonia was detected by the indophenol method. Care must therefore be taken when using nitrile gloves in ammonia synthesis.

We stress that the contamination levels that we observed herein are not definitive: they depend on cleaning procedures and environmental factors such as ambient ammonia concentration. Nonetheless, our experiments provide examples of how contamination in a given set-up can be quantified.

Mass spectrometry. Isotope-labelled ammonia can be detected via mass spectrometry owing to the difference in atomic weight between ¹⁴NH₃ and ¹⁵NH₃. Unfortunately, the mass difference between H₂O and isotope-labelled ¹⁵NH₃ is only 0.008 AMU, so suppression of the water signal—for example, by lowering the ionization potential coupled with very high resolution—is necessary in order to quantify the ¹⁵NH₃ signal. Other strategies to mitigate the interference from water have thus far yielded only qualitative data²¹.

Gas-phase Fourier-transform infrared spectroscopy. Fourier-transform infrared spectroscopy can distinguish between ¹⁴NH₃ and ¹⁵NH₃, on the basis of the atomic mass difference and the corresponding change in the vibrational frequencies. This manifests itself as a roughly 5-cm⁻¹ shift in the wagging mode of ammonia (see Extended Data Fig. 3), centred around 940 cm⁻¹, in accordance with the prediction of the quantum-mechanical harmonic oscillator²².

NMR spectroscopy. All NMR experiments were performed at 25 °C on a Bruker AVANCE III HD spectrometer operating at a ¹H frequency of 800.182 MHz and equipped with a 5-mm TCI CryoProbe (Bruker Biospin) or a Bruker AVANCE III HD spectrometer operating at a ¹H frequency of 400.13 MHz equipped with a Prodigy probe (Bruker Biospin). One way to confirm the successful electrochemical production of NH₃ from isotope-labelled ¹⁵N₂ experiments would be a standard 'pulse and acquire' NMR experiment tuned to the resonance frequency of ¹⁵N. Despite using a ¹⁵N-labelled precursor, the low production yield—coupled with unfavourable NMR properties of ¹⁵N (for example, low gyromagnetic ratio and long T₁ relaxation constants)—limits the sensitivity of ¹⁵N for this application. ¹H NMR is the better choice for sensitivity—it can differentiate ¹⁵NH₄⁺ from ¹⁴NH₄⁺ because ¹⁴N is a spin-1 nucleus and ¹⁵N is a spin-1/2 nucleus. Consequently, the scalar interaction between ¹H and ¹⁵N in ¹⁵NH₄⁺ results in a splitting of the

¹H resonance into two symmetric signals, with a spacing of 73 Hz; the magnitude of the ¹H-¹⁵N scalar interaction. Conversely, the ¹H resonance for ¹H coupled to ¹⁴N in ¹⁴NH₄⁺ is split into three symmetric signals with a spacing of 52 Hz. For the samples prepared in H₂O, the water resonance was suppressed with the excitation sculpting method using a 3-ms 180° shaped pulse centred at 4.70 p.p.m. The perfect-echo variant was chosen to reduce *J*-modulation for the samples analysed at 800 MHz. A total of 1,024 transient scans were recorded with an inter-scan delay of 1 s. 64,000 complex points were acquired for each free induction decay with an acquisition time of 3.4 s. The processed spectra were zero-filled to 64,000 real points, and an exponential apodization function with lb = 0.3 Hz was applied before Fourier transformation. D₂O (3 vol%; 99.9%, Sigma-Aldrich) was added for deuterium locking and referencing. For the samples analysed at 400 MHz it was necessary to add 10 vol% D₂O to achieve sufficient lock signal. For the samples prepared in THF/ethanol the 1D-NOESY (nuclear Overhauser spectroscopy) pre-saturation method was used to suppress the two THF signals. A train of 100 ms square pulses centred at 3.66 p.p.m. with a frequency modulation of 1.82 p.p.m. was applied during the relaxation delay (3 s) and mixing time (100 ms). ¹³C continuous-wave decoupling was applied during the acquisition time to decrease the intensity of the THF satellite signals. A total of 512 transient scans were recorded. 16,000 complex points were acquired for each free induction decay with an acquisition time of 3.4 s. Linear prediction was used to double the number of complex points and the free induction decay was subsequently zero-filled to 32,000 real points. An exponential apodization function with lb = 1 Hz was applied before Fourier transformation. 5 vol% THF-d₈ (99.9%, Sigma-Aldrich) was added for deuterium locking and referencing. Calibration samples were prepared with varying concentrations of ¹⁴NH₄Cl (99.8%, Merck) and ¹⁵NH₄Cl (98 atom% ¹⁵N, Sigma-Aldrich).

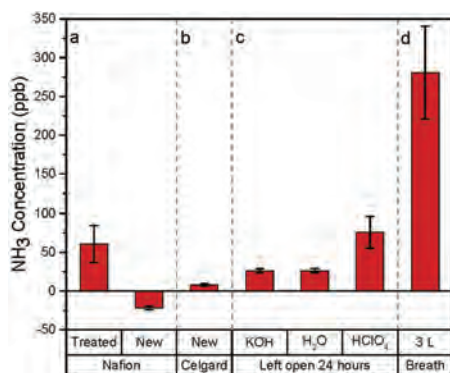
Gas circulation set-up for isotope measurements. Although we stress the importance of isotope labelling experiments, we acknowledge that the high price and small volume of ¹⁵N₂ gas bottles makes such measurements challenging. Furthermore, the low activity of the nitrogen reduction reaction requires the experiment to run for an extended time, with a continuous supply of N₂ gas. Typically, a few litres or tens of litres are required for each measurement, and most of the gas is lost as exhaust. Nevertheless, the price of US\$2,100 for 5 litres of 98% ¹⁵N₂ is negligible compared to having an incorrect scientific report published, which can potentially mislead the entire field. Therefore, we designed a circulation set-up in which ¹⁵N₂ gas was continuously cycled and resupplied to the electrode surface. A simplified schematic and picture of our set-up is shown in Extended Data Fig. 4. A four-way valve is central to the set-up, and enables the choice between purging mode (that is, gas flowing through the entire set-up to the exhaust) and circulating mode (gas being cycled in the enclosed system by a pump). The volume of the enclosed cycling system is about 100 ml (4.46 mmol N₂), which for the present conversion range is plenty. The inlet gas passes through a Cu impurity trap and a cold trap, described in detail in the following section, to remove any impurity supplied to the system. A water trap before the exhaust limits the possibility of back-flow. Before flowing ¹⁵N₂ gas, Ar gas is first flowed through the whole set-up for 30 min to remove any ¹⁴N₂ gas that is present in the system. After sufficient purging with Ar, ¹⁵N₂ is flowed for 20 min with a flow rate of 10 ml min⁻¹. Then the four-way valve is switched to circulating mode, and the isotope experiments are performed. ¹⁴N₂ experiments are performed in the exactly the same manner, except for the unnecessary Ar purging beforehand. The set-up also enables the flow of 10% H₂ in Ar through the gas line that is used for the activation of the copper catalyst. **Cleaning of ¹⁵N₂ gas.** Cleaning of the ¹⁵N₂ gas (98 atom% ¹⁵N, Sigma-Aldrich) is very important, because ¹⁵N₂ may contain substantial impurities in the form of ¹⁵NH₃ along with ¹⁵NO_x species¹⁰. We tested the purity of our ¹⁵N₂ by first saturating our solution of 0.1 M KOH with Ar to remove any excess ¹⁴N₂, followed by bubbling around 200 ml of ¹⁵N₂. We circulated the 200 ml ¹⁵N₂ gas for 1 h to duplicate the long-term electrochemical measurement. The resulting solution was analysed by colorimetric tests to detect NH₃, NO₂⁻ and N₂H₄, and by NMR to differentiate ¹⁴NH₄⁺ from ¹⁵NH₄⁺. With NMR spectroscopy, as shown in Extended Data Fig. 5, we observed a detectable amount of ¹⁴NH₄⁺, which is an unavoidable impurity. However, we could not observe any ¹⁵NH₄⁺ species. Colorimetric tests also confirmed less than 10 p.p.b. of NH₃ in the solution, as shown in Extended Data Fig. 6a. Given the result, we concluded that ¹⁵NH₃ contamination in our system is negligible. Unlike ammonia, we clearly observed greater than 10 p.p.b. of nitrite from the colorimetric test, as shown in Extended Data Fig. 6c. NO₂⁻ can easily be reduced to NH₄⁺ and would give a false positive, even in the isotope-labelled tests. To remove these impurities, a Cu impurity trap was introduced, composed of 2 g Cu-Zn-Al oxide catalyst in a U-shaped stainless steel tubing^{34,35}. The Cu catalyst was reduced before each experiment in a 5% H₂/Ar stream at 300 °C for 2 h. The gas flow was switched to Ar at 300 °C for 30 min, and the Cu impurity trap was cooled to -100 °C using an ethanol slurry, prepared by mixing ethanol with liquid nitrogen. Ar flow through the Cu impurity trap was used to purge the entire system for 30 min, including the gas-tight electrochemical cell.

The electrolyte was then injected using a syringe to the Ar-purged electrochemical cell to prevent exposure to air and moisture. Ar was bubbled through the electrolyte for an additional 30 min to remove dissolved $^{14}\text{N}_2$. Finally, $^{15}\text{N}_2$ was introduced to the electrochemical system through the reduced Cu impurity trap. After bubbling $^{15}\text{N}_2$ gas for 15 min (about 200 ml), the gas was circulated in a closed loop using a glass pump (Makuhari Rikagaku Garasu). Using this cleaning procedure, three repeated measurements were carried out. The first test with the cleaning procedure showed up to 25 p.p.b. of ammonia, as seen in Extended Data Fig. 6b. We assume this is due to leftover contamination of the catalyst, or unaccounted impurity from the environment. Both, however, were in the form of $^{14}\text{NH}_4^+$, as observed by NMR, and should therefore not interfere with the isotope-labelling measurements. For the second and third tests with the cleaning procedure, no ammonia was detected. Regarding the nitrite measurements, small amounts of nitrite in the gas stream were evidently removed, and we could not detect any nitrite after the cleaning procedure, as shown in Extended Data Fig. 6d. No hydrazine was measured before the cleaning procedure as shown in Extended Data Fig. 6e. Such a cleaning procedure is important to definitively prove the catalytic conversion from $^{15}\text{N}_2$ to $^{15}\text{NH}_3$. Other techniques may be used to clean the $^{15}\text{N}_2$ gas, such as using a commercial gas purifier (MicroTorr MCI-902F; SAES Pure Gas), with certified <5 p.p.t.v of NH_3 and <1 p.p.t.v of NO_x impurities.

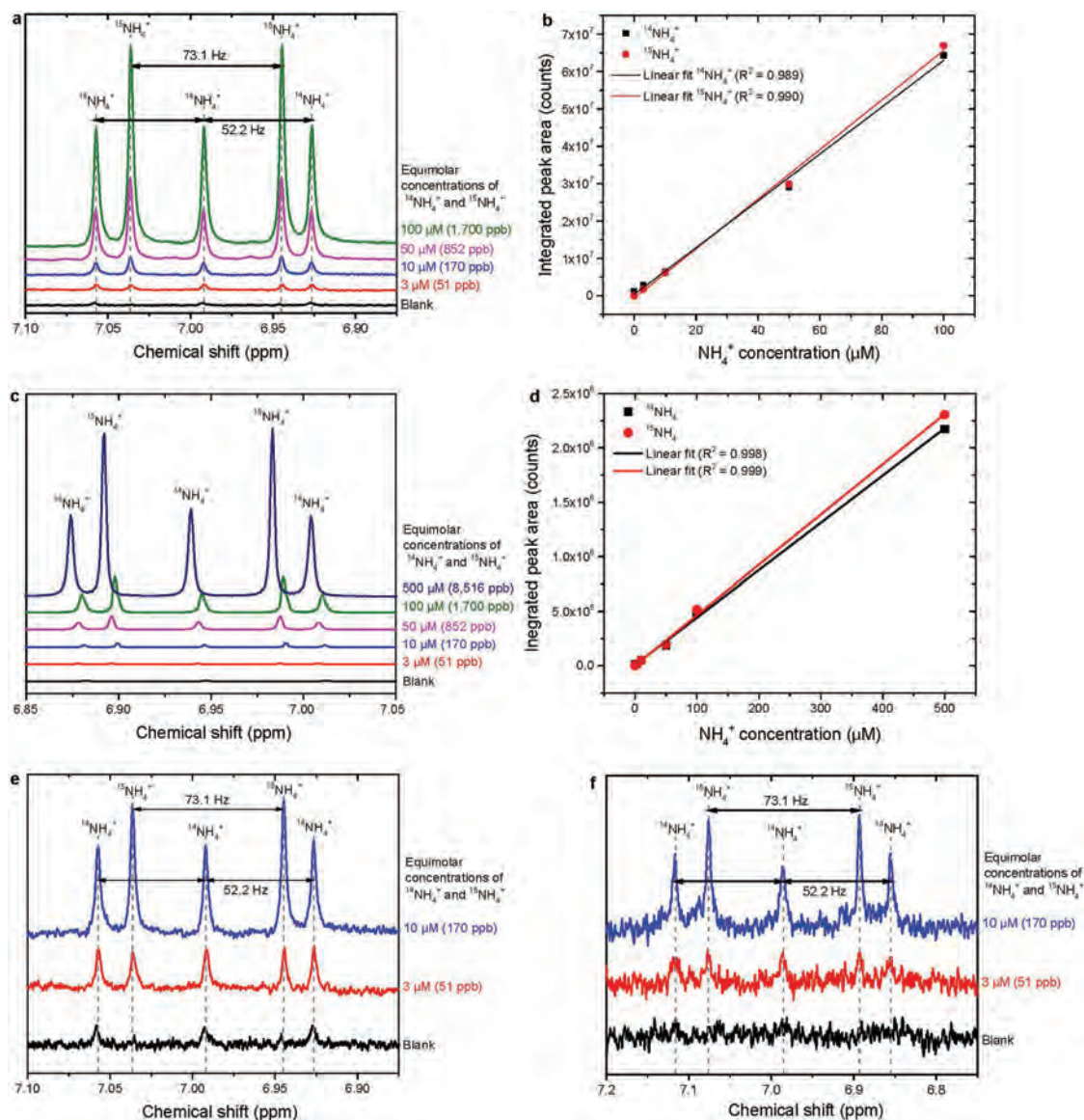
Data availability

The datasets generated during and/or analysed during the current study are available from the corresponding author on reasonable request.

- Čoćli, V. et al. Experimental aspects in benchmarking of the electrocatalytic activity. *ChemElectroChem* **2**, 143–149 (2015).
- Gritzner, G. Standard electrode potentials of M^+/M couples in non-aqueous solvents (molecular liquids). *J. Mol. Liq.* **156**, 103–108 (2010).
- Brass, M., Pritzel, T., Schulte, E., and Keller, J. U. Measurements of vapor–liquid equilibria in the systems $\text{NH}_3\text{--H}_2\text{O}$ – NaOH and $\text{NH}_3\text{--H}_2\text{O}$ – KOH at temperatures of 303 and 318 K and pressures 0.1 MPa < p < 1.3 MPa. *Int. J. Thermophys.* **21**, 883–898 (2000).
- Ma, L. et al. In situ DRIFTS and temperature-programmed technology study on $\text{NH}_3\text{--SCR}$ of NO_x over Cu-SSZ-13 and Cu-SAPO-34 catalysts. *Appl. Catal. B* **156–157**, 428–437 (2014).
- Ma, L. et al. Characterization of commercial Cu-SSZ-13 and Cu-SAPO-34 catalysts with hydrothermal treatment for $\text{NH}_3\text{--SCR}$ of NO_x in diesel exhaust. *Chem. Eng. J.* **225**, 323–330 (2013).
- Cook, R. L. & Sammells, A. F. Ambient temperature gas phase electrochemical nitrogen reduction to ammonia at ruthenium/solid polymer electrolyte interface. *Catal. Lett.* **1**, 345–349 (1988).
- Furuya, N. & Yoshida, H. Electroreduction of nitrogen to ammonia on gas-diffusion electrodes modified by Fe-phthalocyanine. *J. Electroanal. Chem. Interfacial Electrochem.* **263**, 171–174 (1989).
- Furuya, N. & Matsui, K. Electroreduction of carbon dioxide on gas-diffusion electrodes modified by metal phthalocyanines. *J. Electroanal. Chem. Interfacial Electrochem.* **271**, 181–191 (1989).
- Kordali, V., Kyriacou, G. & Lambrou, C. Electrochemical synthesis of ammonia at atmospheric pressure and low temperature in a solid polymer electrolyte cell. *Chem. Commun.* 1673–1674 (2000).
- Pospíšil, L. et al. Electrochemical conversion of dinitrogen to ammonia mediated by a complex of fullerene C_{60} and γ -cyclodextrin. *Chem. Commun.* 2270–2272 (2007).
- Xu, G., Liu, R. & Wang, J. Electrochemical synthesis of ammonia using a cell with a Nafion membrane and $\text{SmFe}_{0.7}\text{Cu}_{0.3-x}\text{Ni}_x\text{O}_3$ ($x = 0\text{--}0.3$) cathode at atmospheric pressure and lower temperature. *Sci. China Ser. B* **52**, 1171–1175 (2009).
- Kugler, K., Luhn, M., Schramm, J. A., Rahimi, K. & Wessling, M. Galvanic deposition of Rh and Ru on randomly structured Ti felts for the electrochemical NH_3 synthesis. *Phys. Chem. Chem. Phys.* **17**, 3768–3782 (2015).
- Li, S.-J. et al. Amorphizing of Au nanoparticles by $\text{CeO}_x\text{--RGO}$ hybrid support towards highly efficient electrocatalyst for N_2 reduction under ambient conditions. *Adv. Mater.* **29**, 1700001 (2017).
- Chen, S. et al. Electrocatalytic synthesis of ammonia at room temperature and atmospheric pressure from water and nitrogen on a carbon-nanotube-based electrocatalyst. *Angew. Chem. Int. Ed.* **56**, 2699–2703 (2017).
- Marnellos, G. & Stoukides, M. Ammonia synthesis at atmospheric pressure. *Science* **282**, 98–100 (1998).
- Murakami, T., Nohira, T., Goto, T., Ogata, Y. H. & Ito, Y. Electrolytic ammonia synthesis from water and nitrogen gas in molten salt under atmospheric pressure. *Electrochim. Acta* **50**, 5423–5426 (2005).
- Wang, B. H., De Wang, J., Liu, R., Xie, Y. H. & Li, Z. J. Synthesis of ammonia from natural gas at atmospheric pressure with doped ceria– $\text{Ca}_3(\text{PO}_4)_2\text{--K}_3\text{PO}_4$ composite electrolyte and its proton conductivity at intermediate temperature. *J. Solid State Electrochem.* **11**, 27–31 (2006).
- Köleli, F. & Kayan, D. B. Low overpotential reduction of dinitrogen to ammonia in aqueous media. *J. Electroanal. Chem.* **638**, 119–122 (2010).
- Amar, I. A. et al. Electrochemical synthesis of ammonia based on doped-ceria-carbonate composite electrolyte and perovskite cathode. *Solid State Ionics* **201**, 94–100 (2011).
- Amar, I. A., Lan, R., Petit, C. T. G., Arrighi, V. & Tao, S. Electrochemical synthesis of ammonia based on a carbonate-oxide composite electrolyte. *Solid State Ionics* **182**, 133–138 (2011).
- Amar, I. A. et al. Electrochemical synthesis of ammonia from N_2 and H_2O based on $(\text{Li},\text{Na},\text{K})_2\text{CO}_3\text{--Ce}_{0.8}\text{Gd}_{0.18}\text{Ca}_{0.02}\text{O}_{2-\delta}$ composite electrolyte and CoFe_2O_4 cathode. *Int. J. Hydrogen Energy* **39**, 4322–4330 (2014).
- Licht, S. et al. Ammonia synthesis by N_2 and steam electrolysis in molten hydroxide suspensions of nanoscale Fe_2O_3 . *Science* **345**, 637–640 (2014).
- Lan, R., Alkhamzi, K. A., Amar, I. A. & Tao, S. Synthesis of ammonia directly from wet air at intermediate temperature. *Appl. Catal. B* **152–153**, 212–217 (2014).
- Amar, I. A., Lan, R. & Tao, S. Electrochemical synthesis of ammonia directly from wet N_2 using $\text{La}_{0.6}\text{Sr}_{0.4}\text{Fe}_{0.8}\text{Cu}_{0.2}\text{O}_{3-\delta}\text{--Ce}_{0.8}\text{Gd}_{0.18}\text{Ca}_{0.02}\text{O}_{2-\delta}$ composite catalyst. *J. Electrochem. Soc.* **161**, H350–H354 (2014).
- Amar, I. A., Lan, R., Petit, C. T. G. & Tao, S. Electrochemical synthesis of ammonia based on $\text{Co}_3\text{Mo}_3\text{N}$ catalyst and $\text{LiAlO}_2\text{--}(\text{Li},\text{Na},\text{K})_2\text{CO}_3$ composite electrolyte. *Electrocatalysis* **6**, 286–294 (2015).
- Cui, B. et al. Electrochemical synthesis of ammonia directly from N_2 and water over iron-based catalysts supported on activated carbon. *Green Chem.* **19**, 298–304 (2017).
- Van Tarnelen, E. E. & Akermark, B. Electrolytic reduction of molecular nitrogen. *J. Am. Chem. Soc.* **90**, 4492–4493 (1968).
- Becker, J. Y., Avraham (Tsarfaty), S. & Posin, B. Nitrogen fixation: Electrochemical reduction of titanium compounds in the presence of catechol and N_2 in MeOH or THF. *J. Electroanal. Chem. Interfacial Electrochem.* **230**, 143–153 (1987).
- Köleli, F. & Röpke, T. Electrochemical hydrogenation of dinitrogen to ammonia on a polyaniline electrode. *Appl. Catal. B* **62**, 306–310 (2006).
- Kim, K. et al. Communication—electrochemical reduction of nitrogen to ammonia in 2-propanol under ambient temperature and pressure. *J. Electrochem. Soc.* **163**, F610–F612 (2016).
- Zhu, D., Zhang, L., Ruther, R. E. & Hamers, R. J. Photo-illuminated diamond as a solid-state source of solvated electrons in water for nitrogen reduction. *Nat. Mater.* **12**, 836–841 (2013).
- Dong, G., Ho, W. & Wang, C. Selective photocatalytic N_2 fixation dependent on $g\text{-C}_3\text{N}_4$ induced by nitrogen vacancies. *J. Mater. Chem. A* **3**, 23435–23441 (2015).
- Banerjee, A. et al. Photochemical nitrogen conversion to ammonia in ambient conditions with FeMoS -chalcogels. *J. Am. Chem. Soc.* **137**, 2030–2034 (2015).
- Li, J., Li, H., Zhan, G. & Zhang, L. Solar water splitting and nitrogen fixation with layered bismuth oxyhalides. *Acc. Chem. Res.* **50**, 112–121 (2017).
- Liu, J. et al. Nitrogenase-mimic iron-containing chalcogels for photochemical reduction of dinitrogen to ammonia. *Proc. Natl Acad. Sci. USA* **113**, 5530–5535 (2016).
- Hu, S. et al. Effect of $\text{Cu}(\text{I})\text{--N}$ active sites on the N_2 photofixation ability over flowerlike copper-doped $g\text{-C}_3\text{N}_4$ prepared via a novel molten salt-assisted microwave process: the experimental and density functional theory simulation analysis. *ACS Sustain. Chem. Eng.* **5**, 6863–6872 (2017).
- Hirakawa, H., Hashimoto, M., Shiraiishi, Y. & Hirai, T. Photocatalytic conversion of nitrogen to ammonia with water on surface oxygen vacancies of titanium dioxide. *J. Am. Chem. Soc.* **139**, 10929–10936 (2017).

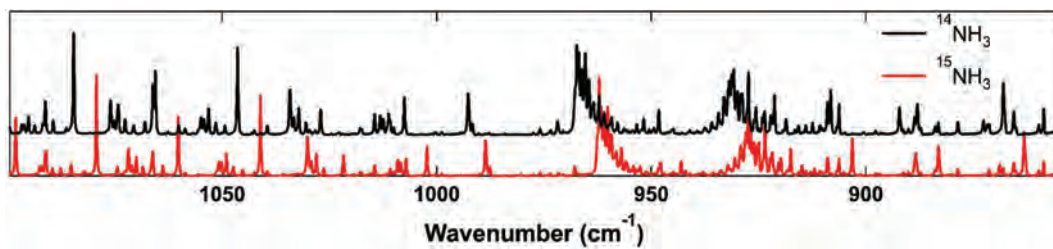


Extended Data Fig. 1 | Concentrations of ammonia produced by various possible contamination sources. All measurements were performed three times; the top of the bars show the mean, the errors show the standard deviation. The following were tested for contamination: **a**, new and treated Nafion membranes; **b**, new Celgard membrane; **c**, 2 ml of 0.1 M solutions of MilliQ H₂O left open overnight; **d**, 2 ml 0.1 M KOH, into which one person had breathed 3 l of air through a glass straw.



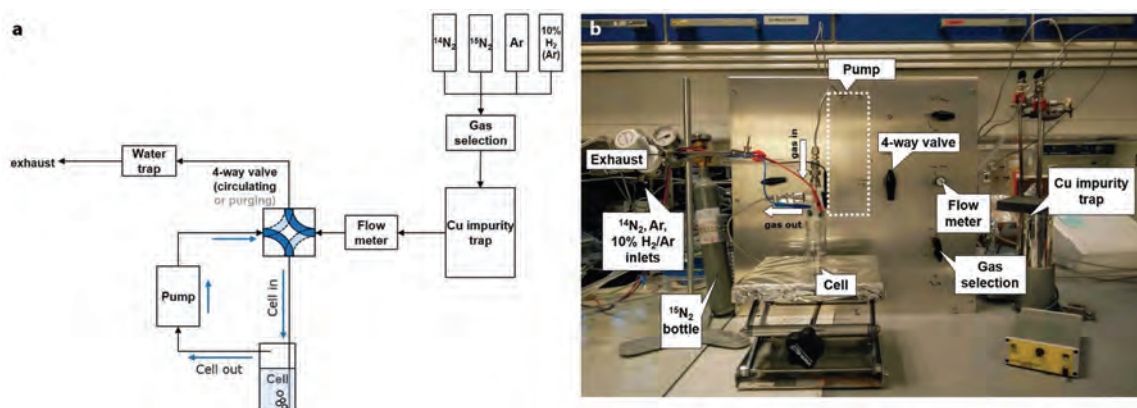
Extended Data Fig. 2 | NMR data. Spectra were acquired using a Bruker AVANCE III HD 800 MHz spectrometer equipped with a 5 mm TCI CryoProbe. Solutions contain equal concentrations of $^{14}\text{NH}_4^+$ and $^{15}\text{NH}_4^+$ from NH_4Cl . **a**, Spectrum of a solution of 600 μl 0.1 M KOH, acidified with 0.5 M H_2SO_4 to a pH of 1. CH_3OH (200 μM) was added as an internal reference. **b**, Integrated peak areas from **a** for both $^{14}\text{NH}_4^+$ and $^{15}\text{NH}_4^+$. **c**, Spectrum of a solution of 500 μl 0.1 M LiClO_4 in THF and ethanol with a ratio of 99:1, respectively, with 2 μl 4 M HCl and 50 μl THF- d_6 .

d, Integrated peak areas from **c** for both $^{14}\text{NH}_4^+$ and $^{15}\text{NH}_4^+$. The variation of chemical shift of the NMR peaks is due to slight differences in the pH, volume, and/or temperature of the samples. **e**, Magnified view of the samples in **a** that contain the lowest concentrations of $^{14}\text{NH}_4^+$ and $^{15}\text{NH}_4^+$. **f**, Spectra of samples with the same concentrations as those in **a**, using a Bruker AVANCE III HD 400 MHz spectrometer equipped with a 5 mm Prodigy probe.



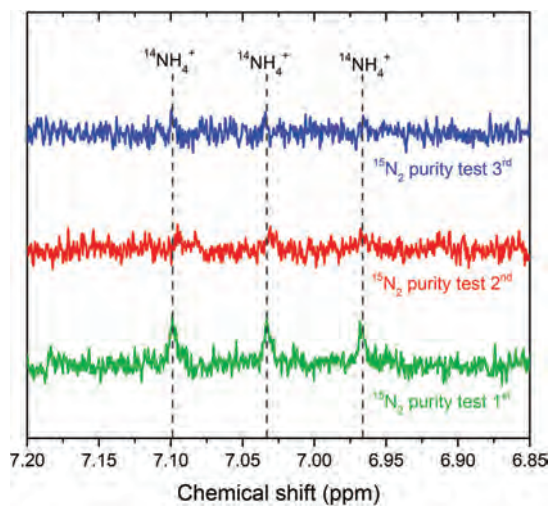
Extended Data Fig. 3 | Gas phase Fourier-transform infrared spectra of labelled and unlabelled ammonia. Spectra were acquired on a Nicolet iS50 spectrometer fitted with a 2-m path length gas cell heated to 135°C.

The total volume of the vaporized sample was 100 μl . The ammonia concentration was 1,000 p.p.m. in H_2O before vaporization.

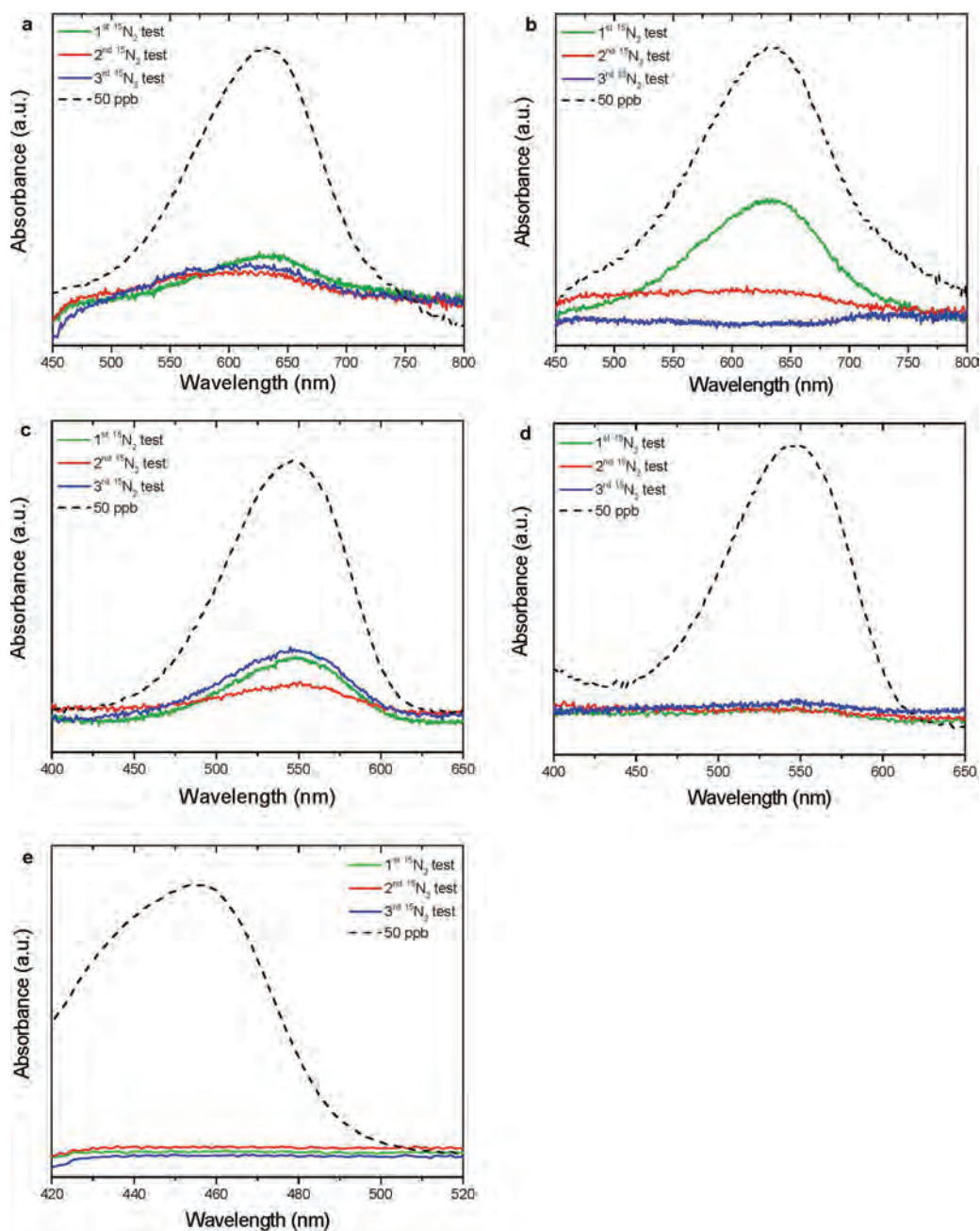


Extended Data Fig. 4 | The set-up for gas ($^{15}\text{N}_2$, $^{14}\text{N}_2$, Ar or 10% H_2 in Ar) circulation through the electrochemical cell. a, Schematic of the set-up. b, Photograph of the set-up with the components labelled. The

pump that circulates the gas through the set-up is situated behind the metal panel, and its position is outlined by the white dashed rectangle.



Extended Data Fig. 5 | ^1H NMR spectra of 0.1 M KOH samples after purging the solution with $^{15}\text{N}_2$ gas. Spectra were acquired using a Bruker AVANCE III HD 800 MHz spectrometer equipped with a 5-mm TCI CryoProbe. No $^{15}\text{NH}_4^+$ was seen in the measurements.



Extended Data Fig. 6 | Concentration of ammonia, nitrite and hydrazine in the gas supply. a–e, Three sequentially repeated measurements of the concentrations of: ammonia (using the indophenol method) without cleaning the gas stream (a); ammonia (using the

indophenol method) with the described cleaning procedure (b); nitrite concentration without cleaning the gas stream (c); nitrite concentration with the described cleaning procedure (d); and hydrazine without cleaning the gas stream (e).

Extended Data Table 1 | Literature data on the electrochemical reduction of N₂ to ammonia in near-ambient conditions

Reference	Catalyst	Reactant	Electrolyte	T (°C)	E(V)	Rate (μmol h ⁻¹ cm ⁻²)	FE (%)	C _{NH3} (ppm)	Comment	¹⁵ N
Sclafani et al. (1983) ⁷	Fe	N ₂ , H ₂ O	6 N KOH	45	-1.06 V vs SCE	0.0002	-	-	Polyethylene membrane No specified blank test Acid trap used	no
Cook et al. (1988) ²⁵	Ru	N ₂ , H ₂	Nafion	25	-	1.75 × 10 ⁻⁵	0.0015	-	Ar blank test Open-circuit blank test Acid trap used	no
Furuya et al. (1989) ²⁷	Fe-phthalocyanine	N ₂ , H ₂	1 M KOH	25	-	2.02 -0.680	0.34 -0.12	-	No blank test	no
Furuya et al. (1989) ²⁸	Sn-phthalocyanine	N ₂ , H ₂	1 M KOH	25	-0.4 V vs RHE	-	1.83 -1.18	-	No blank test	no
Furuya et al. (1990) ²⁷	Fe PbO-TiO ₂ ZnS ZnSe	N ₂ , H ₂	1 M KOH	25	-1.0 V vs RHE	4.82 3.37 20.4 23.2	0.12 0.27 0.96 1.29	-	No blank test	no
Kordali et al. (2000) ²⁹	Ru	N ₂ , H ₂ O	Nafion	90	-1.02 V vs Ag/AgCl	0.076	0.24	4.89* (acid trap)	Nafion used/ Open circuit blank test Ar blank test	no
Pospisil et al. (2007) ⁴⁰	C ₆₀ -γ-cyclodextrin complex / Hg electrode	N ₂ , H ₂ O	0.1 M KCl	60	-1.2 V vs Ag/AgCl	-	-	-	No blank test Acid trap used	no
Xu et al. (2009) ⁴¹	SmFe _{0.7} Cu _{0.1} Ni _{0.2} O ₃	N ₂ , H ₂	Nafion	80	2.0 V (two-electrodes)	40.7	90.4	19.6* (acid trap)	Nitrates used in synthesis NH ₃ used in synthesis Acid trap used No blank test	no
Zhang et al. (2010) ⁸	SmBaCuNiO _{5.5}	N ₂ , H ₂	Nafion	80	2.5 V (two-electrodes)	31.3	-	15.1* (acid trap)	Nitrates used in synthesis Ammonia used in synthesis Acid trap used No blank test	no
Lan et al. (2013) ⁹	PI	Air, H ₂ O	NH ₄ ⁺ exchanged Nafion	80	1.6 V (two-electrodes)	4.10	0.51	-	NH ₄ ⁺ exchanged Nafion Acid trap used No blank test	no
Kugler et al. (2015) ⁴²	Ru	N ₂ , H ₂	0.5 M H ₂ SO ₄	25	-	0.432	-	0.58	(NH ₄) ₂ [(RuCl ₄ (H ₂ O)) ₂ (μ-N)] used for preparing Ru electrode Acid electrolyte No blank test	no
Bao et al. (2017) ²⁵	Tetrahexahedral Au nanoparticles	N ₂ , H ₂ O	Nafion, 0.1 M KOH	25	-0.2 V vs RHE	0.0968	4.00	41.2* ppb/hr	Nitrate used in synthesis Cetyltrimethylammonium bromide used in synthesis Ar blank test Open circuit blank test	no
Li et al. (2017) ⁴³	Amorphous Au nanoparticles/CeO ₂ -RGO	N ₂ , H ₂ O	0.1 M HCl, Nafion	25	-0.2 V vs RHE	-	10.10	-	Nitrate used in synthesis Ar blank test Open circuit blank test	no
Shi et al. (2017) ¹⁸	Au sub-nano-clusters on TiO ₂	N ₂ , H ₂ O	0.1M HCl, Nafion	25	-0.2 V vs RHE	-	3.11	-	Ar blank test Open circuit blank test	no
Chen et al. (2017) ⁴⁴	Fe ₂ O ₃ /carbon nanotubes	N ₂ , H ₂ O	Nafion	20	-2.0 V vs Ag/AgCl	0.013	0.027	-	Open circuit blank test	no
Chen et al. (2017) ²⁰	Li ⁺ -incorporated poly(N-ethylbenzene-1,2,4,5-tetracarboxylic diimide) (PEBCD)	N ₂ , H ₂ O	H ₂ SO ₄ added 0.5 M Li ₂ SO ₄ , Nafion	25	-0.7 V vs RHE	0.11869	1.71	-	Diamine used in synthesis N as imide in catalyst, HNO ₃ used in electrode preparation Ar blank test No catalyst blank test ¹⁵ N ¹⁴ N gas used with NMR	yes
Kong et al. (2017) ²⁷	γ-Fe ₂ O ₃ nanoparticles	N ₂ , H ₂ O	i) 0.1 M KOH ii) Anion-exchange membrane (FAA-3, Fumatech)	i) 25 ii) 65	i) 0.0 V vs RHE ii) 1.6 V (two-electrodes)	i) 0.044 ii) 0.056	i) 1.96 ii) 0.04	i) - ii) 0.252	Nafion used for half-cell Acid trap used for MEA Ar blank test	no
Yao et al. (2018) ²⁹	Au	N ₂ , H ₂ O	0.1 M KOH	25	-0.5 V vs RHE	0.014	0.12	0.14	Blank measurement performed for SEIRAS experiment, but not for catalytic test	no
Song et al. (2018) ²¹	CNS (N-doped carbon nanospikes)	N ₂ , H ₂ O	0.25 M LiClO ₄	25	-1.19 V vs RHE	5.71 ± 0.42	11.56 ± 0.85	69.97* ± 5.13*	Argon blank test isotope labelled GCMS Blank tests without active catalyst	yes

Refs 7-9,18,21,25-28,36-44.

Ambient conditions are noted as 25 °C.

All pressures were ambient (1 atm). Turnover frequencies were not reported.

*Calculated (or estimated) concentrations from parameters given in the papers.

Extended Data Table 2 | Electrochemical reduction of N₂ to ammonia at high temperature or pressure

Reference	Catalyst	Reactant	Electrolyte	T (°C)	P (atm)	E(V)	Rate (μmol h ⁻¹ cm ⁻²)	FE (%)	C _{NH3} (ppm)	Comment	¹⁵ N
Marnellos et al. (1998) ⁴⁵	Pd	N ₂ , H ₂	SrCe _{0.95} Yb _{0.05} O ₃	570	1	-	17.4	78	-	OCV blank test Acid trap used	no
Murakami et al. (2005) ⁴⁶	Ni	N ₂ , H ₂ O	0.5 mol% Li ₃ N in molten LiCl-KCl-CsCl	300	1	0.4 V vs. Li ⁺ /Li	72	23	-	Not continuous process: N ₂ → Li ₃ N → NH ₃	no
Wang et al. (2006) ⁴⁷	Ag-Pd	N ₂ , CH ₄	Y doped Ce-Ca ₃ (PO ₄) ₂ -K ₃ PO ₄	650	1	1.0 V (two-electrodes)	25.0	-	-	Ammonium and nitrate salts used in synthesis Acid trap used No blank test	no
Köleli et al. (2010) ⁴⁸	Polypyrrole (C ₄ H ₂ NH) _n	N ₂ , H ₂ O	Aqueous 0.1 M Li ₂ SO ₄ /0.03 M H ⁺	25	59.2	-0.165 V vs. NHE	-	-	0.903 *	Ar blank test No catalyst blank test.	no
Amar et al. (2011) ⁴⁹	La _{0.8} Sm _{0.4} Fe _{0.8} Cu _{0.2} O _{3.5} -Ce _{0.8} Sm _{0.2} O _{2.8}	N ₂ , H ₂	La _{0.9} Sm _{0.4} Fe _{0.8} Cu _{0.2} O _{3.5} and Ce _{0.8} Sm _{0.2} O _{2.8}	450	1	0.8 V (two-electrodes)	19.4	-	5.22 * (acid trap)	Nitrates used in synthesis Ammonia used in synthesis Acid trap used No blank test	no
Amar et al. (2011) ⁵⁰	CoFe ₂ O ₄ with Ag	N ₂ , H ₂	Carbonate-LiAlO ₂ composite	400	1	0.8 V (two-electrodes)	0.835	-	0.512 * (acid trap)	Nitrate used in synthesis Ammonia used in synthesis Acid trap used No blank test	no
Amar et al. (2014) ⁵¹	CoFe ₂ O ₄ -Ce _{0.8} Gd _{0.18} Ca _{0.02} O _{2.8}	N ₂ , H ₂ O	Ca, Gd co-doped Ce-ternary carbonate composite	400	1	1.6 V (two-electrodes)	0.234	0.17	0.156 * (acid trap)	Nitrate used in synthesis Ammonia used in synthesis Acid trap used No blank test	no
Licht et al. (2014) ⁵²	Fe ₂ O ₃ (Ni-monel electrode)	N ₂ , H ₂ O	Molten NaOH/KOH	200	1	1.23 V (two-electrodes)	8.64	35	-	Ar blank test Open circuit blank test Water trap used	no
Lan et al. (2014) ⁵³	Pr _{0.8} Ba _{0.4} Fe _{0.8} Cu _{0.2} O _{3.5}	Air, H ₂ O	Ce _{0.9} Gd _{0.2} O _{2.9} -(Li,Na,K) ₂ CO ₃	400	1	1.4 V (two-electrodes)	0.385	0.6	0.336 * (acid trap)	Nitrates used in synthesis Ammonia used in synthesis Acid trap used No blank test	no
Amar et al. (2014) ⁵⁴	La _{0.8} Sm _{0.4} Fe _{0.8} Cu _{0.2} O _{3.5} -Ce _{0.8} Gd _{0.18} Ca _{0.02} O _{2.8}	N ₂ , H ₂ O	Ce _{0.8} Gd _{0.18} Ca _{0.02} O _{2.8} -(Li/Na/K) ₂ CO ₃	400	1	1.4 V (two-electrodes)	0.18	0.1	0.06 * (acid trap)	Nitrates used in synthesis Ammonia used in synthesis Acid trap used No blank test	no
Amar et al. (2015) ⁵⁵	Co ₃ Mo ₃ N with Ag	N ₂ , H ₂	LiAlO ₂ -(Li,Na,K) ₂ CO ₃	450	1	0.8 V (two-electrodes)	1.18	2.85	1.57 * (acid trap)	Nitrates used in synthesis Ammonia used in synthesis Acid trap used No blank test	no
Cui et al. (2017) ⁵⁶	Fe ₂ O ₃ /AC (stainless steel electrode)	N ₂ , H ₂ O	Molten NaOH/KOH	250	1	1.55 V	29.8	4.9	-	Nitrate used in synthesis Acid trap used No catalyst blank test	no

Refs ⁴⁵⁻⁵⁶.

Ambient conditions are noted as 25 °C and 1 atm. Turnover frequencies were not reported.

*Calculated (or estimated) concentrations from parameters given in the papers.

Extended Data Table 3 | Electrochemical reduction of N₂ to ammonia in non-aqueous electrolytes

Reference	Catalyst	Reactant	Electrolyte	T (°C)	P (atm)	E(V)	Rate (μmol h ⁻¹ cm ⁻²)	FE (%)	C _{NH3} (ppm)	Comment	¹⁵ N
van Tamelen et al. (1968) ⁵⁷	Titanium complex (Pt electrode)	N ₂	Titanium tetraisopropoxide, aluminum chloride in 1,2-dimethoxyethane	-	1	80 V (two-electrodes)	-	-	851 *	Ar blank test, No catalyst blank test	no
Becker et al. (1987) ⁵⁸	Cp ₂ TiCl ₂ (Pt electrode)	N ₂	0.3 M n-tetrabutylammonium perchlorate in THF	25	1	-2.05 V vs. SCE	-	0.28	-	Acid trap used Ammonium used as an electrolyte (n-Bu ₄ NClO ₄)	no
Tsuneto et al. (1993) ¹³	Li (on metal electrode, Ag)	N ₂	0.2 M LiClO ₄ , 1 vol% EtOH in THF	25	1	-	2.09	8.4	1.65 *	Ar blank test	no
Tsuneto et al. (1994) ²⁴	Li (on metal electrode, Fe)	N ₂	0.2 M LiClO ₄ +0.18M EtOH in THF	25	50	-4 V vs Ag/AgCl/AgCl(sat)	14.34	57.7	-	Ar blank test	no
Köhlér et al. (2006) ⁵⁹	Polyaniline	N ₂	30 mM H ₂ SO ₄ + 0.1M LiClO ₄ in MeOH	25	49.3	-0.12 V vs. NHE	0.16	16.3	0.443 *	Ar blank test Aniline in catalyst	no
Kim et al. (2016) ⁶⁰	Ni	N ₂ , H ₂ O	10 mM H ₂ SO ₄ in 2-propanol/H ₂ O (9:1, v/v)	25	1	3.7 V (two-electrodes)	0.0554	0.89	0.126 *	No blank test	no
Kim et al. (2016) ²⁸	Ni	N ₂ , H ₂ O	0.1 M LiCl in ethylenediamine (EDA)	25	1	1.8 V (two-electrodes)	0.129	17.2	-	Neosepta CMX membrane (cation exchange membrane) used Ethylenediamine used as a solvent Ar blank test ¹⁵ N ₂ test using MS	yes
Zhou et al. (2017) ³⁰	Fe/FTO Fe/SS	N ₂ , H ₂ O	[P _{6,6,6,14}][eFAP] (ionic liquid)	20	1	-0.8 V vs. NHE	0.017 0.073	60 45	-	Acid trap used ¹⁵ N ₂ test using NMR Ar blank test Open circuit blank test	yes

Refs 13,24,29,30,57-60.

Ambient conditions are noted as 25 °C and 1 atm. Turnover frequencies were not reported.

*Calculated (or estimated) concentrations from parameters given in the papers.

Extended Data Table 4 | Photochemical reduction of N₂ to ammonia in non-aqueous electrolytes

Reference	Catalyst	Reactant	Electrolyte	Source	Bandgap (eV)	Rate ($\mu\text{mol h}^{-1} \text{mg}^{-1}$)	TOF (s^{-1})	C _{NH₃} (ppm)	Comment	¹⁵ N
Zhu et al. (2013) ⁶¹	Hydrogen terminated diamond	N ₂	H ₂ O	High pressure HgXe lamp, $\lambda > 190 \text{ nm}$	5.5	$\sim 0.64^* \mu\text{mol h}^{-1} \text{cm}^{-2}$ illuminated			Ar control Dark control IR spectra of NH ₃ isotopes	Yes
Dong et al. (2015) ⁶²	Nitrogen vacancies on graphitic carbon nitride (g-C ₃ N ₄)	N ₂	Aqueous 20% Methanol	300 W Xe lamp, $\lambda > 420 \text{ nm}$	2.74	1.24		$\sim 41^*$ (2.4 mM)	Ar control Dark control N containing electrode UV-vis Nessler's reagent LCMS of indophenol	Yes
Banerjee et al. (2015) ⁶³	FeMoS-Chalcogenols	N ₂	Aqueous pyridinium hydrochloride and sodium ascorbate	150 W Xe lamp		0.03 [*]	3.1×10^{15} [*]	5.21	Dark control Ar control Control without proton or electron source NMR and LCMS of indophenol	Yes
Li et al. (2017) ⁶⁴	Layered bismuth oxyhalides	N ₂	H ₂ O	Visible light	2.81	104.2			Ar control With and without oxygen vacancies control	No
Liu et al. (2015) ⁶⁵	FeMoS-FeS-SnS chalcogel	N ₂	Aqueous PyriH and NaAc	Xenon lamp $\lambda > 190 \text{ nm}$	0.7		8.7×10^{15} [*]	16	Dark control, NMR	Yes
Hu et al. (2017) ⁶⁶	Cu doped g-C ₃ N ₄	N ₂	DI water, Ethanol	High pressure Na lamp 400-800 nm	2.56	0.264 [*] (8.8 mg L ⁻¹ g _{cat} ⁻¹ h ⁻¹)		70.4 [*] (352 mg/L)	UV-vis Nessler's reagent LCMS on indophenol No blank tests No Argon control	Yes
Hirakawa et al. (2017) ⁶⁷	Surface oxygen vacancies on TiO ₂	N ₂	H ₂ O	High pressure Hg lamp $\lambda > 280 \text{ nm}$		7.6×10^{11} ^{**}	2.9×10^{19} [*]	$\sim 3^*$ (175.9 μM)	Argon control Dark control Nessler's reagent LCMS on indophenol	Yes

Refs ⁶¹⁻⁶⁷.

Ambient conditions are noted as 25 °C and 1 atm.

*Calculated (or estimated) turnover frequency, rate and concentration from parameters given in the papers.

Paper IV

Cyclic Stabilization Method on Lithium Mediated Electrochemical Nitrogen Reduction

Suzanne Z. Andersen*, Michael J. Statt*, Vanessa J. Bukas*, Sarah Groot Shapel, Jakob Bruun Pedersen, Kevin Kreml, Mattia Saccoccio, Debasish Chakraborty, Jakob Kibsgaard, Peter Christian Kjærgaard Vesborg, Jens Nørskov, and Ib Chorkendorff

In preparation

* these authors contributed equally

Cyclic Stabilization Method on Lithium-Mediated Electrochemical Nitrogen Reduction

Authors: Suzanne Z. Andersen^{1†}, Michael J. Statt^{2†}, Vanessa J. Bukas^{1†}, Sarah G. Shapel¹, Jakob B. Pedersen¹, Kevin Krempf¹, Mattia Saccoccio¹, Debasish Chakraborty¹, Jakob Kibsgaard¹, Peter C. K. Vesborg¹, Jens Nørskov^{1*}, and Ib Chorkendorff^{1*}

Affiliations:

¹Department of Physics, Technical University of Denmark, Kongens Lyngby, Denmark.

²SUNCAT Center for Interface Science and Catalysis, Department of Chemical Engineering, Stanford University, Stanford, CA, USA.

[†]These authors have contributed equally

*Correspondence to: jkno@dtu.dk, ibchork@fysik.dtu.dk.

Abstract: Lithium-mediated nitrogen reduction is a proven method to electrochemically synthesize ammonia; however, the process has thus far been unstable, and the continuous deposition of lithium limits the practical applicability of the process. In addition, very little is understood about the mechanism. Herein we report a novel method of cycling the potential between lithium reduction potential, and a less negative potential wherein we do not reduce out further lithium. We show that this leads to improved stability of the system, with a significant increase in faradaic efficiency. In addition, we develop a simple model of the process, which can account for a number of observations including the increased efficiency upon cycling.

